

An FtsZ-centric approach to divide gene-expressing liposomes

Noguera López, Jonás

DOI

[10.4233/uuid:0161174a-4915-480f-970d-77c70a992da9](https://doi.org/10.4233/uuid:0161174a-4915-480f-970d-77c70a992da9)

Publication date

2019

Document Version

Final published version

Citation (APA)

Noguera López, J. (2019). *An FtsZ-centric approach to divide gene-expressing liposomes*. [Dissertation (TU Delft), Delft University of Technology]. <https://doi.org/10.4233/uuid:0161174a-4915-480f-970d-77c70a992da9>

Important note

To cite this publication, please use the final published version (if applicable). Please check the document version above.

Copyright

Other than for strictly personal use, it is not permitted to download, forward or distribute the text or part of it, without the consent of the author(s) and/or copyright holder(s), unless the work is under an open content license such as Creative Commons.

Takedown policy

Please contact us and provide details if you believe this document breaches copyrights. We will remove access to the work immediately and investigate your claim.

An FtsZ-centric approach to divide
gene-expressing liposomes

An FtsZ-centric approach to divide gene-expressing liposomes

Dissertation

for the purpose of obtaining the degree of doctor
at Delft University of Technology
by the authority of the Rector Magnificus prof.dr.ir. T.H.J.J. van der Hagen
chair of the Board for Doctorates
to be defended publicly
on Monday 16th December 2019 at 15:00 o'clock

by

Jonás NOGUERA LÓPEZ

Licenciado en Biología, Universidad de Oviedo, Spain
born in Gijón, Spain

This dissertation has been approved by the promotors.

Composition of the doctoral committee:

Rector Magnificus,
Dr. C. J. A. Danelon,
Prof.dr. A. M. Dogterom,

chairperson
Delft University of Technology, promotor
Delft University of Technology, promotor

Independent members:

Prof.dr. P. Bassereau,
Prof.dr. G.H. Koenderink,
Prof.dr. G. Rivas Caballero,
Dr. M. Loose,
Prof.dr. H. Geerlings,

Institut Curie, France
Delft University of Technology
CSIC, Spain
IST Austria, Austria
Delft University of Technology, reserve member



Keywords: synthetic biology, artificial cell, minimal cell, cell division, FtsZ, FtsA, ZipA, ZapA, Min system, liposome, PURE system, supported lipid bilayer, fluorescence microscopy.

Printed by: Ridderprint, www.ridderprint.nl

Cover by: Jonás Noguera López

Copyright © 2019 J. Noguera López

Casimir PhD series Delft-Leiden 2019-45

ISBN 978-90-8593-427-1

An electronic copy of this dissertation is available at

<http://repository.tudelft.nl/>

A mi abuelo.

Table of contents

1 Introduction: constructing a minimal cell	9
<i>Preface</i>	
1.1 Minimal cell model	11
1.2 In this thesis	13
<i>The divisome</i>	
1.3 FtsZ	14
1.4 FtsA	15
1.5 ZipA	15
1.6 ZapA	16
1.7 Assembly of downstream division proteins and divisome activation	16
1.8 <i>In vitro</i> reconstitution of <i>E. coli</i> early division proteins	17
<i>The Min system</i>	
1.9 MinC	21
1.10 MinD	21
1.11 MinE	22
1.12 Molecular dynamics of the Min oscillations	22
1.13 <i>In vitro</i> reconstitution of the Min system	23
<i>Technologies</i>	
1.14 PURE system	28
1.15 Biomimetic membranes	29
1.16 Microscopy techniques	32
2 Synthesized FtsZ and other key division proteins on SLBs	35
2.1 Introduction	36
2.2 Materials and Methods	37
2.3 Results	43
2.4 Discussion	56
3 In-vesicle synthesis of FtsZ	63
3.1 Introduction	64
3.2 Materials and methods	65
3.3 Results	69
3.4 Discussion	77

4 FtsZ-MTS on SLBs and inside liposomes	81
4.1 Introduction	82
4.2 Materials and methods	83
4.3 Results	85
4.4 Discussion	94
5 The cell-free synthesized Min system on SLBs	101
5.1 Introduction	102
5.2 Materials and methods	103
5.3 Results	110
5.4 Discussion and conclusions	125
5.5 Supplementary information	137
6 General conclusions	145
6.1 The PURE system is a versatile tool and its use should be continued in the development of minimal cells	146
6.2 Synthesized <i>E. coli</i> division-related proteins can be implemented in artificial cells	147
6.3 A new minimal machinery model arises	148
Appendix: DNA constructs and sequences	151
7.1 DNA sequences for expression of Min proteins in <i>E. coli</i> .	152
7.2 DNA sequences for expression in the PURE system	154
References	161
Summary	179
Samenvatting	181
Acknowledgements	183
Curriculum vitae	187
List of publications	189

Chapter 1

Introduction: constructing a minimal cell

“There is grandeur in this view of life, with its several powers, having been originally breathed into a few forms or into one; and that, whilst this planet has gone cycling on according to the fixed law of gravity, from so simple a beginning endless forms most beautiful and most wonderful have been, and are being, evolved.”

- Charles Darwin, *The Origin of Species*.

Preface

What is life but a tangled mess of interconnected processes, that furiously seek one sole thing: to perpetuate itself? Life is selfish¹. This concept, i.e. that life is the interconnected process, rather than a physical property of the matter that constitutes the organism, was captured by the Chilean biologists Humberto Maturana and Francisco Varela in their work *De Máquinas y Seres Vivos* (About Machines and Living Beings)². They coined the word *autopoiesis* (from Greek; *auto*, meaning self and *poiesis*, creation) to try to explain the property of living organisms that separate them from the dead matter. In their own words:

“[A living organism] is a machine organized (defined as a unity) as a network of processes of production (transformation and destruction) of components which [...] through their interactions and transformations continuously regenerate and realize the network of processes (relations) that produced them”²

Autopoiesis has also been defined as a ratio between the complexity of the organized machine, and the complexity that surrounds that machine³. In this scenario, autopoietic machines, i.e. living beings like unicellular organisms, are defined as a complex network of processes that creates more of its own complex network⁴.

Over more than 3500 million years, life has evolved to outstanding levels of complexity by modifying, nucleotide by nucleotide, the genes of the organisms and their frequency in the population. While such complexity is nothing but fascinating, and has maintained scientists occupied for centuries, one could wonder how much of it is actually dispensable. What are the foundations of life? Or more specifically, what are the minimal requirements for a cell to be alive?

In nature, some unicellular species exhibit outstanding levels of gene reduction. Let's take for example *Pelagibacter ubique*, which holds the honor of possessing the shortest genome of all free-living bacteria with a surprising length of 1.31 Mbp⁵. To compare, the well-known gram-negative bacterium *E. coli* exhibits up to 4500 genes encoded in a 4.64 Mbp genome⁶. Still, some parasitic species have experienced even more intense evolutive pathways towards genome reduction. *Mycoplasma genitalium*, with 580 Kbp and 515 protein-coding genes, is probably one of the known organisms with the shortest genome alive today. *Nanoarchaeum equitans*, another parasitic species, shows a 491 Kbp genome coding for a total of 536 proteins. These two species are interesting paradigmatic examples of genome complexity reduction. While *M. genitalium* possesses a longer genome than *N. equitans*, its number of protein-coding genes is lower. This exemplifies one of the challenges when considering complexity reduction in biology, i.e. how can it be measured. While not ideal, genome length or total number of proteins are good proxies to this complexity that are easily calculated and interpreted.

Despite the high reductionism of some of these parasitic species, the theoretical minimal set of genes (MSG) that sustains life might be much lower than the one exhibited by *M. genitalium* or *N. equitans*⁷. The first cross-species investigation of ortholog genes to theoretically assess the MSG was done between *Haemophilus influenzae* and *M. genitalium* and indicated that only 256 conserved genes were shared between these two bacteria⁸. Later, the MSG number was reduced to 206 by Gil et al.⁹ after an exhaustive consideration of all available data at the time. However, the MGS concept cannot be defined without taking into account the characteristics of the hypothetical medium surrounding the minimal cell. For example, Luisi et al. proposed that, if a minimal cell was to grow in rich medium¹⁰ the MGS number could be reduced even further to approximately 150 genes.

Notwithstanding the number of genes of the hypothetical MSG, a minimal cell must be able to self-maintain and self-reproduce in order to be alive¹¹. Yet one more requisite is the coding of these two functions in a heritable molecule, which in turn gives rise to evolvability. Typically, implementation of these features in a minimal cell is done following one of two approaches.

In the top-down approach, all non-essential genes of a modern reference species are removed or replaced by synthetic ones in order to reduce the length of the genome¹²⁻¹⁵. This approach does not necessarily need or seek to understand the functions of the removed genes. To the contrary, this can be done by removing one gene at a time or by random mutagenesis screening¹⁶. Since this approach depends in the first place on the chosen organism of reference, the set of genes of the reduced genome will probably be different to the set of genes of another reduced organism. Therefore, the minimality of this approach can be questioned in that there could be other organisms that present, potentially or de facto, a higher reduction in complexity.

The bottom-up approach, or biochemical approach can be considered much more challenging¹⁴. It does not start from an existing living cell, but aims to assemble essential cellular functions (evolvability, self-maintainability, self-reproducibility) with a minimal set of organic and non-biotic molecules under controlled conditions¹⁷⁻¹⁹. The goal is to understand the fundamental principles of cellular biology by rational construction of each one of its components. Here, a distinction can be made between the synthetic and the semi-synthetic approach. In the former, only organic and inorganic molecules which are assumed to have been present at the time of the first living organism, are used for the construction of a synthetic protocell. The focus is to understand the transition from chemistry to biology and the origins of life^{14,20}. In the latter approach, any modern biomolecules present in any domain of life (Archaea, Bacteria, Eukarya) or viruses are potential candidates to be used as building blocks for a semi-synthetic cell¹⁷. The capacity to combine and adapt genes from different organism, ultimately, will produce highly controllable, designable and predictable organisms, with applications in biotechnology and medicine¹⁴.

1.1 Minimal cell model

In the group of Christophe Danelon, we envision a minimal cell as a semi-synthetic biological entity with the necessary complexity, but no more, to evolve, self-maintain and self-reproduce. In our model (Figure 1.1 *Left*), the vertebral spine that powers every cellular subsystem is the cell-free, in-vesicle synthesis of protein. To this end, we use the PURE system, an *in vitro* transcription and translation machinery reconstituted from purified components (further information in Section 1.14, page 28). This flow of information, i.e. from DNA, to RNA to proteins, is what in molecular biology is known as the central dogma of molecular biology. Such a machinery must be encapsulated in a cell boundary. This is a necessary requirement to establish an *in* and an *out* and define the cell as an independent unit in space. In our model, this boundary takes the shape of a spherical, semipermeable phospholipid membrane (a liposome; Section 1.15.2, page 31) capable of maintaining proteins and other macromolecular particles in the interior of the cell, protect it from external damage and contaminants and provide it with the most basic structural scaffold for the organization of proteins and other molecules. Finally, our cell is governed by the presence in the cytosol of a minimal genome. Its purpose is to control the

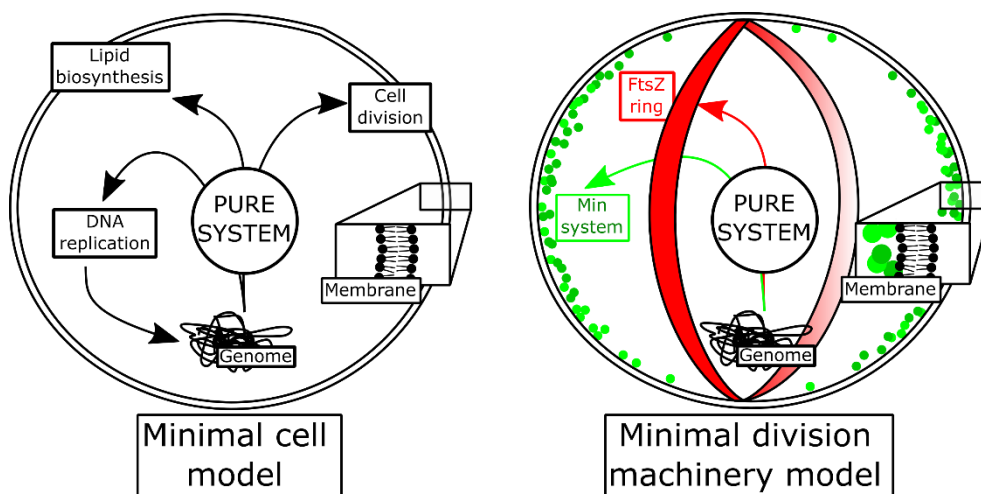


Figure 1.1 Idealized models for the construction of minimal cells with a division machinery

Our general minimal cell model (*Left*) consists of a cell which metabolic center core is formed by the PURE system. This system, encapsulated in a liposome and guided by a minimal genome, generates a set of cellular subsystems. In turn, this subsystems provide the cell with the essential processes of life, i.e. evolvability, self-maintenance and self-reproduction. Our minimal division machinery (MDM) model (*Right*), builds upon the general model. In the MDM model, cell division is carried out by FtsZ, anchored to the membrane by FtsA and/or ZipA. This ring, with constriction capabilities, is spatially regulated by the Min system, a three-protein network that oscillates pole-to-pole to establish a time-average gradient minimum at the midcell, where the Z-ring is allowed to assemble. The concerted action of the FtsZ-ring and the Min system divides the cell.

functions of the cell through a specifically designed proteome, ultimately synthesized by the PURE system.

These three components (PURE system, membrane, genome) must coordinate to give rise to the three essential functions of life: evolvability, self-maintainability, self-reproducibility. In our model, we envision each of these essential features arising as a consequence of three cellular submodules: DNA replication, membrane synthesis and cellular division. In first place, DNA replication is intimately linked to self-reproduction and the emergence of evolvability. Our strategy to minimal cell DNA replication makes use of the bacteriophage $\Phi 29$ machinery. Amplification of encapsulated DNA can be achieved by expressing the phage's DNA polymerase and terminal protein on a template modified to contain two origins of replication at both extremes of the template²¹. Second, membrane synthesis is connected to both cell maintenance and self-reproduction. Our strategy involves the expression of key *E. coli* enzymes involved in phospholipid metabolism²². Finally, cell division is linked to reproduction and the emergence of evolvability. We follow two different strategies to achieve division. In a passive approach, we use the phospholipid enzymatic machinery to create a membrane excess in the cell. Eventually, the energetically unfavorable surface per volume ratio would relax by spontaneously producing daughter cells. In an active, or mechanical approach, we aim to synthesize and assemble some type of cytoskeleton able to exert a mechanical force on the membrane. Two systems are being explored, the ESCRT system and an FtsZ based system.

Throughout this thesis, our working minimal division machinery (MDM) model is based on the FtsZ approach (Figure 1.1 *Right*). In this model, we aim to assemble the *E. coli* protein FtsZ

into a cytokinetic ring in the interior of the cell. Attached to the membrane by partner proteins (FtsA or ZipA), FtsZ would realize a constriction force that eventually would pinch the cell. To regulate the FtsZ ring, and therefore division, we propose the use of the *E. coli* Min system. In the cell, this system oscillates pole-to-pole to ensure that division occurs only at midcell. In this thesis, we intend to exploit the bacterial division machinery and its associated regulatory system to implement an artificial cytokinetic network able to divide a liposome.

1.2 In this thesis

Bacterial division machinery is a fascinating, interconnected and highly complex network of proteins. The unravelling of its structure and function commenced almost three decades ago with the identification of a cytoskeletal assembly related to the *ftsZ* gene²³. Such discovery shook the long-believed notion that prokaryotes were a mere unorganized collection of proteins-containing sacculi, and opened the door for the investigation of bacterial cytoskeletons.

Enormous research efforts have been done *in vitro* to help us understand the basic principles of this machinery. However, such studies mainly focused on the physiological attributes of division. In this thesis, we propose a different focus. Can we engineer an artificial division system for minimal cells, based on the bacterial division machinery? Can this artificial system be spatiotemporally regulated with yet another engineered artificial protein network? To answer these fairly intimidating questions, we propose the following outline.

In Chapter 1 of this thesis, we review the concept of minimal cells, describe the working model of the Danelon laboratory and revise the current knowledge on *E. coli* division machinery. Additionally, we describe some of the key technologies utilized in this book for the consecution of this thesis' goals.

Next, we focus on the engineering of a functional, cell-free synthesized minimal version of the *E. coli* division machinery. In Chapter 2, we used supported lipid bilayers (SLBs) and cell-free synthesized *E. coli* early division proteins to reconstitute some crucial cytoskeletal patterns. We demonstrate that cell-free expression with the PURE system of physiologically active division-related proteins is possible. In Chapter 3, we show the interaction of these synthesized proteins with liposomes. In particular, we show the capacity of in-vesicle synthesized FtsZ to bundle and trigger the deformation of liposomes into elongated and lemon-shape conformations. This establishes a direct link between vesicle genotype and shape. In Chapter 4, we utilized both SLBs and liposomes to study the possibilities of chimeric, multifunctional FtsZ proteins. Our artificial FtsZs were capable of targeting to phospholipids while still maintaining the capacity to rearrange in dynamical cytoskeletal structures. Dynamics involved bundle fusion and ring shrinking, processes of great interest to the formation of cytokinetic machineries.

In Chapter 5 of this thesis, we focus on the reconstitution on planar membranes of reaction-diffusion powered spatiotemporal patterns with cell-free synthesized Min proteins. We show that physiologically active Min proteins can be expressed from their genes and highlight the importance of optimization of *in vitro* conditions to realizing complex behaviors in artificial settings.

Finally, in Chapter 6 we discuss some general considerations regarding the implementation of a minimal division machinery in artificial cells and propose an extended MDM model that integrates all the lessons learned during the realization of this thesis.

The divisome

In many prokaryotes like *E. coli*, division commences with the assembly at the midcell of a very well-coordinated multi-protein complex, named the divisome^{24,25}. This complex, with 12 essential proteins and over 15 non-essential ones^{26–36}, spans from the nucleoid to the outer cell membrane and assembles in a highly hierarchical fashion²⁴.

1.3 FtsZ

The first known event of division is the arrival of FtsZ to midcell²³. FtsZ (Filamentous temperature sensitive mutant Z), is a cytosolic protein with a molecular weight of ~40 kDa highly conserved among bacteria, and the most conserved among the essential proteins of the divisome³⁷.

In the cell, FtsZ undergoes a GTP powered dynamic cycle between a monomeric and a polymeric state. In the monomeric state, FtsZ polymerizes upon GTP binding^{38,39–42}. These polymers, known as protofilaments, are on average 30 monomers long^{39,43,44}. Once self-associated, and as long as free Mg^{2+} is available, the GTPase activity of FtsZ becomes active^{38,45,39}. GTP hydrolysis, in turn, weakens the self-interaction between two adjacent monomers, promoting the disassembly of the protofilament³⁹. This way, monomers and small oligomers are dynamically interchanged between the cytoplasm and the protofilaments. This turnover exhibits a rapid half-time of approximately 10 seconds^{46,47}. While in this active cycle, protofilaments can further self-interact through lateral interactions to form longer and thicker structures known as filaments or bundles^{35,43,48,49}. Eventually, these filaments will coalesce in the cell into a single ring-like structure known as the Z-ring⁵⁰. This structure is the scaffold upon which the divisome will be assembled and plays a major role in the regulation of the divisome activity and perhaps on the generation of a constriction force⁵¹.

The crystal structure of FtsZ has been resolved and three domains can be identified³⁷. In the N-terminus, the globular domain is responsible for most of the molecular dynamics of FtsZ. This domain is responsible for GTP binding and hydrolysis, FtsZ self-interaction, polymerization and lateral interactions^{37,52}. FtsZ is considered a structural homologue of tubulin due to its grand similarity to this protein⁵³. In this regard, it is not surprising that, like FtsZ, tubulin binds and hydrolyzes GTP, polymerizes upon GTP binding and establishes lateral interactions with neighboring filaments⁵⁴. An interesting feature of the FtsZ globular domain is the presence of the catalytic site at opposite sides of the domain^{37,53}. This feature explains both the GTP-dependent polymerization as well as the activation of the GTPase activity only when in polymeric state. Connected to the N-terminal globular region through an unstructured flexible linker⁵⁵, FtsZ has a yet another conserved 12-amino acid domain at its very C-terminus⁵⁶. This short peptide is responsible for the binding of FtsZ to a variety of protein partners^{56,57}.

While *in vivo* the Z-ring is anchored to the inner leaflet of the cytoplasmic membrane, FtsZ does not show a membrane binding domain. This function is tackled by two other early and essential division proteins, FtsA and ZipA, which arrive at the Z-ring right after or together with FtsZ, modulate their dynamics and recruit downstream division proteins²⁴.

1.4 FtsA

FtsA (Filamentous thermosensitive mutant A) arrives at midcell together with FtsZ⁵⁸. It anchors FtsZ protofilaments to the cell-membrane by interacting with the FtsZ's CCTP domain^{59,60}. Interestingly, FtsA might have a dual activity over FtsZ dynamics. While FtsA stabilizes and supports the Z-ring⁶¹, *in vitro* studies have suggested that FtsA might destabilize as well FtsZ's protofilaments⁵⁹. In the cell, FtsZ and FtsA are kept to a constant FtsZ:FtsA ratio of 1:10^{62,62}. Proper ratio is important for allowing division in *E. coli*, as overexpression of any of these proteins is toxic⁶³.

FtsA forms part of the actin family of ATPases⁶⁴ and has been shown to have an actin-like structure⁶⁵. The protein exhibits an ATP binding pocket core intercalated between two globular domains⁶⁶, although only a marginal ATPase activity has been found⁶⁷. ATP binding is required for interaction with FtsZ and the membrane^{68,69}. In the current model, upon ATP binding, FtsA would carry out a conformational change that promotes its interaction with FtsZ, triggers polymerization of FtsA and forces the activation of a C-terminal amphipathic helix capable of targeting to the membrane^{69,56,57,60}. The C-terminal amphipathic MTS might be disordered in solution⁶⁵, but transposes into a helix in contact with the membrane⁷⁰. This helix seems to function only as a general anchor that can be transplanted and swapped with other membrane anchors with similar characteristics⁷¹.

An interesting FtsA polymorphic, FtsA_{R286W} (FtsA*) which is impaired for self-interaction, compensates in the cell for the loss of other essential divisome proteins like ZipA⁷², meaning that FtsA* alone can anchor the Z-ring to the membrane and recruit downstream division proteins.

1.5 ZipA

ZipA (FtsZ interacting protein A) arrives together with ZipA and FtsA to the divisome and anchors the Z-ring to the membrane²⁴. ZipA can interact both with monomers and FtsZ polymers through a C-terminal globular domain (FtsZ binding domain; FBD) and a hydrophobic transmembrane N-terminal domain that integrates in the lipid bilayer^{73,74}. These two domains are linked through a flexible, unstructured peptide with two distinct regions, the proline/arginine (P/Q) domain and the charged domain^{75,75}. ZipA is essential for the structural integrity of the Z-ring and has been shown to bundle FtsZ protofilaments^{76,77}. ZipA can self-interact to form homodimers⁷⁸. This could be related to its ability to bundle FtsZ protofilaments. The globular domain of ZipA has been shown to be monomeric in solution, but the full length ZipA (with the N-terminal unstructured and transmembrane domains intact) are able to dimerize^{79,78}.

ZipA is highly integrated in the *E. coli* divisome interactome. In one hand, ZipA is recruited to the division septum only if FtsZ is present⁷⁶ and in the other, it is required for recruitment of other downstream essential proteins like FtsK and the FtsEX complex, as well as FtsQ, FtsL and FtsN^{61,80,34,80}. However, ZipA is a protein that is not well-spread outside γ -proteobacteria⁷³ and as stated above, FtsA* (and other FtsA's impaired for self-interaction) can easily bypass ZipA essentiality. The presence of FtsZ, FtsA and ZipA at the midcell and their organization in a ring-like structure is known as the protoring⁸¹.

1.6 ZapA

While not essential, other proteins are involved in the stabilization and modulation of the protoring dynamics. ZapA (FtsZ associated protein A) is an important protein that cross-links FtsZ protofilaments and stabilizes the Z-ring^{82,32}. Mutants with a ZapA deletion, albeit non-lethal, provoke a disintegration of the Z-ring into disperse, incoherent FtsZ clusters⁸³. Additionally, ZapA has been found to participate in the coordination between chromosome segregation and progression of the septum division as well as in the spatial regulation of the divisome through the ZapA-ZapB-MatP network, even in the absence of the Min and NO systems^{84,85,86}. The correct functioning of this network, of which ZapA is primordial, avoids the chromosome to be bisected before chromosome segregation is completed⁸⁵.

ZapA is in a dimer-tetramer equilibrium in solution⁸⁷. This equilibrium can be shifted towards any state depending on ZapA concentration. At high concentrations, ZapA is shifted towards the tetramer conformation. It has been shown that the active form of ZapA, i.e. the form capable of crosslinking FtsZ protofilaments is the tetramer form⁸⁸.

The protein structure of ZapA consists of a globular domain at its N-terminus that interacts with the globular domain of FtsZ⁸⁹. At the C-terminus, ZapA exhibits a coiled-coil domain responsible for homodimerization and tetramerization⁸⁹. When ZapA self-interacts, their globular domains get positioned at opposite sides of the complex, allowing to cross-link FtsZ protofilaments⁸⁹.

1.7 Assembly of downstream division proteins and divisome activation

Once the protoring proteins assemble at midcell, recruitment of downstream division proteins commences²⁴. After a temporal delay, FtsK arrives at the division septum⁹⁰. FtsK is a DNA translocase that has been related to the segregation of the bacterial chromosome during division through its cytoplasmic domain⁹¹⁻⁹³. Nonetheless, their essential domain seems to be located in the transmembrane part and it has been suggested to be responsible for the transduction of signals from the early to the late division proteins of the divisome^{91,92,94}. Next, the proteins FtsQ, FtsL and FtsB arrive to the division septum. These proteins seem to form a subcomplex inside the divisome, and probably arrive to midcell already as a complex⁹⁵. They are related with the transduction of signals from other components of the divisome and participate in the activation of the peptidoglycan (PG) enzymatic machinery⁹⁶. Next, FtsW, a protein with ten transmembrane segments arrives to midcell and recruits FtsI, an enzyme related to the synthesis of PG^{97,98}. Finally, FtsN, a single pass membrane protein, arrives at midcell⁹⁶.

In the current model, the arrival of FtsN to midcell triggers the activation of the divisome from an assembly phase to a constriction phase. FtsN contains a small N-terminal cytoplasmic domain, a transmembrane domain and a large periplasmic domain⁹⁹. Through its N-terminal domain, FtsN interacts with FtsA at midcell¹⁰⁰. This interaction could promote a change on the polymerization state of FtsA, which in turn might signal late division proteins to start constriction¹⁰¹. The activity of FtsN seems to involve a positive feedback loop. The presence of a small concentration of FtsN at the division septum promotes the remodeling of the PG layer through activation of cytoplasmic FtsA. This remodeling, in turn, recruits FtsN to the division site, which activates more FtsA^{101,102}. FtsN might also interact with the FtsQLB complex to indirectly promote the activation of FtsW and FtsI¹⁰³. In this model, FtsZ activity in the Z-ring would involve the treadmilling of FtsZ clusters around midcell in a circular motion¹⁰⁴. This

treadmilling would guide the recruitment of the late division proteins and PG remodeling machinery, ensuring that the synthesis of new cell wall is homogeneous¹⁰². The progression of the septum would finally close up to complete division.

1.8 *In vitro* reconstitution of *E. coli* early division proteins

In 2013, Loose and Mitchison¹⁰⁵ reconstituted on SLBs the *E. coli* protoring proteins FtsZ, FtsA and ZipA. They aimed to study the fundamental mechanisms responsible for the Z-ring assembly *in vivo*. They observed that, while FtsZ/FtsA assembled in dynamic bundles and vortices, FtsZ/ZipA produced static filament networks (Figure 1.2). Interestingly, FtsZ/FtsA vortices underwent a rapid reorganization and rotated clock-wise at a velocity of 6.56 μm per minute. These vortices had a diameter close to the *E. coli* circumference (0.7-1.4 μm). They further studied whether these rotations were due to a sliding or treadmilling mechanism. By complementing their Alexa Fluor 488 labelled FtsZ assays with traces of Cy5 labelled FtsZ, they showed that, while structures reorganized, single Cy5 labelled FtsZ monomers remained static, indicative of a treadmilling activity. Analysis of single filaments showed two types of dynamics. In the first one, FtsZ filaments polymerized from one end and, after a small delay time, the

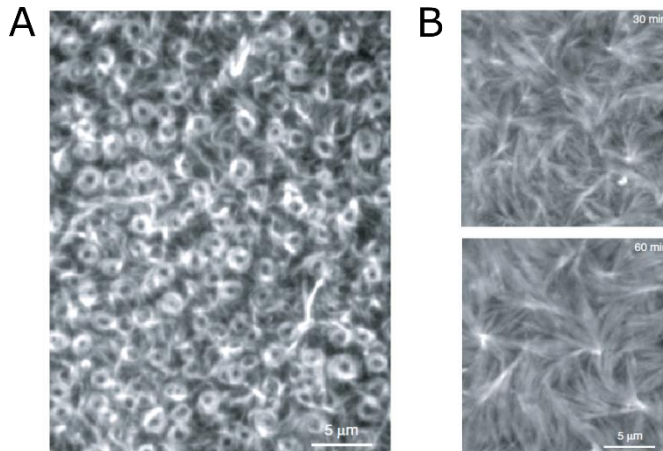


Figure 1.2 Purified proteins FtsZ, FtsA and ZipA reorganize on SLBs

A) Purified FtsZ and FtsA self-organized in chiral vortices and filaments. B) Purified FtsZ and ZipA produced straighter bundles than FtsZ/FtsA reconstitutions and the suprastructure was static. Figure adapted from reference¹⁰⁵.

opposite end started to depolymerize, but a faster rate. This, eventually ended with the total depolymerization of the filament. In other cases, both rates (polymerization and depolymerization) were similar and the filaments travelled on the membrane in a typical treadmilling fashion. With FtsZ/ZipA experiments, they observed a homogeneous increase of protein on the membrane and the delay time to produce the bundles was much shorter than with FtsA. In addition, FtsZ monomers in these conditions showed a longer life-time than in FtsZ/FtsA filaments. They used these experiments to argue that the reorganization of FtsZ on the membrane does not arise from an intrinsic quality of FtsZ (at least not only) but that it necessitates FtsA or ZipA activity for such dynamics to emerge.

Loose and Mitchison studied further the signal on the membrane of FtsZ/FtsA filaments as a function of time. In a first experiment, they let FtsZ and FtsA monomers to interact in solution for a few minutes without the presence of GTP. Upon addition of GTP, they observed that, at

first, the concentration of FtsA increased gradually while FtsZ remained at similar levels than before. This was followed by a second phase where both FtsZ and FtsA concentration increased at a similar pace, following a similar curve over time. In a second experiment, when both nucleotides (GTP and ATP) were added from the beginning and FtsZ was at low concentration, FtsA signal on the membrane rose linearly and FtsZ concentration stayed at basal levels. When extra FtsZ was added, FtsA concentration in the membrane increased rapidly. However, FtsZ described a significant decrease on the membrane, before following a smooth signal recovery. This behavior seemed to show that FtsA was able to depolymerize FtsZ filaments. To better study this effect, they assembled FtsZ filaments in solution on top of a membrane and in the absence of FtsA. After addition of FtsA, they observed that FtsZ signal on the membrane underwent a damped oscillation, consistent with a lagged negative feedback. In the case of ZipA, this did not happen. The authors concluded that the organization of FtsZ/FtsA on the membrane arises from a dual characteristic of FtsA. In one hand, FtsA promotes FtsZ assembly on the membrane, but in the other, it destabilizes FtsZ polymers in a delayed-time manner. Based on their observations, they proposed a model where the reorganization of the Z-ring *in vivo* is based on the polymerization dynamics of FtsZ that arise from the interaction of FtsA with the membrane (Figure 1.3). They think that their data support a Z-ring with high adaptability to the constricting septum and that this would act as scaffold for a force generated by the synthesis of the cell wall.

The notion that FtsZ dynamics on SLBs are a direct consequence of the membrane anchor used (FtsA or ZipA), was contradicted by an article in 2018 by Ramirez-Diaz and colleagues¹⁰⁶. In their work, they studied the dynamics of a membrane targeted FtsZ. This chimeric protein allowed them to study FtsZ behavior on SLBs without the presence of FtsA or ZipA. Still, they found that FtsZ dynamics ranged from self-organizing chiral vortices (as observed by Loose and Mitchison) to static but nonetheless dynamic filament bundles. In their study, they managed to establish a link between the local concentration of FtsZ on the membrane and the different morphologies, suggesting that FtsZ reorganization dynamics are an intrinsic feature of this protein. In turn, the influence of FtsA and ZipA on the FtsZ filament morphology, might be ligated to their ability to recruit FtsZ to the membrane rather than in organizing FtsZ dynamics.

In 2013, Cabre et al.¹⁰⁷ realized a series of experiments where liposome encapsulated FtsZ and ZipA proteins were let to interact. After feeding the liposomes with GTP, FtsZ polymerized and bundled, but, more interestingly, a shrinkage of the liposome membrane was observed. That same year, Osawa and Erickson made interesting observations with FtsZ and the hypermorph FtsA* (self-interaction impaired FtsA) inside vesicles. When FtsZ and FtsA* were encapsulated inside vesicles, they observed the formation of Z-ring-like structures that were able to constrict and deform the liposomes over time (Figure 1.4). In a small fraction of the liposomes, they reported division events, claiming that liposome division was achieved by the minimal FtsZ/FtsA* machinery. It is worth notice that they could not obtain similar results with wild-type FtsA.

In 2018, Furusato and colleagues¹⁰⁸ explored an alternative strategy for the reconstitution of early *E. coli* divisome proteins in liposomes. They argued that, since reconstitution of some membrane proteins (like FtsA and ZipA) can be problematic due to difficulties during purification, and since detergents used for protein purification can hamper the correct topology of reconstituted proteins on the membrane, a better alternative was the *de novo* synthesis of proteins inside liposomes. For gene expression, they used the PURE system. After validating the synthesis of the FtsZ, FtsA and ZipA DNA templates for gene expression, they

1 - Introduction: constructing a minimal cell

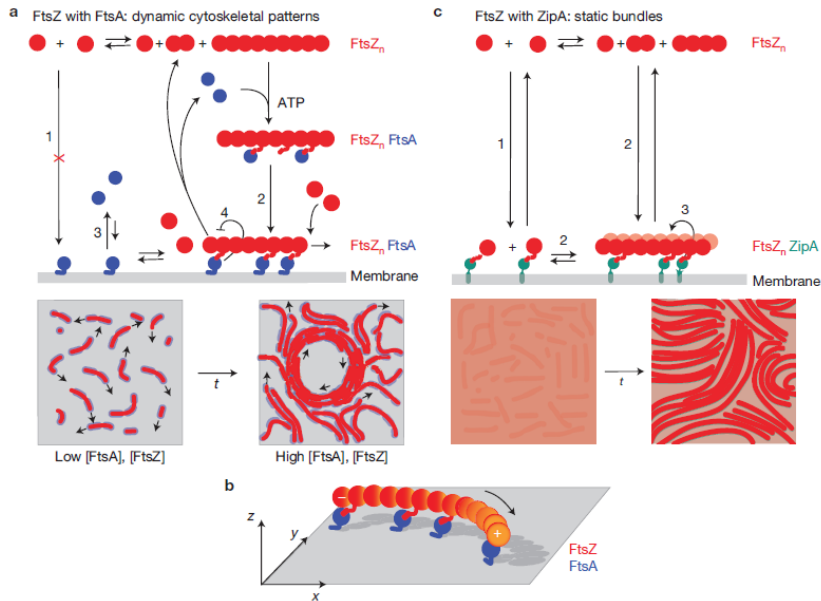


Figure 1.3 Model proposed by Loose and Mitchison to explain the emergence of FtsZ dynamics

A) FtsA cannot recruit FtsZ monomers to the membrane but necessitates first the polymerization of FtsZ. The process requires ATP binding. B) Cartoon of a protofilament anchored by FtsA to the membrane. The spontaneous curvature of FtsZ protofilaments, as well as the presence of a plus (polymerization) and a minus (depolymerization) end, gives rise to the chiral vortices and treadmilling behavior. C) Model for the anchoring of FtsZ to the membrane by ZipA. Both single monomers and protofilaments are recruited by ZipA. The result is a static structure. Figure from reference¹⁰⁵.

confirmed that synthesized proteins were able to assemble on the outside of liposomes through a series of flotation assays. Next, they studied the in-vesicle expression of single proteins. They observed that synthesized FtsZ dispersed on the lumen of the liposomes, but some punctate fluorescence was observed as well (Figure 1.5, first panel). When Ficoll70 was added at 12% (m/v), bundles were observed (Figure 1.5, second panel). In the case of FtsA, the protein stayed on the lumen and punctate fluorescence was observed as well. This pattern changed in vesicles containing 20% DOPC (mol%), from a lumen distributed to a membrane attached pattern. In the case of ZipA, POPC liposomes exhibited protein recruitment in the membrane, which contrasted with 20% DOPG liposomes, where recruitment was reduced. When FtsZ and FtsA were co-expressed in vesicle, the proteins localized on the membrane, indicating that FtsA was able to recruit FtsZ (Figure 1.5, third panel). They screened different FtsZ:FtsA DNA ratios and observed that a weaker recruitment of proteins to the membrane, or the formation of protein cluster in the lumen, was produced, depending whether the ratio was lower, or higher than the standard condition, respectively. In the other hand, the synthesis of FtsZ and ZipA produced a partial recruitment of ZipA to the membrane. Interestingly, the FtsZ/ZipA recruitment adopted a clustered shape that sometimes promoted the deformation of the vesicle (Figure 1.5, fourth panel). They assayed the role of FtsZ's GTP binding and hydrolysis on the formation of liposome-deforming clusters with the synthesis of FtsZ mutants. Still, they found that FtsZ mutants deficient for GTP binding or hydrolysis were recruited to the membrane, produced clusters and deformed the liposomes.

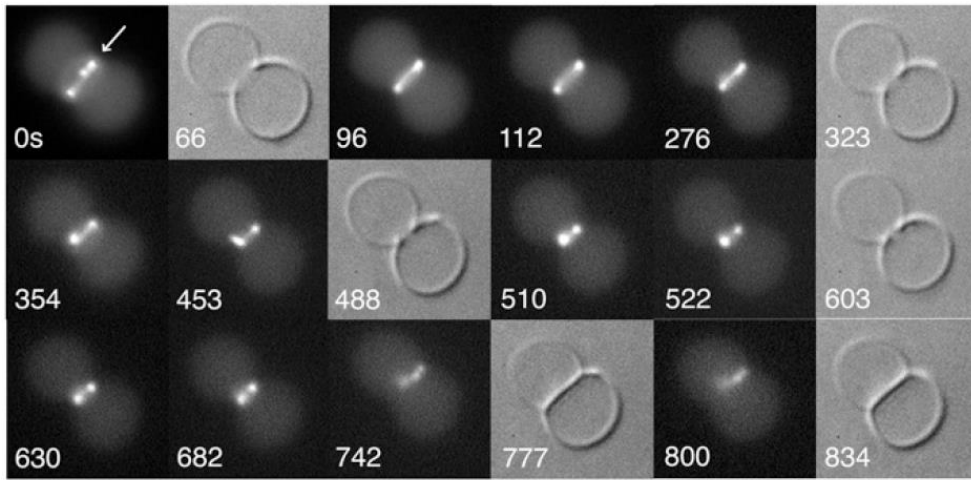


Figure 1.4 Purified proteins FtsZ and FtsA* produce a protein ring that constricted over time
 Liposomes with encapsulated FtsZ and FtsA* (an FtsA mutant impaired for self-interaction) assembled in protein rings at the inner leaflet of the membrane. Such structure (white arrow) constricted over time up to liposome division (around 742 second). Scale bar: 10 μm . Figure from reference¹⁰⁹.

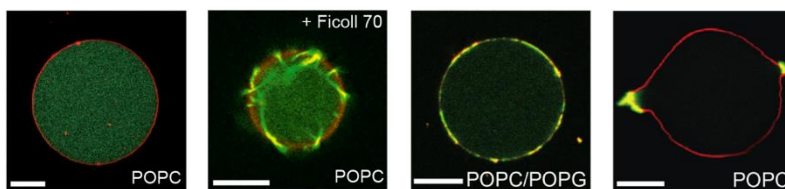


Figure 1.5 De novo expression of *E. coli* early divisome proteins inside vesicles.
 The colors correspond to the liposome membrane (red) and FtsZ (green). First panel from the left, encapsulated synthesized FtsZ is homogeneously distributed in the lumen. Second panel, same conditions as in A, but with 12% of Ficoll70 (m/v). In this case FtsZ bundles were produced. Interestingly they stayed cortically instead of occupying all the lumen. Third panel, co-synthesized FtsZ and FtsA recruited on the inner leaflet of the vesicle. Fourth panel, co-synthesized FtsZ and ZipA produced liposome-deforming clusters. Scale bars: 10 μm . Figure adapted from reference¹⁰⁸.

The Min system

One of the main regulators of the positioning of the divisome in *E. coli* is the Min system. This system carries out a dynamic cycle of oscillations from pole to pole of the cell by a mechanism that involves the interaction of two of its proteins (MinD and MinE) with each other and with the membrane¹¹⁰⁻¹¹². The wavelength and the period of the Min oscillations has been found to range between 3-8 μm ^{110,113} and 40-120 seconds^{113,114}, respectively, which averages a typical wave velocity of $\sim 0.07 \mu\text{m}$ per second. An inhibitor of FtsZ polymerization, MinC, is a passive passenger of these oscillations and the responsible of guiding FtsZ assembly at midcell^{115,116}. The Min system exerts its topological specificity by establishing a time-averaged MinC concentration gradient which is minimal at midcell, where the Z-ring is allowed to assemble. While yet more data must be gathered regarding the molecular activity of the MinCDE proteins, some of the basic principles have been elucidated.

1.9 MinC

MinC is a ~ 25 -kDa cytosolic protein. Its structure consists of a C-terminal domain (residues 116-231)¹¹⁶ which is responsible of dimerization of MinD and interaction with MinC and FtsZ proteins¹¹⁷. The N-terminus of MinC (residues 1-115) constitutes the second domain and is responsible of the direct interaction with FtsZ at its H10 helix¹¹⁸. Both domains have a role in inhibiting the assembly of FtsZ in a coherent Z-ring¹¹⁹. The N-terminal domain weakens longitudinal interactions between FtsZ monomers within the protofilament and increases the detachment rate of FtsZ-GDP¹²⁰. Additionally, MinC's N-terminal domain decreases the association rate of FtsZ and GTP by capping the minus end (H10 helix region) of FtsZ protofilaments¹¹⁸. In the presence of MinD, MinC's C-terminal domain becomes competent to interact with the FtsZ's C-terminus, inhibiting lateral interactions between protofilaments¹²¹. Yet, the detailed mechanism by which MinC interacts with the H10 helix of FtsZ and the mechanism by which MinD activates MinC remain to be elucidated^{122,116}.

1.10 MinD

MinD is a cytosolic ~ 30 -kDa ATPase¹²³. Upon ATP binding and as long as free Mg^{2+} is available in solution, MinD homodimerizes (MinD·ATP)¹²⁴. MinD·ATP dimers directly interact with the inner cell membrane through association with a 10-amino acid long, C-terminal amphipathic helix¹²⁵. Monomers, in the other hand, are not efficiently recruited to the membrane due to the weak interaction of a single C-terminal helix¹¹². MinD·ATP interacts with MinC and MinE only in the dimer state, but interestingly, the two interaction sites in MinD overlap, meaning that MinC and MinE compete with each other to interact with MinD·ATP¹²⁴. Upon ATP hydrolyzation, MinD·ADP dimer becomes instable, promoting monomerization.

MinD is also believed to have a function in the inhibition of FtsZ polymerization. In this model, it has been proposed that MinD activates the inhibiting functions of MinC through direct interaction with the C-terminal H10 helix of FtsZ. It is believed that membrane-bound MinD can activate MinC by recruiting it to the membrane, where FtsZ is tethered, and subsequently enhance MinC-FtsZ interaction¹²².

1.11 MinE

MinE is a soluble, small ~10-kDa protein that spontaneously dimerizes in solution¹²⁶. Its protein structure shows a membrane targeting sequence (MTS), an α helix and three β 1 strands¹²⁷. Upon interaction with membrane bound MinD, MinE changes its basic structure. In the model of Park and colleagues¹²⁸ (Figure 1.6), the two MTSs and their adjacent β 1 strands are first released from the main MinE structure. Next, one of the MTSs tethers to the membrane while at the same time, the other released β 1 strand forms together with flanking residues an α helix that binds MinD. In this configuration, MinE triggers MinD's ATPase activity, which in turn results in the disassembly of the MinD dimer and its release from the membrane. MinE can stay membrane-bound and target other MinD dimers, or it dissociates from the membrane and changes back to its original structure.

1.12 Molecular dynamics of the Min oscillations

While the molecular mechanism of Min oscillations is not yet fully understood, some of the general interactions between the Min system proteins have been elucidated.

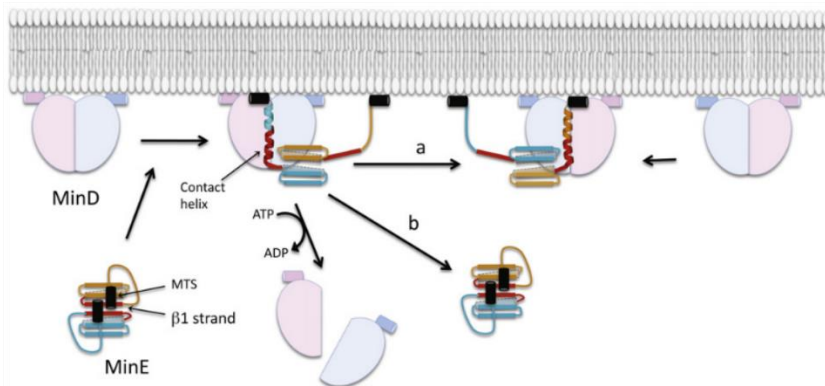


Figure 1.6 MinD-mediated structural change of MinE proposed by Park and colleagues

In this model, MinE, formed by a dimer containing in total 6-stranded β -sheets and two MTSs, interacts with MinD on the membrane. This interaction triggers a conformational change on MinE, upon which the β 1 strands (red) and MTSs (black) are released from the protein structure. Then, one of the MTSs interacts with the membrane, while the other forms a α -helix that is stabilized by contact with MinD. After MinD's ATPase stimulation and release from the membrane, MinE can associate with another MinD, or transform back to its original configuration and dissociate into the solution. Image taken from reference¹²⁸.

In the current model, cytosolic MinD binds ATP (MinD·ATP) which triggers dimerization¹²⁴. This recruits MinD·ATP to the inner cell membrane¹¹². MinD·ATP recruits then MinC dimers. Next, MinE dimers recognize MinD·ATP on the membrane and bind them. This results in the displacement of MinC from the MinCD complex back to the cytoplasm¹²⁸. At this stage, MinE, in its MinD bound configuration, stimulates MinD's ATPase activity, and after ATP hydrolysis, MinD·ADP is released to the cytosol¹²⁹. Bound MinE can then diffuse back to the cytoplasm and change back to its original configuration, or stay temporarily on the membrane¹²⁸. In the latter case, MinE is still able to keep releasing membrane-bound MinD·ATP¹³⁰. Inactive MinD·ADP monomers in solution can dimerize again upon exchange of ADP for ATP and re-bind the membrane, typically far from its most recent binding location, where MinE is still

present. This interplay between MinDE proteins gives as a result the oscillation, pole to pole, of the Min system. As mentioned before, MinC travels passively with the oscillation, creating a time-averaged gradient concentration that is maximum at the poles, therefore only allowing the Z-ring to assemble at midcell, where it is minimum.

Several models have been proposed as an explanation for the formation of Min oscillations, but it remains unclear whether Min oscillations behavior arises due to reaction-diffusion principles or through mechanical communication^{131,132}.

1.13 *In vitro* reconstitution of the Min system

In 2008, Loose et al.¹³³ reported the first successful attempt to reconstitute the MinDE oscillations *in vitro*. They used a combination of SLBs and fluorescence microscopy to observe the formation of Min waves, a spatiotemporal pattern consisting in a membrane-bound protein front that followed a consistent movement in a given direction. Waves were organized in parallel fronts and seemed to emanate from rotating spirals (Figure 1.7 A and B). Propagation velocities and wavelengths varied between 0.28-0.8 $\mu\text{m}/\text{second}$ and 55-100 μm , respectively. This was much unexpected because oscillations *in vivo* can never supersede cell length. They observed that increasing concentrations of MinE (at a fixed MinD concentration) promoted a faster wave velocity, and shortened the wavelength. FRAP analysis of the waves revealed that the waves were not formed by a net movement of proteins on the membrane. Their model introducing MinE cooperativity was able to explain the obtained results more accurately than previous ones.

These interesting results were further investigated in 2011 with a similar approach¹³⁰. This time, they followed the three MinCDE proteins. Their approach allowed them to observe and describe a precise profile of the progression of the Min waves on SLBs. They found that, in a typical wave, the concentration of MinD increased faster than MinC and MinE at the front of the wave (Figure 1.7 C). Then, MinD accumulation rate slowed down until reaching a flat peak, followed by a decrease in concentration. In contrast, MinC and MinE concentration increased linearly starting from the front of the wave. Like MinD, MinE and MinC showed a decrease of concentration at the rear of the wave, although this was a more abrupt drop than in the MinC case. By measuring the protein density within the wave, they were able to draw the MinE/MinD ratio profile along the wave. The ratio started increasing smoothly at the front of the wave at a value of around ~ 0.25 and increased smoothly through the middle of the wave up to ~ 0.4 . Then, at the trail edge of the wave, the ratio sharply increased to a peak of ~ 0.9 before collapsing back to values of around ~ 0.5 . This indicated that, while at the beginning of the wave there is 4 times more MinD than MinE, at the end the amount of MinE increases to roughly equimolar levels to MinD. They also observed that the highest MinE/MinD ratio coincided with the peak of higher MinD and MinE detachment. Interestingly, they detected the presence of a bright band of MinE right at the rear of the waves, before collapsing. This was manifested as a sharp, small but clear jump of MinE signal in the intensity profiles. They found that the bright, abrupt MinE peak at the rear of the wave was not generated by MinE cooperativity (this article did not see proof of MinE cooperativity) but by MinE persistent binding, that is, the capacity of MinE to change MinD partner on the membrane. Consistent with this, they showed that MinE was able to diffuse on an immobile MinD carpet (at MinD saturation levels), and that the residency time of MinE along the wave was clearly higher than for MinD, supporting the notion of rapid rebinding.

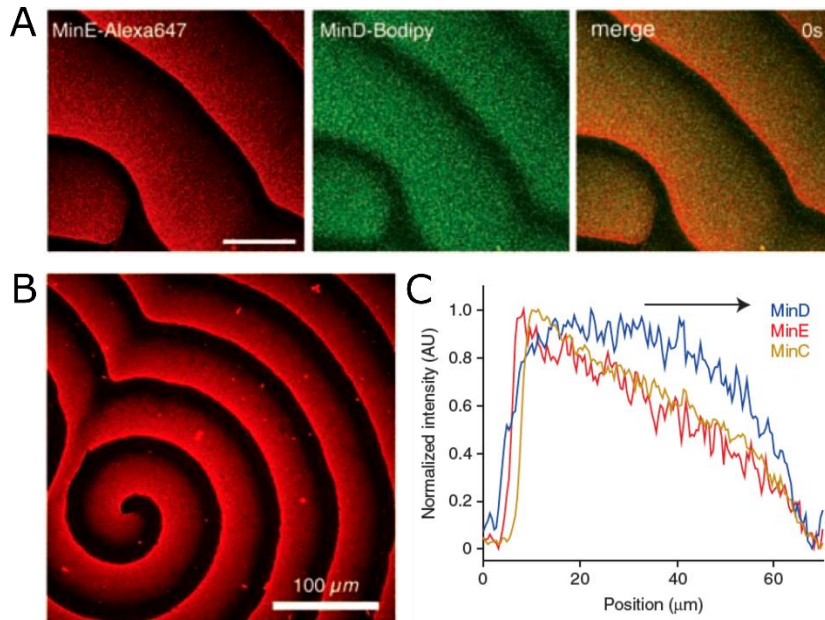


Figure 1.7 Min proteins on planar membranes self-organize in Min waves

A) Typical travelling waves. Scale bar: 50 μm . B) Detail of a vortice. C) Intensity profile of each one of the Min proteins along a travelling wave. Panels A and B are from reference¹³³. Panel C is from reference¹³⁰.

Other researches have studied further the organization of Min waves on planar membranes. For example, Vecchiarelli and colleagues¹³⁴ observed that the flow of the solution, the phospholipid composition of the SLB and the KCl concentration of the buffer influenced wave properties. Min waves were observed to travel in the opposite direction of flow. Phospholipid composition changed the width and the velocity of Min waves: the higher the negative charge density, the narrower the waves and the lower the wave velocity. And finally, increasing KCl promoted wider MinD bands and higher wave velocities. Additionally, Kretschmer et al. showed how different modifications of the MinE MTS influenced the length scales of Min protein patterns¹³⁵.

Since cell shape plays an essential role in Min pattern formation, several studies have focused on reconstitution of Min oscillations in 3D compartments with the aim to elucidate the relationship between compartment geometry and oscillation properties. Zieske and Schwille¹³⁶ successfully reconstituted Min protein oscillations in cell-shaped, open polydimethylsiloxane (PDMS) compartments. Of notice, the length scale of the compartments was approximately ten times the length scale *in vivo*. Membrane bilayers were formed at the bottom and the sides of the compartments. When MinD and MinE were reconstituted on top of the bilayer coating these compartments, *in vivo*-like pole-to-pole oscillations were produced. Elongating the compartments resulted in multiple oscillations next to each other. They also tried cylindrical compartments. In these conditions, three types of patterns were observed: oscillations that underwent a change in the angle of the oscillatory wave front; circular patterns moving around a circle and oscillations along a fixed axis.

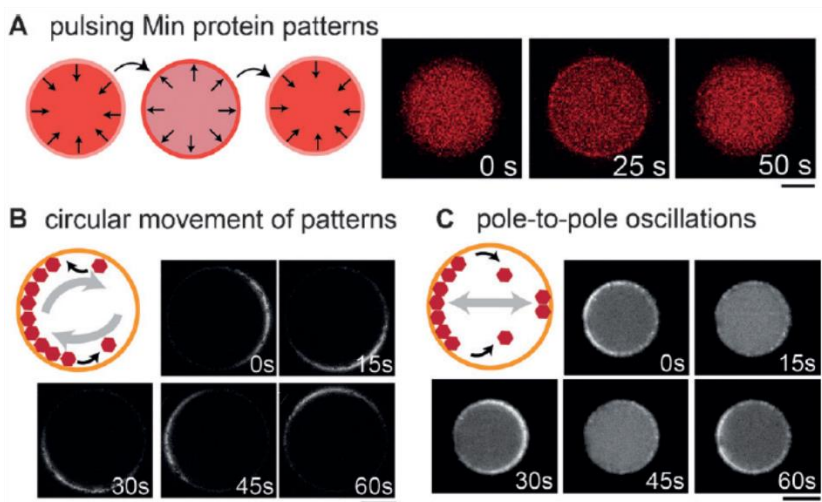


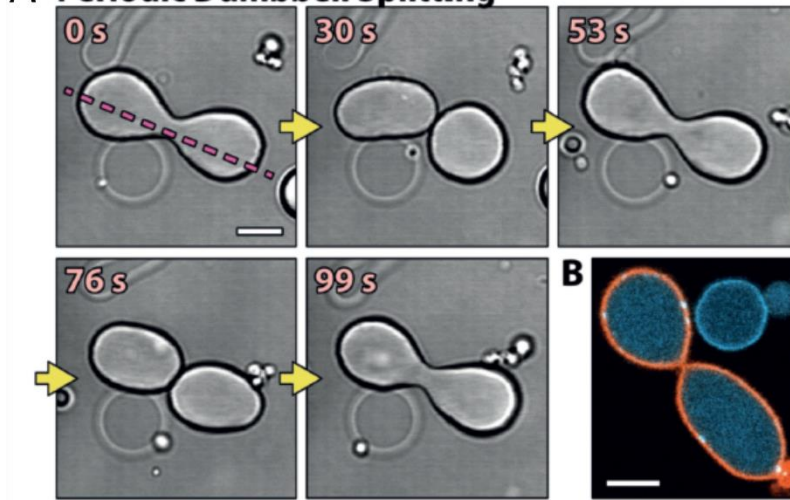
Figure 1.8 Min proteins encapsulated in droplets produce spatiotemporal patterns

A) Min oscillation pattern consisting of periodic association of Min proteins to the membrane, followed by release. B) In this pattern, Min waves travel around the vesicle. This pattern is characterized by a constant proportion of Min proteins both in the membrane and in the lumen. C) Pole-to-pole oscillations of the Min proteins along an axis. Images taken from reference¹³⁷.

Zieske and colleagues followed up with the study of Min oscillations in fully enclosed compartments¹³⁷. Their approach consisted on the encapsulation of MinDE proteins in microdroplets which were interfaced with phospholipid monolayers. The dynamics of the Min proteins could be classified into three groups: pulsing Min protein patterns, circular movement and pole-to-pole oscillations, as shown in Figure 1.8. In microdroplets with Min proteins and FtsZ-MTS, antagonistic protein localization was reconstituted.

In 2018, Litschel et al.¹³⁸ made a set of interesting observations in deflated GUVs with encapsulated MinDE. While under isotonic conditions MinDE oscillatory patterns resembled the one mentioned above for fully enclosed microdroplets (Figure 1.8), under hypertonic stress, deflated vesicles underwent strong shape deformation in coordination with the MinDE oscillations (Figure 1.9). They reported two qualitatively different types of shape transformation. In the periodic dumbbell splitting, the vesicle started with a dumbbell shape with the MinDE proteins bound to the membrane (Figure 1.9 A). Upon release of the Min proteins to the lumen, the dumbbell shape was split into two vesicles connected via a thin neck. Finally, along with the recruitment of MinDE to the membrane (following the typical Min oscillatory patterns described), the vesicle recovered its dumbbell shape again. In the second type of transformation, referred as periodic budding, the vesicles underwent a process of budding and a subsequent fusion with the bud vesicle (Figure 1.9 B). The cycle started with the vesicle in an oblate or flattened state with the Min proteins bound to the membrane. After the Min proteins located to the lumen, the vesicle transitioned to an elongated or prolate configuration. In the

A Periodic Dumbbell Splitting



B Periodic Budding

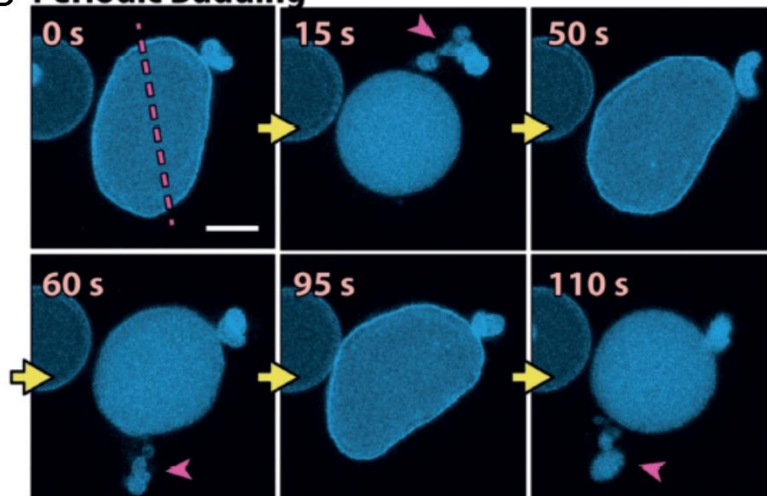


Figure 1.9 Min proteins MinDE inside deflated GUVs produce strong remodelling of the liposome shape

Deflated liposomes with encapsulated Min system undergo dramatic changes on vesicle shape. This change is coordinated with the Min oscillations in the lumen. A) Starting from a dumbbell shape, Min dynamics in the liposome triggered the splitting of the vesicle in two parts joined by a thin neck. The association of Min proteins to the membrane promoted a dumbbell configuration again. Scale bars: 5 μm . B) In the periodic budding pattern, the vesicle underwent a transformation between a flattened and an elongated shape. The cycle starts with the association of the Min proteins to the membrane. Their release following the typical Min pulsing oscillations produced a transition to the elongated form. In this configuration, a budding process was observed. However, the bud vesicles were still connected through a thin neck. Upon budding, the vesicle became spherical, and the bud vesicles were fused again with the mother vesicle. Finally, the liposome changes back to the flatten shape. Scal bar: 5 μm . Modified from reference¹³⁸.

1 - Introduction: constructing a minimal cell

next phase, a small portion of the vesicle membrane split in a manner similar to budding (although still connected to the mother vesicle through a thin neck) and the vesicle became almost spherical. Next, the liposome recovered the buds, became spherical and recruited Min to the membrane again. Finally, the vesicle became oblate to start the cycle again. When Min oscillations were not strong enough, budding was not produced but the vesicle still transitioned back and forth between the oblate and prolate form. Of notice, only pulsing patterns produced extensive shape changes. The authors speculated that the shape transformations might be due to an increase in membrane surface or a decrease on the spontaneous curvature of the vesicle upon interaction of the MinD MTS with the membrane. It is interesting, nonetheless, to observe how a system whose mainly known function in bacteria is to spatially regulate the position of the division septum, might be capable of promote such strong membrane shape deformations, at least *in vitro*.

Technologies

This thesis has extensively used some methodologies and technologies to study and explore the possibilities of the early *E. coli* divisome proteins FtsZ, FtsA, ZipA and ZapA, and of the Min system as a division machinery for artificial cells. The PURE system has been the most predominant technology throughout this thesis (Chapters 2 to 5). Planar membranes were used as platforms for the study of protein organization in open cell-free assays (Chapter 2, 4 and 5). Liposomes (Chapter 3 and 4) were utilized not only as a platform to study protein organization in a more cell-like environment than with SLBs, but were also regarded as one of the essential components of our model minimal cell (Section 1.1, page 11). Finally, TIRF and LSCM were used as fluorescence imaging techniques in SLBs and liposomes, respectively. In the next lines, some of the key concepts regarding these technologies are described.

1.14 PURE system

The protein synthesis using recombinant elements (PURE) system, is a cell-free expression platform developed by Professor Takuya Ueda and coworkers (University of Tokyo)^{139,140}. It contains the required enzymes and co-factors for the *in vitro* transcription and translation of DNA-encoded proteins, tRNA aminoacylation and energy regeneration (36 proteins; Figure 1.10).

The composition and concentration of each component in the PURE system is well-characterized and has the sole purpose of synthesizing DNA-encoded proteins. This is probably the grand advantage of the PURE system and the feature that greatly differentiates it from other cell-free expression platforms like cell-free extracts. Cell-free extracts formulated for *in vitro* expression are usually prepared by bursting open the model cell of choice and isolating the cytoplasmic content from the membrane, large macromolecular particles and other structures like the cell wall¹⁴¹. Cell extracts offer a good protein yield and the production cost is relatively low. However, while some of the cellular components are removed, the resulting extract contains elements that are not directly involved in gene expression. Some elements could be even detrimental to the synthesis of specific proteins, e.g. proteases, or even to influence the activity or function of the synthesized protein. In high contrast, all components in the PURE system are purified from the bacterium *E. coli* with the notable exception of the RNA polymerase (and two other enzymes), which comes from the T7 bacteriophage, and added in known concentrations. Additionally, the T7 polymerase is a single-subunit enzyme with a high promoter specificity that does not require the interaction with transcription factors, therefore efficiently producing mRNA. Since the composition and concentration of the PURE system are known, the system enjoys more reliable and predictable protein synthesis properties than with other platforms of unknown or batch-to-batch changing composition.

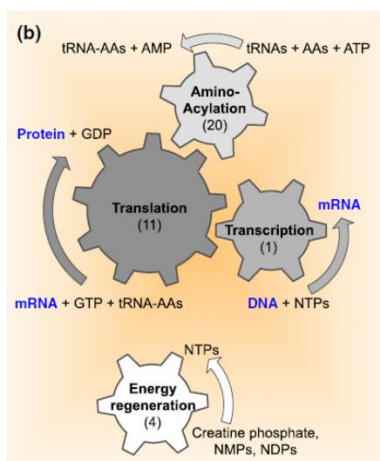


Figure 1.10 Summary of the reactions in the PURE system

The PURE system is a cell-free transcription and translation machinery reconstituted from purified components in a known concentration. All components in the system are directly involved in the synthesis of proteins from DNA, including energy regeneration and aminoacylation. The main reactions taking place in the system are depicted. The number of enzymes per each step of the process is indicated in brackets. From reference¹⁴².

There are two commercially available PURE system: PURExpress® (New England Biolabs) and PUREflex® (GeneFrontier; PUREflex). One of the most remarkable features of PUREflex is that all its proteins are untagged. This means that proteins synthesized in PUREflex can easily be isolated through a Ni-NTA purification column or any other method. Recently, an improved new PUREflex version has been developed (PUREflex®2.0) by modifying the purification of all the components and optimizing the co-factor composition. The improved kit exhibits a higher protein yield and a longer operational life-span¹⁴³.

In our model minimal cell, the PURE system machinery serves as a vertebral metabolic pathway upon which the cell is powered (Figure 1.1, page 12). To this effect, in this thesis, we used both PUREflex and PUREflex 2.0 to cell-free synthesize *E. coli* division proteins in batch mode and inside vesicles.

1.15 Biomimetic membranes

1.15.1 Supported lipid bilayers

Supported lipid bilayers (SLBs) are biomimetic membranes standing on a solid surface like gold, mica or glass^{144,145}. A great variety of SLBs exists, depending on the type of surface and the manner that the phospholipids interact with the surface. For example, while typical SLBs exhibit a thin water layer between the surface and the membrane, polymer-cushioned lipid bilayers sit on a layer of dextran¹⁴⁶, cellulose¹⁴⁷ or other materials. Hybrid bilayers, in the other hand, usually present an alkanethiol monolayer attached to the surface while supporting a lipid monolayer at the solution side¹⁴⁸ (Figure 1.11 A).

Several methods for the formation of SLBs have been developed, such as the Langmuir-Blodgett or Langmuir-Schäfer depositions¹⁴⁹. However, the most straightforward mechanism is the direct spreading of small unilamellar vesicles (SUVs) onto hydrophilic surfaces like glass¹⁵⁰. The production of SUVs can be performed by sonication and centrifugation of large multilamellar

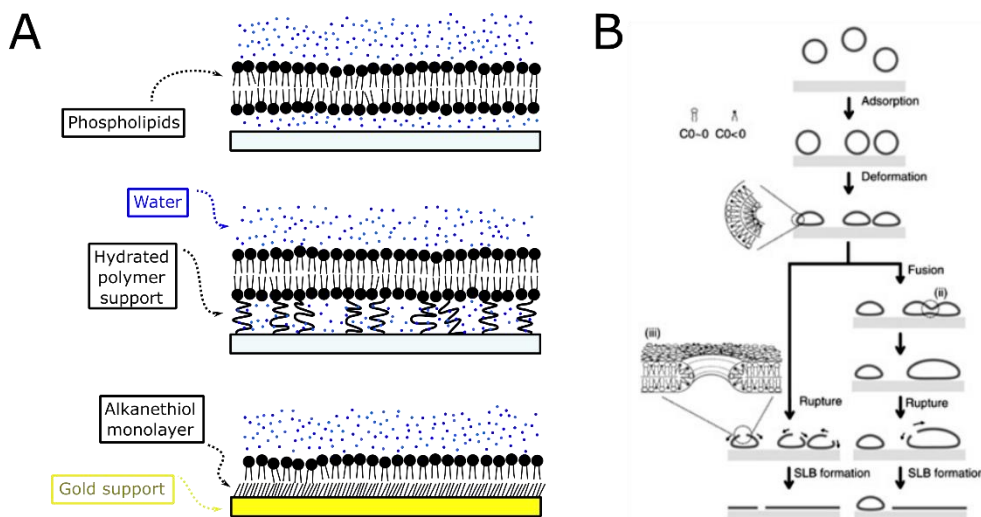


Figure 1.11 Different types of SLBs and dynamics of SUV rupture during SLB formation

A) From top to bottom: supported lipid bilayer, polymer-cushion lipid bilayer and hybrid lipid bilayer. B) Process of rupture of SUVs during SLB formation. First, SUVs adsorb on the support and flatten. Next, SUVs can break and spread on the surface, or fuse with neighboring vesicles, break and spread on the membrane. The edges of the lipid bilayer can promote the rupture and spread of adjacent vesicles. From reference¹⁴⁴.

vesicles (LMVs) or by extrusion of LMVs through a 50-200 nm size porous polycarbonate membrane at high pressure. The SUVs are then exposed to the solid support and allow to burst on the surface. Increased temperature, as well as the addition of divalent cations like Ca^{2+} , have a positive effect on the production of the SLB¹⁵¹. The rupture of the vesicles to form the membrane can occur in different ways. First, the SUVs are adsorbed on the surface and deformed due to the interaction forces. In this situation, they can then burst resulting in patches of lipid bilayers or fuse with neighboring vesicles before rupture and membrane formation (Figure 1.11 B). The edges of the SLB are energetically unfavorable due to exposure of hydrophobic acyl chains to the aqueous solution, promoting rupture of adjacent surface-bound vesicles. Finally, large SLB patches coalesce in order to minimize the exposure to the surrounding buffer, resulting in a complete SLB.

While SLBs stand on a solid support, the interaction with the surface is not direct. A thin water layer of around 10-20 Å is still present between the membrane and the surface. This allows the phospholipids to diffuse freely in the lateral dimension. Despite this thin layer, the SLB is still influenced by the solid support underneath. For example, transmembrane proteins with large cytoplasmic extracellular domains can be denatured upon contact with the solid support. Despite this, SLBs are very popular biomimetic membrane systems due to their numerous advantages. The solid support confers extreme resistance to the membrane, allowing the SLBs to last for weeks or months. In contrast, experiments involving free standing membranes are limited to a few hours. In this line, SLBs are being designed to be air¹⁵² or cooling resistant¹⁵³, features of great interest in their biotechnological applications. SLBs can be produced with a wide range of phospholipid compositions and, since the formation of the membrane is decoupled from the sample preparation, both steps can be optimized separately. Due to the planar nature of SLBs, experiments with this type of biomimetic membranes permit a high control and easy manipulation of the composition of the sample. Finally, an SLB is

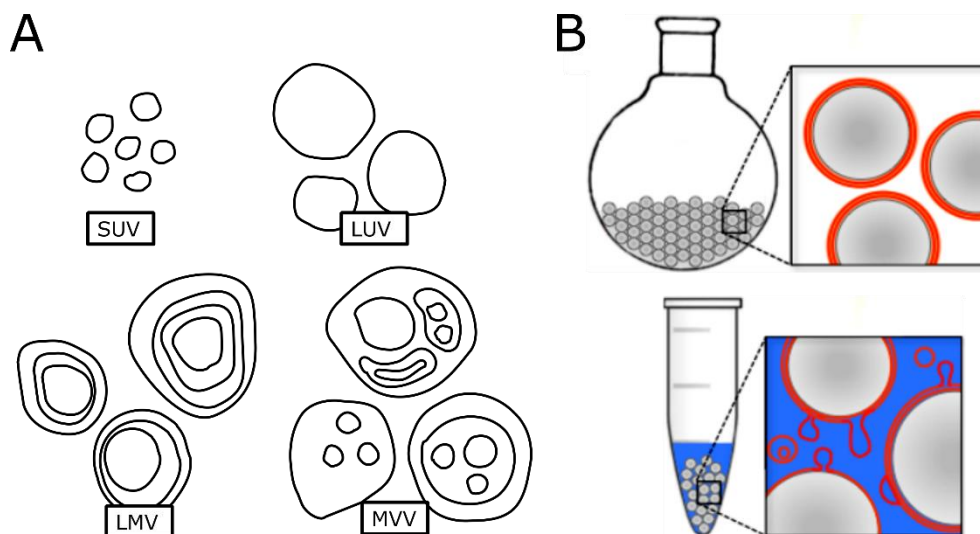


Figure 1.12 Different types of liposomes by size and lamellarity and formation of liposomes with the matrix-assisted swelling method

A) Different types of liposomes categorized by size and lamellarity. SUVs (small unilamellar vesicles), LUVs (large unilamellar vesicles), LMVs (large multilamellar vesicles) and MVVs (multivesicular vesicles). B) Matrix assisted swelling method to produce large and giant liposomes. The method consists of lipid-coated micrometer sized glass beads as a support of the lipid film (Top). The lipid-coated beads are transferred to a test tube and the lipid film is swollen with an aqueous solution (Bottom). This method is compatible with volumes of 20 μL or lower, while generating a high liposome yield. Adapted from reference¹⁵⁴.

highly accessible to surface specific detection techniques, such as atomic force microscopy and evanescence based microscopy like total internal reflection.

In this thesis, we considered the use of SLBs as a suitable membrane platform to study the self-organization and activity of *E. coli* protoring proteins and the MinCDE system. However, the use of SLBs is a choice of convenience before transitioning into the use of a more cell-like biomimetic membrane.

1.15.2 Liposomes

Liposomes are spherical lipidic vesicles containing at least a lipid bilayer. Liposomes can be subdivided by size: small (<200 nm), large (0.2-10 μm) or giant (>10 μm); and by lamellarity or number of lipid layers: unilamellar (one layer), multilamellar (more than one concentric layer) and multivesicular (vesicles in vesicles; Figure 1.12 A). They are generally used as biomimetic models of the cellular membrane and they are extensively used in the drug-delivery industry¹⁵⁵. In the minimal cell field, they are usually regarded as a model of a cell, and frequently used to study in-vesicle cell-free protein synthesis¹⁵⁶.

The production of liposomes is straightforward. Back in the 60's, Bangham and colleagues¹⁵⁷ observed under the electron microscope that dried egg lecithin spontaneously reacted with water to form lipid vesicles. Methods suitable for cell-free expression have been developed. For example, the lipid film swelling method¹⁵⁸ consists in the formation of a dry lipid film and its subsequent hydration with an aqueous solution containing the compounds to be encapsulated. Mechanical film resuspension methods build on this idea by actively promoting the film swelling and releasing of free liposomes from the hydrated film¹⁵⁶. This can be as simple as

vortex of the test tube or by sonication. In the other hand, ethanol injection methods consist in the direct mixing of a solution of phospholipid in ethanol (or methanol) with an aqueous solution containing the translation machinery or any other component intended to be encapsulated in the liposome. Depending on the concentration of the lipid solution, small vesicles (low concentration) or heterogeneous, large multilamellar and clustered vesicles (high concentration) can be formed¹⁵⁹. Other methods involve the use of an oil phase. For example, water in oil-emulsion transfer works by dissolving a lipid solution of the desired composition in an oil phase. This solution is heated in order to evaporate any organic solvent, mixed with an aqueous solution containing the components to be encapsulated and finally shaken to produce an emulsion. Finally, the emulsion is transfer to an aqueous phase containing the external solution, and centrifuged to produce the liposomes^{160,161}.

Although many methods are available for the expression of *de novo* proteins in vesicles, not all of them are equally suitable for the study of protein activity. In particular, methods requiring an oil phase intermediate will most surely contaminate the liposome's membrane. In turn, this can have a significant influence in membrane permeability and perhaps partially denature integral or associated membrane proteins. Moreover, liposome yield can be low depending on the lipid composition of choice, and an osmotic imbalance can be created between the inside and outside of the liposomes¹⁶². In the other hand, swelling methods support a wide range of lipid compositions and do not utilize oil intermediates. However, they suffer in general from a poor liposome yield and micro-liter handling is difficult. An improved porous matrix-assisted swelling method that successfully overcomes these limitations was proposed by Nourian et al.¹⁵⁴ (Figure 1.12 B).

We have used liposomes in this thesis in order to study the activity of cell-free synthesized *E. coli* FtsZ and ZapA and the chimeric protein FtsZ-MTS both outside and inside liposomes.

1.16 Microscopy techniques

1.16.1 TIRF

Total internal reflection fluorescence microscopy (TIRFM) takes advantage of an electromagnetic phenomenon known as *evanescent wave*¹⁶³, which consists on a standing wave whose intensity decreases exponentially. This wave is formed when the incident angle of the excitation light beam illuminating a sample is greater than a certain critical angle, resulting in the reflection of the excitation beam. In conventional epifluorescence, refraction of the beam occurs during transition from the coverslip to the sample, due to the difference in refractive indices of the two media. The critical angle θ_c is given by the Snell's law:

$$\theta_c = \sin^{-1} \left(\frac{n_1}{n_2} \right)$$

1

where n_1 and n_2 are the refractive index of the sample and the coverslip, respectively. If the angle of incidence is greater than the critical angle, reflection instead of refraction occurs at the coverslip-sample interface. This is only possible if $n_1 > n_2$. When this happens, some energy is able to penetrate through the interface and create a standing evanescent wave (Figure 1.13). Due to the rapid decay of the intensity of the wave, only molecules very close to the refraction plane (< 100 nm) will be illuminated. This feature allows TIRFM to achieve a high signal-to-noise ratio in areas close to the refraction plane, while permitting the real-time monitoring of the sample thanks to its wide-field nature.

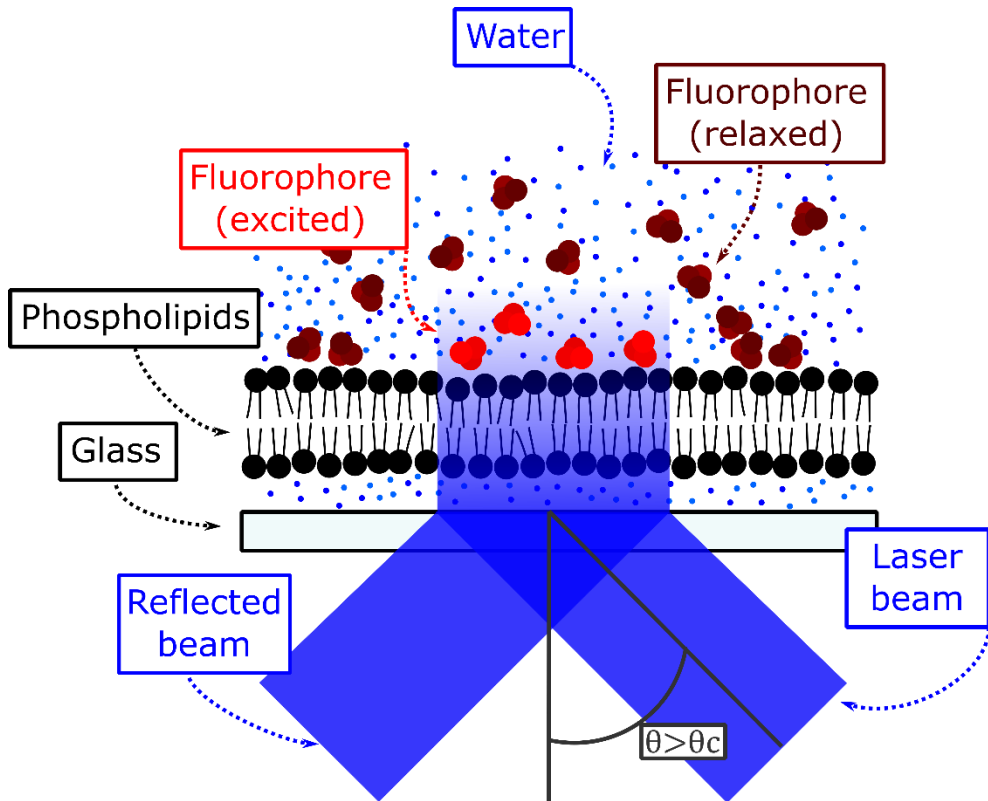


Figure 1.13 TIRFM principle

TIRFM takes advantage of the formation of an evanescent wave when the angle of incidence of the excitation beam is greater than the critical angle. The evanescent wave intensity decreases exponentially as a function of the distance to the reflexion plane, therefore illuminating only a small area on top of the glass surface.

1.16.2 Laser scanning confocal microscope

Laser scanning confocal microscopy (LSCM) is a fluorescence imaging technique that increases the optical resolution and contrast of a sample through the use of a spatial filter to block out-of-focus light. This filter, known as pinhole, can control the focal plane of the laser light, therefore allowing to excite a reduced area or point of the specimen, in contrast to typical wide-field fluorescence microscopy. This overcomes some of the limitations of conventional fluorescence microscopes like the background noise that originates from excited molecules in the vicinity of the focal plane. Moreover, it allows the optical sectioning of specimens for 3D reconstruction. However, the acquisition of the image is slow because the laser must realize a scanning motion to reconstruct the image.

Chapter 2

Synthesized FtsZ and other key division proteins on SLBs

The construction of a minimal cell from the bottom-up, stands head and shoulders above the most exciting challenges of today's biology. In particular, the implementation of a division mechanism in a minimal cell is of great interest, as this is an essential attribute of life. A promising approach consists in using key bacterial division proteins. In this chapter, we explored the potential of cell-free synthesized *E. coli* division proteins FtsZ, FtsA, ZipA and ZapA to reconstitute basic cytoskeletal properties. We utilized the PURE system as a minimal transcription-translation machinery for the synthesis of proteins in vitro. Protein activity was assayed on planar membranes and found that Ficoll70, a general macromolecular crowder, was required to allow the formation of filament networks with the purified proteins FtsZ and ZipA. Moreover, the cell-free synthesized FtsZ, FtsA and ZipA showed capable of self-organizing on the membrane, while cell-free synthesized ZapA, an FtsZ crosslinker, was able to compensate the absence of Ficoll70 when mixed both with purified or cell-free synthesized FtsZ. This confirmed that cell-free synthesis of active *E. coli* proteins is possible. Taken together, we believe that our results open the door for the use of synthesized division proteins in the implementation of an artificial divisome in minimal cells.

2.1 Introduction

Of all division proteins in *E. coli*, FtsZ is regarded as the most important. It arrives first at midcell, marking the future site of division, and it is responsible for the recruitment and assembly of the divisome¹⁶⁴. The cytoplasmic molecular activity of FtsZ includes self-interaction of monomers upon GTP binding, forming polymers known as protofilaments^{39,43,44}, and a Mg²⁺-dependent GTPase activity^{38,45}. After hydrolysis of the nucleotide, the self-interaction between two adjacent monomers becomes unstable, promoting the disassembly of the protofilament^{46,47}. Protofilaments can further self-interact through lateral interactions to form longer and thicker structures known as filaments or bundles^{35,43,48,49}. In the cell, the activity of FtsZ results into the assembly at midcell of a ring-like cytoskeleton structure known as the Z-ring⁵⁰. Two other early and essential division proteins, FtsA and ZipA arrive at the Z-ring right after or together with FtsZ²⁴. Both FtsA and ZipA contain a membrane targeting sequence (MTS) and an FtsZ interacting region, therefore effectively anchoring the Z-ring on the cytoplasmic membrane^{24,61}. The FtsA MTS consists in an amphipathic helix at the C-term of the protein (amino acids 405 to 420)⁷⁰. Interestingly, it has been shown that FtsA promotes the destabilization of FtsZ filaments¹⁰⁵. In addition, FtsA self-interacts and assembles into short polymers^{67,165-167}, an activity that is related with the downstream recruitment of other late division proteins and the maturation of the divisome¹⁶⁸. In the other hand, the MTS from ZipA consists of a transmembrane domain at the N-term of the protein (amino acids 1 to 22)¹⁶⁹. The assembly at midcell of FtsZ, FtsA and ZipA is known as the protoring⁶¹. Unlike FtsA, ZipA does not polymerize, although it seems to promote the bundling of FtsZ protofilaments¹⁶⁹. While not essential, other proteins can regulate the physiological activity of the Z-ring in the cell. For example, ZapA is an important cross-linker of FtsZ protofilaments and stabilizer of the Z-ring⁸².

In 2014, M. Loose and T. J. Mitchison⁵⁹ tested, *in vitro*, the organization of fluorescently labelled FtsZ, FtsA and ZipA on supported lipid bilayers (SLBs). When FtsZ and ZipA were mixed, they observed self-assembly of slightly curved, static filament networks on top of the membrane. The morphology and dynamics of this assembly contrasted with the ones obtained with FtsZ and FtsA in this same study: dynamic protein rings of around 1 μm of diameter self-organized on top of the membrane. Additionally, these rings underwent treadmilling dynamics on the membrane.

In this chapter, we have tested and visualized the self-organization of the cell-free synthesized protoring proteins (i.e. FtsZ, FtsA and ZipA) plus the FtsZ crosslinker ZapA on top of an SLB. This is an important step towards the utilization of key *E. coli* division proteins for the *in vitro* reconstitution of a minimal divisome in liposomes (Chapter 3). Purified proteins FtsZ and the globular domain of ZipA fused at the N-term with a 6-histidine tag (sZipA) have also been used to establish initial working conditions when combined with individual synthesized proteins. The *in vitro* transcription and translation machinery (IVTT) utilized has been the PURE system, a set of reconstituted proteins and ribosomes for the cell-free production of proteins¹³⁹. Such approach offers advantages with respect to traditional *in vitro* assays with purified proteins, e. g. the possibility of producing non-tagged protein versions, *in situ* production of proteins, high control over the presence of contaminants, a more physiological environment for protein testing than oversimplified buffers, etc.

Following this approach, we found that cell-free synthesized *E. coli* FtsZ, FtsA, ZipA and sZipA sustained the formation of cytoskeletal structures on SLBs. Interestingly, we found that the use of Ficoll70, a general macromolecular crowder, was needed in order to promote the formation of protein bundles in the conditions tested. Nonetheless, the use of Ficoll70 could be bypassed

by synthesized ZapA. Taken together, our results showed that synthesized divisome proteins maintain important wild-type functionality on SLBs.

2.2 Materials and Methods

2.2.1 Purified proteins and DNA templates for cell-free expression in PURE_{flex}

E. coli purified proteins FtsZ and the cytoplasmic domain of ZipA fused to a 6-histidine tag at its N-term (sZipA), were kindly provided by Germán Rivas laboratory at Centro de Investigaciones Biológicas (CSIC, Madrid). Purification and labelling of FtsZ¹⁷⁰ and sZipA⁷⁷ was done as previously described. While FtsZ was fluorescently labelled with Alexa Fluor 647 (FtsZ-647), sZipA was labelled with Alexa Fluor 488 (sZipA-488). FtsZ-647 was stored in a buffer containing 50 mM Tris-HCl at pH 7.4, 500 mM KCl, 5 mM MgCl₂ and 5% (v/v) glycerol. sZipA-488 was stored in a buffer containing 20 mM Tris pH 7.5, 50 mM KCl, 1 mM EDTA and 10% of glycerol. Both FtsZ-647 and sZipA-488 were stored in 5 μ L aliquots at -80 °C.

Table 2.1 Standard PCR program

Repetitions	Temperature (°C)	Time (seconds)
1x	98	30
	98	10
35x	55	15
	72	25
1x	72	5 minutes

Preparation of *ftsZ* and *ftsA* DNA templates for expression in PURE_{flex} was done as follows. First, gene fragments were PCR amplified (standard program; Table 2.1) from chromosomal *E. coli* BL21 DNA with the primers ChD 509 and ChD 374 (*ftsZ*) and ChD 508 and ChD 376 (*ftsA*). The list of primers and their sequence can be seen in Table 2.2. These primers contained overhangs for the pET11-a plasmid. Next, the PCR products were digested with DpnI (New England BioLabs® Inc.) and ligated into a linearized pET11-a plasmid (equimolar concentrations) via Gibson Assembly (Gibson Assembly® Master Mix of New England BioLabs® Inc) for 1 hour at 50 °C. Next, the assembled products were transformed into *E. coli* TOP10 competent cells via heat shock, after which the cells were centrifuged and resuspended in 50 μ L of fresh liquid LB media and incubated at 250 rpm for 1 hour at 37 °C. Next, cultures were plated in solid LB medium with 0.05 ng/ μ L ampicillin and grew overnight at 37 °C. A few selected colonies that grew on the plates were cultured in 1 mL of liquid LB medium with 0.05 μ g/ μ L of ampicillin at 250 rpm for 6 hours at 37 C. Plasmid purification (PureYield™ Plasmid Miniprep System, column method, Promega) was carried out and production of linear DNA constructs from the above purified plasmids was done with the primers ChD 194 and ChD 181 in a standard PCR amplification reaction program (Table 2.1). The PCR products were analyzed on a standard DNA agarose gel (1%; Et. Br. or SYBR safe) to check for inserts. Positive colonies were grown overnight at 37 °C and 250 rpm in fresh LB medium with 0.05 ng/ μ L of ampicillin, and stored at -80 °C in 10% glycerol (v/v).

zipA DNA template (*E. coli* K12) was ordered directly from Integrated DNA Technologies® as a linear DNA fragment with overhangs for pET11-a. The construct contained all the required elements to be expressed in a PURE_{flex} reaction (i.e. *t7* promoter, RBS, the gene sequence, stop codon and *t7* terminator). *zipA* construct was inserted into a linearized pET11-a via Gibson Assembly (equimolar concentrations; 1 hour at 50 °C). Plasmid transformation into *E. coli* TOP10 competent cells, its purification and storage at -80 °C was done as described for *ftsZ*.

Table 2.2 List of primers and sequence

Name	Sequence (5' to 3')
ChD 73	GCGAAATTAATACGACTCACTATAGGGAGACC
ChD 181	CAAAAAACCCCTCAAGACCCGTTTAGAGG
ChD 194	TAATACGACTCACTATAGGGGAATTGTGAGCGGATAACAATTCCCCT
ChD 374	TCCTTCGGGCTTTGTTAGCAGCCGGATCCTTAATCAGCTTGCTTACGCAG
ChD 376	CITTCGGGCTTTGTTAGCAGCCGGATCCTTAAAACCTTTTTCGCAGCCAAC
ChD 508	TTTGTTTAACTTTAAGAAGGAGATATACATATGATCAAGGCGACGGACAG
ChD 509	TAACTTTAAGAAGGAGATATACATATGTTTGAACCAATGGAACCTTACC
ChD 5024	ACTTTAAGAAGGAGATATACATATGCATCACCATCATCACCATCATGGTTTCTGGACCAG CCGTAAAG

Production of *szipA*, this is, *zipA* without the nucleotides coding for the transmembrane domain of ZipA plus the bases coding for a 6-histidine tag fused at the N-terminal part of the protein (6His- Δ 22-ZipA), was done starting from a purified *pET11-a-zipA*. First, the *zipA* containing plasmid was amplified with primers ChD 524 (contains the 6-*his*) and ChD 507 (Table 2.2) in order to obtain a DNA fragment coding for 6His- Δ 22-ZipA. Additionally, the primers contained overhangs for pET11-a. Next, the *szipA* fragment was inserted into a linearized pET11-a via Gibson Assembly. Purification of *pET11-a-szipA*, production of linearized DNA template and storage of cell-cultures at -80 °C was done as described for *ftsZ*.

zapA DNA template (*E. coli* K12) was ordered directly from Integrated DNA Technologies®. The construct came inserted in a pIDTSMART-AMP plasmid and contained all the elements required to be expressed in PURE_{flex} (i.e. *t7* promoter, RBS, the gene sequence, stop codon and *t7* terminator). Transformation of this plasmid into *E. coli* TOP10 competent cells, its purification and the production of the linear construct was done as described for *ftsZ*. *p3-phi29* construct was used to perform negative controls and was produced as described by van Nies et al.²¹. Amplification of the linear construct was performed by PCR with primers ChD 73 and ChD 374 (Table 2.2) following a standard PCR program (Table 2.1).

2.2.2 Reaction chambers

To perform activity assays, two types of reaction chambers were fabricated. Silicone disposable chambers were prepared before each experiment and discarded afterwards in the following way. First, a 1 mm thick, squared piece of silicone sheet (Silicone Isolators™ Sheet Material with double side SecureSeal™ adhesive) of ~1x1 cm was cut. Next, a hole of ~3 mm in diameter was carved in the piece with a puncher and placed on top of a pre-cleaned coverslip. This assembly creates a reaction cavity with a glass bottom and silicone walls. Once the sample

2 - Synthesized FtsZ and other key division proteins on SLBs

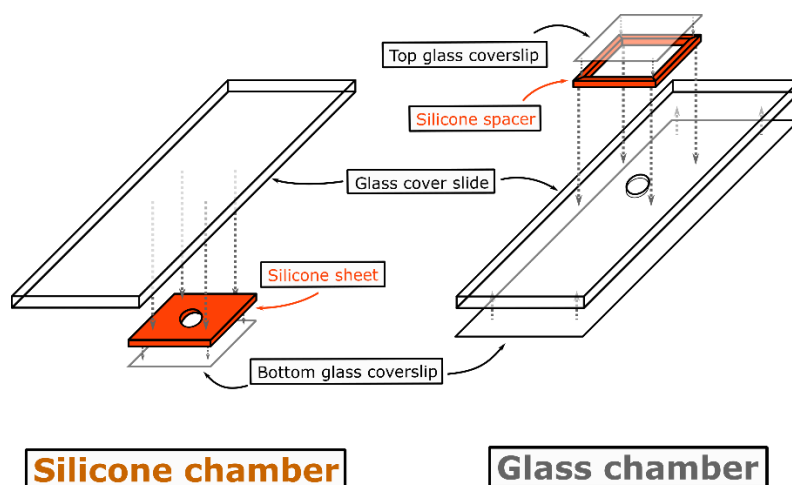


Figure 2.1 Reaction chambers

Two different types of reaction chambers were manufactured. Each step of the process is illustrated. Dashed arrows indicate how each piece of the chamber was assembled. Silicone chambers (*Left*) were produced before each experiment and discarded afterwards. Glass chambers were reusable, except the top glass coverslip which was discarded after each experiment.

was pipetted in the reaction cavity, the chamber was closed by fixing a cover slide on top of the chamber (Figure 2.1). Pre-cleaned glass coverslips were prepared by bath sonication (Sonorex digitec, Bandelin) for ~10 minutes in a 2% (v/v) Helmanex III solution, followed by ~10 minutes in Milli-Q water. Next, the coverslips were rinsed with abundant Milli-Q water and 100% ethanol and stored in 100% ethanol. Right before use, coverslips were rinsed again with abundant Milli-Q water and ethanol 100%, dried with a gentle flow of nitrogen gas, and treated with oxygen plasma for at least 10 minutes (Basic Plasma Cleaner, Harrick Plasma).

Reusable glass chambers were manufactured to improve the tendency of silicone chambers to leakage. Additionally, they were more economical due to the possibility of reusability. We proceeded by sand blasting one or more holes of ~3 mm in diameter in a 76x26x1 mm glass cover slide. Then, a 76x26x0.15 mm pre-cleaned coverslip was glued to one side of the sand blasted cover slide with UV glue NOA81 (Norland products). To cure the glue, the glass assembly was exposed 5 minutes to UV light (365 nm wavelength with 36 W of power; Promed UVL-36 with four UV-9W-L bulbs). Finally, the chamber was kept at 50 °C during at least 3 days. This assembly creates a chamber with glass bottom and walls that can be reused for a few tens of experiments. To close the chamber, a squared frame spacer made out of silicone sheet was stick around the reaction cavity. Then, a clean glass coverslip was fixed on top of the spacer thanks to the SecureSeal™ adhesive (Figure 2.1). Preparation of pre-cleaned glass coverslips was done as described for silicone chambers.

Cleaning of reusable glass chambers was done with a sequence of bath sonication in diverse solvents and solutions. First, the chambers were rinsed with abundant Milli-Q water and 100% ethanol, followed by Milli-Q water again. Then, they were sequentially sonicated during ~10 minutes in a solution of 50% chloroform in methanol (v/v), followed by a 1 M KOH solution, then in 100% ethanol, followed by a 2% Helmanex III solution and finally in Milli-Q water. Between each bath, the chambers were rinsed with the solution they were going to be sonicated next. Finally, the chambers were rinsed once more with abundant Milli-Q water before storing them in 100% ethanol. Silicone frame spacers were cleaned as well with abundant Milli-Q

water and 100% ethanol before storing them for later use. Top glass coverslips were discarded after each experiment.

2.2.3 Phospholipids and lipid compositions

Phospholipids used in this chapter were purchased from Avanti® Polar Lipids Inc. and all were dissolved in chloroform (Table 2.3). Phospholipids were typically aliquoted in glass vials and wrapped with Parafilm M (Bemis©) before storing at -20 °C. In order to produce small unilamellar vesicles (SUV; Section 2.2.4) two different compositions were used (Table 2.4).

Table 2.3 Phospholipids

Name and abbreviation of the phospholipids employed in this chapter.

Abbreviation	Name
DOPC	1,2-dioleoyl-sn-glycero-3-phosphocholine
DOPG	1,2-dioleoyl-sn-glycero-3-phospho-(1'-rac-glycerol)
DGS-NTA	1,2-dioleoyl-sn-glycero-3-[(N-(5-amino-1-carboxypentyl)iminodiacetic acid)succinyl] (nickel salt)

Table 2.4 Phospholipid compositions

The abbreviation and concentration (mol %) at which each phospholipid was mixed for each different composition. These compositions were used to produce supported lipid bilayers.

Composition	DOPC	DOPG	DGS-NTA
1	76.2	19.0	4.8
2	80.0	20.0	--

2.2.4 Production of SUVs by extrusion

In order to produce a solution containing small unilamellar vesicles (SUVs), phospholipids were mixed in a glass vial up to a total lipid mass of 500 µg. The lipidic composition differed for each experiment and it is specified in the relevant sections. Then, the lipid mixture was dried under a gentle flow of argon followed by ~20 minutes in a desiccator. The films were rehydrated with 400 µL of SLB buffer (50 mM Tris-HCl, pH 7.5, 300 mM KCl, 5 mM MgCl₂) to a phospholipid concentration of 1.25 µg/µl. The vials were vortexed to produce a solution containing large multilamellar vesicles (LMVs) for at least 1 minute or until the lipid film is totally removed and dispersed in the buffer. Next, the LMV solution was extruded (Avanti Polar Lipids, Inc.) through a 0.1 µm pore polycarbonate membrane (Nuclepore track-etched membrane, Whatman) 10-20 times. The resultant SUV solution is stored in 5 µL aliquots at -20 °C.

2.2.5 Production of SLBs

The protocol to produce SLBs differed depending whether a silicone chamber or a glass chamber was utilized (Section 2.2.2). In the case of silicone chambers, a pre-cleaned glass coverslip was first abundantly rinsed with 100% ethanol and dried under a gentle flow of nitrogen gas. Then, the glass coverslip was treated with oxygen plasma for at least 10 minutes. Immediately after, a squared silicone sheet piece of ~1x1 cm with a 3 mm diameter hole was

2 – Synthesized FtsZ and other key division proteins on SLBs

gently pressed with clean tweezers against the glass coverslip to ensure that both layers were properly fixed. Right after, 5 μL of 0.9 $\mu\text{g}/\mu\text{L}$ phospholipid SUV solution was pipetted inside the chamber, followed by 5 μL of 6 mM CaCl_2 . The chamber was placed next to a wet tissue inside a petri dish to avoid drying and incubated at 37 $^\circ\text{C}$ for \sim 10 minutes to produce an SLB. Finally, the membrane was washed three times with SLB buffer before use.

Glass chambers were first rinsed with 100% ethanol, dried with a flow of nitrogen and treated with oxygen plasma for at least 10 minutes. Next, 5 μL of 0.9 $\mu\text{g}/\mu\text{L}$ phospholipid SUV solution was injected into the chamber followed by 5 μL of 6 mM CaCl_2 . Finally, the chamber was incubated \sim 30 minutes at 37 $^\circ\text{C}$. Before use, the membrane was washed three times with SLB buffer.

2.2.6 Cell-free protein synthesis in bulk with PURE $_{\text{frex}}$

Cell-free synthesis of proteins in bulk was realized with PURE $_{\text{frex}}$ (GeneFrontier Corporation, Chiba, Japan). Unless otherwise specified in the relevant sections, the preparation of a PURE $_{\text{frex}}$ reaction was as follows. First, 10 μL of PURE $_{\text{frex}}$ Solution I, 1 μL of Solution II and 1 μL of Solution III was pipetted in a new, clean PCR tube. Optionally, the reaction was supplemented with 1 U/ μL of SUPERase In $^{\text{TM}}$ RNase Inhibitor (Invitrogen $^{\text{TM}}$). Next, the DNA template (single expression) or templates (co-expression) were diluted to a typical DNA concentration of 5-15 nM. Finally, Milli-Q water was added up to a total volume of 20 μL . During the preparation of the reaction solution, both the reactants and solution were kept on ice to prevent gene expression from starting. Next, the PURE $_{\text{frex}}$ reaction was incubated at 37 $^\circ\text{C}$ for 3 hours in a thermocycler (Bio-Rad C1000 Touch).

2.2.7 SDS-PAGE analysis of synthesized proteins

The analysis on SDS-PAGE of synthesized proteins was done as follows. Cell-free bulk expression of DNA templates was realized with a standard reaction of PURE $_{\text{frex}}$ (Table 2.5) with the exception of the addition of 0.5 μL of BODIPY-Lys-tRNA $_{\text{Lys}}$ (FluoroTect $^{\text{TM}}$ GreenLys, Promega) to the solution. After incubation at 37 $^\circ\text{C}$ for 3 hours, the translation products were mixed with 2x SDS Laemmli sample buffer and heated at 65 $^\circ\text{C}$ for 3 minutes. Next, the protein ladder (Spectra Multicolor Broad Range Protein Ladder; Thermo Fischer Scientific) and samples were placed on ice before being loaded and run in a 12% SDS polyacrylamide gel electrophoresis (PAGE) gel. Table 2.6 shows the volumes of the components for the production of the resolving and stacking gel for a 12% SDS-PAGE. Visualization of the *de novo* synthesized proteins was carried out by illuminating the SDS-PAGE with a 488 nm wavelength laser in a fluorescence gel imager (Typhoon, Amersham Biosciences).

Table 2.5 Typical PURE^{flex} reaction

Name of the reactant, volume (in μL) and final concentration of each one of the elements typically used to prepare a PURE^{flex} reaction. The DNA template 2, marked with an asterisk (*), is only added when a co-expression is carried out.

Reactant	Volume (μL)	Concentration
Solution I	10	x1
Solution II	1	x1
Solution III	1	x1
SUPERase In	1	1 U/ μL
DNA template 1	x	5-15 nM
DNA template 2 (*)	y	5-15 nM
Milli-Q water	20-13-x-y	
Total	20	

Table 2.6 Volumes of components of the resolving gel and stacking gel for a standard 12% SDS-PAGE gel preparation.

SDS: sodium dodecyl sulfate. AA: acrylamide. BAA: bis-acrylamide. APS: ammonium persulfate. TEMED: tetramethylethylenediamine

Component	Resolving gel 4% (mL)	Stacking gel 12% (mL)
Milli-Q	3.15	1.6
1.5 M Tris-HCl pH 8.8	1.875	-
0.5 M Tris-HCl pH 6.8	-	0.625
20% SDS w/v	0.0375	0.0125
AA/BAA 37.5%/0.8%	2.4	0.265
10% APS	0.0375	0.0125
TEMED	0.005	0.0025

2.2.8 Activity assays with purified proteins

Activity assays with purified proteins were done in silicone chambers as described below. First, the SLB was incubated for ~ 10 minutes at room temperature with $10 \mu\text{L}$ of $1 \mu\text{M}$ of sZipA-488 diluted in SLB buffer. After this, the membrane was washed 3 times with SLB buffer. An FtsZ-647 protein solution was next prepared in an Eppendorf tube, typically to a total volume of $20 \mu\text{L}$. Added volumes of each component varied depending on the final volume of the mixture.

For assays carried out in reaction buffer (50 mM Tris-HCl, pH 7.6, 150 mM KCl, 5 mM MgCl_2), $2 \mu\text{L}$ of a 10x reaction buffer was added, followed by an appropriate volume of Milli-Q water. Then, the purified protein FtsZ-647 was added to the desired concentration, followed by GTP to a final concentration of 3.33 mM. Optionally, a solution containing 125 g/L of Ficoll70 was added. The final concentration is specified in the relevant sections. The volume

2 – Synthesized FtsZ and other key division proteins on SLBs

of deionized water depended on the volume of purified protein or Ficoll70 solution. For assays carried out in PURE $_{\text{frex}}^{108}$, 10 μL of PURE $_{\text{frex}}$ Solution I, 1 μL of PURE $_{\text{frex}}$ Solution II and 1 μL of PURE $_{\text{frex}}$ Solution III and a volume of Milli-Q water were mixed. Then, FtsZ-647 was added to the desired final concentration, followed by GTP to a final concentration of 3.33 mM. Optionally, a solution containing 125 g/L of Ficoll70 was added to the desired final concentration. The volume of deionized water depended on the volume of purified protein or Ficoll70 solution.

Next, the assembled silicone chamber was emptied from SLB buffer and, unless otherwise specified, 5 μL of the protein mixture was immediately injected. Prior microscopy visualization at room temperature, the chamber was sealed following the methods described in Section 2.2.2 for silicone chambers.

2.2.9 Activity assays with synthesized proteins

Activity assays with synthesized proteins involved first the preparation of a standard PURE $_{\text{frex}}$ reaction (Section 2.2.6) with either *ftsZ*, *zapA* or both (co-expression). After incubation of the PURE $_{\text{frex}}$ mixture for 3 hours at 37 °C, the translation products were placed on ice to stop the reaction. Next, the protein mixture was prepared by mixing 3.5-9 μL of the translation products with 2.5-3.33 mM of GTP and Milli-Q to a final volume of 5-10 μL . Optionally, FtsZ-647 (to the desired final concentration) and Ficoll70 (usually 5%), was mixed with the translation products. Then, the mixture was injected in a silicone or glass chamber (Section 2.2.2), and proteins were visualized under the microscope at room temperature or 37 °C.

In the case of activity assays with *in situ* synthesized proteins, the PURE $_{\text{frex}}$ reaction was prepared as described above. However, the PURE $_{\text{frex}}$ mixture was immediately injected in a glass chamber with preformed SLB. Next, the chamber was typically incubated at 37 °C for 3 hours in a thermocycler. The translation products were finally extracted from the chamber to produce the corresponding protein mix as described for activity assays with synthesized proteins.

2.2.10 Microscopy and image analysis

Images were acquired with an Olympus IX81 Inverted TIRF microscope equipped with a 150x UApoNTIRF oil objective (NA 1.45). Excitation laser lines of 640 nm (FtsZ-647) and 488 nm (sZipA-488) were utilized to visualize the purified proteins. Images were captured with an EM-CCD camera (iXion X3 DU897, Andor technologies). Olympus cell^TTIRF illuminator and Andor IQ3 were used as control and acquisition software. Experiments were carried out at room temperature or at 37 °C.

Analysis of the acquired images was done with ImageJ¹⁷¹. In general, images were adjusted for brightness and contrast. Optionally, a background subtraction was carried out with a roll balling radius of 50-250 pixels, depending on the image, and if specified in the relevant sections, average images (AVG) were produced by taking the average pixel intensity of a sequence of pictures of the same region of the sample.

2.3 Results

2.3.1 Purified proteins FtsZ-647 and sZipA488 self-assemble on SLBs when supplemented with Ficoll70

In order to establish the working conditions for activity assays with cell-free synthesized proteins, we first sought to reproduce, with purified proteins, some of the reconstitution

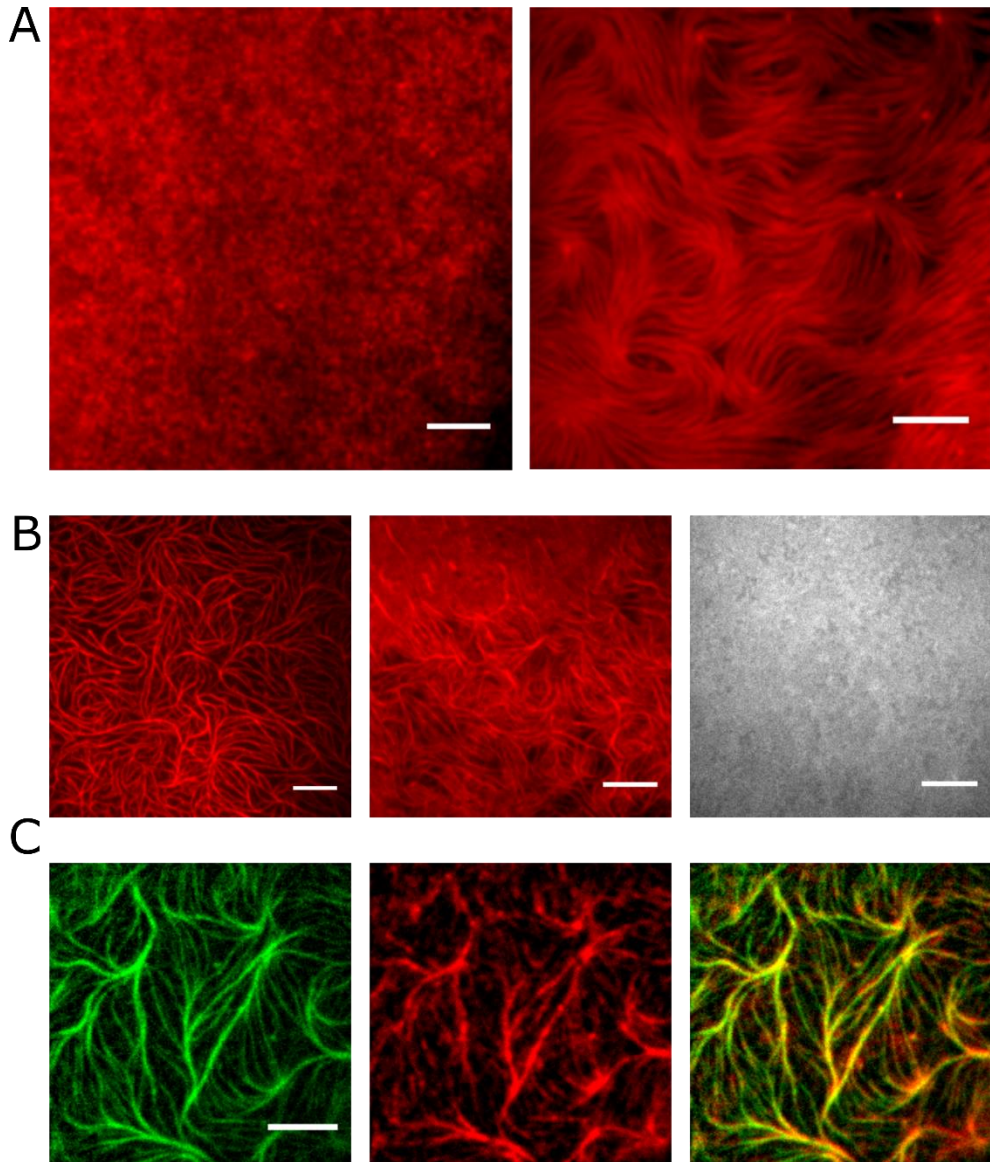


Figure 2.2 Purified FtsZ-647 and sZipA-488 in reaction buffer

TIRFM images of FtsZ-647 and sZipA-488 on top of an SLB (composition 1; Table 2.4). Red channel represents FtsZ-647 while gray and green channels represent sZipA-488. Scale bar in all images: 5 μm . A) Left, 4 μM FtsZ-647 and 1 μM sZipA resulted in recruitment of FtsZ to the membrane but no clear filaments were formed. Right, 6 μM of FtsZ-647 and 2 μM of sZipA-488 supplemented with 12.5% of Ficoll70 formed thick, dense filament networks. B) *Left*, 3 μM of FtsZ-647 and 1 μM of sZipA-488 with 12.5% of Ficoll70. Network filaments were formed on the surface. Compared to the image in A (*Right*), the network looked less dense and the bundles seemed thinner. *Center*, 1.5 μM FtsZ-647 and 0.5 μM sZipA-488 with 12.5% of Ficoll70. Filaments and networks could still be formed, but they were less dense and thinner than in *Left*. *Right*, 1 μM of sZipA-488 with 12.5% of Ficoll70. Under these conditions, only recruitment to the membrane was observed. This highlights the dependence of sZipA-488 on FtsZ-647 to self-assemble into filaments. C) When

2 – Synthesized FtsZ and other key division proteins on SLBs

FtsZ-647 and sZipA-488 bundled on the membrane, both proteins co-localized. Here, 3 μM of FtsZ-647 and 1 μM of sZipA-488, supplemented with 12.5% of Ficoll70 was utilized. *Left*, sZipA channel. *Center*, FtsZ-647 channel. *Right*, merge.

experiments carried out in literature. For example, Loose et al.⁵⁹ demonstrated that FtsZ and the cytoplasmic domain of ZipA (sZipA) self-organize into filaments on top of an SLB in a simple buffer. We proceeded similarly to Loose et al. by diluting 4 μM of FtsZ-647 and 1 μM of sZipA-488 (final concentrations) in 5 μL of reaction buffer and let the proteins interact on top of an SLB (composition 1; Table 2.4). Under these conditions, we observed protein recruitment to the membrane but we failed to confirm the presence of filaments (Figure 2.2 A *Left*). Nonetheless, the protein on the membrane did not look homogeneous but seemed to show some puncta which could consist of very small and short filaments. To promote the bundling of FtsZ-647 protofilaments, we increased the concentration of FtsZ-647 (6 μM) and sZipA-488 (2 μM), and supplemented the assay with 12.5% of Ficoll70 (m/v), a general macromolecular crowder commonly used in this kind of reconstitution assays (for example¹⁷²). Under these conditions, large areas of the membrane presented thick and dense FtsZ-647 filament networks (Figure 2.2 A *Right*). We found that lower protein concentrations also sustained the formation of protein filaments and filament networks as long as Ficoll70 levels remained at 12.5%. For example, 3 μM of FtsZ-647 together with 1 μM of sZipA-488 (Figure 2.2 B *Left*) and 1.5 μM of FtsZ-647 together with 0.5 μM of sZipA-488 (Figure 2.2 A *Right*); although it must be noticed that the lower the concentration, the thinner the filaments in the networks and less abundant the bundles. sZipA-488 self-organized in the form of bundles as well and clearly co-localized with FtsZ-647 (Figure 2.2 C). In any case, sZipA-488 bundles were clearly dependent on the presence of FtsZ-647 (Figure 2.2 B *Right*).

Next, we tested the formation of filaments and networks in the PURE_{flex} system. This is an important step prior investigating cell-free synthesized proteins. We proceeded similarly as above by diluting 4 μM of FtsZ-647 and 1 μM of sZipA-488 together with 12.5% Ficoll70. Then, the proteins were let to interact on top of an SLB (composition 1; Table 2.4) in PURE_{flex}. Almost immediately, we detected the presence of filaments on large areas of the membrane (Figure 2.3 *Left*), although single filaments looked thinner than the ones produced in simple buffer. The overall morphology of protein self-assembly consisted in this case in a high density of single filaments rather than in a network, as observed with FtsZ-647 in reaction buffer (Figure 2.2 A). The effect of Ficoll70 in these assays was similar to the assays in reaction buffer. For example, the absence of Ficoll70 totally or almost totally abolished the production of FtsZ-647 filaments (Figure 2.3 *Center*). If protein filaments were observed, these were thin, short and scarce. We assayed further the influence of Ficoll70 in the formation of filaments and found that concentration levels of this agent as low as 1.5% still triggered the formation of FtsZ-647/sZipA filaments (3 μM of FtsZ-647 and 1 μM of sZipA) in large areas of the membrane (Figure 2.3 *Right*).

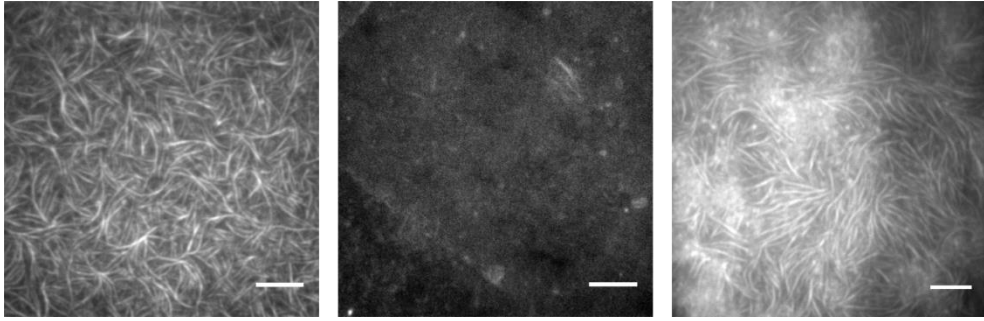


Figure 2.3 Purified FtsZ-647 and sZipA-488 in PUREflex

TIRFM images of FtsZ-647 and sZipA-488 on top of an SLB in PUREflex. Scale bars: 5 μm . Gray channel represents sZipA-488. *Left*, 4 μM of FtsZ-647 and 1 μM of sZipA-488 supplemented with 12.5% of Ficoll70. A high density of filaments was observed. *Center*, 3 μM of FtsZ-647 and 1 μM of sZipA-488. No Ficoll70 was added. Overall, recruitment of sZipA-488 to the membrane was observed. In rare occasions, filaments could appear on the membrane. *Right*, 4 μM of FtsZ-647 and 1 μM of sZipA-488 supplemented with only 1.5% of Ficoll70. Filaments were formed on some areas of the membrane in these conditions, although with a lower density and the networks encompassed smaller areas than in *Left*.

2.3.2 Synthesized FtsZ is recruited to the membrane by purified sZipA-488 and forms filaments

Next, we sought to test whether cell-free synthesized FtsZ (Figure 2.4 A) would be able to self-organize on top of an SLB. To do this, we prepared a standard PUREflex reaction with 15 nM of *ftsZ* DNA and incubated the mix at 37 $^{\circ}\text{C}$ for 3 hours. Then, 7 μL of the translation products were injected into a chamber along with 1 μM of sZipA-488 and 5% Ficoll70 to a final volume of 10 μL .

Under these conditions, protein filaments were observed on the membrane at room temperature (Figure 2.5 A). Interestingly, when 12.5% of Ficoll70 (instead of 5%) and only 5 μL of translation products were included (final volume stayed at 10 μL), we could not detect clear filaments (Figure 2.5 B Top) except in a few areas of the membrane (Figure 2.5 B Bottom). No filaments could be detected when the synthesized $\Phi 29$ terminal protein (TP; Figure 2.4 E) was used as a negative control, either when injecting 7 μL (5% Ficoll70; Figure 2.5 C Left) or 5 μL (12.5% Ficoll70; Figure 2.5 C Right) of the translation products.

2.3.3 *In situ* synthesized FtsA recruits to the membrane and facilitates the bundling of FtsZ-647

Next, we wondered whether cell-free synthesized FtsA (Figure 2.4 A) would be able to recruit and facilitate the bundling of FtsZ-647 on SLBs. Since FtsA is a membrane associated protein, we decided to synthesize FtsA *in situ*, i.e. directly inside the chamber on top of a membrane. To do this, we prepared a standard PUREflex reaction directly inside a glass chamber with 15 nM of *ftsA* DNA. Next, we harvested the pre-ran solution from the chamber and mixed 3.5 μL of the synthesized FtsA solution with 2.5 μM of FtsZ-647, 5% Ficoll70 and 1.25 mM of GTP

2 - Synthesized FtsZ and other key division proteins on SLBs

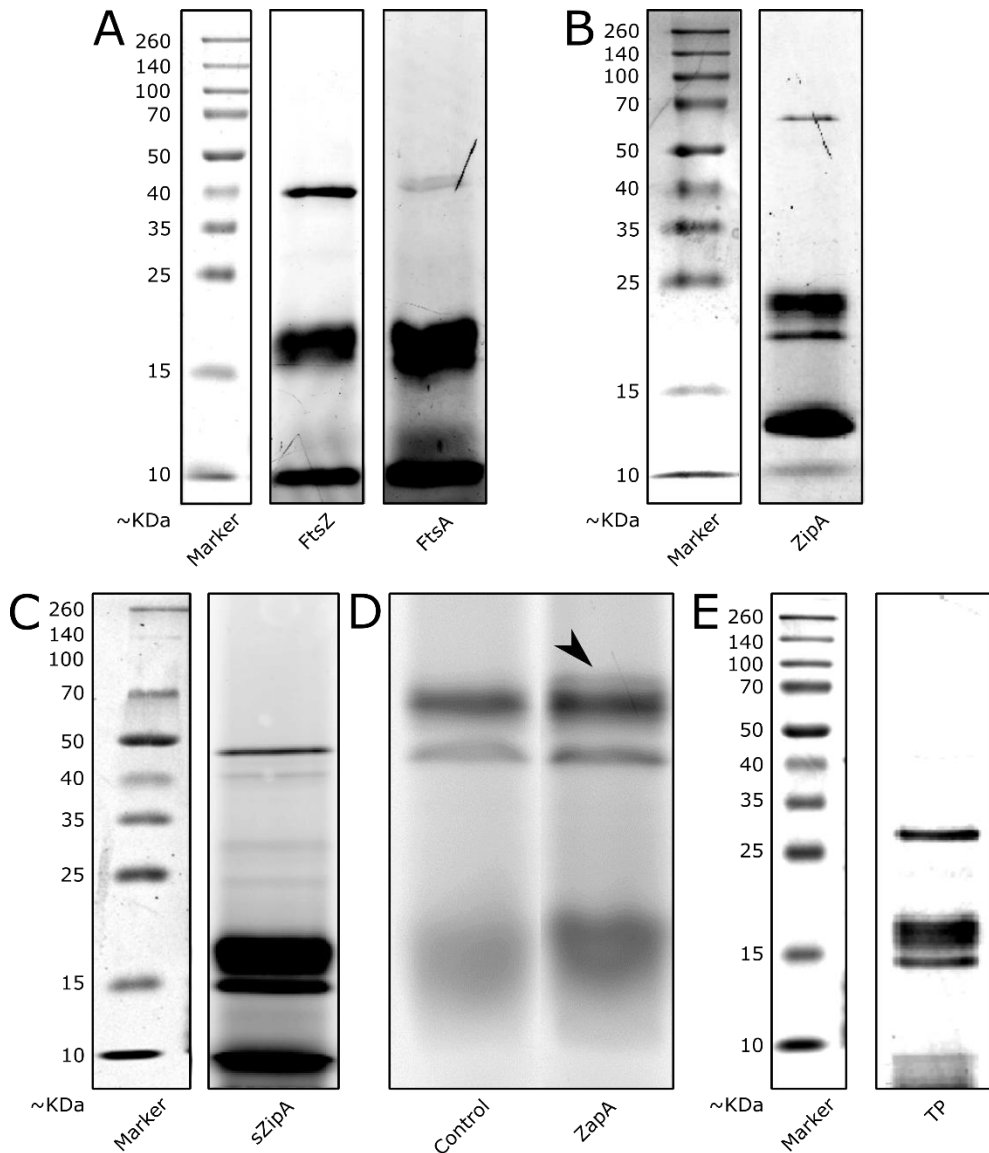


Figure 2.4 Expression of DNA templates in PUREfrex

The DNA templates coding for the proteins used in this chapter were expressed in a standard PUREfrex reaction supplemented with GreenLys and analyzed in a 12% SDS-PAGE. The protein ladder (Marker) is shown at the left of each panel with the exception of ZapA (D) where the left lane (Control), corresponds to a PUREfrex expression with no DNA template. The right lane (ZapA), corresponds to an expression with *zapA*. Black arrowhead indicates the band corresponding to the synthesized ZapA. A) FtsZ (~40 KDa) and FtsA (~45 KDa). B) ZipA (~36 KDa). C) sZipA (~34 KDa). D) ZapA (~13 KDa). E) TP (~31 KDa).

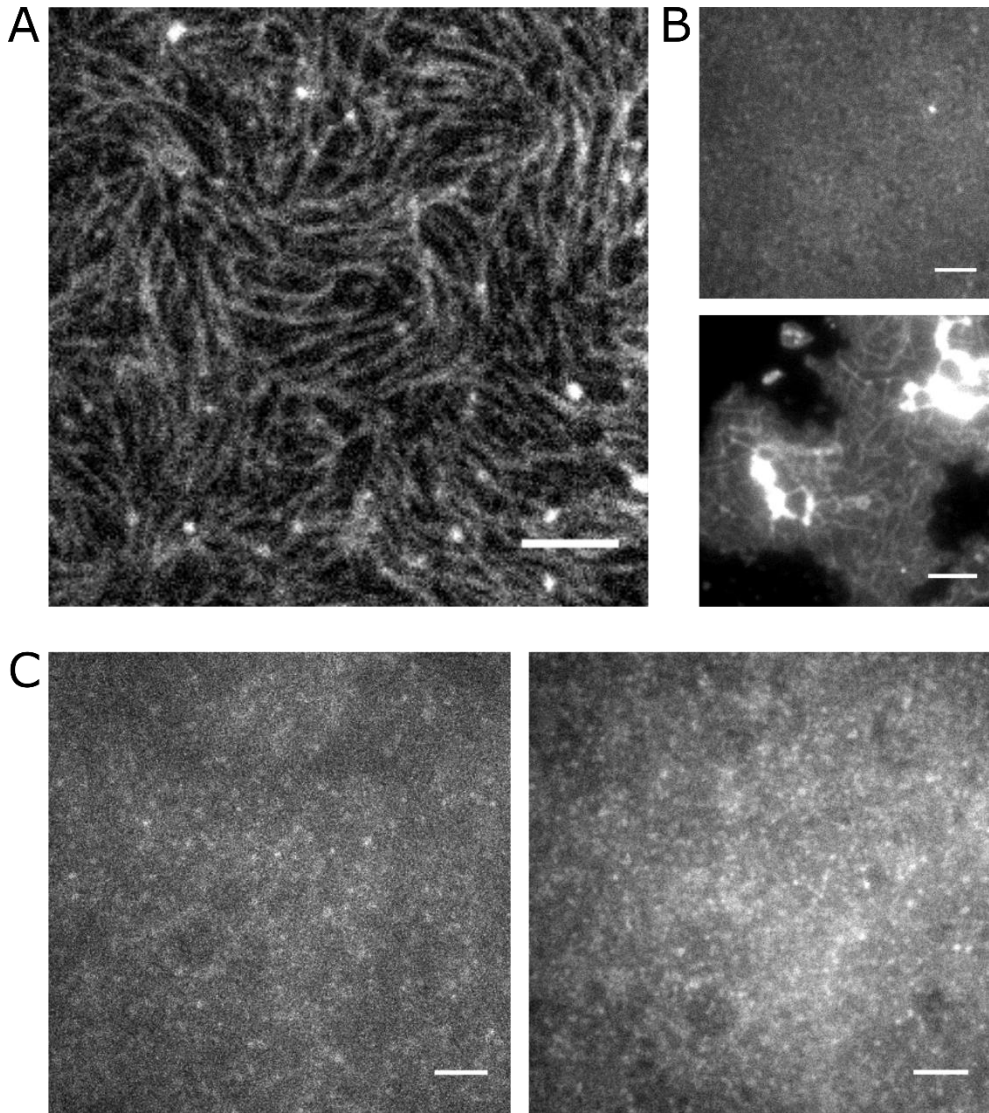


Figure 2.5 Synthesized FtsZ is recruited to the membrane by sZipA-488 and forms filaments

TIRFM images of sZipA-488 with cell-free synthesized FtsZ on top of an SLB in PURE*flex*. Scale bar in all images: 5 μm . Gray channel represents sZipA-488. A) 7 μL of synthesized FtsZ on top of an SLB incubated with 1 μM of sZipA-488 showed the presence of protein filaments. Here, 5% of Ficoll70 was used. B) 5 μL of synthesized FtsZ on top of a SLB incubated with 1 μM of sZipA plus 12.5% Ficoll70. Most of the membrane showed no filaments (*Top*) except a few areas (*Bottom*). C) Synthesized TP on top of a SLB incubated with 1 μM of sZipA. Either when 7 μL of synthesized TP (5% Ficoll70; *Left*) or 5 μL (12.5% Ficoll70; *Right*) were used, no structures were seen on the membrane.

2 - Synthesized FtsZ and other key division proteins on SLBs

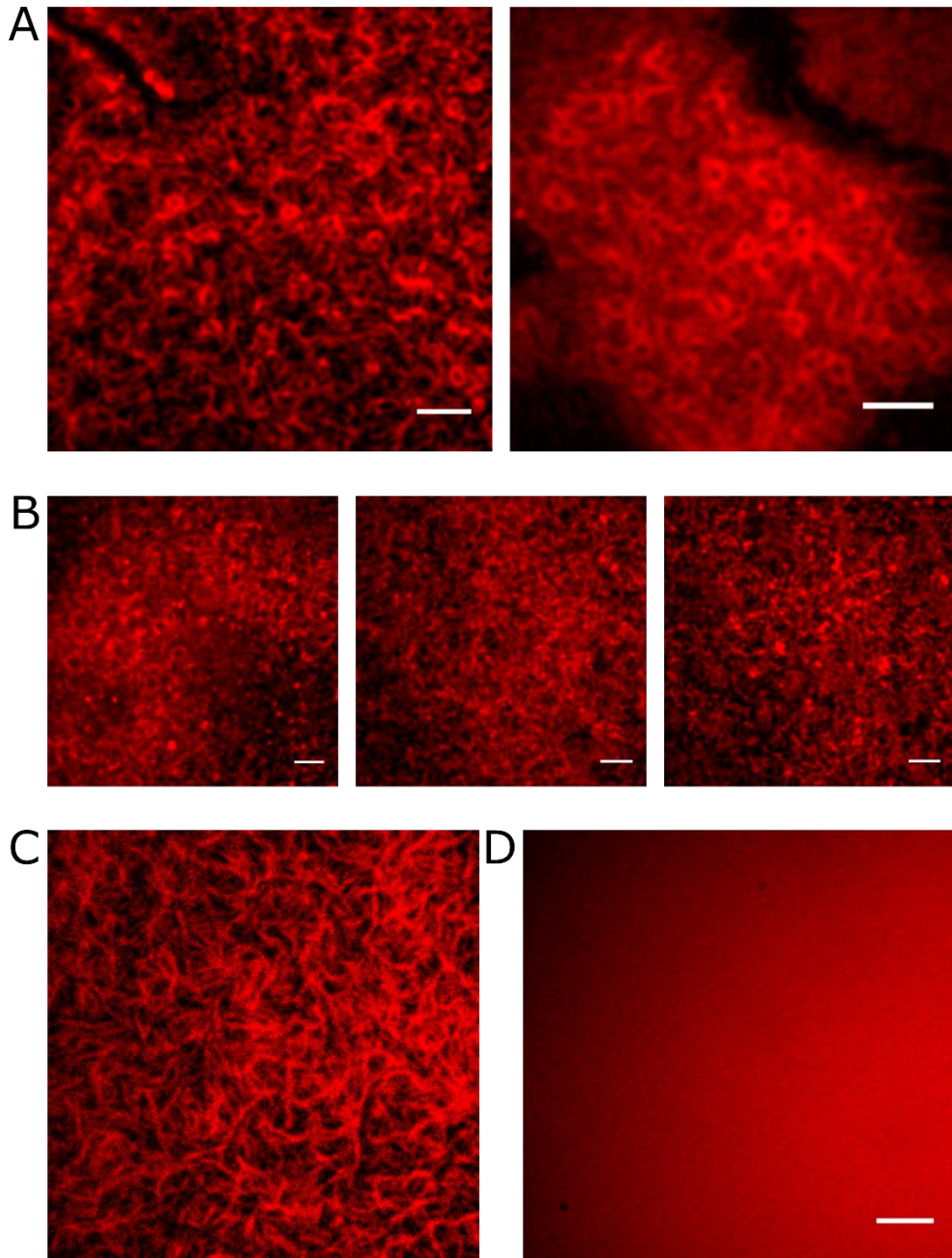


Figure 2.6 Cell-free synthesized FtsA is recruited to the membrane and facilitates the bundling of FtsZ-647

TIRFM images of FtsZ-647 with cell-free synthesized FtsA on top of an SLB in PURE/frex. Scale bar in all images: 5 μ m. Red channel represents FtsZ-647. A) 3.5 μ L of the synthesized FtsA solution supplied with 2.5 μ M of FtsZ-647 together with 5% Ficoll70 and 1.25 mM of GTP and ATP. This sample showed short, thick, highly curved filaments and some degree of filament networks (*Left*). In some areas of the membrane, the presence of protein rings was clear (*Right*). B) Under the same

conditions as in A, we explored different FtsZ-647 concentrations: 2 μM (*Left*), 1.5 μM (*Center*) and 1 μM (*Right*). We observed a positive correlation between FtsZ-647 concentration and the length, thickness and density of filament networks. C) Purified FtsZ-647 and synthesized FtsA formed longer and straighter filaments than the ones observed in A, when the sample was visualized at room temperature (2 μM FtsZ-647 and 2.5 mM of GTP and ATP). D) FtsZ-647 is not recruited to the membrane when synthesized TP is added to the sample under similar conditions to A (1.5 μM FtsZ-647, 5% Ficoll70 and 4 mM GTP and ATP, imaging performed at 37 °C).

and ATP. Finally, 5 μL of this mix was injected into the chamber and the membrane (composition 2, Table 2.4) was visualized at 37°C. Immediately, we observed the presence of thick filaments over extensive areas of the membrane (Figure 2.6 A Left) and, very frequently, numerous protein rings (Figure 2.6 A Right). Under the same conditions, we assayed alternative FtsZ-647 concentrations (2, 1.5 and 1 μM ; Figure 2.6 B) and found that lowering concentrations of FtsZ-647 led to a decrease in the length, thickness and abundance of filaments. For example, at 1 μM of FtsZ-647, filaments were infrequent and short and the surface mainly consisted of puncta (Figure 2.6 B Right). Interestingly, when the visualization was realized at room temperature instead of at 37 °C, the filaments were longer and were able to self-organize in the form of clear filament networks (2 μM FtsZ-647 and 2.5 mM of GTP and ATP; Figure 2.6 C). In contrast, *in situ* cell-free synthesized TP was not able to trigger the formation of FtsZ-647 filaments (1.5 μM FtsZ-647; Figure 2.6 D), highlighting the importance of the synthesized FtsA in the FtsZ organization.

2.3.4 *In situ* synthesized sZipA and full-length ZipA recruit and facilitate the bundling of FtsZ-647

Next, we wonder whether PURE_{flex} synthesized ZipA (Figure 2.4 B) would be able to trigger the recruitment and self-organization of purified FtsZ-647 on the membrane (composition 2; Table 2.4). To do this, we proceeded similarly as in Section 2.3.3. First, we expressed *in situ* 3.5 nM of *zipA* DNA template in a standard PURE_{flex} reaction in a silicone chamber. We mixed 3.5 μL of the harvested synthesized ZipA solution with 3 μM of FtsZ-647, 5% Ficoll70 and 2.5 mM GTP. 5 μL of the protein mix were introduced in the chamber and visualized at 37 °C. Under these conditions, we observed recruitment of FtsZ-647 to the membrane, but failed to detect the presence of filaments (Figure 2.7 A).

While recruitment of FtsZ-647 was successful, we reasoned that the final concentration of synthesized ZipA might have not been high enough to trigger polymerization or bundling. To generate a higher ZipA concentration, we

decided to carry out two consecutive PURE_{flex} *zipA* expressions in the same chamber. We utilized 3.5 nM of *zipA* for the two PURE_{flex} reactions and the protein mix was prepared as described above. Under these conditions, we observed recruitment of FtsZ-647 to the membrane, but failed again to observe protein filaments (Figure 2.7 B).

Next, we hypothesized that the standard conditions of the PURE_{flex} reaction might not be optimal for the production of active ZipA. Therefore, we expressed only 1 nM of *zipA* for 6 hours at 25 °C. The protein mix was produced as before and the sample was visualized at 25 °C. While most of the fields of view showed FtsZ-647 recruitment only, in certain areas we could observe dense puncta, very short filaments and half or even complete protein rings as a consequence of the high degree of curvature of some of the filaments (Figure 2.7 C).

Finally, we assayed the synthesized sZipA (Figure 2.4 C) in similar conditions as above with the exception of the SLB composition, which contained DGS-NTA this time (composition 1;

2 – Synthesized FtsZ and other key division proteins on SLBs

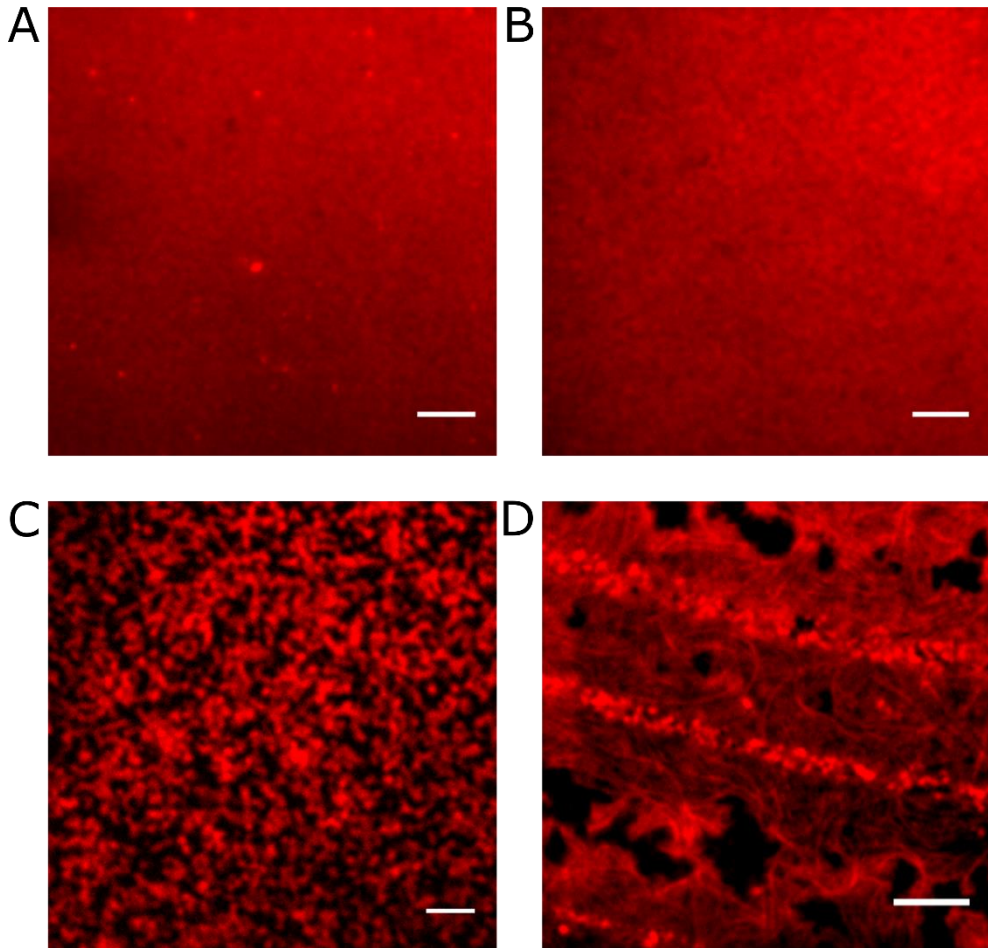


Figure 2.7 Purified FtsZ-647 with synthesized ZipA

TIRFM images of FtsZ-647 with cell-free synthesized ZipA on top of an SLB in PURE*flex*. Scale bar in all images: 5 μm . Red channel represents FtsZ-647. A) *In situ* synthesized ZipA was able to recruit FtsZ-647 to the membrane, although no filaments were observed under these conditions (3.5 μL of synthesized ZipA, 3 μM of FtsZ-647, 5% Ficoll70 and 2.5 mM GTP. Imaging was performed at 37 $^{\circ}\text{C}$). B) Two consecutive *in situ* expressions of *ZipA* led to the recruitment of FtsZ-647 to the membrane although no filaments were detected under the conditions tested (3.5 μL of the second translation products, plus 3 μM of FtsZ-647, 5% Ficoll70 and 2.5 mM GTP). C) Synthesized ZipA was able to recruit and bundle FtsZ-647 when it was expressed at low temperature (25 $^{\circ}\text{C}$) for 6 hours under the conditions tested (3.5 μL of the translation products, plus 3 μM of FtsZ-647, 5% Ficoll70 and 2.5 mM GTP; images taken at 25 $^{\circ}\text{C}$). D) Synthesized sZipA was able to recruit and facilitate the bundling of FtsZ-647 in a membrane containing DOPC, DOPG and DGS-NTA (composition 1; Table 2.4) under the conditions tested (3.5 μL of the translation products, 3 μM of FtsZ-647, plus 5% of Ficoll70 and 2.5 mM of GTP; imaging was performed at 37 $^{\circ}\text{C}$).

Table 2.4). To do this, we expressed *in situ* 15 nM of *szipA* in standard conditions. Next, the protein mix was produced as before and the sample was visualized at 25 °C. In this setting, we observed both recruitment to the membrane, and long filaments on the surface (Figure 2.7 D), although their presence was rare.

2.3.5 Synthesized ZapA triggers the bundling of purified FtsZ-647/sZipA-488 filaments

Since molecular crowders are unspecific and their presence and concentration hard to regulate when considering their *in-situ* production inside artificial cells, we envisioned ZapA, a natural crosslinker of FtsZ, as a promising alternative to Ficoll70. To explore the possibilities of synthesized ZapA as FtsZ-bundling agent, we first expressed in a standard PURE_{flex} reaction 5 nM of *zapA* (Figure 2.4 D) and assayed the activity of the synthesized protein in a standard SLB experiment with sZipA-488. On top of the membrane (composition 1; Table 2.4), we injected 10 µL of a sample consisting of 8 µL of the pre-ran PURE_{flex} solution, 2 µM of FtsZ-647 and 2.5 mM of GTP. Ficoll70 was not utilized. Visualization at 37 °C showed the presence of extensive areas of dense, long FtsZ-647 filaments (Figure 2.8 A Left). We found that, over time, the fluorescent signal intensity of FtsZ-647 on the membrane decreased and the filaments appeared thicker (Figure 2.8 A Right). Despite these preliminary results, we encountered repeatability issues, i.e. samples where membrane areas exhibiting FtsZ-647 filaments were rare (Figure 2.8 B).

We found that carrying out the expression of *zapA* at 25 °C for 5 hours and supplemented with 2 µL of the human peptidyl-tRNA hydrolase (Pth), facilitated the reproducibility of the experiments when using 7 µL of synthesized ZapA (Figure 2.8 C). Additionally, we explored the effect of reducing the volume of synthesized ZapA while maintaining a fixed total volume of the assay (10 µL) and concentrations of purified FtsZ-647 (2 µM), sZipA-488 (1 µM) and GTP (2.5 mM). Figure 2.8 D shows the result of adding 4, 3 or 2 µL of synthesized ZapA. We found that reducing volumes of synthesized ZapA produced less clear and abundant filaments on the membrane down to 2 µL (Figure 2.8 D Right), which looked similar to other experiments performed with purified protein without Ficoll70 (Figure 2.2 A).

2.3.6 Co-synthesized FtsZ and ZapA self-organized on an sZipA-488-SLB

In Sections 2.3.2 and 2.3.5, we tested separately the activity of synthesized FtsZ and ZapA, respectively. Here, we sought to co-synthesize FtsZ and ZapA to test whether PURE_{flex} is able to produce sufficient amounts of both proteins to support their self-organization on the membrane. We prepared a PURE_{flex} reaction with 1 nM of *ftsZ* and 5 nM of *zapA*. This unbalance of DNA template concentration is justified when considering the apparent stronger expression of *ftsZ* with respect to *zapA* (Figure 2.4 A and D). Due to the presence of *zapA*, we supplemented the reaction with Pth and let it incubate at 25 °C for 5 hours. Next, a mix was prepared with 9 µL of the translation products plus 50 nM of FtsZ-647 and 2.5 mM of GTP into a final volume of 10 µL. The amount of added FtsZ-647 is below the critical concentration threshold for FtsZ bundling and served reporting purposes. Ficoll70 was not utilized in this case due to the presence the synthesized ZapA. Finally, the mix was injected into a glass chamber where an SLB (composition 1; Table 2.4) had previously been formed and incubated with sZipA-488. Under these conditions, FtsZ-647 recruitment was overall observed (Figure 2.9 Left) and in many areas, bright protein dots were detected as well (Figure 2.9 Right).

2 - Synthesized FtsZ and other key division proteins on SLBs

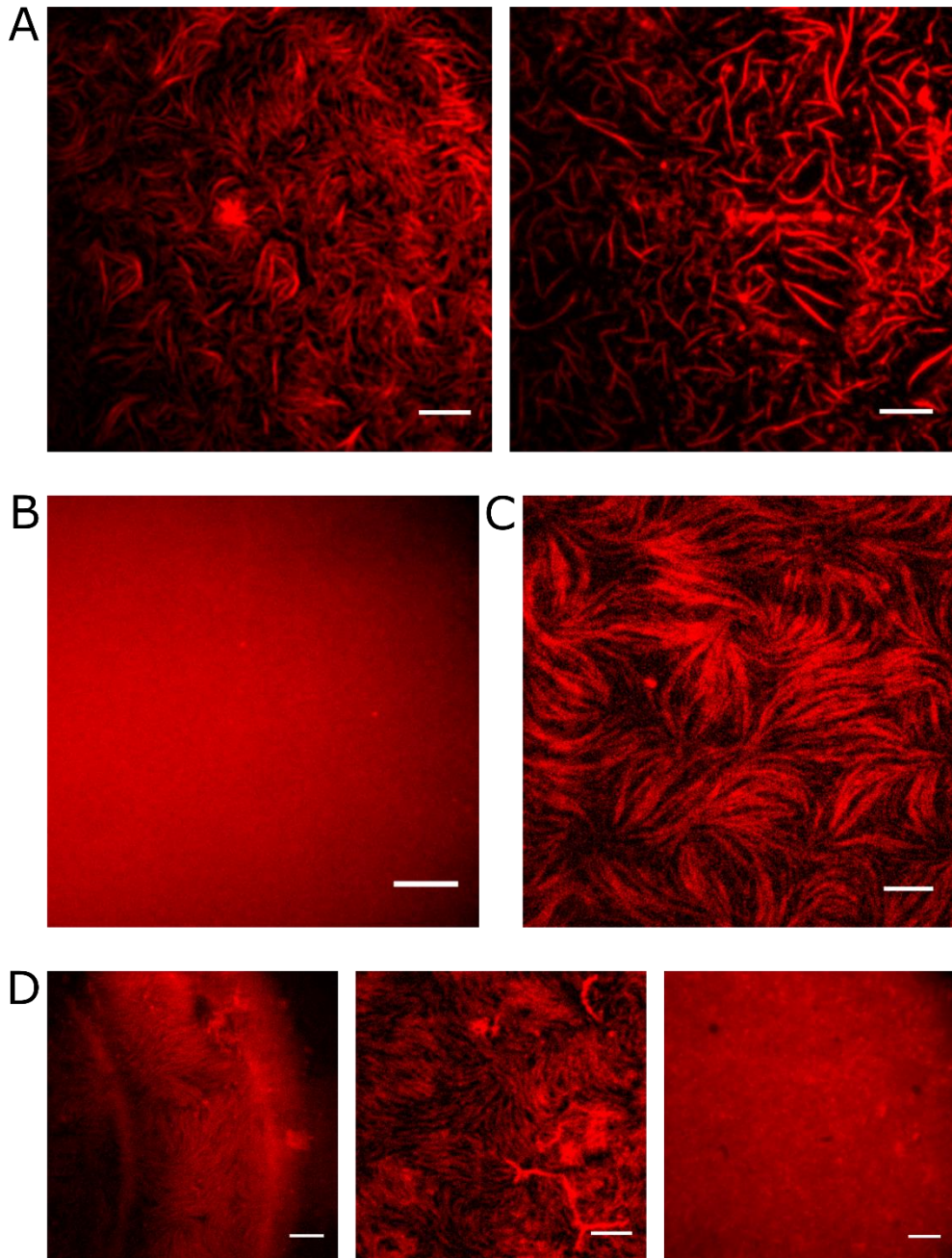


Figure 2.8 Synthesized ZapA triggers the bundling of FtsZ-647/sZipA-488 filaments on SLBs in the absence of Ficoll70

TIRFM images of FtsZ-647 together with sZipA-488 and cell-free synthesized ZapA on top of an SLB in *PUREflex*. In all cases the membrane is composed of DOPC, DOPG and DGS-NTA (composition 1; Table 2.4). Scale bar in all images: 5 μm . Red channel represents FtsZ-647. A) 8 μL of synthesized ZapA was able to trigger the bundling of 2 μM of FtsZ-647 on top of an sZipA-488-SLB under the conditions tested (1 μM of sZipA-488, 2.5 mM GTP and visualization at 37 $^{\circ}\text{C}$).

In *Left*, a region of the membrane imaged a few minutes after injecting the sample in the chamber. In *Right*, another region of the membrane visualized ~30 minutes after starting the visualization. B) The assays performed with synthesized ZapA suffered from reproducibility issues. Here, and under similar conditions as in A, filaments were very rare and overall only FtsZ-647 recruitment could be observed. C) The expression of ZapA at 25 °C for 5 hours and supplemented with Pth produced more reproducible results than the standard PURE*flex* expression. Under these conditions (2 μM FtsZ-647, 1 μM sZipA-488, 2.5 mM GTP), FtsZ-647 filaments were formed on the membrane. D) Lower volumes of synthesized ZapA than in C, were utilized here (from left to right: 4, 3 and 2 μL of synthesized ZapA). As shown in *Right*, addition of only 2 μL of synthesized ZapA in a total volume of 10 μL seemed to be insufficient to trigger the bundling of FtsZ-647.

We increased the concentration *ftsZ* DNA to 2 nM, while keeping *zapA* at 5 nM and tested the activity of the synthesized products in the same conditions as above with the exception that 0.1 μM of reporting FtsZ-647 was supplied. Recruitment of FtsZ-647 to the membrane was observed, mostly in the form of bright dots (Figure 2.10 A *Top*). To assure that the total DNA template concentration was not a limiting factor during co-expression, we ran a PURE system reaction with 4 nM of *ftsZ* and 7 nM of *zapA* at 25 °C for 5 hours. Under these conditions, we obtained mainly four distinct morphologies. First, we observed recruitment in the form of dots, similarly as before (Figure 2.10 A *Bottom*). Second, in a few areas, short, moderately sparse filaments could be detected (Figure 2.10 B). Third, some areas exhibited clear filament networks on the surface (Figure 2.10 C *Left*), although their morphology was somehow different to the one observed in previous experiments due to their low filament density and the apparent lack of a preferred curvature. Finally, in other areas of the membrane, isolated filaments (not arranged in a network) with a similar morphology as the one just described were observed (Figure 2.10 C *Right*).

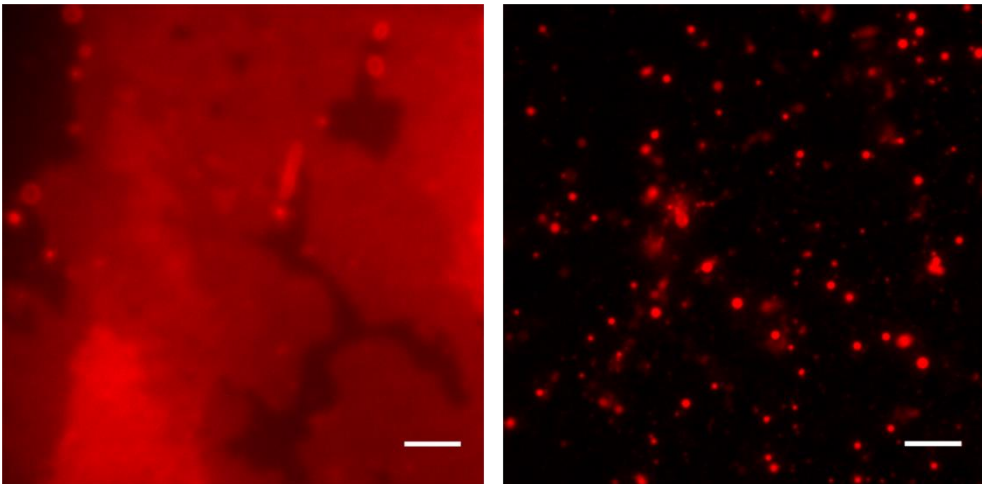


Figure 2.9 Co-synthesized FtsZ and ZapA on a sZipA-488-SLB

TIRFM images of an SLB (composition 1; Table 2.4) pre-incubated with 1 μM of sZipA-488, and containing 9 μL of a pre-ran PURE*flex* solution with 1 nM of *ftsZ* and 5 nM of *zapA*, along with 50 nM of FtsZ-647 and 2.5 mM of GTP. Both images were constructed by averaging a few tens of captures of the same sample region over a span of a few seconds. Red channel corresponds to FtsZ-647. In both images, scale bar: 5 μm. In *Left*, area of the sample with recruitment of FtsZ-647. In *Right*, a different area of the membrane showing the presence of bright dots. This phenotype was quite common in this sample.

2 - Synthesized FtsZ and other key division proteins on SLBs

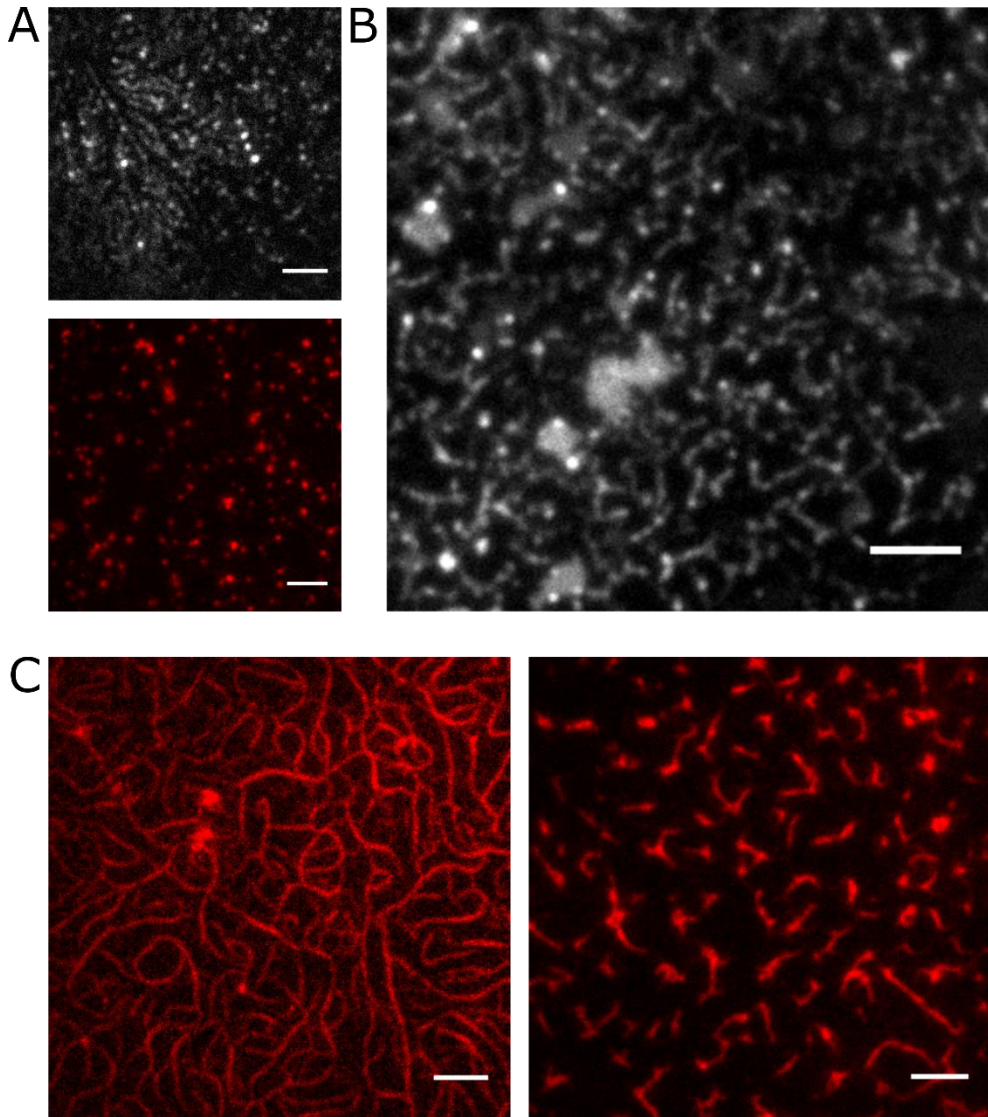


Figure 2.10 Co-synthesized FtsZ and ZapA bundle and self-organize in the form of filament networks on top of an SLB

TIRFM images of the activity assay carried out on top of a SLB (composition 1; Table 2.4) previously incubated with 1 μM of sZipA-488, with the translation products resulting from a PURE $_{flex}$ reaction containing 2 nM of *ftsZ* and 5 nM of *zapA* (A *Top*) or 4 nM of *ftsZ* and 7 nM of *zapA* (A *bottom*, B and C). The protein mix injected in the chamber contained 9 μL of the translation products, plus 50 nM of FtsZ-647 in the case of A *Top*, and 0.1 μM in the rest, plus 2.5 mM of GTP. Red channel corresponds to FtsZ-647. White channel corresponds to sZipA-488. In all images, scale bar: 5 μm . A) Co-synthesized FtsZ and ZapA produce a dot phenotype on the membrane. In *Top*, sample containing the translation products of 2 nM of *ftsZ* and 5 nM of *zapA*. In *Bottom*, sample containing the translation products of 4 nM *ftsZ* and 7 nM *zapA*. B) Here, a phenotype consisting on short filaments was observed. The morphology of the filaments seemed to be in a middle point between single filaments and networks. C) In many regions of the sample, clear filaments and network structures appeared as well. In *Left*, the phenotype consisted in a low density network of

flexible and thick filaments. In *Right*, similar although shorter filaments than in *Left*, did not arrange in networks.

2.4 Discussion

Here, we have tested and visualized the self-organization dynamics of the synthesized FtsZ, FtsA, ZipA, sZipA and ZapA on top of an SLB, and explored the viability of PURE_{flex} as our main IVTT system. Achieving functional PURE_{flex} synthesized proteins is an important step towards their utilization in liposome division (Chapter 3) and artificial cells.

In this chapter, we have successfully demonstrated that cell-free synthesized FtsZ retains essential wild-type features like monomer polymerization and bundling, plus FtsA and ZipA interaction. Furthermore, we have shown that synthesized FtsA and sZipA are able to recruit purified FtsZ to the membrane and facilitate its bundling. We also succeeded to triggering the bundling of purified FtsZ with cell-free synthesized ZapA. Consistent with these results, we achieved the crosslinking and bundling of co-synthesized FtsZ/ZapA protofilaments in an sZipA-SLB. Taken together, our experiments validate the use of PURE_{flex} for synthesis of key division proteins in artificial cells.

In the other hand, some of the results obtained challenge our view of the FtsZ-FtsA-ZipA dynamics on top of SLBs. For example, we failed to detect the presence of long, mildly curved purified FtsZ-647 filaments with synthesized ZipA in the conditions tested, in contrast with the results obtained with synthesized sZipA. Unlike previous reports in the literature, we found that Ficoll70 was a necessary reagent of the activity assays in order to obtain the bundling of FtsZ, unless synthesized ZapA was present.

2.4.1 Cell-free synthesized FtsZ retains basic wild-type functionality

The arising of cytoskeletal FtsZ suprastructures on SLBs requires monomer tail-to-head polymerization, monomer and protofilament interaction with ZipA or FtsA, and protofilament bundling through lateral interactions. In Section 2.3.2, we have shown that assembly of synthesized FtsZ and sZipA-488 on top of an SLB produced bundles and extensive filament networks (Figure 2.5 A). Such an achievement implies that the synthesized FtsZ harbors basic wild-type functionality.

This high level of functionality, meaning the recruitment and bundling capacity of the synthesized FtsZ, necessitates also a fine tuned 3-D protein structure. In particular, the recruitment of synthesized FtsZ by sZipA-488 to the membrane requires the FtsZ CTV to be functional¹⁷³. Since this region is located at the C-terminal extreme of FtsZ, recruitment of FtsZ is very sensitive to protein truncations. In the other hand, both the T7 loop and the GTP binding pocket must be well positioned and aligned to permit not only polymerization of monomers but also to self-assemble into specific morphologies¹⁷⁴. Additionally, FtsZ longitudinal and lateral interactions rely on several electrostatic interactions on the front, back and lateral faces of the protein, respectively^{175,176}. Hence, changes in the 3-D protein structure of the protein could impair the morphology of the filament structure. On the contrary, we observed a highly similar filament network phenotype between synthesized FtsZ (Figure 2.5) and purified proteins (Figure 2.2 B *Left* and Figure 2.3 *Left*), the latter results being in agreement with the literature^{59,106,177}.

2.4.2 Synthesized FtsA recruits and facilitates the bundling of FtsZ-647 in the membrane

Taken together, our results in Section 2.3.3 and Figure 2.6 demonstrate that cell-free synthesized FtsA recruits purified FtsZ-647 to the membrane and facilitates its bundling into short, curved filaments. Very frequently, we detected the presence of protein rings in these samples (Figure 2.6 A *Left*), and in some areas they were particularly abundant (Figure 2.6 A *Right*). This contrasts with the long, less curved filaments obtained in our experiments with synthesized sZipA (Figure 2.7 D), consistent with previous observations by Loose and Mitchison⁵⁹ with purified FtsZ and sZipA. As discussed above for synthesized FtsZ (Section 2.4.1), FtsA activity requires a correct 3-D protein structure to interact with the membrane, and recruit and facilitate the bundling of FtsZ-647^{56,68,70,165,178}. Hence, our data suggest successful synthesis of functional FtsA.

Interestingly, we observed that, while exhibiting a high capacity to recruit FtsZ in our SLB activity assays (Figure 2.6), synthesized FtsA showed an apparent low expression in the SDS-PAGE analysis (Figure 2.4 A). Although qualitative, signal intensity comparison of GreenLys protein bands can still be useful. In Figure 2.4 A we observed a marked difference in signal intensity between FtsZ and FtsA samples. Of course, the measured signal intensity of the expressed proteins will be influenced by the relative occurrence of Lys residues in the protein. However, the slightly higher proportion of Lys in FtsA ($\frac{21}{420} = 5.0\%$) than in FtsZ ($\frac{17}{383} = 4.4\%$) suggests that the amount of synthesized FtsA is lower than FtsZ. In fact, *in vivo* FtsZ:FtsA protein ratio is ten to one⁶². Additionally, other factors like *in situ* expression of FtsA, could facilitate integration of the amphipathic MTS on the membrane, which in turn would promote an efficient recruitment of FtsZ.

2.4.3 Cell-free synthesized ZipA produces short, curved FtsZ filaments while synthesized sZipA triggers the formation long, mildly curved bundles

Our data in Section 2.3.4 clearly indicates that PURE_{flex} synthesized ZipA is able to recruit FtsZ-647 to the membrane. This implies that synthesized ZipA is able to integrate into the lipid bilayer its transmembrane domain and to interact with FtsZ-647. Nonetheless, we did not observe FtsZ bundling when ZipA was synthesized in *in situ* (Figure 2.7 A). The lack of bundling could be due to a low yield of expressed ZipA, despite the attempts to run two consecutive expression reaction. We also considered the possibility that the limiting factor was the production of active ZipA, rather than the total protein production. In Figure 2.7 C, we assayed an *in situ* expression of ZipA at 25 °C for 5 hours. The low expression temperature was designed with the purpose of slowing down the translation machinery to allow ZipA to fold adequately. Also, it would grant the protein more time to get integrated in the membrane and avoid the aggregation of ZipA, especially through its highly hydrophobic MTS. Under these conditions, we obtained indications of FtsZ bundling in the form of puncta or short, curved filaments. Sometimes, they could arrange in the form ring-like structures. This data suggests that expression of *zipA* is sensitive to temperature.

The structures obtained with synthesized ZipA differed from the morphology observed with purified sZipA in literature⁵⁹, where extensive areas of thick, long filament networks were produced. Interestingly, this morphology is consistent with the data obtained in our experiments with sZipA (Figure 2.7 D). The different morphology between ZipA and sZipA assays could be a consequence of the lack of the physiological transmembrane domain in the case of sZipA. For example, it is known that while the full-length ZipA is capable of

homodimerization, the globular domain is not^{78,79}. While the replacement of the hydrophobic transmembrane domain of ZipA with a 6-histidine tag can be a useful workaround to allow its successful purification, our results suggest that even small modifications in wild-type proteins might alter their activity^{78,169}. Nonetheless, other factors might contribute to the different results obtained with ZipA and sZipA, like for example a lower propensity of sZipA to aggregate.

2.4.4 FtsZ filament network morphology is highly variable

Our data supports a model where FtsZ filament network morphology is highly variable and depends on several factors like membrane anchor, FtsZ concentration at the membrane and temperature. In general, we obtained short, curved filaments and protein rings with synthesized FtsA (Figure 2.6 A), and long, straighter filaments with sZipA (Figure 2.2 B and Figure 2.7 D). However, when ZipA was synthesized and visualized at 25 °C, we obtained as well short filaments and some ring-like structures (Figure 2.7 C). In a study by Ramirez-Diaz et al.¹⁰⁶, the authors found that the morphology of the filament network was more related to the local concentration of FtsZ on the membrane than the FtsZ anchor. This would imply that the differences observed by Loose and Mitchison between FtsZ/FtsA and FtsZ/sZipA networks would be more related to the intrinsic capacity of each anchor to attract FtsZ to the membrane than to any other specific interaction. The observations of Krupka et al.¹⁷⁹, where they found that low, physiological levels of sZipA produced protein rings similar to those typically attributed to FtsA, would be consistent with this idea.

In addition, we found that synthesized FtsA with FtsZ-647 at 25 °C produced longer and less curved filaments (Figure 2.6 C) than obtained at 37 °C. As discussed above, such an observation seems to imply that, at 25 °C, a higher concentration of FtsZ is present on the membrane than at 37 °C. This could be explained by the slowing down of the FtsZ GTPase activity at temperatures below 37 °C which in turn would stabilize the filaments on the membrane¹⁸⁰. Similarly, the FtsZ filament destabilization activity of FtsA⁵⁹ might be negatively affected by temperature, promoting an increase of FtsZ concentration at the membrane.

2.4.5 Cell-free synthesis of the FtsZ cross-linker ZapA leads to filament bundling

The use of ZapA in place of macromolecular crowders in general, and Ficoll70 in particular, is a preferred strategy in the context of FtsZ-containing artificial cells. While general molecular crowders are unspecific, ZapA directly interacts with FtsZ protofilaments, therefore avoiding undesirable effects over other cellular systems or chemical reactions¹⁸¹. Additionally, ZapA is a molecule which can be fabricated *in situ* inside the cell, and easy to control at the genetic, translational or protein level.

In Figure 2.8, we have demonstrated the cell-free synthesis of a functional ZapA, capable of triggering the bundling of FtsZ-647/sZipA-488 protofilaments under regular conditions without the presence of Ficoll70. ZapA is believed to be a tetramer in its active form^{87,88}. The 3-D structure of the ZapA tetramer has been resolved, suggesting that a conserved region of positive residues in the globular domain of ZapA is an important area for FtsZ interaction^{176,182}. Hence, our results imply that the synthesized ZapA retains the wild-type protein structure.

Since ZapA is active in its tetrameric form, a linked ZapA could be synthesized in order to promote oligomerization at lower protein concentration. This would be facilitated by the orientation of monomers in the complex. As Figure 2.11 A shows, the relative proximity of some of the terminal sections of the monomers in the tetramer could facilitate the fusion of monomer 1 with 2 and monomer 3 with 4, via an unstructured amino acid linker (Figure 2.11

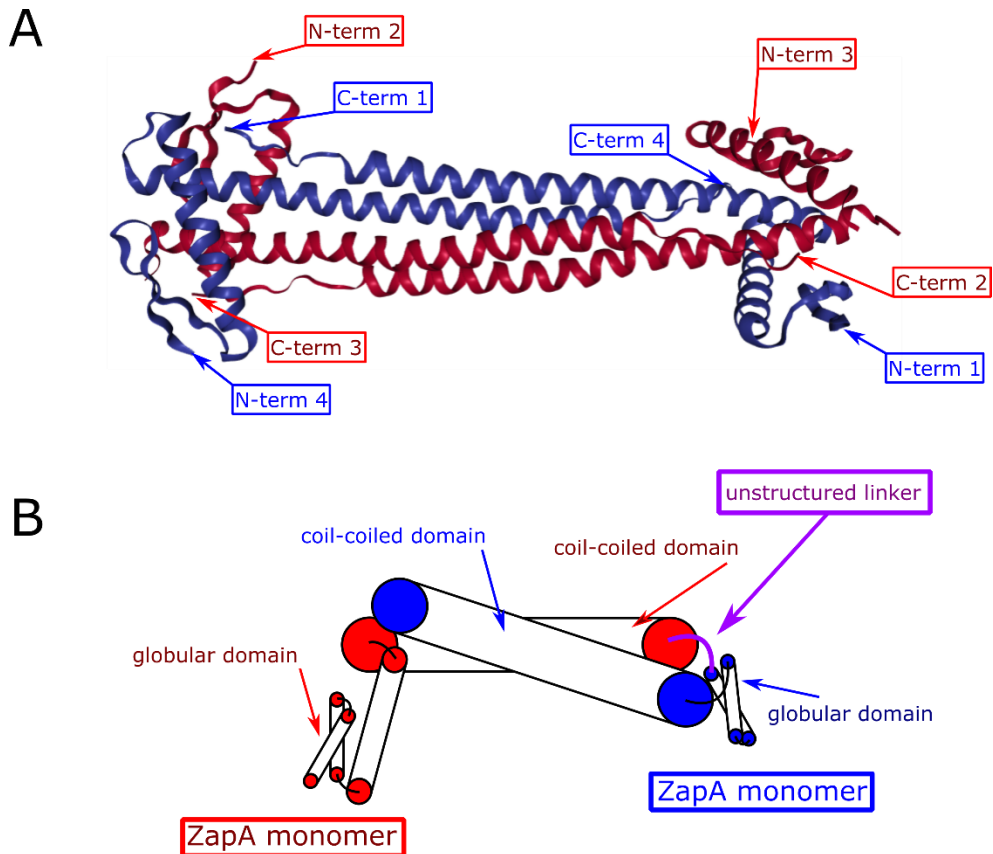


Figure 2.11 ZapA tetramer structure and schematic of linked ZapA

A) ZapA tetramer structure (PDB 4P1M)¹⁸³. It is believed that ZapA is active in its tetrameric or dimeric form. In a tetramer, the C-term of monomer number 1 is relatively close to the N-term of monomer number 2. The same occurs with the C-term number 3 and the N-term number 4. This is not the case with C-term monomer 2 and N-term monomer 3. Two unstructured amino acid linkers could be added to link monomers 1 with 2 and 3 with 4, but not monomer 2 and 3. B) Schematic of a linked ZapA dimer. Two different monomers (red and blue) could join together through an unstructured amino acid linker (magenta).

B). However, the C-terminal section of monomer 2 would be too far away from the N-terminal section of monomer 3. Two linked dimers could interact normally to form tetramers. Thanks to the relatively low molecular weight of *E. coli* ZapA monomers (~13 kDa), a DNA template containing the linked ZapA dimers could be cell-free synthesized and tested with the purified FtsZ-647 and sZipA-488 on SLBs.

2.4.6 Co-expression of *ftsZ* and *zapA* generates protein filament networks.

Our experiments showed that assays involving separately synthesized FtsZ (Section 2.3.2) and ZapA had been successful (Section 2.3.5). Moreover, our data in Section 2.3.6 and Figure 2.10 clearly demonstrates that co-synthesized FtsZ and ZapA are able to bundle and form filament networks. The presence of FtsZ/ZapA filaments was dependent on the *ftsZ:zapA* DNA template ratio. While 1 nM:5 nM produced no visible bundles, both 2:5 and 4:7 produced at least a type of cytoskeleton structure, which suggests the existence of an optimal FtsZ:ZapA protein

ratio. In addition, the morphology of the observed structures was dependent on this ratio. While in Figure 2.10 B we observed short, straight filaments, Figure 2.10 C *Left* showed thick, ‘floppy’ bundles arranged in filament networks. This morphology contrasted with the denser but less ‘floppy’ networks produced with FtsZ-647 and synthesized ZapA (Figure 2.8 A), suggesting that the long interaction (3 hours) of both synthesized proteins in solution (without having access to the sZipA-SLB), stabilized this type of ‘floppy’ structure.

2.4.7 Total volume and geometry of the activity assays might be a factor contributing to the dynamics of FtsZ, FtsA and ZipA

The data gathered during our experiments, clearly pointed to the general macromolecular crowder Ficoll70 as a necessary component to efficiently trigger the bundling of FtsZ, unless the crosslinker ZapA was utilized (Section 2.3.5). While Ficoll70 has been used in literature to bundle FtsZ, usually the activity assays performed with the *E. coli* protoring proteins do not necessarily require it^{105,172,179}, especially at the protein concentration we used compared to other studies (0.7-1.5 μM of FtsZ and 0.125-1.7 μM of FtsA in Loose and Mitchison¹⁰⁵).

A plausible explanation would involve the unconventional experimental set up of our activity assays, i.e. the low reaction volume and geometry of the chambers. Compared with previous studies, our SLB assays have been conducted in 10-fold^{105,179} or 20-fold⁴⁴ lower volume. Our experimental design, i.e. the use of the PURE system, constrained the use of large assay volumes (100 μL in Loose and Mitchison¹⁶) due to its high economical cost. It is generally recognized that protein pattern formation involving membrane-bound states is influenced by geometrical factors and the number of proteins¹⁸⁴⁻¹⁸⁶. To test the effect of geometry in our activity assays, reaction chambers with different dimensions could be produced. However, the sand-blasting method described in Section 2.2.2 would not be precise enough. An alternative, is the use of aluminium chambers as described in Section 5.2.7 (page 107).

2.4.8 PURE_{flex} is a promising candidate to support cell-free expression of key *E. coli* division proteins in artificial cells

Our data validates PURE_{flex} as a promising candidate to cell-free synthesize key *E. coli* division proteins. In Figure 2.3, we showed that purified proteins FtsZ-647 and sZipA-488 self-organized into protein bundles in a PURE_{flex} context, implying that PURE_{flex} is a viable background for FtsZ-FtsA-ZipA interaction. Expression of DNA templates was successful (Figure 2.4) and our experiments involving the activity of synthesized FtsZ, FtsA, ZipA, sZipA and ZapA produced cytoskeleton structures in many of the conditions tested. PURE_{flex} also proved capable of synthesizing more than one protein at a time (FtsZ and ZapA; Figure 2.10) and enabled the self-assembly of FtsZ/ZapA bundles and filament networks. Such an achievement is of capital importance in the development of artificial cells based on the PURE system.

PURE_{flex} also proved highly versatile. For example, expression reactions were done directly on top of a membrane in the case of FtsA and ZipA (Section 2.3.3 and 2.3.4). This probably helped these proteins to get integrated in the membrane and avoid aggregation, especially in the case of ZipA, a recalcitrant protein hard to purify^{77,172}. Additionally, expressions at low temperature (25 °C; Figure 2.7 C), or the addition of cofactors (Pth; Section 2.3.5 and 2.3.6) facilitated the correct folding of ZipA and expression of *zapA*, respectively.

2.4.9 Conclusion

Taken together, we can conclude that the cell-free synthesized proteins FtsZ, FtsA, ZipA, sZipA and ZapA are functional on SLBs in a PURE_{flex} context. The successful observation of self-organization in these conditions highlights the compatibility of the *E. coli* division proteins with the PURE system and prompt us to test them in vesicles (Chapter 3).

Acknowledgements

We thank Germán Rivas' lab at Centro de Investigaciones Biológicas (CSIC) in Madrid for providing the purified proteins used in this chapter. We thank Ilias Zarguit for excellent laboratory work and fruitful discussions. We thank Daniël Lam and Jeremie Capoulade for the TIRFM training and technical support.

Chapter 3

In-vesicle synthesis of FtsZ

Evolving, self-maintaining, self-reproducing. These are the essential features of that special state of matter that we call *alive*. In the exciting field of synthetic biology, one of the *holy grails* is the building, brick by brick, of biological particles exhibiting such characteristics. This formidable challenge can be broken up into distinct, smaller pieces, each one accomplishing a specific function like for example cellular division, also called cytokinesis. In this chapter, we aimed at the reconstitution, in vesicle, of a membrane deforming machinery with the ultimate goal of dividing artificial model cells. We approached this task by challenging key *E. coli* division proteins to assemble on, and to deform free-standing liposome membranes. While typical in-vesicle assays relay on purified proteins, our approach involved the cell-free synthesis of proteins via the PURE system, a well characterized mix of purified components for transcription and translation. We found that FtsZ and ZipA protein self-organization took place in the form of bundles on the outer leaf-let of the liposomes, although membrane deformation was not evident. In contrast, in-vesicle synthesis of FtsZ generated straight bundles in the lumen that were capable, in many cases, of elongating the liposomes. Our work establishes a clear link between genotype and phenotype, i.e. liposome membrane deformation can be triggered by *in situ* protein synthesis from a DNA template. We believe that establishing this link enables the creation of evolvable artificial cells.

3.1 Introduction

In *E. coli*, division commences with the assembly at midcell of the divisome, a very well-coordinated protein complex^{24,25}. Among the ten essential proteins that constitute this complex²⁴, FtsZ is the first to assemble upon GTP binding into the Z-ring, a dynamic ring-like structure made of bundled FtsZ polymers^{39,43,44,50}. The Z-ring is anchored to the cytoplasmic leaflet of the inner cell membrane through two other essential proteins, FtsA and ZipA, which contain a membrane targeting sequence (MTS) and an FtsZ interacting region^{24,61}. Together, these three proteins form a ring-like structure known as the protoring⁸¹, and constitute the basic cytoskeleton upon which the matured divisome is assembled. Once mature, the divisome exerts a constriction motion and starts with the synthesis of the division septum, until division is complete⁴⁶. The activity of the divisome can be regulated and facilitated by, despite non-essential, other proteins. For example, ZapA is an important protein that cross-links FtsZ protofilaments and stabilizes the Z-ring⁸². While the role of FtsZ in the generation of constriction force *in vivo* is not clear, several *in vitro* studies have shown that FtsZ has some constriction capabilities. In 2013, a study by Osawa and Erickson (Figure 1.4 , page 20)¹⁸⁷, showed that when wild-type FtsZ and a deficient self-interacting FtsA was encapsulated inside spherical liposomes, protein rings were generated on the inner membrane of the bilayer and constriction took place in some of them. These type of experiments showed that, at least *in vitro* and for a subset of liposomes, FtsZ has membrane remodeling and constriction force capabilities¹⁸⁸.

Recently, Furusato et. al.¹⁰⁸ studied the *de novo* expression of proto-ring proteins in vesicle. They used an FtsZ version with a sfGFP fused to the C-terminal region (FtsZ-sfGFP). This fusion protein was reported to present a different GTP hydrolysis rate than the wild-type version as well as being recruited much stronger by any protein anchor. Despite this, they found that co-expression of FtsZ-sfGFP and full-length ZipA inside vesicles led to the formation of protein clusters that deformed the liposome. Importantly, these clusters were independent of GTP binding or hydrolysis, as well as the presence of the sfGFP. In their study, they also reported that the use of Ficoll70 inside of FtsZ-sfGFP-expressing vesicles led to protein bundles that stayed cortically. In this case, no expression of protein anchor was assayed.

Here, we aimed to reconstitute an artificial, FtsZ-based division mechanism in liposomes. Our approach consisted in the encapsulation of a cell-free transcription and translation system reconstituted from purified components (PURE system), together with a selection of DNA constructs coding for FtsZ membrane anchoring proteins, i.e. FtsZ and ZapA. The *in situ* production of untagged proteins represents an advantage compared with other conventional reconstitution approaches. In one hand, traditional approaches rely on the use of purified proteins. This limits the collection of available proteins, depending on purification protocols and whether the protein of interest is recalcitrant (e.g. membrane-bound proteins). In the other hand, the PURE system offers a more physiological environment than the reaction buffers typically employed. Nonetheless, *in situ* expression of proteins inside the synthetic-cell is ultimately an essential requirement, not only to mimic a key feature of natural biological cells but also to avoid death by dilution, which is unavoidable if proteins are not synthesized *in situ*.

In this chapter, we tested the protein self-organization of the in-vesicle synthesized FtsZ and ZapA. We found that under slightly higher K^+ and Mg^{2+} concentration than required for a PURE system reaction and in the absence of Ficoll70, we triggered the formation of protein bundles in the lumen. These filaments were able to deform the membrane, triggering the creation of fusiform and lemon-shape liposomes.

3.2 Materials and methods

3.2.1 Preparation of DNA templates for gene expression and purified proteins

Purified protein FtsZ-647 was utilized. A description can be found in Section 2.2.1 (page 37).

The *ftsZ*, *zapA* and *p3-phi29* constructs were prepared as described in Section 2.2.1 (page 37). The *eyfp* construct codes for an eYFP with the necessary genetic parts to be synthesized in the PURE system and was produced as specified in van Nies et al.¹⁸⁹. A complete and detailed account of the DNA sequences and their features can be found in the Appendix (page 154). The purified proteins FtsZ-647 and sZipA-488 utilized in this chapter were kindly provided by Germán Rivas, from *Centro de Investigaciones Biológicas*, CSIC, Madrid (Section 2.2.1, page 37).

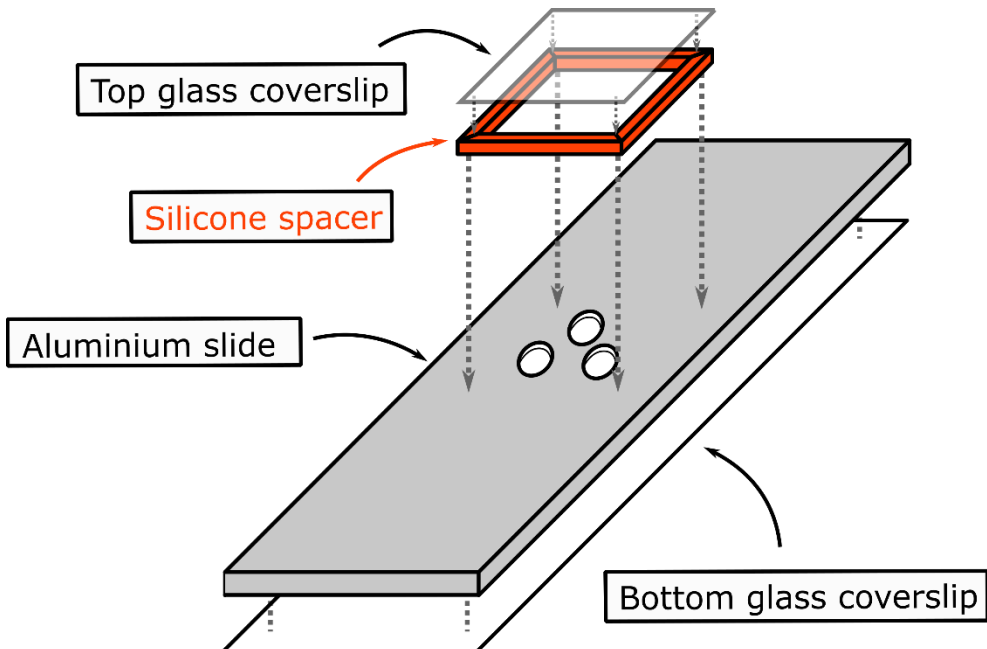


Figure 3.1 Aluminium chamber

Reusable aluminium chambers were manufactured. Dashed arrows indicate how each piece of the chamber was assembled. This type of chambers allowed for a higher control over the geometry of the reaction cavities and were reusable, except for the top glass coverslip which was discarded after each experiment.

3.2.2 Reaction chambers

Home-made silicone reaction chambers were fabricated and handled as described in Section 2.2.2 (page 38). Aluminium chambers were produced in order to have a higher control over the geometry of the reaction cavity compared to glass chambers. Aluminium chambers were easier to fabricate, reusable and could be designed to accommodate up to three reaction cavities at the same time. To manufacture these chambers, we proceeded by drilling three holes of 4 mm in diameter on the center of a 76x26x2 mm aluminium slide in an equilateral triangular position. Next, a pre-cleaned, 0.15 mm thick coverslip was glued with UV glue NOA81 (Norland products) to one side of the drilled aluminium sheet, on top of the holes. To cure

the glue, the assembly was exposed 5 minutes to UV light (365 nm wavelength with 36 W of power; Promed UVL-36 with four UV-9W-L bulbs). Finally, the chamber was kept at 50 °C during at least 3 days. This assembly creates three reaction cavities with glass bottom and aluminium walls with a total volume capacity of ~25 µL. The chamber can be reused for a few tens of experiments. To close the chamber, a squared frame spacer made out of silicone (Silicone Isolators™ Sheet Material with double side SecureSeal™ adhesive) sheet is stick around the reaction cavities. Then, a clean glass coverslip is fixed on top of the spacer thanks to the SecureSeal™ adhesive (Figure 3.1). Preparation of pre-cleaned glass coverslips was done as described in Section 2.2.2 (page 38) for silicone chambers. Before use, aluminium chambers were flushed with Milli-Q water (Millipore Corporation) and 100% ethanol. Then, the chambers were dried with a flow of nitrogen gas and plasma cleaned (Basic Plasma Cleaner, Harrick Plasma) for 10 minutes with air. The chambers were subsequently washed three times with the buffer employed in the feeding solution (Section 3.2.5 and 3.2.6). Cleaning of reusable aluminium chambers was done as described for glass chambers in Section 2.2.2, with the exception of the sonication in KOH solution that was omitted, due to the reactive properties of KOH and aluminium.

In the case of immobilization of liposomes on the surface, the chambers were functionalized first with BSA-biotin (Thermo Fisher Scientific) and Neutravidin (Sigma-Aldrich). To do this, 10 µL of 1 mg/mL of BSA in 1 mg/mL of BSA-biotin was incubated at room temperature for 10 minutes and washed three times with the feeding solution buffer. Next, the chambers were incubated with 10 µL of 1 mg/mL of Neutravidin for 10 minutes at room temperature followed by three washes with the feeding solution buffer.

3.2.3 Phospholipids

Phospholipids were purchased either from Avanti® Polar Lipids Inc. or ThermoFisher Scientific Invitrogen™ (Table 3.1) and all were dissolved in chloroform. Phospholipids were typically aliquoted in glass vials and wrapped with Parafilm M (Bemis©) before storing at -20 °C. DHPE-TxR was additionally wrapped in aluminium foil to avoid photobleaching. These phospholipids were eventually mixed to produce custom made compositions. For a complete list of all the phospholipid compositions employed in this chapter, see Table 3.2.

3.2.4 Preparation of lipid-coated beads

Liposomes were produced by natural swelling following the method described by Nourian et al.¹⁵⁴, where a porous matrix is utilized to increase the yield of large and giant liposomes. First, a phospholipid mixture was prepared in a 25 mL round-bottom flask in the appropriate proportions up to a total mass of 5 mg of phospholipids (except when DSPE-PEG-biotin and DHPE-TxR were added. See Table 3.2). Every time a different phospholipid was added to the round-bottom flask, extra chloroform was pipetted with the same tip to ensure that all the phospholipid mass was used. To facilitate swelling of the lipid film, and unless otherwise indicated, 30% (v/v) of 100 mM of rhamnose in methanol was added to the lipid mixture^{21,22}. Next, 212-300 µm diameter glass beads (Sigma-Aldrich®) were placed in the round-bottom flask to a typical ratio of 3.34 µg of lipids per mg of beads. Chloroform was removed by rotary evaporation at 200 mbar and 50 rpm for at least two hours or until chloroform was totally evaporated by visual inspection. Next, using a clean spatula, the beads were aliquoted into 1.5 mL Eppendorf tubes and desiccated overnight. Aliquots were gently flushed with argon and wrapped in Parafilm M, before storing at -20 °C. Lipid-coated beads containing a fluorescent dye were covered with aluminium foil to avoid photobleaching.

Table 3.1 Phospholipids used for the production of liposomes

The name, abbreviation and the company from where the phospholipids were purchased are listed. Avanti: Avanti® Polar Lipids Inc. Invitrogen: ThermoFisher Scientific Invitrogen™.

Abbreviation	Name	Company
DOPC	1,2-dioleoyl-sn-glycero-3-phosphocholine	Avanti
DOPE	1,2-dioleoyl-sn-glycero-3-phosphoethanolamine	Avanti
DOPG	1,2-dioleoyl-sn-glycero-3-phospho-(1'-rac-glycerol)	Avanti
Cardiolipin or CL	1,3-bis(sn-3'-phosphatidyl)-sn-glycerol	Avanti
DGS-NTA	1,2-dioleoyl-sn-glycero-3-[(N-(5-amino-1-carboxypentyl)iminodiacetic acid)succinyl] (nickel salt)	Avanti
DSPE-PEG-Biotin	1,2-distearoyl-sn-glycero-3-phosphoethanolamine-N-[biotinyl(polyethylene glycol)-2000] (ammonium salt)	Avanti
DHPE-TxR	1,2-Dihexadecanoyl-sn-Glycero-3-Phosphoethanolamine, Triethylammonium Salt	Invitrogen
--	Cholesterol	Avanti

Table 3.2 Lipidic composition of liposomes

Abbreviation and concentration at which each phospholipid was mixed for each different composition. The phospholipids DOPC, DOPE, DOPG, Cholesterol, DGS-NTA and CL were always added together up to a total phospholipid mass of 5 mg. The phospholipids DSPE-PEG-biotin and DHPE-TxR, due to the low concentration at which they were mixed, were added over the total phospholipid mass of 5 mg.

Composition	DOPC (mol%)	DOPE (mol%)	DOPG (mol%)	Cholesterol (mol%)	DGS-NTA (mol%)	CL (mol%)	DSPE-PEG-biotin (mass%)	DHPE-TxR (mass%)
1	76	--	19	--	5	--	1	--
2	64	--	16	16	4	--	1	--
3	51	35	11	--	0.5	2	1	0.5
4	51	35	12	--	--	2	1	0.5

3.2.5 Activity assays on the outside of liposomes with purified proteins

A swelling solution consisting in reaction buffer (50 mM Tris-HCl pH 7.5, 150 mM KCl, 5 mM MgCl₂) supplemented with 0.2 M sucrose was prepared in a 1.5 mL Eppendorf tube to a final volume of 20 μ L. Next, 20-30 mg of lipid-coated beads (composition 1 or 2; Table 3.2) were mixed with the swelling solution and incubated at room temperature for at least two hours. In this case, 100 mM of rhamnose in methanol was not used. The tube was rotated and tapped every 30 minutes to allow a better release of liposomes from the beads. After the swelling, four freeze-thaw cycles were carried out with liquid nitrogen. Next, the feeding solution was prepared with reaction buffer plus 0.2 M glucose, 12.5% or 1.5% of Ficoll70 (m/v) and 2 μ M of purified sZipA-488. Two microliters of liposome-containing swelling solution were placed together with 7 μ L of feeding solution inside a silicone reaction chamber, upon which it was sealed and imaged at room temperature. Then, 2 or 3 μ M of FtsZ-647 and 5 or 2.5 mM of GTP were added in sequential order. At each step, the sample was imaged. The specific concentration of each protein and nucleotide depended on the experiment and are indicated in the relevant sections.

Table 3.3 Composition of a typical swelling solution for expression inside liposomes

Swelling solution contained either PURE*frex* or PURE*frex* 2.0, but not both. The volume of the DNA construct added (x) could vary depending on its molar concentration and the number of different constructs. The final concentration of each different construct was always 5 nM. When PURE*frex* 2.0 was used, the relevant volumes are denoted with an asterisk (*).

Reactant	Volume (μ L)	Final concentration
PURE <i>frex</i> I (2.0*)	10 (10*)	1x
PURE <i>frex</i> II (2.0*)	1 (1*)	1x
PURE <i>frex</i> III (2.0*)	1 (2*)	1x
SUPERase	0.5	0.5 U/ μ L
FtsZ-647	2	2 μ M
DNA construct	x	5 nM
Milli-Q water	5.5 - x (4.5 - x*)	
Total	20	

3.2.6 Protein activity assays inside liposomes

First, a swelling solution containing either PURE*frex* or PURE*frex* 2.0, 0.5 U/ μ L of SUPERase In™ (Ambion) (SUPERase) and 2 μ M of purified FtsZ-647 was mixed in a 1.5 mL Eppendorf tube to a final volume of 20 μ L. In the case of single or co-expression of DNA inside liposomes, 5 nM of (each) DNA template was included (Table 3.3). Next, 20-30 mg of lipid-coated beads (compositions 3 or 4; Table 3.2) were placed together with the swelling solution. The solution was incubated for at least 2 hours at room temperature (only purified proteins) or on ice to avoid the start of the reaction (with a DNA construct). During incubation, the tube was rotated and tapped every 30 minutes to allow a better release of liposomes from the beads. After swelling, four freeze-thaw cycles were carried out with liquid nitrogen. Next, a feeding solution was prepared with either 1x PURE*frex* or PURE*frex* 2.0 buffer and 1 μ L of 100 μ g/mL of

Proteinase K in a final concentration of 10 µg/mL. Then, 2 µL of liposome-containing swelling solution was injected together with 7 µL of feeding solution inside a glass reaction chamber, upon which it was sealed and incubated at 37 °C.

The percentage of filament-containing liposomes (F ; Figure 3.5 and Figure 3.6) was calculated as shown below:

$$F = 100\left(\frac{f}{N}\right)$$

2

where f is the number of liposomes containing an FtsZ-647 protein filament in the lumen and N is the total number of liposomes in the sample. Truncated liposomes, i.e. liposomes whose perimeter was not totally visible in the image were not considered. The criterion followed to identify filaments inside liposomes is as follows: in general, only linear structures inside a liposome whose length was three times or longer than its width, were considered as filaments. In the case where more than one structure was found inside the liposome and the length of the structures was two to three times longer than their width, a valid filament was still counted if these structures were aligned inside the lumen. Due to the high number of liposomes per sample, the counting was automatized. To do this, a HAAR cascade algorithm¹⁹⁰ was used in order to create a classifier to detect liposomes in microscopy images. To train a 30 stages classifier, we used 4584 positive and 327 negative instances. In order to facilitate the manipulation, counting and cropping of detected liposomes not only for posterior analysis but also for improvement of the HAAR classifier, a script was developed in Python 3.6 (<https://www.python.org/>).

In order to analyze the roundness of liposomes (Figure 3.7), we proceeded first by manually measuring in ImageJ2 the apparent long and short axis of each liposome. Then, we calculated the elongation ratio (E) as follows:

$$E = \frac{\text{long axis}}{\text{short axis}}$$

3

Both long and short axis were measured in µm. E equals to 1 for perfectly round liposomes ($\text{long axis} = \text{short axis}$) and gives higher values with increasing elongation of the liposome.

3.3 Results

3.3.1 FtsZ-647 and sZipA-488 polymerize on liposomes and deform the membrane

First, we tested the capacity of the purified proteins FtsZ-647 and sZipA-488 to polymerize and deform the membrane on the outside of liposomes. To do this, we produced a liposome solution (composition 1; Table 3.2) containing DGS-NTA to allow the recruitment of sZipA on the membrane and DSPE-PEG-biotin for liposome immobilization. To enhance the accumulation of liposomes on the silicone chamber surface, the swelling solution was supplemented with sucrose. Then, we prepared a feeding solution containing glucose and 12.5% of Ficoll70. Sequentially, 2 µM of sZipA-488, 2 µM of FtsZ-647 and 5 mM of GTP were added (final concentration). After the addition of sZipA-488, liposomes could be observed, indicating that sZipA-488 was able to interact with the liposome's membrane (Figure 3.2 A Left). Additionally, we observed a great number of fused liposomes on the surface, spontaneously forming an SLB. After the addition of FtsZ-647, the protein was also recruited

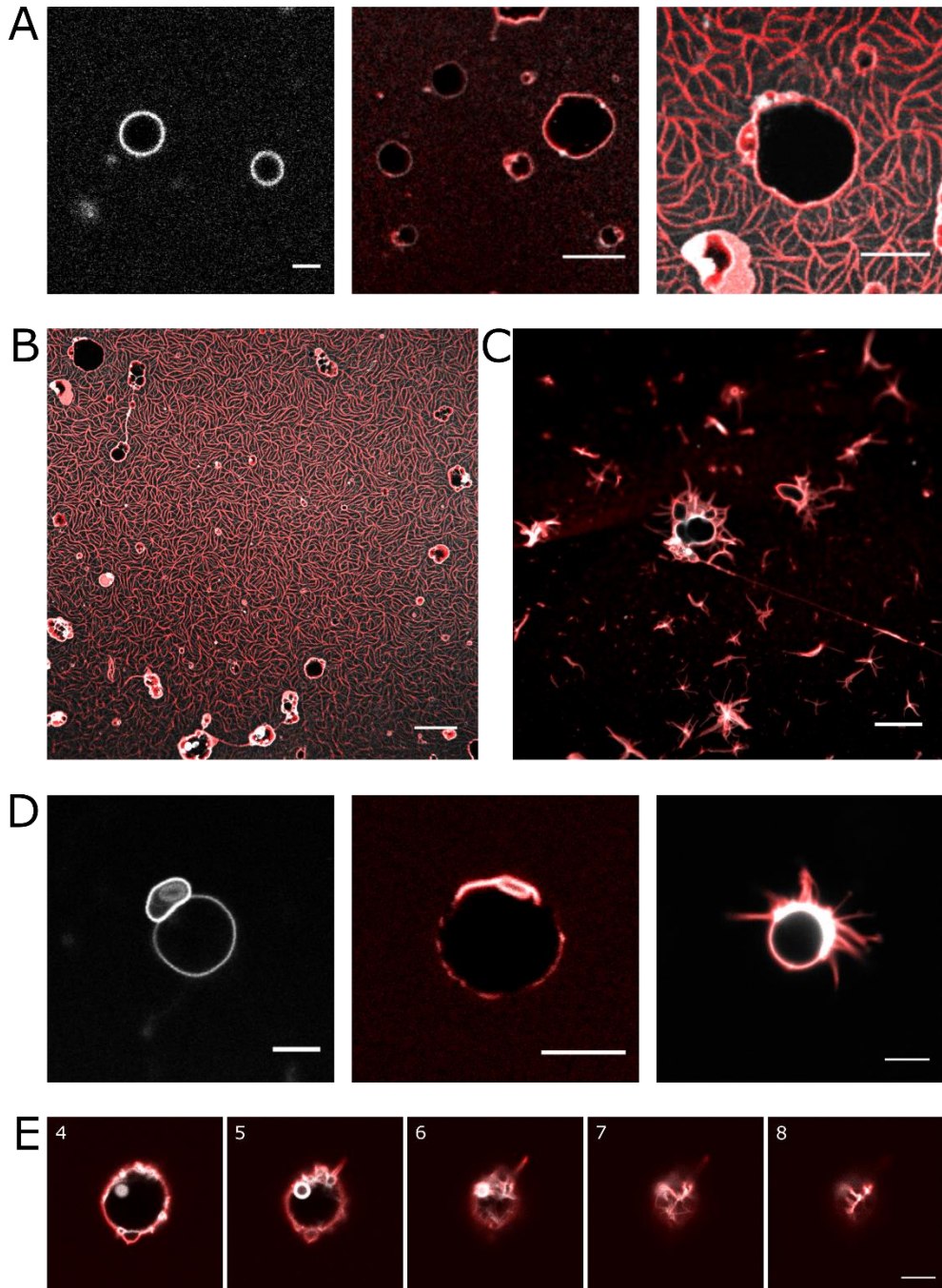


Figure 3.2 Purified proteins assayed on the outside of liposomes

LSCM images of purified FtsZ-647 and sZipA-488 proteins assayed on the outside of liposomes. Red channel represents FtsZ-647, and white channel represents sZipA-488. The lipidic composition of liposomes in A and B is composition 1 (Table 3.2), plus the addition of 2 μM of FtsZ-647 and 2 μM of sZipA-488. The liposomes were immobilized on the surface with

3 – In-vesicle synthesis of FtsZ

Neutravidin. A) *Left*, recruitment of sZipA on the membrane of some immobilized liposomes. Scale bar: 2 μm . *Center*, after the addition of 2 μM FtsZ-647, the protein was recruited to the liposome membrane. Scale bar: 5 μm . *Right*, the addition of 5 mM of GTP triggered the formation of protein filaments. The possible deformation of the membrane is not clear. Scale bar: 5 μm . B) Due to spontaneous fusion of liposomes on the surface, an SLB was formed. Extensive areas showing FtsZ-647/sZipA-488 protein filament networks were formed. Scale bar: 10 μm . Panels C-E correspond with liposomes with the lipid composition 2 (Table 3.2), plus the addition of 6 μM of FtsZ-647 and 2 μM of sZipA-488. In this case, liposomes were not immobilized to avoid spontaneous fusion on the surface, although the swelling and feeding solutions were supplemented with sucrose and glucose, respectively, to promote accumulation of liposomes onto the chamber bottom. C) General view of liposomes on the surface after the sequential addition of 2 μM of sZipA-488, 6 μM of FtsZ-647 and 2.5 mM of GTP. Filaments were formed and protein protrusions from the edge of the liposome are clear. Scale bar: 10 μm . D) *Left*, after the addition of 2 μM of sZipA-488, the protein was recruited to the liposome membrane. Scale bar: 5 μm . *Center*, after the addition of 6 μM of FtsZ-647, the protein is recruited to the liposome membrane. Scale bar: 5 μm . *Right*, the addition of 2.5 mM of GTP triggered the formation of protrusions. E) Optical sectioning carried out with a liposome on the surface of the chamber. The distance from the surface, in micrometers, is depicted on the upper-left corner of each image. Filaments on top of the liposome were clearly visible after 6 μm . Scale bar: 5 μm .

to the liposomes' membrane and the SLB (Figure 3.2 A *Center*). Finally, upon addition of GTP, large areas formed filament networks on the SLB (Figure 3.2 B). Nevertheless, liposomes did not markedly deform (Figure 3.2 A *Right*). Next, we carried out a similar experiment but with an increased concentration of FtsZ-647 (6 μM) and cholesterol was added to the liposome membrane (composition 2, Table 3.2). Moreover, the feeding solution contained 2 μM of sZipA-488, 1.5% of Ficoll70, 2.5 mM of GTP and glucose. While the liposomes were not immobilized with neutravidin to reduce spontaneous fusion of the liposomes, the glass surface of the silicone chamber was still passivated with BSA. sZipA-488, FtsZ-647 and GTP were sequentially added and liposomes were visualized. When sZipA-488 (Figure 3.2 D *Left*) and FtsZ-647 (Figure 3.2 D *Center*) were added, we obtained similar results as before with the exception that we did not observe the presence of significant areas with spontaneous SLBs. Upon addition of GTP (Figure 3.2 C and D *Right*) we detected potential liposome deformation events in the form of spikes and membrane projections. Additionally, optical sectioning of liposomes suggested the presence of filaments on their surface (Figure 3.2 E).

3.3.2 FtsZ-647 bundles inside liposomes under increased concentrations of K^+ and Mg^{2+}

Next, we were interested in observing the self-organization of purified FtsZ-647 inside liposomes in the background of PURE_{flex}. Because it has been shown that increasing amounts of K^+ and Mg^{2+} leads to longer FtsZ polymers and reduces the rates of GTP hydrolysis and subunit exchange^{191,192}, we wondered if this could lead to a greater tendency of purified FtsZ-647 to bundle inside liposomes. To test this, we encapsulated 2 μM of FtsZ-647 in PURE_{flex} 2.0 with additional K^+ and Mg^{2+} (a total of 240 mM and 18.7 mM, respectively; a 33% increase of the original concentration). K^+ and Mg^{2+} concentration was increased by adding potassium glutamate and magnesium acetate to the swelling and feeding solution. The liposome composition contained TxR for liposome visualization but no DGS-NTA (composition 4; Table 3.2). No membrane anchors of FtsZ were used. Samples were incubated at 37 °C for up to 6 hours in the chamber. After 4 hours, large FtsZ-647 protein filaments inside liposomes could be observed (Figure 3.3 B). In contrast, when the concentration of K^+ and Mg^{2+} was reduced to a total of 210 and 16.3 mM, respectively, the frequency of liposomes (composition 3; Table 3.2) exhibiting protein bundles was greatly reduced (Figure 3.3 A).

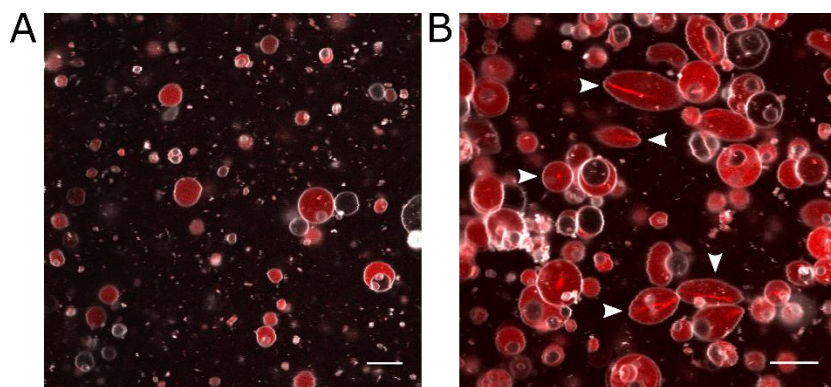


Figure 3.3 FtsZ-647 encapsulated together with PURE *frex* inside liposomes, bundles when both the swelling and the feeding solution are supplemented with extra K^+ and Mg^{2+}
 LSCM images of $2\ \mu\text{M}$ of encapsulated FtsZ-647, taken after 4 hours of incubation at $37\ ^\circ\text{C}$. White channel: liposome membranes. Red channel: purified FtsZ-647. Scale bar: $10\ \mu\text{m}$. A) Typical image of liposomes when only extra $20\ \text{mM}$ of K^+ and $2.3\ \text{mM}$ of Mg^{2+} were added. Protein bundles could be detected, but were infrequent. B) Typical image of liposomes when extra $60\ \text{mM}$ of K^+ and $4.7\ \text{mM}$ of Mg^{2+} were added. Filaments inside liposomes were very frequent. White arrow heads indicate some of the liposomes containing protein filaments

3.3.3 In-vesicle synthesis of FtsZ triggers the formation of protein bundles inside liposomes

Next, we sought to determine the effect of synthesized FtsZ and ZapA on protein self-organization inside liposomes. First, we verified the in-vesicle expression of proteins by encapsulating $5\ \text{nM}$ of *eyfp* inside liposomes (composition 3; Table 3.2). The reaction chamber was treated with BSA-Biotin and Neutravidin to immobilize liposomes, which facilitate the tracking of individual vesicles. Under these conditions, we detected the presence of synthesized eYFP after 30 minutes of expression. Figure 3.4 A displays the eYFP fluorescent intensity in the lumen of a single liposome every 5 minutes over the span of 70 minutes and shows a clear increase in intensity. The overnight incubation of the sample led to the production of a clear eYFP signal inside many of the liposomes (Figure 3.4 B, C).

As already seen in Section 3.3.2, the frequency of liposomes presenting protein filaments was low when the concentration of K^+ and Mg^{2+} was set to 210 and $16.3\ \text{mM}$, respectively. We hypothesized that increasing FtsZ concentration through in-vesicle expression could lower the requirement for high K^+ and Mg^{2+} concentration and promote bundle formation. As a negative control, we first tested the expression inside liposomes (composition 4; Table 3.2) of an unrelated protein (the protein TP from the phage $\Phi 29$ from DNA construct *p3-phi29*), to establish an activity baseline with $207\ \text{mM}$ and $16.1\ \text{mM}$ of K^+ and Mg^{2+} , respectively. The frequency of filament-containing liposomes (F) was monitored for up to 6 hours (Figure 3.5 A Left and B). At the final time point, this value reached $F=0.3\%$ ($\text{sd}=0.1$, $n=3$) of the total liposome population. Next, we tested whether the expression of *ftsZ* or *zapA* influences F under the same conditions. While the samples expressing *zapA* did not affect the frequency of filament-containing liposomes ($F=0.5\%$, $\text{sd}=0.3$, $n=3$; Figure 3.5 A Right and B), the samples expressing *ftsZ* increased this frequency up to $F=2.4\%$, $\text{sd}=1.0$, $n=3$, approximately eight times that of the baseline (Figure 3.5 A Right and B), indicating that the synthesized FtsZ favored the formation of bundles.

3 - In-vesicle synthesis of FtsZ

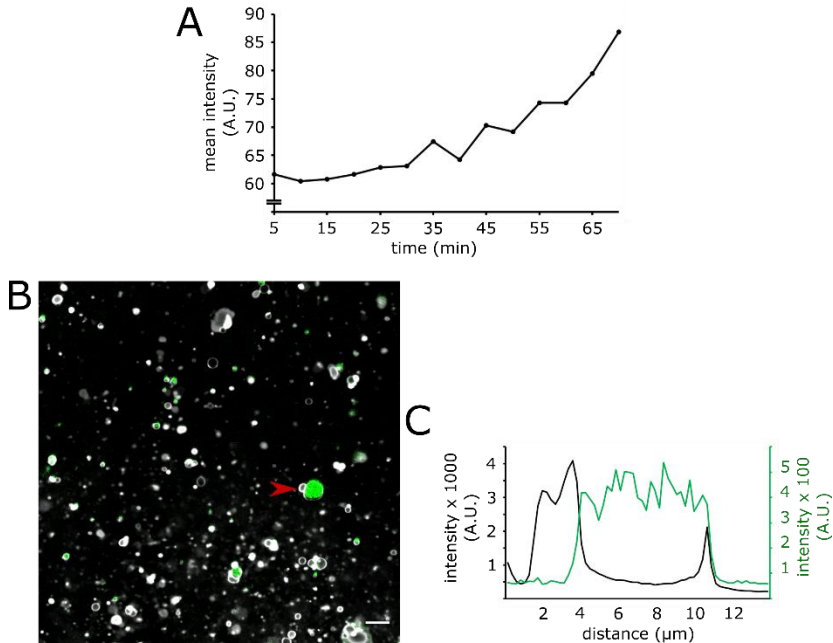


Figure 3.4 eYFP is synthesized inside liposomes.

Expression of the DNA template *eyfp* was carried out inside liposomes. A) One single vesicle was tracked for 70 minutes from the start of the reaction. The expression of *eyfp* over time was monitored and the mean pixel intensity (A.U.) of the inner area of the liposome was plotted as a function of time (minutes). The mean pixel intensity increases overtime. B) The sample was left to incubate at 37 °C overnight. Green channel represents eYFP and the white channel represents the liposome membrane (TxR). Scale bar: 10 μ m. C) Fluorescent intensity profile of the liposome marked with a red arrowhead in B. In green the channel corresponding with eYFP and in black, the channel corresponding with the liposome membrane (TxR).

Next, we sought to test whether GTP availability was a limiting factor for the synthesis or activity of FtsZ inside liposomes. Additional 1 or 2 mM of GTP was supplemented in a reaction with the *ftsZ* gene. The samples were incubated at 37 °C and the protein activity was monitored for up to 6 hours (Figure 3.5 C and D). Under these conditions, both GTP concentrations gave similar frequencies than without extra nucleotide ($F \approx 2$ -2.5%, $n=1$), suggesting that GTP is not a limiting factor under these conditions.

Next, we wondered whether the co-expression of *ftsZ* and *zapA* would have an influence on F . We reasoned that the presence of both FtsZ and ZapA might further promote the bundling of protein filaments. We performed three different types of co-expression: *ftsZ* plus *zapA*, *ftsZ* plus *p3-phi29* and *zapA* plus *p3-phi29*. In all cases, the concentration of each DNA template was 5 nM. As shown in Figure 3.6 A, after 6 hours, co-expression of *zapA* and *p3-phi29* gave an F value similar to the baseline ($F=0.3\%$, $sd=0$, $n=2$), while co-expression of *ftsZ* and *zapA* ($F \approx 2.2\%$, $sd=0.5$, $n=2$) and co-expression of *ftsZ* and *p3-phi29* ($F=1.2\%$, $sd=1.5$, $n=2$) were higher.

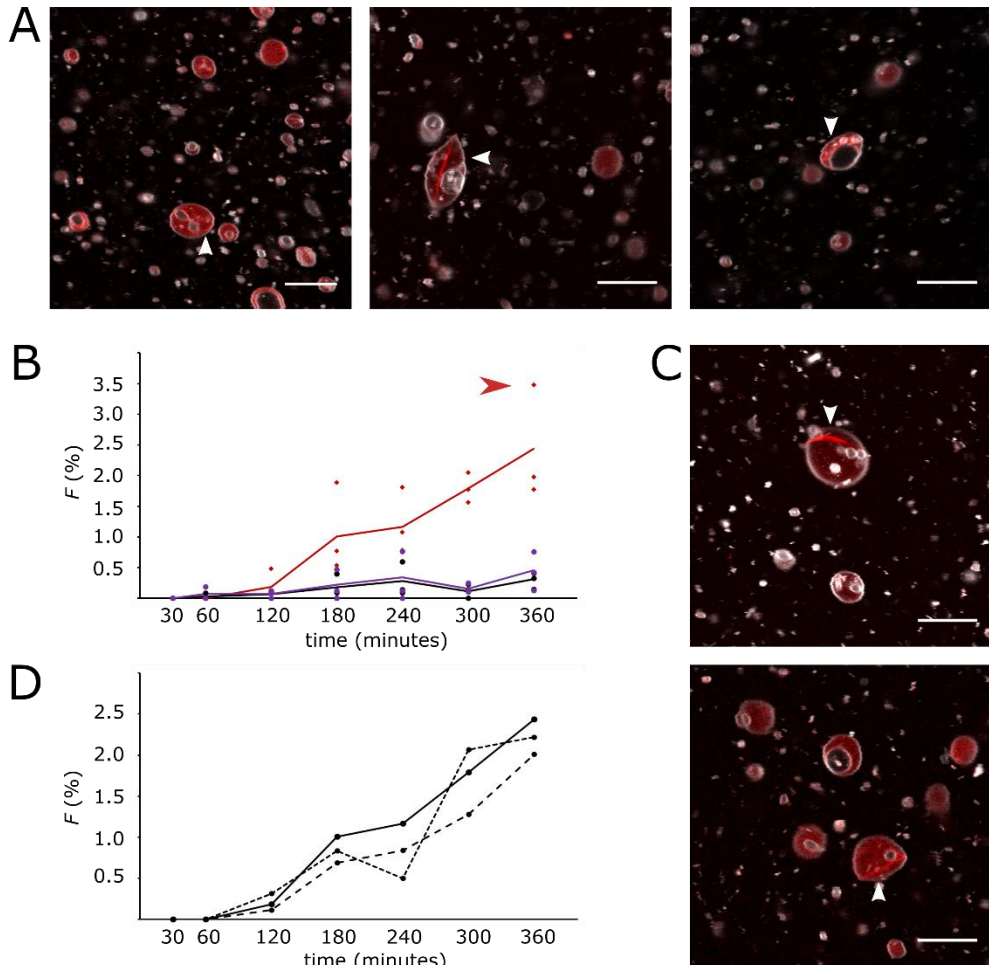


Figure 3.5 In-vesicle expression of *ftsZ* and *zapA*.

LSCM images of protein-expressing liposomes. A) Image of liposomes expressing *tp-phi29* (Left), *ftsZ* (Center) or *zapA* (Right) after 6 hours of expression. In all cases protein filaments were detected (white arrowheads). B) The averaged fraction of filament-containing liposomes (F) when *p3-phi29*, *ftsZ* or *zapA* were expressed inside liposomes was tracked during 6 hours (lines). Each condition was repeated 3 times (dots). The samples expressing *p3-phi29* and *zapA* showed a baseline activity of $F \approx 0.3\%$, while the sample expressing *ftsZ* increased the fraction of filament-containing liposomes eight times ($F \approx 2.4\%$). The data marked with a red arrowhead has been used for the analysis of liposome roundness in Section 3.3.4. C) Images of liposomes expressing *ftsZ* with 1 mM (Top) or 2 mM (Bottom) of extra GTP after 5 (Top) or 6 (Bottom) hours of expression. Protein filaments inside liposomes were detected (white arrowheads). D) F value of samples expressing *ftsZ* (from A) or expressing *ftsZ* with 1 or 2 mM of extra GTP (from C) was tracked during 6 hours. All samples showed a similar proportion of filament-containing liposomes ($F = 2-2.5\%$). Scale bar in all images: 10 μm .

3 - In-vesicle synthesis of FtsZ

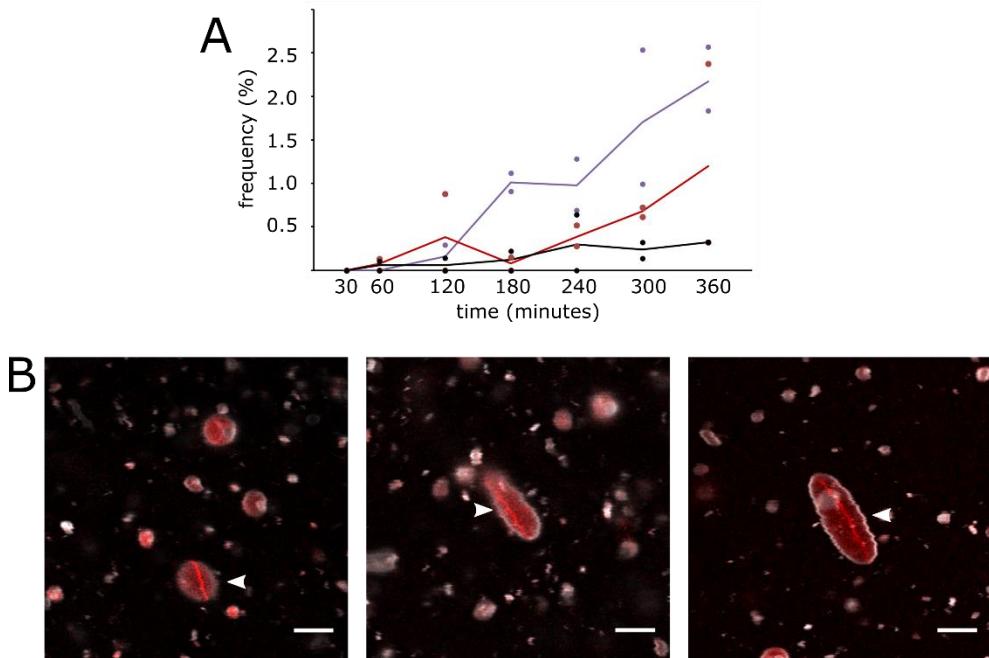


Figure 3.6 In-vesicle co-expression of *ftsZ* and *zapA*

Co-expression of a combination of the constructs *ftsZ*, *zapA* and *p3-phi29* inside liposomes was carried out. A) The fraction of filament-containing liposomes (F) when *ftsZ* plus *zapA*, *ftsZ* plus *p3-phi29* or *zapA* plus *p3-phi29* were expressed inside liposomes was tracked during 6 hours. While the *zapA* and *p3-phi29* combination showed a baseline activity of $F=0.3\%$, both the *ftsZ* plus *zapA* ($F=2.2\%$) and *ftsZ* plus *p3-phi29* ($F=1.2\%$) combinations showed a higher fraction of filament-containing liposomes. B) Image of liposomes expressing *ftsZ* plus *zapA* (Left), *ftsZ* plus *p3-phi29* (Center) or *zapA* plus *p3-phi29* (Right) combinations after 6 hours of expression. FtsZ-647 is shown in the red channel and liposome membrane in the white channel (TxR). Scale bar in all images: 5 μm .

3.3.4 FtsZ protein bundles push-out the liposome membrane from the inside

Many of the liposomes containing an FtsZ filament in their lumen seemed to present an elongated morphology (Figure 3.3 B, Figure 3.5 A, C and Figure 3.6 B). If filaments were indeed the cause of liposome deformation, we wondered what the level of membrane stretching was and sought to quantify it by measuring the general roundness of the liposome population. We performed the analysis in one of the samples expressing *ftsZ* for 6 hours (Figure 3.5 B). We divided the total population of this sample (774 liposomes) in liposomes where no filament was detected (734 liposomes; negative subpopulation) and liposomes containing at least one filament (30 liposomes; positive subpopulation). From the negative subpopulation, 60 liposomes were selected at random to constitute the control sample while we kept the positive subpopulation intact to constitute the testing sample. Next, we proxied the roundness of each liposome in both samples. The elongation ratio (E) that we utilized (Equation 3) equals to 1 for perfectly spherical liposomes, and gives higher values with increasing elongation of the liposome. We found that the control sample had a significantly lower ratio than the sample population ($E=1.17$, $sd=0.11$ $n=60$ and $E=1.59$, $sd=0.78$, $n=30$, respectively; Mann-Whitney U test, $U=241$, $p<0.05$, two-tailed; Figure 3.7 A).

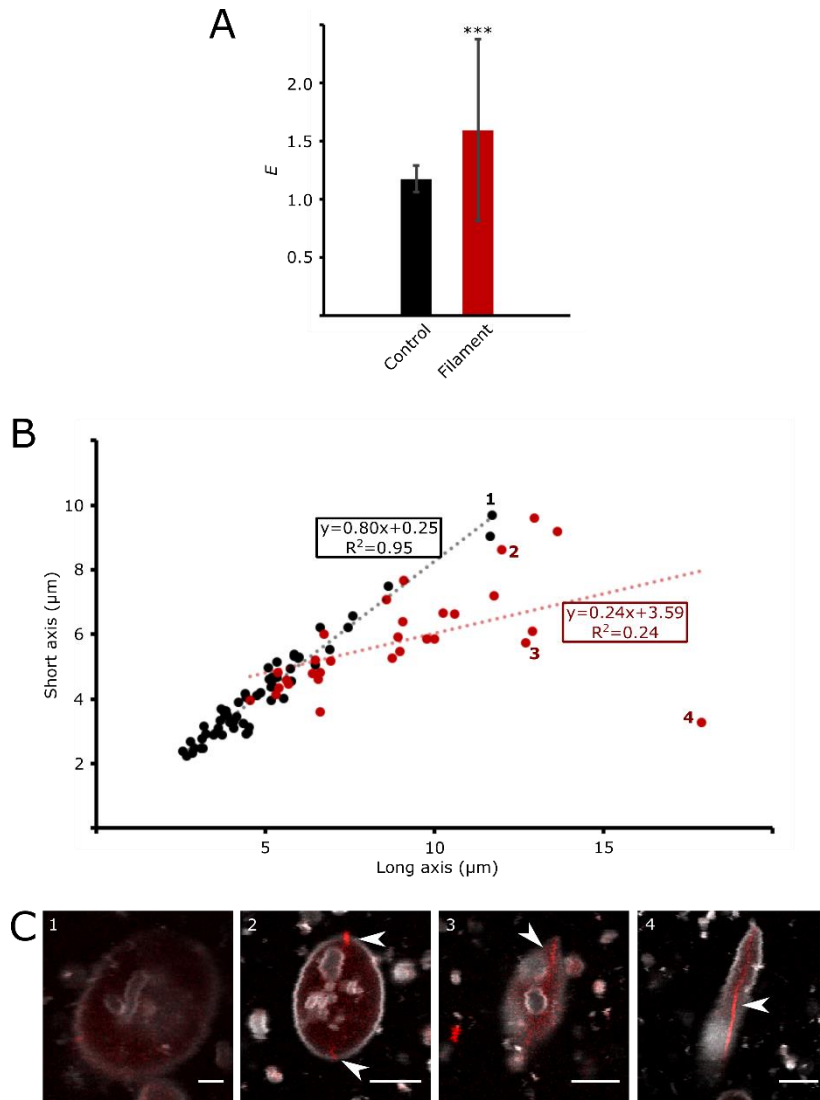


Figure 3.7 FtsZ/FtsZ-647 filaments formed inside liposomes deform and elongate the vesicle.

A) Comparison of the mean elongation ratio (E) between the control sample (constituted of a random selection of liposomes not containing an FtsZ filament in their lumen; $n=60$) and the testing sample (all filament-containing liposomes; $n=30$). The data used here have been taken from one of the samples expressing *ftsZ* in Figure 3.5 B (after 6 hours of expression; marked with a red arrowhead). Error bars in standard deviation (sd). The difference between groups is significant (p -value < 0.001). B) Data represented as a plot of the long, versus short axis (μm) of both the control (black dots) and testing sample (red dots). Two simple linear regressions were calculated for both the control sample [$0.80(\text{long axis}) + 0.25$, $R^2=0.95$] and the testing sample [$0.24(\text{long axis}) + 3.59$, $R^2=0.24$]. C) LSCM images of liposomes from the data in A and B. The number at the upper-left corner of each image corresponds to the numbered data points in B. As can be seen, the farther away the data points from the trend line of the control sample, the more elongated the liposome. Scale bar in all images: $5 \mu\text{m}$.

Additionally, we plotted the length (μm) of the short against the long axis of each liposome in both the control and the test samples (Figure 3.7 B, C) and the data were fitted by linear regression (Figure 3.7 B). The control sample showed a slope relatively close to 1 (0.80), as expected for spherical liposomes, and almost all variation of the sample could be explained by the model ($R^2=0.95$). In the other hand, the test sample showed a lower slope (0.24) and the data were more dispersed ($R^2=0.24$). Interestingly, almost no filament-containing liposome was observed presenting an apparent diameter of $5 \mu\text{m}$ or lower unlike with the control sample.

3.4 Discussion

Here, we have explored the possibilities of creating an FtsZ-based artificial division system for synthetic cells. We envisioned this system as a reconstitution of the Z-ring in liposomes. Furthermore, we sought to test the potential of the PURE system as our main *in vitro* transcription and translation machinery. We regard the in-vesicle synthesis of proteins as a major milestone on the construction of artificial cells, not only as a way to genetically control the *cellular* dynamics but also as a necessary feature to develop self-reproducing minimal cells.

In this study, we have shown the self-organization of purified FtsZ-647 and cell-free synthesized FtsZ and ZapA inside liposomes. We found that under

increasing concentrations of K^+ and Mg^{2+} , purified FtsZ-647 condenses and bundles in the form of filaments even in the absence of any crowding agent like Ficoll70. Interestingly, when FtsZ was synthesized in vesicle and under non-condensing conditions, eight times increase in the frequency of filament-containing liposomes was observed compared to the control condition. Strikingly, the in-vesicle assembled FtsZ filaments pushed out and deformed the liposomes.

3.4.1 The assembly of protein filaments inside the liposome lumen can be triggered with an increased concentration of K^+ and Mg^{2+}

FtsZ is incontestably one of the most important proteins of bacterial cell division. For already some time it has been believed that, at least in part, FtsZ is responsible for the constriction of the inner cell membrane. Although this hypothesis has been challenged by new *in vivo* results^{104,164,193-195}, *in vitro* studies performed already several years ago showed the capacity of FtsZ to remodel membranes^{51,187,188,196,197}. In some conditions FtsZ can assemble protein rings on the inner leaflet of liposome membranes, which generates constriction forces^{187,197,198}. For this reason, we still consider FtsZ a potential and promising synthetic cell division mechanism. Nonetheless, it has been calculated that *in vivo*, the Z-ring would not be able to exert more than approximately 100 pN of constriction force¹⁹⁵. This is insufficient to compete with the cell turgor, even when the matured Z-ring consists of condensed filaments. *In vitro*, the formation of bundles seems to be important to generate enough deforming force as well¹⁸⁷ and therefore a synthetic cell would be expected to require the presence of an FtsZ protofilament condenser. However, the required force to do this would be in the order of 10 pN or less¹⁹⁹.

Since we were able to synthesize an active FtsZ protein in the previous chapter (Section 2.3.2, page 46), we decided here to investigate its self-organization in the inside of liposomes. Despite FtsZ being a protein that evolved to indirectly interact with phospholipid membranes through its membrane binding partners, we managed to bundle purified FtsZ-647 protofilaments in the lumen of liposomes under low protein concentration compared to experiments in literature (for example $7 \mu\text{M}$ FtsZ-YFP and $7 \mu\text{M}$ FtsA* in Osawa and Erickson¹⁰⁹, or $12 \mu\text{M}$ FtsZ and $5 \mu\text{M}$ sZipA in Cabre et al.¹⁰⁷), without any crowding agent like ficoll70 or the

presence of FtsA or ZipA. Under these conditions, a high proportion of the total liposome population contained FtsZ-647 bundles (Figure 3.3 B). This was done in the PURE_{flex} system with an increased K⁺ and Mg²⁺ concentration (240 mM and 18.7 mM, respectively). Increasing concentration of K⁺ and Mg²⁺ was already known in literature to enhance FtsZ polymerization¹⁹¹. Interestingly, when the levels of K⁺ and Mg²⁺ were reduced to 200 mM and 16.3 mM, respectively, the presence of filaments was greatly reduced (Figure 3.3 A).

One interesting feature of these filaments is their tendency to be straight (Figure 3.3 B) compared to the ones seen typically in literature^{107,187,188,196,197,200-202}. Usually, when FtsZ filaments are assembled inside vesicles, they take the shape of the liposomes, or arrange in a mesh, either cortically or in the vesicle lumen (Figure 1.5, page 20). This morphological difference could be attributed to the complex buffer of the PURE_{flex} system or the presence of a relatively high ionic strength. *In vivo*, while the cytoplasm is expected also to be highly complex and dense (e.g. 200-400 mM of K⁺ and 2-3 mM of free Mg²⁺)^{203,204} other FtsZ-interacting proteins are present to recruit filaments to the membrane and modulate lateral interactions.

3.4.2 The assembly of FtsZ filaments inside liposomes can be genetically controlled

In Figure 3.5 B we showed how the in-vesicle expression of *ftsZ* increased the proportion of filament-containing liposomes to $2.4\% \pm 1.0$ under a total K⁺ and Mg²⁺ concentration of 207 mM and 16.1 mM, respectively. In contrast, when the unrelated *tp-phi29* gene was expressed, this value only reached $0.3\% \pm 0.1$, eight times less than with *ftsZ*. This result shows that the formation of bundles is dependent on the expressed FtsZ protein, and is therefore genetically controlled. This achievement is key in the production of synthetic cells, since it establishes a clear link between genotype and phenotype. Although the most likely cause of filament formation is the total concentration of active protein, our experimental system is not equivalent to the incorporation of purified protein from the beginning of the experiment, since in our case FtsZ concentration increases over time. In this regard, it would be interesting to examine the dynamics of filament formation as a function of the increasing amount of FtsZ.

We attempted to achieve similar results by in vesicle expressing *zapA* under the same conditions as above. We expected the synthesized ZapA to have enough crosslinking capacity to trigger the formation of bundles. However, the proportion of liposome-containing liposomes was similar to the baseline (Figure 3.5 B). One of the reasons might be a low production of ZapA. In Chapter 2 of this thesis, we have already shown an example of a GreenLys SDS-PAGE of in-bulk synthesized ZapA and, while the protein is clearly produced, the signal is low (Figure 2.4 D). This could be an effect of the relatively lower density of Lys in the amino acid sequence of the protein ($\frac{4}{109} = 3.7\%$), for example compared to FtsZ ($\frac{17}{383} = 4.4\%$). Optimized synthesis conditions like the use of chaperones could be also tried to increase the level of active protein. Finally, ZapA might be less efficient at interacting or bundling FtsZ protofilaments in solution than when attached to the membrane. This could explain why we achieved the bundling of FtsZ filaments on SLBs without the presence of Ficoll70 (Section 2.3.5, page 52) but failed to observe the same here.

Co-expression inside liposomes was also carried out (Figure 3.6). We tried three different combinations: *ftsZ* plus *zapA*, *ftsZ* plus *tp-phi29* and *zapA* plus *tp-phi29*, the latter two conditions corresponding to negative controls of dual-gene expression. In the first place, we were looking for a favorable effect when expressing both FtsZ and ZapA. We expected that the *ftsZ* and *zapA* combination would give more filament-containing liposomes (higher *F*) than

the single expression of *ftsZ*. This was not the case, with an $F = 2.2\% \pm 0.5$, compared to the $2.4\% \pm 1.0$ obtained with the expression of *ftsZ* (Figure 3.5 B and Figure 3.6 B). This might not be so unexpected after all, considering the lack of effect detected when only *zapA* was synthesized. In the case of *ftsZ* and *tp-phi29*, F equaled to $1.2\% \pm 1.5$, further away from the 2.4% reached with single *ftsZ* expression. As we have seen in Figure 2.4 (page 47), expression of *p3-phi29* seems highly efficient compared to the expression of *ZapA*, even though the occurrence of Lys is higher in TP ($\frac{26}{266} = 10.1\%$) than in FtsZ (4.4%) and in *ZapA* (3.7%), which may bias the estimation of protein concentration from a GreenLys gel analysis.

With these results, we have established a strong link between the genetic material in the liposome and the presence of filaments.

3.4.3 Filament-containing liposomes show an elongated morphology

Surprisingly, we found that the in-vesicle filaments are able to deform outwards the membrane of the liposomes into elongated shapes, mostly fusiform and lemon-shape (Figure 3.3 B, Figure 3.6 B and Figure 3.7 C). Although there are abundant cases in literature where FtsZ filaments are assembled in the lumen of liposomes^{107-109,188,198}, the overall shape of the liposomes is never affected if the filaments are not attached to the membrane. For example, Furusato et. al.¹⁰⁸ synthesized *de novo* FtsZ-sfGFP inside liposomes containing 12% Ficoll70 and obtained a cortical network of bundles. Despite the thickness and high number of bundles, the liposomes remained spherical. This was not the case when a membrane anchor was included. Of course, the type of phospholipids utilized in the different studies matters when considering vesicle shape remodeling. For example, it is known that increasing concentrations in the liposome membrane of acidic, e.g. phosphatidylglycerol (PG), with respect to neutral phospholipids, e.g. phosphatidylcholine (PC) influences the bending elasticity and tension of the vesicle, increasing the resistance of the liposome to stretching¹⁹⁹.

We quantified the elongation of one sample expressing *ftsZ* in vesicle after 6 hours of incubation (Figure 3.7). We found that the mean elongation factor (E) of the control sample (no filament detected in the lumen) was 1.17 ± 0.11 , while it reached 1.59 ± 0.78 for the positive sample, i.e. when at least a filament was found inside the liposome. Both subpopulations show pronounced heterogeneity of E values (Figure 3.7 A). First, not all filament-containing liposomes are elongated. The reason could be as simple as having a bundle not strong or long enough to deform the liposome. Second, laser-confocal microscopy images capture only a planar section of the liposomes. This means that the liposomes that do not align perfectly to the focus plane will seem less elongated than they actually are. In these conditions, it is expected that the standard deviation of E is higher for the filament-containing liposomes than for the control sample.

3.4.4 Conclusions and outlook

To conclude, in Section 3.3.3 we demonstrated the relationship between the expression of genes and the presence of FtsZ filaments. This shows the potential of the PURE system to be used as the protein factory to decode DNA sequences and generate active proteins in model synthetic cells. In Section 3.3.4, we have demonstrated that non-membrane-bound FtsZ filaments influence the liposome shape. The link between genotype and function that we have described here is one of the most important features that an artificial cell must harbor to be capable of Darwinian evolution.

Future lines of research should aim to synthesize FtsZ membrane anchors like ZipA or FtsA (Section 2.3.3 and Section 2.3.4). Alternatively, a modified FtsZ fused to a membrane targeting

sequence could be utilized in order to reduce the load on the PURE system (Chapter 4), although the expression of chimeric proteins would probably result in less physiological protein filaments.

Acknowledgements

We thank Germán Rivas' lab at Centro de Investigaciones Biológicas (CSIC) in Madrid for providing the purified proteins used in this chapter. We thank Ilias Zarguit for excellent laboratory work and fruitful discussions. We thank Jeremie Capoulade for the LSCM training and technical support. We thank Alicia Soler and Duco Blanken for help with the LSCM.

Chapter 4

FtsZ-MTS on SLBs and inside liposomes

Metabolism is a defining feature of living organisms. The synthesis of DNA-encoded proteins is one of the most fundamental enzymatic pathways in the cell, pillar of a myriad of other metabolic routes. In model artificial cells constructed from the bottom-up, this task can be carried out by a purified and well-defined collection of enzymes and compounds known as the PURE system. However, in its current state, this technology is limited by a low protein yield and synthesis life-span. A plausible workaround of these limitations is the creation of chimeric proteins with multiple functionalities, therefore reducing the load on the metabolic machinery. In this chapter, we assayed the activity of two chimeric versions of FtsZ, engineered to target phospholipid bilayers in the absence of its native membrane-anchoring proteins ZipA and FtsA. Our engineered FtsZ's contained a 6-histidine tag (FtsZ-His) or the membrane targeting sequence from FtsA (FtsZ-A), which consists of 15 residues, at their C-terminus. We found that our chimeric FtsZ proteins were recruited to planar membranes and sustained the formation of dynamic cytoskeletal structures. Dynamical behaviors included condensation of filaments and constriction of protein rings. These structures could also form on the outer leaflet of free-standing liposome membranes. However, no activity was detected when FtsZ-His was synthesized in vesicles. Further optimization will be required, in particular to tune the relative amounts of membrane-targeted and cytosolic FtsZ variants. We believe that our chimeric FtsZ proteins retain crucial dynamics necessary in the construction of artificial divisomes. Moreover, they are a good alternative to multi-protein complexes in the context of minimal cells with challenged metabolic machineries.

4.1 Introduction

Division in rod-shaped bacteria like *E. coli* is governed by a multiprotein complex known as the divisome^{164,205}. This complex assembles at midcell guided and regulated by the dynamic activity of a ring-like structure known as the Z-ring⁵⁰. This structure is composed of FtsZ, a cytoplasmic essential protein²⁰⁶. FtsZ's core functionality, i.e. polymerization upon GTP binding³⁹ and Mg²⁺ dependent GTPase activity⁴⁵, resides at its N-terminal globular domain. This domain is as well responsible for the further assembly of FtsZ protofilaments into bundles, giving rise to the cytoskeletal structures observed both *in vivo* and *in vitro*^{105,188}. At the C-terminus of the protein, a short 12 amino acid domain (CTV) regulates the lateral interactions of FtsZ protofilaments¹⁷⁶. However, its main task is to interact with a wide range of different division related proteins²⁰⁷. While FtsZ does not possess the ability to directly interact with the membrane, the Z-ring is anchored to the inner leaflet of the cytoplasmic membrane via two other divisome proteins: FtsA and ZipA. FtsA is an essential protein belonging to the acting family of ATPases⁶⁴. It contains a membrane targeting sequence (MTS) consisting of an amphipathic helix of 15 amino acids long at the C-terminus of the protein⁷⁰. This C-terminal domain is involved as well in other functions. For example, residue W415 is required for FtsA localization at the Z-ring and its deletion causes self-interaction deficiencies⁶⁷. Nonetheless, the globular domain of FtsA is the main responsible of many of the most essential tasks of FtsA. It is essential for self-interaction¹⁶⁵, recruitment of other late division proteins like FtsN (residues 83 to 176)¹⁰⁰ and very importantly, interaction with the FtsZ's CTV domain¹⁷⁸. In the other hand, ZipA, an essential divisome protein, contains a hydrophobic transmembrane domain at the C-terminus which efficiently integrates in lipid bilayers. It is connected to the globular domain through a flexible and unstructured positively charged linker (residues 29 to 85)⁷⁵. Like with FtsA, ZipA's globular domain mediates the interaction with the FtsZ's CTV domain^{57,169}.

An amphipathic helix similar to the one in FtsA is the amphipathic helix (MTS) of MinD⁷⁰. It has been shown that MinD's MTS is transplantable. The MTS from *Escherichia coli* MinD or *Bacillus subtilis* MinD is a transplantable sequence and is able to target any peptide to the membrane²⁰⁸. In 2008, Osawa and Erickson¹⁹⁷ refined this idea by swapping the FtsZ CTV's domain with the MinD's MTS sequence, and inserting a YFP between the flexible linker and the MTS, producing a chimeric protein (FtsZ-YFP-MTS). They showed that this protein was able to produce Z-rings *in vivo*, although progression of the division was blocked. They also assayed this FtsZ-MTS in tubular liposomes and they claimed that the protein assembled in Z-rings capable of partial membrane constriction. After this, many studies have been performed using this FtsZ version *in vitro*^{36,68,71,86,87}. For example, Ramirez-Diaz et al.³⁶ studied the self-organization patterns produced by this protein on supported lipid bilayers (SLBs). Since FtsZ-YFP-MTS was able to directly target the membrane, FtsA or ZipA were not needed. Interestingly, they observed protein patterns highly similar to the ones found by Loose and Mitchison⁵⁹ with FtsZ-FtsA-ZipA, including filament networks and dynamic rings. This allowed them to relate the formation of these patterns exclusively with the intrinsic dynamics of FtsZ, and not as a result of the FtsZ-FtsA or FtsZ-ZipA interaction, as was regarded before⁵⁹.

MTS-containing FtsZ could be utilized for the implementation of an FtsZ-based minimal divisome in model artificial cells. In this context, *in situ de novo* synthesis of proteins is an important feature of a self-sufficient cell. However, despite the numerous experiments focused on the *in vitro* reconstitution of FtsZ-MTS filaments, no experiments have been reported on cell-free synthesis of FtsZ-MTS. In this chapter, we will explore the possibilities of PURE_{flex} synthesized FtsZ-MTS on SLBs and in liposomes as a plausible minimal and functional

divisome. The goal is to obtain an FtsZ-MTS capable of membrane binding, polymerization and bundling into filament networks and protein rings. Since one of the limitations of the PURE system is its relatively low protein yield compared to *in vivo* production or cell-free extracts, the use of multi-function fusion proteins offers an attractive alternative to the wild-type versions. However, FtsZ-MTS versions as the FtsZ-YFP-MTS are not suitable in a PURE system context due to its relatively high molecular weight and folding into distinct domains. Consequently, we constructed two versions of FtsZ-MTS by attaching at the C-terminus of the protein a 6-histidine tag (FtsZ-His) or the MTS from FtsA (FtsZ-A).

On planar membranes, we confirmed the production of dynamic cytoskeleton patterns with FtsZ-His and FtsZ-A, indicating that the synthesized proteins possessed the capacity of membrane binding, polymerization and bundling. On the outside of liposomes, cell-free synthesized FtsZ-His assembled into bundles but we did not observe liposome membrane deformation. Moreover, in-vesicle synthesis of FtsZ-His was not able to recruit FtsZ to the membrane under the conditions tested.

4.2 Materials and methods

4.2.1 Purified proteins and DNA templates for cell-free expression

Purified protein FtsZ-647 was utilized. A description can be found in Section 2.2.1 (page 37).

Two different FtsZ DNA templates were prepared. *ftsZ-his* codes for a wild-type *E. coli* FtsZ with a 6-histidine tag fused at the C-term as a membrane targeting sequence (MTS). Like *ftsZ-his*, *ftsZ-a* codes for an *E. coli* wild-type FtsZ but with the MTS from the *E. coli* FtsA₍₄₀₅₋₄₂₀₎(FtsA). *ftsZ*, *zapA* and *p3-phi29* DNA templates were also utilized and were prepared as described in Section 2.2.1. A complete and detailed account of the DNA sequences and their features can be found in the Appendix (page 154).

To prepare *ftsZ-his*, a standard PCR (Table 2.1, page 37) was performed on a regular *ftsZ* DNA template with the primers ChD 509 and ChD 600 (Table 4.1). Both primers contain overhangs for the plasmid pET11-a and primer ChD 600 also introduces a 6-histidine DNA sequence at the 5' end of *ftsZ-his*. After NdeI digestion at 37 °C for 1 hour, a Gibson assembly (Gibson Assembly® Master Mix of New England BioLabs® Inc) of the PCR product was performed with a linearized pET11-a plasmid (equimolar concentrations) for 1 hour at 50 °C. Next, the assembled products were transformed into *E. coli* TOP10 competent cells via heat shock, after which the cells were centrifuged and resuspended in 50 µL of fresh liquid LB medium and incubated at 250 rpm for 1 hour at 37 °C. Next, cultures were plated in solid LB medium with 0.05 ng/µL of ampicillin and grew overnight at 37 °C. A selection of colonies that grew on the plates were cultured in 1 mL of liquid LB medium with 0.05 ng/µL of ampicillin at 250 rpm for 6 hours at 37 °C. Plasmid purification (PureYield™ Plasmid Miniprep System, column method, Promega) was carried out and production of linearized DNA constructs from the above purified plasmids was done with the primers ChD 194 and ChD 181 (Table 4.1) in a standard PCR amplification reaction program (Table 2.1, page 37). The PCR products were analyzed on a standard DNA agarose gel (1%; Et. Br. or SYBR safe) to check for inserts. Positive colonies were grown overnight at 37 °C and 250 rpm in fresh LB medium with 0.05 ng/µL of ampicillin, and stored at -80 °C in 10% glycerol (v/v).

To prepare *ftsZ-a*, primers ChD 194 and ChD 764 (Table 4.1) were used to amplify a regular *ftsZ* DNA template with a standard PCR program. Since ChD 764 contains at its 3' end the DNA region of FtsA coding for the MTS (nucleotide positions 1215 to 1260 of the FtsA ORF),

Table 4.1 List of primers and sequence

Name	Sequence (5' to 3')
ChD 181	CAAAAAACCCCTCAAGACCCGTTTAGAGG
ChD 194	TAATACGACTCACTATAGGGGAATTGTGAGCGGATAACAATTCCCCT
ChD 509	TTAACTTTAAGAAGGAGATATACATATGTTTGAACCAATGGAACCTTACC
ChD 600	TCCTTTCGGGCTTTGTTAGCAGCCGGATCCTTAATGGTGATGATGGTGATGATCAGCTTGCTTACGAG
ChD 764	TTACATCATCTGATCCAAACGCAGTATTAAGATAATAACGCCCGCGATGGCTATGATAGCTAACAGTACATGACCGAACCGAGGTATCAGCTTGCTTACGCAGGAATGC

the PCR product resulted in the *FtsZ-a* DNA template. In this case, no T7 terminator was inserted at the 3' end of the construct, as such a feature is not essential for termination of the T7 RNA polymerase on a linear DNA.

4.2.2 PURE_{flex} synthesis of proteins in bulk

The synthesis of proteins in batch mode was always carried out as described in Section 2.2.6 (page 41), regarding the expression of proteins with PURE_{flex}. For experiments involving single expression of a DNA template, the concentration was always of 5 nM. For two-gene expression experiments, 4 nM of *ftsZ-his* and 7 nM of *zapA* were used. Unless otherwise specified, expression was carried out at 37 °C for 3 hours.

4.2.3 SDS-PAGE analysis of synthesized FtsZ-His

Analysis of the synthesized FtsZ-His on SDS-PAGE was carried out as described in Section 2.2.7 (page 41) unless otherwise specified in the relevant sections.

4.2.4 Production of SLBs

SLB formation was produced as described in Section 2.2.5 (page 40). To test the activity of FtsZ-His, the membrane composition consisted of 1,2-dioleoyl-sn-glycero-3-phosphocholine (DOPC), 1,2-dioleoyl-sn-glycero-3-phospho-(1'-rac-glycerol) (DOPG) and 1,2-dioleoyl-sn-glycero-3-[(N-(5-amino-1-carboxypentyl) iminodiacetic acid) succinyl] (nickel salt) (DGS-NTA) in a 78:18:4 (mol%) ratio. In addition, FtsZ-His was tested with a membrane consisting of *E. coli* polar lipids [phosphatidylethanolamine (PE), phosphatidylglycerol (PG), 1,3-bis(sn-3'-phosphatidyl)-sn-glycerol (cardiolipin or CA) and DGS-NTA (67:23:9:1 mol%)]. To test the activity of FtsZ-A, the membrane composition consisted exclusively of DOPC and DOPG (80:20 mol%). Table 4.2 summarizes the phospholipid composition of each type of membrane.

4.2.5 Activity assays on SLBs

Unless otherwise specified, activity assays on SLBs with PURE_{flex} synthesized proteins were carried out as described in Section 2.2.9 (page 43).

4.2.6 Activity assays of FtsZ-His on the outside of liposomes

Activity assays of FtsZ-His in the outside of liposomes was carried out as described in Section 3.2.5 (page 68), with a few exceptions. First, glucose and sucrose were not added in the swelling and feeding solutions, respectively. Second, the lipid beads were incubated on ice. And third,

Table 4.2 Lipidic composition of SLBs

Abbreviation and concentration (mol%) at which each phospholipid was mixed for each different composition. FtsZ-His was tested on SLBs with compositions A and B. Both compositions contained DGS-NTA to allow the recruitment of FtsZ-His. FtsZ-A was tested on SLBs with composition C. PE, PG and CA refers to the most abundant lipids present in the *E. coli* polar extract.

Composition	DOPC	DOPG	PE	PG	CA	DGS-NTA
A	78	18	--	--	--	4
B	--	--	66	23	10	1
C	78	18	--	--	--	--

assays were performed in glass chambers. The expression of *ftsZ-his* was done as described in Section 4.2.2.

4.2.7 Activity assays of in-vesicle synthesized FtsZ-His and ZapA

Unless otherwise specified, in-vesicle PURE_{flex} synthesis (but not PURE_{flex} 2.0) of proteins was done as described in Section 3.2.6 (page 68). In this case, compositions 1 and 3 of Table 3.2 (page 67) were utilized.

4.2.8 Microscopy

In experiments on SLBs, images were acquired with an Olympus IX81 Inverted TIRF microscope with a 150x UApO_NTIRF oil objective (NA 1.45). Excitation laser line of 640 nm (FtsZ-647) was utilized to visualize the purified protein. Images were captured with an EM-CCD camera (iXion X3 DU897, Andor technologies). Olympus cell[^]TIRF illuminator and Andor IQ3 were used as control and acquisition software. Temperature was controlled with a T-unit bold line (OKOlab). In liposome experiments, images were acquired with a laser scanning confocal microscope (Nikon confocal A1R/Sim) equipped with the laser line 640 nm (FtsZ-647) and a 100x oil immersion objective (1.49 NA).

4.2.8.1 Image analysis

Analysis of images collected in SLBs and liposomes experiments was performed with ImageJ²¹⁰ or ImageJ²¹⁷¹. In general, images were adjusted for brightness and contrast. If specified in the relevant sections, average images (AVG) were computed by taking the average pixel intensity of a sequence of pictures of the same region of the sample. Optionally, a background subtraction was applied to SLB images, with a roll balling radius of 50-250 pixels, depending on the image.

4.3 Results

4.3.1 FtsZ-MTSs are synthesized in PURE_{flex}.

First, we sought to confirm the PURE system expression of *ftsZ-his* and *ftsZ-a*. *ftsZ-his* codes for a *E. coli* wild-type FtsZ plus a 6-histidine tag fused to its C-term. Instead of the 6-histidine tag, *ftsZ-a* codes for an FtsZ with the amphipathic MTS from FtsA. We expressed these constructs (5 nM) in a reaction of PURE_{flex} supplemented with GreenLys and analyzed the translation products on an SDS-PAGE (Figure 4.1). Both FtsZ-His and FtsZ-A bands were compared with a positive control containing the translation products of a regular PURE_{flex} expression with

the *FtsZ* construct. Details concerning *ftsZ* can be found in Appendix (page 154) and has been extensively utilized and validated in this thesis (Section 2.3.2, page 46). For each construct, expression of single bands at the expected molecular weight were achieved, confirming that full-length FtsZ-MTS proteins can be produced.

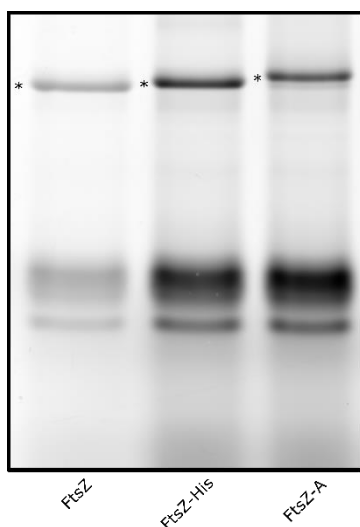


Figure 4.1 SDS-PAGE analysis of PUREfrex expressed MTS-containing FtsZ's constructs.

The translation products of a singled expression of *ftsZ*, *ftsZ-his* and *ftsZ-a* in a regular GreenLys PUREfrex reaction were analyzed on a SDS-PAGE. The resulting protein bands are marked with the symbol (*).

4.3.2 FtsZ-His recruits purified FtsZ-647 to the membrane and produces short bundles

Next, we wondered whether the protein yield of *ftsZ-his* was comparable to that of a regular *ftsZ*. To test this, we carried 2 sets of PURE system reactions: at 22 and 37 °C. Per each condition, we performed three independent PUREfrex reactions with *ftsZ* and three others with *ftsZ-his*. Then, we analyzed the results in two different GreenLys SDS-PAGE (one gel per temperature condition; Figure 4.2 A and B, Left). The band intensities for the two conditions showed similar levels of fluorescent signal (t-test. At 22 °C: $t = 0.82$, $p = 0.46$; at 37 °C: $t = 1.24$, $p = 0.28$; Figure 4.2 A and B, Right). We concluded that cell-free expression of *ftsZ-his* or *ftsZ* yields similar protein production at the two tested expression temperatures. While not a quantitative approach, visual inspection of the fluorescent signal intensities revealed as well that the production of protein at 37 °C was higher than at 22 °C.

Next, we assayed the activity of FtsZ-His on top of an SLB. We started by synthesizing FtsZ-His in a separate reaction of PUREfrex. Then, we placed 6 or 7 μL of the translation products on top of a membrane (composition A, Table 4.2) with 5% of the crowding agent Ficoll70 in a final volume of 10 μL . For visualization purposes, we included 50 nM of purified FtsZ-647. After adding

the sample on the SLB, the membrane was clearly visible, indicating the recruitment of FtsZ-647 (Figure 4.3 A Left). Importantly, we observed in some areas of the sample the presence of protein filaments, suggesting that the synthesized protein retained basic functionality (Figure 4.3 A Center and Right). Because the purified protein does not contain a membrane targeting

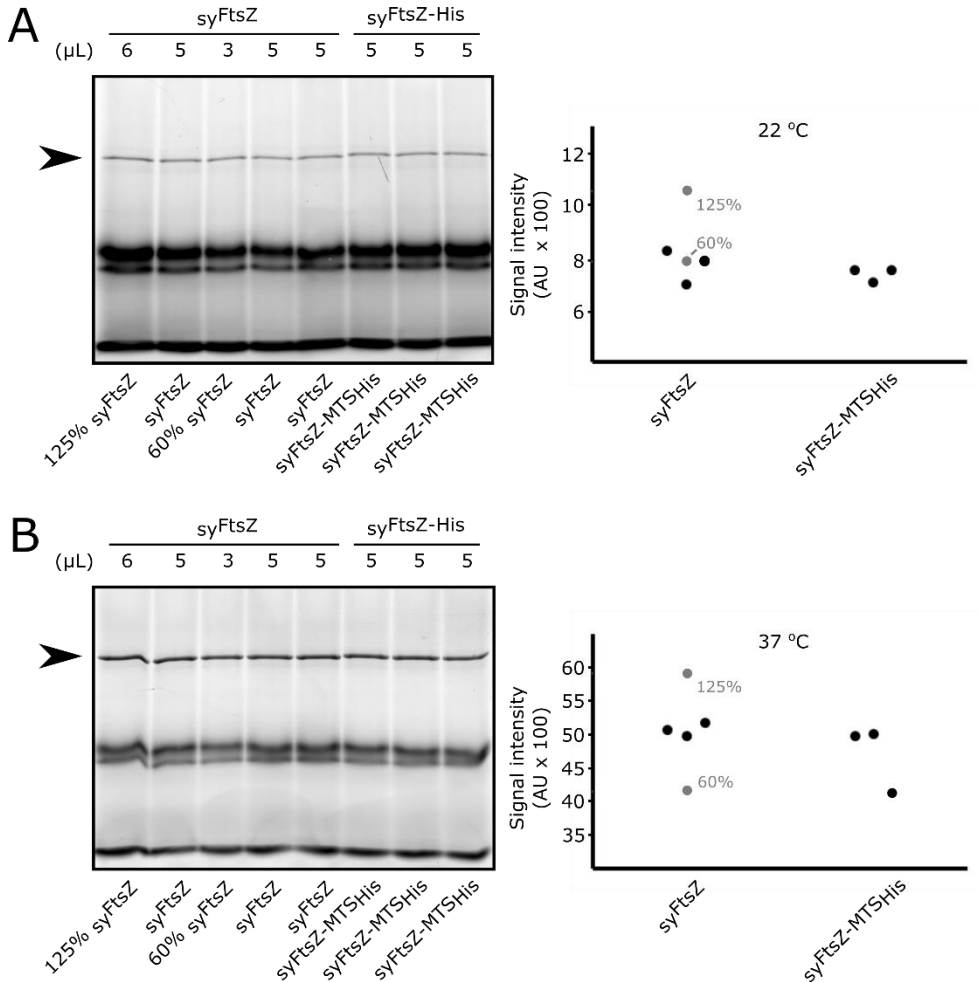


Figure 4.2 SDS-PAGE of the expression of *ftsZ* and *ftsZ-his* at two different temperatures and comparison of protein yield.

Expressions were performed at 22 °C (A) and 37 °C (B) and supplemented with GreenLys. Three separated expressions of *ftsZ* and *ftsZ-his* were performed per condition and visualized in SDS-PAGE (A and B *Left*). Per condition, two wells were loaded with 6 μL and 3 μL of sample instead of the standard 5 μL. In B and C *Right*, protein yield analysis comparing the band intensities in *Left*.

sequence, this result demonstrates that FtsZ-His is able to recruit purified FtsZ-647 to the membrane and stimulate filament formation. The terminal protein (TP) of the phage Φ 29, an unrelated protein, was synthesized under the same conditions and no fluorescence signal on the membrane was detected, confirming that filament formation is FtsZ-His dependent (Figure 4.3 A; *p3-phi29* has been previously validated in our laboratory and in literature²¹).

4.3.3 FtsZ-His forms extensive filament networks on SLBs

While FtsZ-His organized in bundles, their morphology was slightly straighter than the obtained with the wild-type version of FtsZ in this thesis (Figure 2.5, page 48) and in literature¹⁰⁵. We reasoned that the absence of an additional FtsZ interacting protein like FtsA and ZipA might affect FtsZ's bundling activity. In fact, it is known that ZipA promotes bundling

of FtsZ¹⁶⁹. To test whether this observation results from the absence of the other interacting proteins or from the direct association of FtsZ to membrane, we decided to double the concentration of purified FtsZ-647 from 50 to 100 nM. We reasoned that an increase in purified protein concentration might lower the critical concentration threshold for the formation of a dense filament network while lowering the fraction of membrane anchors. However, we did not observe any appreciable difference under these conditions.

Because we suspected that the total volume of the assay might affect the dynamics of filaments and protein network formation, we decided to increase the volume of the assay from 10 to 20 μ L. Additionally, this change allowed us to raise the volume of the added FtsZ-His from 7 to 12 μ L. In this case, and with an FtsZ-647 concentration of 100 or 200nM, we were able to observe thin filament networks as shown in Figure 4.3 B. Additionally, we found that this concentration of purified FtsZ-647 was suitable to visualize isolated filaments and study their behavior. For example, we observed that under the conditions tested (FtsZ-His with 200 nM of purified FtsZ-647 in PURE buffer), preformed protein filaments preferentially landed on the membrane and stayed of the same length for several minutes as shown by the kymographs in Figure 4.3 C, instead of landing of monomers and subsequent rearrangement in filaments. When we increased the concentration of FtsZ-647 from 200 up to 700 nM, we observed the formation of large areas on the membrane with extensive protein networks (Figure 4.3 D). Together, this indicates that FtsZ-His is functional to produce filament networks when supplemented with more than 200 mM of FtsZ-647.

4.3.4 FtsZ-His form extensive filament networks on *E. coli* SLBs

Next, we sought to explore the effect of a more complex membrane composition on the formation of filament networks with FtsZ-His. We produced an SLB composed of *E. coli* polar lipids (composition B, Table 4.2) and synthesized FtsZ-His as previously described (Section 4.3.1). We kept using 700 nM of FtsZ-647 and 5% of Ficoll70 in a total volume of 20 μ L. Under these conditions, we obtained thicker filament networks than before (Figure 4.4 A; compare with Figure 4.3 D). Additionally, we studied the dynamics of the filament networks over the span of several minutes. The networks stayed static over short periods of time. However, occasionally, their suprastructure was able of arrangements over longer periods of 10 to 20 minutes. We identified two basic types of suprastructure dynamics, namely, *bundle condensation* and *ring shrinking* (Figure 4.4 B and C and Figure 4.4 D and E, respectively). *Bundle condensation* was observed as a process where two or more protein filaments fused. This fusion implied that single bundles were able to travel a certain distance over the membrane and fused several filaments; in the most extreme case recorded by us, this implied a distance of approximately 6 μ m and a fusion of 6 filaments (Figure 4.4 B). *Ring shrinking* required the presence of a preformed ring bundle structure embedded in a filament network (Figure 4.4 D and E). It consisted on the progressive reduction of the ring diameter over the span of several minutes. The reduction in diameter could be as high as approximately 50% (from 3,22 μ m to 1.5 μ m (53 %) during the span of 10 minutes; Figure 4.4 E). In contrast, inverse processes to bundle condensation or ring shrinking were never observed. In other words, bundles tended to fuse and rings to shrink, but never the opposite.

4 - FtsZ-MTS on SLBs and inside liposomes

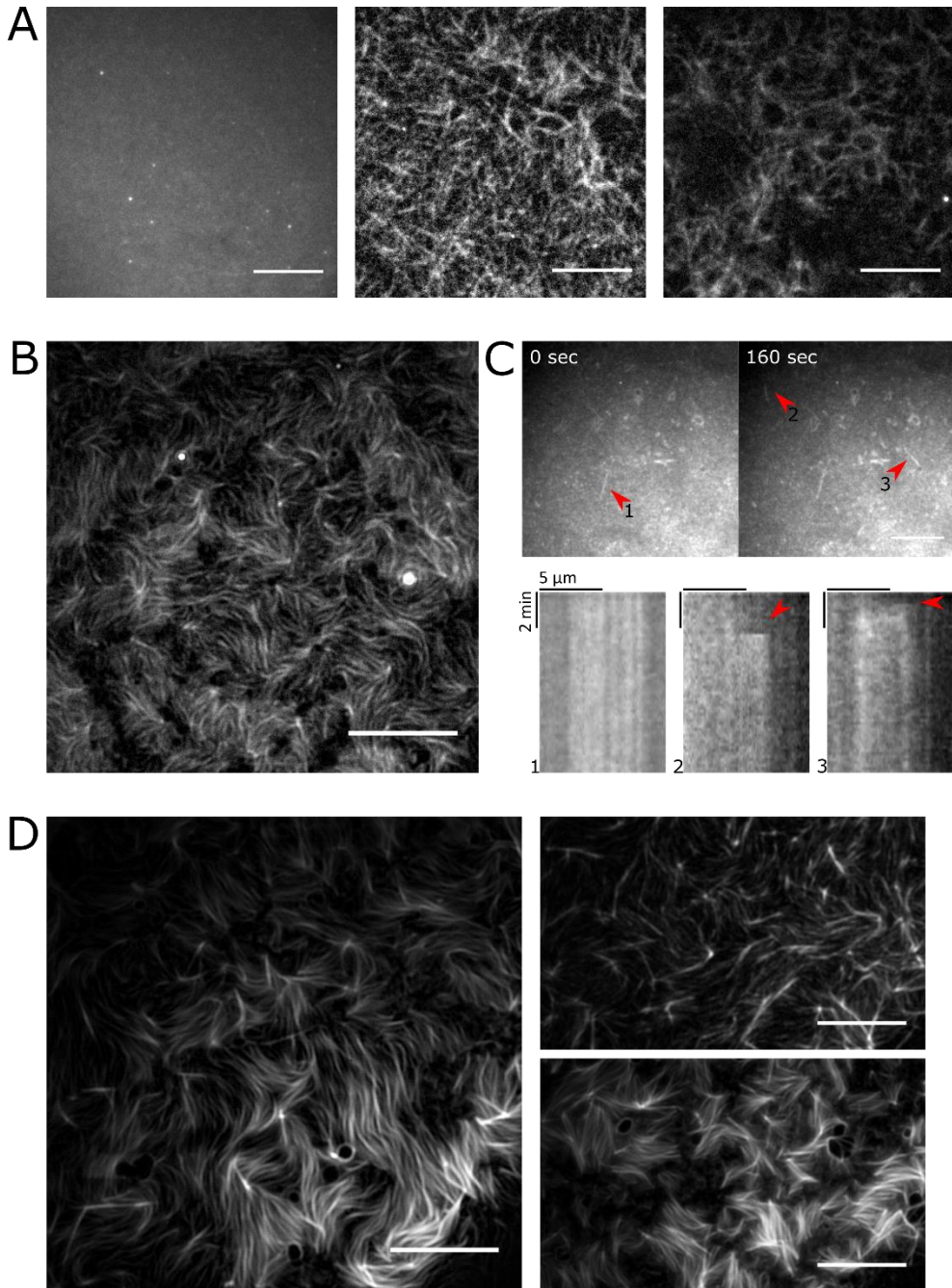


Figure 4.3 FtsZ-His complemented with FtsZ-647 self-assembles into filaments and networks on a minimal SLB

TIRF microscopy images. Scale bars: 10 μm. A) *Left*, recruitment of FtsZ-647 (50 nM) to the membrane was achieved with synthesized FtsZ-His. *Center* and *Right*, some regions of the membrane showed the formation of straight bundles and protein structures. B) FtsZ-His and 200 nM of FtsZ-647 were able to generate thin filament networks on SLBs when the total volume of

the assay was increased to 20 μL . AVG image. C) *Top*, time-lapse images of the landing of single bundles of FtsZ-His (200 nM of FtsZ-647) on the membrane. Time in seconds at the left-top corner. *Bottom*, the dynamics of the filaments marked with red arrows in the top images are shown by a set of kymographs. Filaments formed in solution and landed on the membrane (the landing of the filaments is marked with red arrows in kymographs 2 and 3). Then, they were stabilized and did not grow or shrink (kymograph 1). D) Massive formation of filament networks was achieved when FtsZ-His was placed on the membrane with 700 nM of FtsZ-647. AVG images.

4.3.5 Cell-free synthesized ZapA bundles FtsZ-His filaments in the absence of Ficoll70

We realized an activity assay where 9 μL of cell-free synthesized FtsZ-His was placed together with 1 μM of FtsZ-647 in a total volume of 10 μL . No Ficoll70 was added. Under these conditions, we were unable to detect the presence of filaments, despite the clear signal on the membrane (Figure 4.5 B). Therefore, the production of filaments, whether isolated or in the form of networks, was strictly dependent on the presence of the crowding agent Ficoll70. We have already seen in Section 2.3.5 (page 52) that cell-free synthesized ZapA is able to compensate for the absence of Ficoll70. We sought to verify if the same holds true for FtsZ-His under the absence of FtsA or ZipA. To test this, we ran two separate PURE_{flex} reactions (with 100 nM of FtsZ-647 for visualization purposes) to produce FtsZ-His and ZapA. Then, we combined them on top of a membrane (composition A, Table 4.2) at a total volume of 20 μL . Again, we omitted Ficoll70. We tested up to 5 different FtsZ-His to ZapA ratios (6:14, 8:12, 10:10, 12:8 and 14:6; v/v). We succeeded to detect the presence of areas containing FtsZ filaments (Figure 4.4 F), although they were thin and exhibited a low contrast with the rest of the membrane. The filaments could only be observed with 8 μL of FtsZ-His and 12 μL of ZapA, suggesting the presence of an optimal FtsZ-His:FtsZ-647:ZapA ratio^{182,211}.

4.3.6 FtsZ-A recruits FtsZ-647 to the membrane

One of the drawbacks regarding the use of a 6-histidine tag as a membrane targeting sequence is that the membrane requires the presence of the artificial phospholipid DGS-NTA. Furthermore, the anchoring of the protein is not physiological. Another possibility is the use of a natural MTS, like the one present in FtsA⁷¹. Therefore, we sought to test whether FtsZ-A was able to form similar filaments and bundles as the ones formed by FtsZ-His. To test this, we carried out a PURE_{flex} reaction with 5 nM of *ftsZ-A*. Next, 12 μL of the translation products were placed on top of a SLB (composition C, Table 4.2) together with 100 nM of FtsZ-647 (for visualization purposes) and 5% of Ficoll70 in a total volume of 20 μL . Under these conditions, we observed recruitment of FtsZ-647 on the membrane. We also observed the presence of a special type of FtsZ-A arrangement on the membrane (Figure 4.4 G *Bottom*). While in one hand some long, straight bundles were observed, they seemed to be connected to FtsZ-A clusters or patches. We were unable to detect the presence of protein filaments or networks as seen before (Sections 4.3.3, page 87 and Section 4.3.4, page 88). Hence, we resolved to increase the concentration of purified FtsZ-647 from 100 to 300 nM (Figure 4.4 G *Top*). Still, the aforementioned structures were present, even at a higher density.

4 - FtsZ-MTS on SLBs and inside liposomes

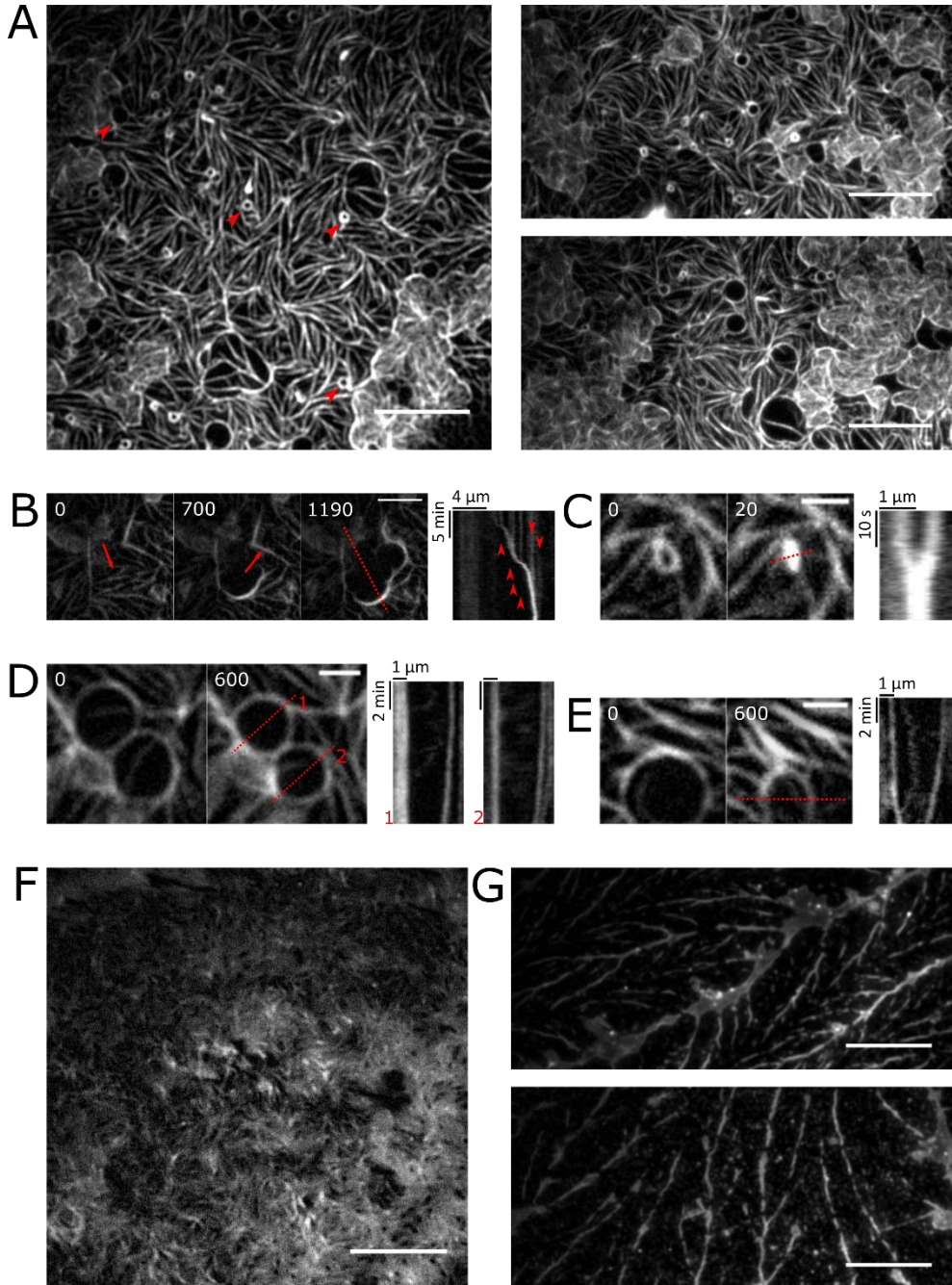


Figure 4.4 FtsZ-His supplemented with FtsZ-647 forms thick filament networks on *E. coli* SLBs and is bundled by synthesized ZapA

TIRF microscopy images. A) FtsZ-His and 700 nM of the purified FtsZ-647 formed thick filament networks on *E. coli* SLBs. Filament rings of different sizes (some examples are marked with red arrowheads) were very common under these conditions. AVG images. Scale bar 10 μm . B) *Left*, time-lapse images show an example of *bundle condensation*. Red arrows mark the bundle's

movement direction. Scale bar 5 μm . *Right*, kymograph along the red dotted line in *Left*. The kymograph shows the dynamics of the bundle over time. The process started at a point on the membrane and the fusion movement occurred in one direction, in a swipe fashion motion. *Bundle condensation* events (6 in total) are marked with red arrowheads. C) *Left*, time-lapse images show another example of *bundle condensation*. Here, both bundles moved and fused. Scale bar: 2 μm . *Right*, kymograph along the red dotted line in *Left*. D) *Left*, time-lapse images showing an example of *ring shrinking*. Scale bar: 2 μm . *Right*, kymographs along the red dotted lines in *Left*. E) *Left*, time-lapse images show another example of *ring shrinking*. Scale bar 2 μm . *Right*, kymograph along the red dotted line in *Left*. F) FtsZ-His is bundled by ZapA on SLBs. However, filaments were thin and difficult to detect. These structures were only observed in a FtsZ-His:ZapA ratio of 8:12 v/v. AVG image. Scale bar 10 μm . G) FtsZ-A is recruited to an SLB lacking DGS-NTA and formed structures on the membrane in the presence of 300 nM (*Top*) or 100 nM (*Bottom*) of FtsZ-647.

4.3.7 FtsZ-His forms filaments on the outer membrane of liposomes

Encouraged by the formation of filaments and protein networks with the FtsZ-His on SLBs, we wondered whether these structures could deform membranes when produced in the outside of liposomes. We started by expressing 5 nM of FtsZ-His for 3 hours at 37 °C in PURE_{flex}. Then, we placed 7 μL of the translation products together with a liposome solution (composition 1; Table 3.2, page 67), 5% of Ficoll70 and 1 μM of purified FtsZ-647. The membrane composition contained DGS-NTA to support FtsZ-His recruitment and a phospholipid conjugated with PEG-Biotin for liposome immobilization. Figure 4.6 A shows the recruitment of FtsZ-647 onto the liposome membrane.

Interestingly, in some areas of the sample, spontaneous formation of SLBs happened, probably due to the fusion of liposomes onto the glass. As can be seen in Figure 4.6 B, these patches showed the presence of filaments and proteins networks. This confirms earlier results (Section 4.3.3) and highlights the compatibility of the chosen membrane composition with the formation of filaments under these conditions. On the liposomes' membrane, protein filaments were difficult to visualize. Therefore, we carried out 100 nm step, optical sectioning of immobilized liposomes. We were able to detect protein bundles on the top of the vesicles (Figure 4.6 C).

4.3.8 Expression of *ftsZ-his* inside liposomes does not recruit FtsZ-647 to the inner liposome membrane

Next, we sought to synthesize FtsZ-His inside liposomes. We expected to obtain protein recruitment in the inner leaf-let of the liposome membrane, and in the best of the cases, the formation of filaments. Therefore, we proceeded to encapsulate the PURE_{flex} system inside liposomes (composition 1 plus 0.5 mass% of DHPE-TxR; Table 3.2, page 67), together with 5 nM of *ftsZ-his* and 100 nM of purified FtsZ-647 for visualization purposes. To inhibit the synthesis of proteins in the outside of the vesicles, we supplemented the feeding solution with Proteinase K. Next, we incubated the liposomes for 3 hours at 37 °C. Under these conditions, we were unable to detect bundles or the association of the purified FtsZ-647 to the membrane. We tried with increased amounts of purified protein (1 and 2 μM of FtsZ-647), but we obtained similar results as before (Figure 4.7 A and B). Since Ficoll70 was not employed here, and we have already observed that the absence of macromolecular crowders prevents the production of protein filaments on SLBs (Section 4.3.5), we sought to assay the co-expression of *ftsZ-his* and *zapA* inside liposomes. Four nM of *ftsZ-his* and 7 nM of *zapA*, together with 100 nM of FtsZ-647. Under these conditions, no filaments or protein recruitment was detected (Figure 4.7 C).

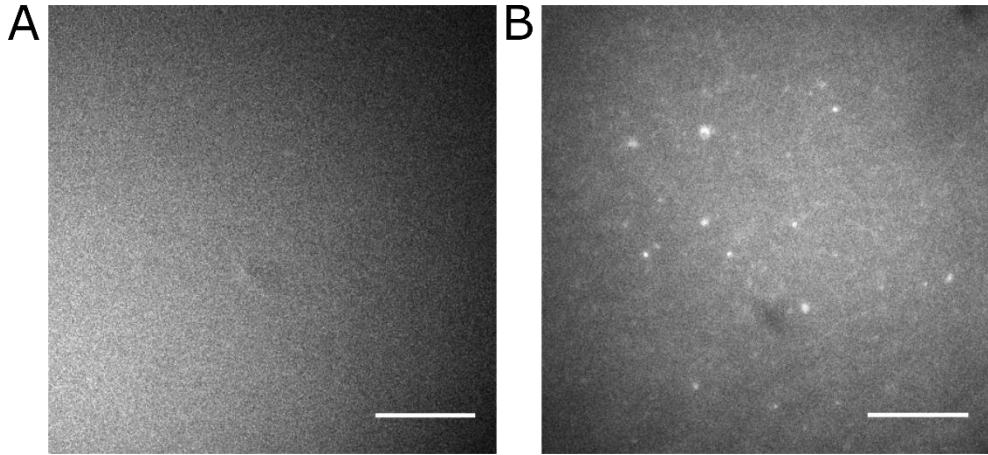


Figure 4.5 FtsZ-647 requires FtsZ-His to be recruited to the membrane and Ficoll70 to form filaments.

TIRF microscopy images. Scale bars: 10 μm . A) The cell-free synthesized Φ 29 terminal protein is unable to recruit FtsZ-647 (50 nM) to the membrane. B) Cell-free synthesized FtsZ-His is capable of recruiting FtsZ-647 (1 μM) to the membrane but fails to organize into bundles in the absence of Ficoll70.

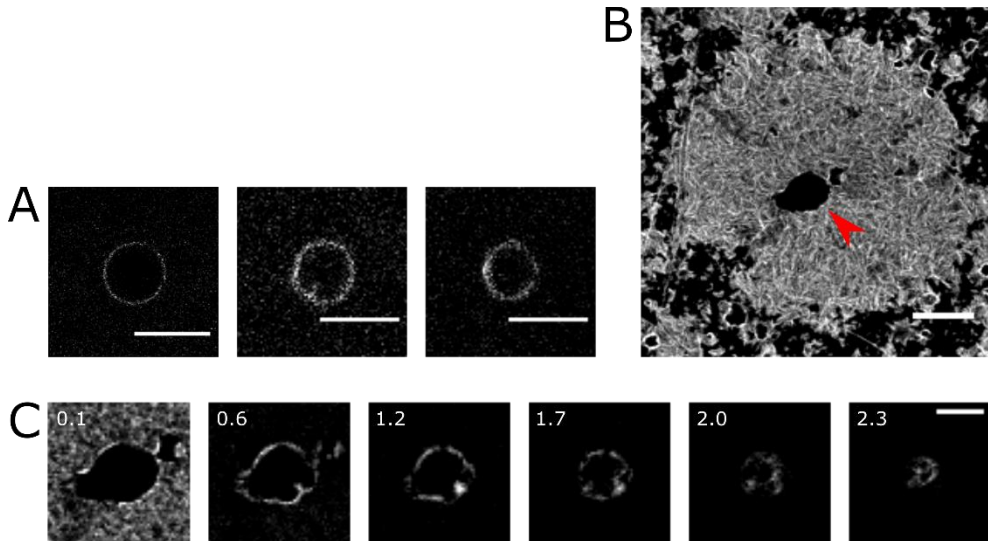


Figure 4.6 FtsZ-His in the presence of liposomes.

LSCM images of synthesized FtsZ-His in the presence of surface immobilized liposomes. A) FtsZ-His in the outside of three different liposomes allowed the recruitment of FtsZ-647 (1 μM) to the membrane, indicative of the functionality of the synthesized protein. Scale bars: *left*, 10 μm ; *center* and *right*, 5 μm . B) Spontaneous formation of SLBs on the glass surface and recruitment of protein filaments (FtsZ-His and 1 μM of FtsZ-647). Red arrowhead indicates the location of an immobilized liposome on the surface. Scale bar: 10 μm . C) Optical sectioning of the immobilized liposome in B. Distance from the membrane, in μm , stated at the upper-left corner of each image. At 2 and 2.3 μm from the surface, small protein filaments could be observed. Scale bar: 5 μm .

4.4 Discussion

The cell-free synthesis of chimeric proteins can be an attractive approach to solve some of the more challenging processes of artificial cells. Besides, it can efficiently lower the load on the PURE system machinery when fused proteins with more than one function are designed. In this chapter, we have tested and visualized the self-organization of the chimeric FtsZ-His and FtsZ-A on SLBs and in the presence of liposomes. We found that FtsZ-His efficiently self-recruits to the membrane, and bundles into straight filaments. Interestingly, FtsZ-His structures were dynamic over periods of 10 to 20 minutes and carried out two distinct processes: *ring shrinking* and *bundle condensation*. In the outside of liposomes, FtsZ-His was recruited and bundled into filaments. However, we were not able to detect FtsZ-His recruitment in the inner leaf-let of the liposome's membrane, even when *zapA* was co-expressed.

4.4.1 Ring shrinking and bundle condensation are key processes for an FtsZ-based liposome division mechanism

In Figure 4.4 D and E, we showed that certain filament rings are able to constrict. With the goal of building a divisome based on FtsZ, this capacity is a key property. Interestingly, we did not observe the opposite of *ring shrinking*, namely, ring expansion, suggesting directionality in the filament dynamics under the conditions tested. The constriction of FtsZ rings with purified proteins has been seen before in literature. Probably, the most impressive example is the study carried out by Osawa and Erickson¹⁰⁹. In this study, they attempted to reconstitute a minimal divisome made of FtsZ and FtsZ_{R286W} inside spherical liposomes. They achieved the formation of rings, and a very small fraction of them were able to constrict. Other studies by Osawa and Erickson made usage of FtsZ-MTS. Here^{197,198}, they performed several experiments with two versions of FtsZ-MTS. They obtained protein rings able to constrict both in the outside and inside of tubular liposomes. Despite the results, the capacity of these reconstituted systems to resolve the constriction neck and finalize division is not clear. In fact, *in vivo*, FtsZ leaves the divisome complex before division is completed¹⁶⁴. One of the reasons for this could be the location of FtsZ in the divisome, where it becomes an obstacle once the constriction reaches a critical point. *In vivo*, it is possible that other proteins carry on with the constriction and finalize division. However, in a minimal system the absence of FtsZ would lead to the relaxation of the neck. Strikingly, results reported by Redfearn²⁰⁹ showed that FtsZ-YFP-MTS inside tubular SLBs arranged in ring-like structures and underwent a constriction motion. The diameter of the rings could go from 3-2 μm down to diameters below the resolution limit of the microscope (≤ 198 nm). Probably, the most surprising results showed by Redfearn is the disappearance of FtsZ-YFP-MTS from the neck once the gap was below the resolution limit, raising the possibility that FtsZ-YFP-MTS was able to finalize the fusion of the gap membrane. Although the capabilities of FtsZ-YFP-MTS explored by Redfearn sound promising to be implemented as an FtsZ-based artificial divisome, the experiments were realized in a concentration range in the order of millimolar (3-25 mM), impossible to replicate in a cell-free synthesized system with the current technology.

Perhaps, the potential capacity of FtsZ filaments to fuse close-positioned membranes could be related to the ability of FtsZ filaments to bundle and fuse to each other. We have observed this phenomenon in our experiments (Figure 4.4 B and C). This property of FtsZ filaments is important because it shows that a potential FtsZ-based divisome could bring the membrane as close as possible. Again, processes like *bundle condensation* have been reported before. For example, Arumugam²¹² observed the annealing of FtsZ-MTS filaments on SLBs. However, their

4 - FtsZ-MTS on SLBs and inside liposomes

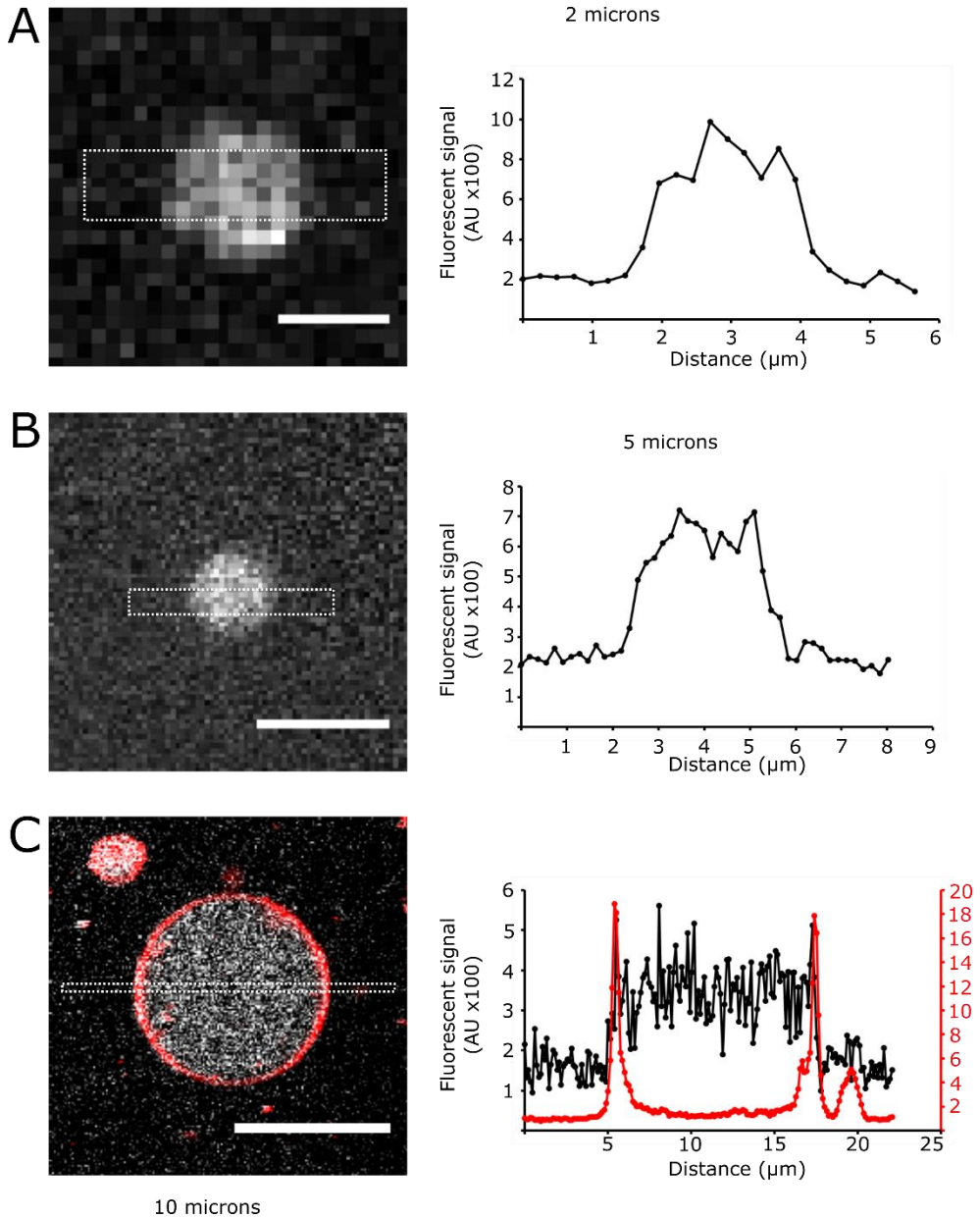


Figure 4.7 In-vesicle synthesis of FtsZ-His.

LSCM images of three different liposomes expressing FtsZ-His. Purified protein channel in grey. Membrane channel in red. The white dotted boxes are 5 pixels in height in the original images. A) *Left*, 2 μM of FtsZ-647 encapsulated. Membrane composition 1 (Table 3.2, page 67). Scale bar: 2 μm . *Right*, signal intensity profile of the white dotted box in *Left*. B) *Left*, 1 μM of encapsulated FtsZ-647. Membrane composition 1 (Table 3.2). Scale bar: 5 μm . *Right*, signal intensity profile of the white dotted box in *Left*. C) *Left*, liposome co-expressing 4 nM of ftsz-his and 7 nM of zapA with 1 μM of encapsulated FtsZ-647. Membrane composition 3 (Table 3.2). Scale bar: 10 μm . *Right*, signal intensity profile of the white dotted box in *Left*.

process involved the end-to-end annealing of filaments able to diffuse freely on the membrane, in contrast to the fusion of bundles integrated in a stable, high density filament structure as we observed (Figure 4.4 A). In tubular liposomes, Osawa and Erickson^{197,198} also observed the shifting and fusion of adjacent FtsZ rings. Interestingly, bundling does not require the presence of a membrane. For example, FtsZ adsorbed on mica is able to fragment, anneal and bundle as well as carry out the cyclization of FtsZ filaments²¹³. However, *ring shrinking* was not observed, raising the question of whether ring constriction requires the interaction of FtsZ with a membrane, whether directly or not.

4.4.2 FtsZ-His and ZapA form a completely synthesized cytoskeletal minimal system.

One of the key results obtained in this chapter is the formation of FtsZ filaments only with the synthesized proteins FtsZ-His and ZapA (Figure 4.4 F). Although we have already shown that cell-free synthesized ZapA is able to bundle FtsZ filaments anchored to the membrane by sZipA (Section 2.3.5, page 52), this is the first time where purified proteins have been used exclusively as reporting molecules.

The filaments obtained were very thin and exhibited a low contrast with the membrane, making very difficult the visualization. The image displayed in Figure 4.4 F was computed by calculating the average pixel intensity of a series of independent images over the same region of the sample. Only in this way the filaments on the membrane were possible to detect. The morphology of the synthesized FtsZ-His/ZapA filament network was more similar to the one obtained in Figure 4.3 D (FtsZ-His/FtsZ-647 filaments on a minimal membrane; composition A, Table 4.2) than the one obtained in Figure 4.4 A (FtsZ-His/FtsZ-647 filaments on an *E. coli* polar lipid SLB; composition B, Table 4.2). This result might suggest that a different membrane composition induces the formation of different filament morphologies. One of the key differences in morphology might be the apparent scarcity of rings in the FtsZ-His/ZapA filament network, which might be essential in the implementation of this system as an artificial divisome. However, the morphological difference might be due to a probably lower concentration of total protein in the case of co-expression, or a lower bundling capacity of the synthesized ZapA. As learned in other parts of this thesis, supplementation of specific enzymes like Pth (Section 2.3.5, page 52) or molecular chaperones like DnaK or GroE (Section 5.3.5.3, page 123) to the expression reaction or activity assay solution might help to increase the fraction of active proteins.

4.4.3 Synthesized FtsZ-His is not recruited to the inner leaflet of liposomes

We have shown that FtsZ-His was able to recruit FtsZ-647 to the outer membrane of liposomes (Figure 4.6). However, we failed to detect the recruitment of FtsZ-647 in the inner leaflet of liposomes upon expression of FtsZ-His (Figure 4.7). A failure in the expression of the protein in the liposomes is improbable due to positive controls carried out in other parts of this thesis (Section 3.3.3, page 72). Alternatively, we have also shown that the lipid composition of the liposome membrane is compatible with the formation of filaments (Figure 4.6B). Despite this, some problems related with the lipid composition and the presence of a His tag can arise.

Perhaps, due to the non-physiological anchoring of FtsZ-His to the membrane, the translation of this protein in close proximity to the membrane might stall the ribosome. Other possibilities are an asymmetrical distribution of DGS-NTA on the liposome's membrane or an imbalance between the concentration of the membrane anchored FtsZ-His and the purified FtsZ (Figure 4.8).

4 - FtsZ-MTS on SLBs and inside liposomes

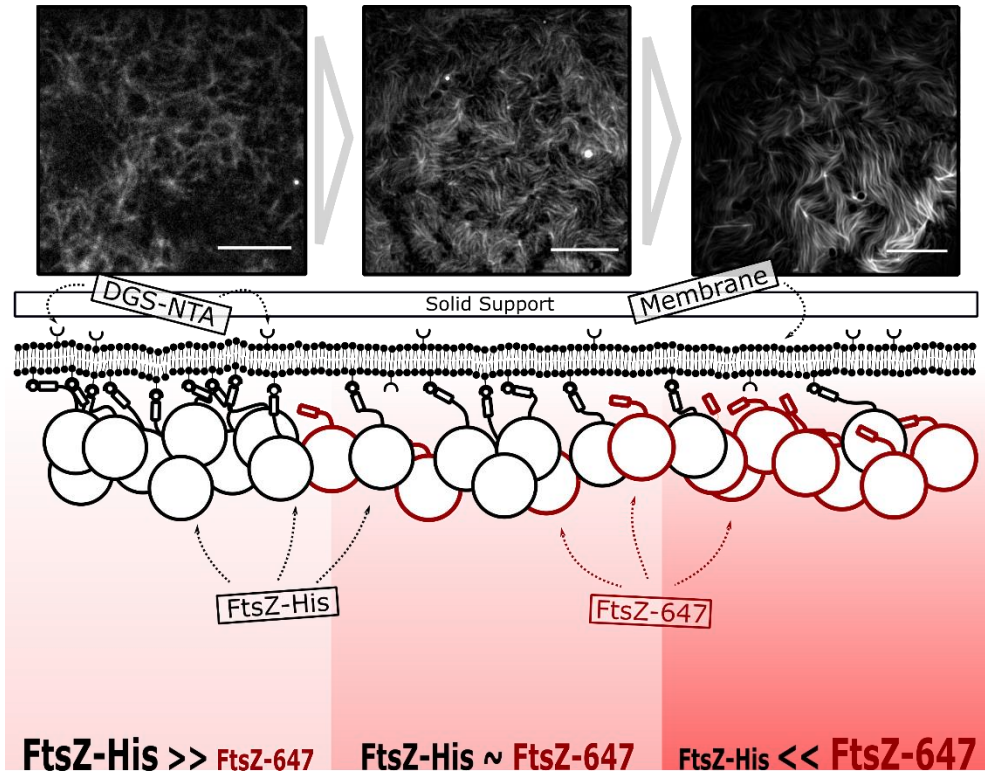


Figure 4.8 The FtsZ-His:FtsZ-647 ratio on the membrane might play a role on the morphology of the protein networks.

The presence of high amounts of synthesized FtsZ-His with respect to FtsZ-647 (50 nM) might produce straight filaments (*Left* picture; taken from Figure 4.3 A Right). However, higher amounts of FtsZ-His per FtsZ-647 might allow mildly curved morphologies. Center picture taken from Figure 4.3 B, with 200 nM of FtsZ-647. Right picture, taken from Figure 4.3 D, with 700 nM FtsZ-647.

4.4.4 FtsZ-His is a superior alternative to FtsZ-YFP-MTS in an IVTT context

One of the most popular options among the artificial FtsZ-MTS protein family is FtsZ-YFP-MTS. This fusion protein, broadly used in literature, is characterized by the presence of a fused YFP tag and the MTS from MinD¹⁹⁷. This convenient fluorescent tag at the C-terminus side of FtsZ has been useful in *in vitro* assays^{109,198,214} by providing an easy way to monitoring its activity.

Incidentally, the presence of this tag, allows the FtsZ part of the protein to *indirectly* interact with the membrane, similarly to the manner that the wild-type FtsZ interacts with the membrane through FtsA or ZipA. This is not the case with FtsZ-His, which interacts with the membrane through a 6-histidine tag, therefore coexisting at a closer distance from the membrane than the wild-type FtsZ *in vivo* (Figure 4.9). Additionally, the MTS amino acid sequence attached to the C-terminus of the protein comes from the wild-type MinD protein, therefore offering a physiological interaction with the membrane.

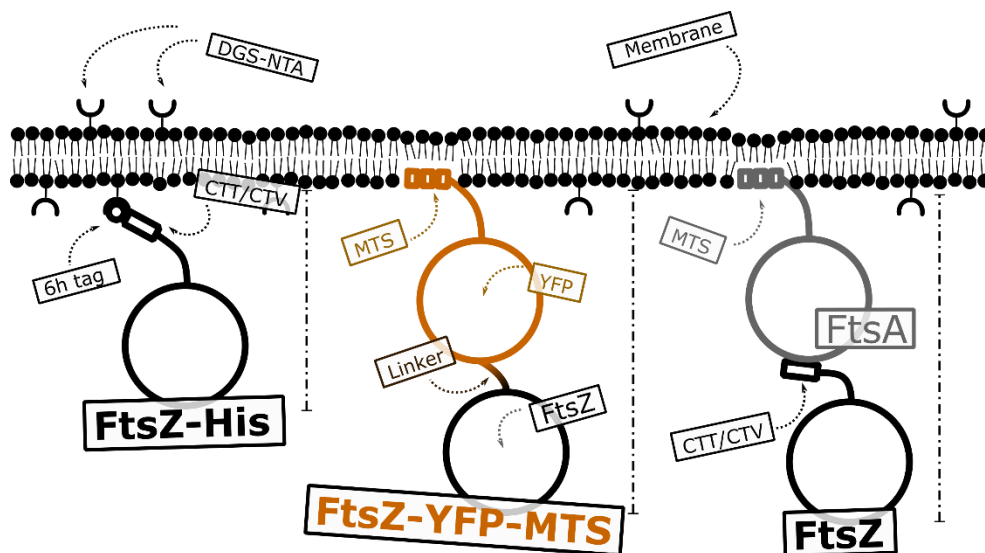


Figure 4.9 Schematic showing some functional and structural differences between FtsZ-His, FtsZ-YFP-MTA and the FtsZ-FtsA interaction.

While FtsZ-His binds to the membrane through its 6-histidine tag via a DGS functionalized with an NTA moiety, both FtsZ-YFP-MTA and FtsA use a physiological amphipathic helix. Due to the relatively high molecular weight of the fluorescent tag, the FtsZ domain of the FtsZ-YFP-MTS protein is situated at a distance of the membrane comparable to that in FtsZ-FtsA. However, FtsZ-His localises closer from the bilayer.

Despite that some of the features of FtsZ-YFP-MTS might be considered an advantage in certain frameworks, FtsZ-His is nonetheless a better alternative in an IVTT context. For example, the presence of a fluorescent tag like YFP, which might be able to oligomerize²¹⁵, might also have a negative influence on some critical functions of the protein and influence FtsZ's physiological activity. It is important to notice that the molecular weight of the YFP tag^{216,217} (calculated from sequence) represents 77% of the FtsZ-YFP-MTS molecular weight. This massive tag, with respect to the total mass of FtsZ-YFP-MTS, might impose a steric hindrance for a physiological FtsZ behavior. FtsZ-His, opportunely, does not contain a fluorescent tag, therefore avoiding such troubles. The simplicity and shorter length of FtsZ-His with respect to FtsZ-YFP-MTS is an advantage as well. Due to the current state of the cell-free synthesis technology and the limitations regarding total protein mass production, shorter versions of a given protein should be expected to reach a higher micromolar final concentration. In the case of cell-free synthesis of general FtsZ-MTS inside liposomes, this might be even essential due to the limited access to nutrients from the outside. Finally, another feature of FtsZ-His is the use of a His-tag as MTS. This method has been tried before in literature^{107,179,218} and in this thesis (Section 2.3.1, page 43) with other proteins like ZipA. The advantage that this method offers compared with the MinD MTS of FtsZ-YFP-MTS is that the attachment of the protein should be less influenced by the phospholipid membrane composition²⁰⁸. In the context of building a synthetic cell, this method is a more flexible alternative than FtsZ-YFP-MTS.

4.4.5 Conclusions and outlook

In this chapter, we have explored the possibilities that FtsZ-MTS offers regarding the reconstitution of protein filament networks on SLBs and the deformation of the liposome's

membrane. In one hand, we have shown that synthesized FtsZ-His is able to polymerize and bundle into filament networks and rings. Very importantly, these rings were able to shrink, suggesting that a divisome based on FtsZ-His could be possible. Despite the ability of FtsZ-His filaments to bundle and to constrict when in the form of Z-rings, its capacity to resolve the constriction neck and finalize scission is not evident. This raises the possibility of using other systems like the SNARE or ESCRT proteins in order to carry out this essential function. Inside liposomes, recruitment of synthesized FtsZ-His to the inner leaflet of the membrane has not been achieved, although this was possible from the outside. Different liposome membrane compositions or MTSs, like for example the transmembrane region of *E. coli* ZipA, could be tried.

Acknowledgements

We thank Germán Rivas' lab at Centro de Investigaciones Biológicas (CSIC) in Madrid for providing the purified proteins used in this chapter. We thank Daniël Lam and Jeremie Capoulade for TIRFM training. We thank Jeremie Capoulade for LCSM training and technical support. We thank Alicia Soler Cantón and Duco Blanken for help with the LCSM.

Chapter 5

The cell-free synthesized Min system on SLBs

Natural cells exert a tight spatiotemporal control over important cellular subsystems that in turn allow them to coordinate basic processes to give rise to complex behavior. Efficient model artificial cells must aim to achieve, perhaps at a simpler level, such type of regulation. Division in bacteria like *E. coli* is carried out by a multiprotein complex, the divisome, which assembles at the midcell and synthesizes the division septum. The Min system regulates the positioning of this complex by a reaction-diffusion powered oscillatory pattern between the cell poles. With the aim of constructing a minimal division machinery for synthetic cells based on the *E. coli* divisome, we regarded the Min system as an attractive mechanism for spatiotemporal regulation of artificial cytokinesis. In this chapter we attempted to reconstitute a functional Min system on planar membranes with the ultimate goal of validating its use in the spatiotemporal regulation of artificial division of synthetic cells. To convey hereditary information in a synthetic cell, the Min system must be encoded in a DNA molecule that can be copied, transcribed and translated. We achieved this with the PURE system, a well characterized mix of purified components, purposely designed for clean, controllable cell-free transcription and translation. We found that cell-free synthesized Min proteins resumed reaction-diffusion-like patterns on planar membranes. Optimization of the PURE system reaction conditions was required in order to obtain such patterns. Our results suggest that the Min system is a potential candidate for effective control and coordination of division and other artificial cellular subsystems in model artificial cells.

5.1 Introduction

In *in vivo*, rod-shaped bacteria like *E. coli* divide through binary fission thanks to a multiprotein complex known as the divisome²⁰⁵. Of all proteins in this complex, FtsZ is the core component and the responsible for the location of the future division septum⁹⁰. FtsZ assembles into a ring-like structure at midcell, the Z-ring²³, upon which the divisome is assembled and controlled¹⁰¹. In turn, the position of the Z-ring is regulated by a variety of other overlapping cellular subsystems like nucleoid-occlusion²¹⁹, the MatP mediated system^{84,85,220} or the Min system. Such a redundancy of mechanisms to control the position of the Z-ring implies that none of them is essential²²¹⁻²²⁴. The most well-studied positioning facilitator is arguably the Min system. In contrast to the others, the Min system relies on geometrical cues of the cell rather than in signaling molecules. Such features make the Min system a sound candidate for *in vitro* regulation of FtsZ in model artificial cells. The Min system is comprised of three proteins: MinC, MinD and MinE. In the cell, the Min proteins self-organize at the inner surface of the cytoplasmic membrane and dynamically oscillate between the two cell poles^{115,225-227}. These oscillations are driven by a reaction-diffusion mechanism involving MinD and MinE, nucleotide exchange and transitions between the cytoplasmic and membrane-bound states²²⁸. MinC, an inhibitor of FtsZ polymerization, passively travels along the dynamic MinDE protein pattern. The oscillations impose a time-averaged intracellular gradient of MinC concentration that is minimal in the middle of the cell, where FtsZ polymerizes as an early stage of divisome maturation²²⁹⁻²³¹.

Probably, the best asset of the Min system regarding the rational construction of an artificial cell is the vast amount of knowledge accumulated during decades of research. The first study published around this subject dates back to the 60's²³² and many studies have been carried out at the microbiological^{123,233-238}, single cell^{110,111,123,125,208,225-227,234,237-246}, biochemical^{110-112,123-125,208,226,227,235,238,242,243,247-255} and *in vitro* reconstitution level. The discovery of the Min proteins oscillations and some of its defining characteristics *in vivo* led to the question of what patterns and dynamics could be reproduced *in vitro*. The first successful attempt to reconstitute MinDE dynamics was carried out by M. Loose et al.¹³³ on SLBs in 2008. They observed the formation of what was called *Min waves*, which consisted on a moving protein front and rear over the membrane surface. Loose et al. recorded the intensity profiles for each protein and studied the dynamics of the system through FRAP experiments. In 2011, they further expanded their original study by following the three Min proteins (MinC, D and E) and studying the intensity profile of each independent protein on the membrane²⁵⁶. The use of TIRF microscopy allowed them to observe important features like the MinE ring at the rear of the Min waves. The original study of 2008¹³³ prompted other researchers to reconstitute the Min system *in vitro*. Different membrane lipid compositions, buffer salt content and concentrations were tried in order to observe the influence of these parameter on the dynamics of the Min waves. For example, Vecchiarelli et al.¹³⁴ studied the influence of flow, lipid composition, and salt concentration on Min patterns. Others found qualitatively different patterns like *amoebas* and *snakes* on SLBs of different compositions¹³². High degrees of sophistication were reached with the *in vitro* reconstitution on SLBs of a combined Min system and FtsZ-ZipA filament network¹⁷², or the combination of FtsZ-YFP-MTS filament networks and ZapA²⁴⁶. Others opted to study the influence of the surface's geometry on the Min patterns in a range of biomimetic membranes. For example, Schweizer et al.²⁵⁷ reported the change in dynamics of Min waves reconstituted on planar surfaces with the presence of obstacles of different sizes and shapes. Additionally, studies reporting the patterns obtained on SLBs formed in open microfabricated cell-shape compartments²⁵⁸ or in fully confined fluidic chambers²⁵⁹ were

carried out. Going beyond planar membranes, studies reconstituting waves on GUV's external membrane¹¹³ or oscillations inside GUV¹³⁸ were carried out.

Despite the efforts made throughout the *in vitro* reconstitution field, up to date and to the best of our knowledge, no successful attempt has been reported on the *in vitro* reconstitution of *de novo* synthesized Min proteins on SLBs. In this chapter, our goal is to achieve the formation of spatiotemporal patterns with cell-free synthesized Min proteins on an SLBs. A successful outcome in this area would open the door to the use of cell-free synthesized Min proteins inside liposomes and in artificial cells with the purpose of regulating an FtsZ-based divisome. We approached this challenge by, in the first place, establishing optimized working conditions with purified Min proteins. We assessed the interactions between the purified MinC, MinD and MinE, as well as with a lipidic membrane in a series of sedimentation assays and examined their activity on top of an SLB. Next, we assayed the synthesized MinD and MinE proteins on SLBs and found that they formed Min waves and other patterns on the membrane. Taken together, our results clearly demonstrate that the *de novo* synthesis of functional Min proteins is possible and opens the door to their utilization in artificial cells.

5.2 Materials and methods

5.2.1 Cloning, expression and purification of Min proteins

Plasmids coding for *E. coli* Min proteins were kindly provided by the laboratory of Petra Schwille in the Max-Planck-Institute of Biochemistry, Germany. A detailed account of these DNA sequences can be seen in the Appendix (page 154). Ten ng of each plasmid was transformed into competent *E. coli* BL21 (DE3) pLysS strains via heat shock and plated on solid LB medium with 50 ng/ μ L of kanamycin. Colonies were grown overnight at 37 °C. Then, single colonies from each transformation were inoculated in 12 mL of liquid LB medium supplemented with 50 ng/ μ L of kanamycin and grown overnight at 37 °C and 250 rpm. Cultures were diluted in 1 L of fresh liquid LB medium (1:100 v/v) supplemented with 50 ng/ μ L of kanamycin and grown overnight at 37 °C and 125 rpm until OD600 = 0.4-0.6. Finally, cultures were induced with 400 μ M of IPTG and grown overnight at 16 °C.

After induction, samples were pelleted and suspended in 10 mL of lysis buffer (50 mM Tris-HCl pH 7.6, 30 mM NaCl, 5 mM MgCl₂, 10 mM imidazole, 10% glycerol (v/v), supplemented with 20 μ L of Set III protease inhibitor cocktail (CalBiochem) and 10 μ L of DNase I). Cells were disrupted by sonication in cycles of 90 seconds (30 seconds on, followed by 59 seconds off) for a total time of 2 hours and 30 minutes. The resulting cell suspension was centrifuged in 50 mL Falcon tubes at 30 000 rcf for 40 minutes at 4 °C.

The purification of the cell lysate (CFE) was performed in Ni-NTA columns. First, 4 mL of Ni-NTA resin was equilibrated with 80 mL of lysis buffer. The CFE was then incubated with the resin in two 50 mL Falcon tubes for 1.5 hours at 4°C. The resin with the cell lysate was then poured in the purification columns and the flow through was collected. Then, the column was washed with wash buffer (50 mM Tris-HCl pH 7.6, 30 mM NaCl, 5 mM MgCl₂, 30 mM imidazole, 10% glycerol) and the flow through was collected. The columns were finally eluted with elution buffer (50 mM Tris-HCl pH 7.6, 30 mM NaCl, 5 mM MgCl₂, 250 mM imidazole, 10% glycerol) and fractions of 0.5 mL were collected.

5.2.2 SDS-PAGE analysis of purified Min proteins

Unless otherwise specified, preparation and casting of the SDS-PAGE was carried out as described in Section 2.2.7 (page 41). To facilitate the analysis, the purified fractions were

pooled in groups of 6-7 fractions (3-3.5 mL). Twenty μL of each pooled fraction was mixed with 5 μL of 5x Laemmli buffer plus 50 mM DTT. Samples were boiled for 10 minutes at 95 $^{\circ}\text{C}$ and 10 μL of each sample was loaded in the gel. To store the purified proteins, the pooled fractions were buffer exchanged in storage buffer (50 mM Tris-HCl pH 7.6, 150 mM KCl, 5 mM MgCl_2 , 10% glycerol) and concentrated 3 to 4 times with 3 kDa Amicon filter (Millipore).

5.2.3 Concentration measurements

The concentration of the purified Min proteins was assessed using two complementary methods: Bradford assay and fluorescence spectrometry. The Bradford assay works by constructing a standard curve with dilutions of a protein of which the concentration is known. Then, the best possible line describing the standard curve is calculated by linear regression. In the next stage of the process, the absorbance of the protein of interest is measured and its value plugged into the previously calculated line fit as long as it resides in the linear regime of the standard curve. Usually, several dilutions of the protein of interest are assayed to maximize the chances of obtaining at least one of the absorbance measures within this linear regime. The solution to this equation is the apparent concentration of the protein of interest. We applied this method to our stock of purified Min proteins: MinC, eGFP-MinC, eGFP-MinD and MinE. Only dilutions of the purified Min proteins that were in the range of the standard curve were considered. The concentration ($\mu\text{g}/\text{mL}$) of the proteins were inferred and the molar concentration (μM) was calculated using sequence predicted protein weights. Bradford assay was performed with the Quick StartTM Bradford Protein Assay (Bio-Rad). The assay was performed using a 250 μL glass bottom 96-well microplate. The standard protein used was Bovine Serum Albumin (BSA) and standard curve was replicated three times per each Min protein in stock. Three different dilutions of each Min protein (100, 200 and 400 times) were produced in reaction buffer (50 mM Tris-HCl pH 7.5, 150 mM KCl, 5 mM MgCl_2) and each of the dilutions replicated three times. Next, 150 μL of each dilution of the standard and the samples was pipetted into the wells of the microplate. Then, 150 μL of dye reagent (Quick StartTM Bradford Protein Assay, Bio-Rad) was added to each well. The assay was incubated for 5 min in the plate reader (CLARIOstar[®] BMG LABTECH), after which the absorbance was measured at 595 nm.

Additionally, we assessed the molar concentration of the stock proteins by fluorescence spectrometry. This method measures the absorbance of a sample at the specific wavelength of a fluorophore which is known to be in the sample. Consequently, only the stock proteins fused to a fluorophore, i.e. eGFP-MinC and eGFP-MinD, were assayed following this approach. In general, the assay works by illuminating the sample with light of a specific wavelength, preferably close to the maximum of excitation of the fluorophore to be detected and away from the absorbance values of contaminating molecules. We decided to use a light wavelength of 488 nm that corresponds with the peak of maximum excitation of eGFP. Then, the absorbance of the light in the chosen wavelength is measured. This value correlates to the concentration of fluorophore in the sample by using the Lambert-Beer law:

$$A = \epsilon lc$$

4

where A refers to the measured absorbance; ϵ is the molar extinction coefficient of the fluorophore of interest in $\text{M}^{-1}\text{cm}^{-1}$ (for eGFP this was $55000 \text{ M}^{-1}\text{cm}^{-1}$); l is the length of the light path in cm (in our case 0.1 cm) and c is the eGFP concentration (M) and can be used as an estimation of the concentration of the protein of interest. Min proteins were diluted 2, 4 and 8 times in reaction buffer in order to increase the chances of measuring a sample in the linear range of absorbance. Three technical replicates were performed for each sample (Thermo

Scientific NanoDrop 2000c spectrophotometer). The blank was realized with reaction buffer. The pedestal was cleaned with Milli-Q water between each measurement.

5.2.4 Preparation of Large Multilamellar Vesicles

Large multilamellar vesicles (LMVs) were prepared with *E. coli* polar lipids (Table 5.1; Avanti® POLAR LIPIDS, INC). First, 200 μL of 25 mg/mL of *E. coli* polar lipids in chloroform was placed in a glass vial and dried under a gentle flow of argon and desiccated for at least 20 minutes to allow the final traces of chloroform to be removed. Next, the lipid film was rehydrated with 200 μL of reaction buffer with 0.365 M sucrose, giving a final lipid concentration of 25 $\mu\text{g}/\mu\text{L}$ of lipids. The vial was vortexed until the solution became turbid and the lipids were dissolved. Finally, the LMV solution was stored in a 1.5 mL Eppendorf tube at $-20\text{ }^{\circ}\text{C}$.

Table 5.1 Phospholipid composition of *E. coli* polar lipid extract

Component	Mass (%)
phosphatidylethanolamine (PE)	67.0
phosphatidylglycerol (PG)	23.2
cardiolipin (CA)	9.8

5.2.5 Sedimentation assays: procedure and analysis

Protein-to-protein and membrane-to-protein interactions of the Min proteins were tested by a series of sedimentation assays. During a sedimentation assay, a sample with proteins and sucrose-loaded phospholipid vesicles (LMVs) is prepared. After incubation, samples are centrifuged. By analyzing the content of the supernatant and the pellet of the samples on an SDS-PAGE, the binding activity of the proteins to the phospholipids and to each other can be assessed.

The preparation of the LMVs was done as described in Section 5.2.4. Next, samples were prepared according to the following instructions, unless otherwise specified in the relevant sections. Min proteins were mixed with 1 mM of ATP, 3 $\mu\text{g}/\text{mL}$ of *E. coli* polar lipids LMVs in reaction buffer with 0.365 M sucrose and in a total volume of 25 μL . The composition of the mixture can be found in Table 5.2. The samples varied in protein composition. The volume of the absent protein, except when the three Min proteins were assayed, was compensated by the same volume of reaction buffer with 0.365 M sucrose. Next, the samples were incubated at $37\text{ }^{\circ}\text{C}$ in a 1.5 mL Eppendorf tube inside a pre-warmed top-bench centrifuge (Eppendorf Centrifuge 5424R) for ~ 10 minutes. Samples were centrifuged for 30 minutes at 21000 rcf upon which pellets on the bottom of the tubes were clearly visible. Twenty μL of the supernatant was pipetted out into a new, 1.5 mL Eppendorf tube (supernatant sample). Then, the pellet was washed two times by letting 20 μL of reaction buffer with 0.365 M sucrose gently fill the tube before discarding the extra 20 μL of solution. Finally, the pellets were resuspended with the remaining 5 μL of buffer (pellet sample) and transferred to PCR tubes to be boiled at $90\text{ }^{\circ}\text{C}$ for 5 minutes in a thermocycler (Bio-Rad C1000 Touch). Afterwards, the samples were placed on ice.

Table 5.2 Composition of sample in a sedimentation assay

Not all three Min protein were present in every sedimentation assay. In the case of the absence of a particular protein or proteins, the assay volume was compensated with reaction buffer (* reaction buffer plus 0.365 M sucrose).

Component	Volume (μL)	Final concentration
25 mM ATP	1	1 mM
25 μg/μL LMVs	3	3 μg/μL
25 μM MinC	2	2 μM
25 μM eGFP-MinD	4	4 μM
25 μM MinE	6	6 μM
Reaction buffer*	up to a total 25 μL	1x

Both pellet and supernatant samples were mixed with 1.5 μL or 5 μL of 5x Laemmli buffer, respectively. Then, the samples were transferred to PCR tubes and boiled at 90 °C for 5 minutes in a thermocycler (Bio-Rad C1000 Touch). Immediately, the samples were put on ice and loaded in a standard 12% Acrylamide/Bis-acrylamide SDS-PAGE. Preparation and casting of the SDS-PAGE was carried out as described in Section 2.2.7 (page 41). The gel was usually ran 30 minutes at 60 V and 1.5 hours at 90 V until the front reached the bottom of the gel. The gel was then stained with SimplyBlue™ SafeStain (Invitrogen™) Coomassie G-250.

Imaging of the gels was performed with ChemiDoc™ XRS+ System with Image Lab™ Software. Images were processed and analyzed using Fiji²⁶⁰ (ImageJ distribution) and Microsoft Excel (2010). The Fiji Gel Analyzer was used to select the lanes, plot their intensity profile and calculate the integrated intensity of the bands of interest. The results were exported to Microsoft Excel (2010). The bands corresponding to the Min proteins were identified by visual inspection by comparing them with the expected protein weights. The fraction of protein found in the pellet with respect to the total amount of protein in the sample (%) was calculated using the following formula:

$$F = 100 \frac{A_p}{A_p + A_s}$$

5

Where F is the fraction of protein in the pellet; A_p is the measured integrated area of the protein band in the pellet and A_s is the measured integrated area of the protein band in the supernatant sample.

5.2.6 Production of SLBs

The formation of supported lipid bilayers (SLBs) was done as described in Section 2.2.5 (page 40) for glass chambers, with a few exceptions. First, LMV solutions were prepared as described in Section 2.2.4 (page 40) with *E. coli* polar lipids or composition 1 from Table 2.4 (page 40). Second, SUV solutions were prepared either by extrusion (Section 2.2.4, page 40) or by sonication. In the latter case, a tip sonicator (Q500 sonicator, Qsonica) with a microtip was employed. The tip was first cleaned with 70% ethanol and Milli-Q. Then, a suspension of LMVs was placed on ice and the tip of the sonicator inserted in the suspension. It was ensured

that the tip of the sonicator did not touch the walls of the tube. The program followed was as indicated below:

Table 5.3 Program use in the creation of SUVs through tip sonication.

Amplitude setting	25%
Pulse on	30 seconds
Pulse off	15 seconds
Total time	1 hour

After sonication, the resulting SUV suspension was centrifuged for 30 min at 20000 rcf (Eppendorf Centrifuge 5424 R) to precipitate the metal particles that were released from the sonicator tip. The supernatant containing the SUV solution was recovered and stored at -25 °C.

5.2.7 Reaction chambers

Both glass and aluminium reaction chambers were used in this chapter. For a description of their production and handling, see Section 2.2.2 (glass; page 38) and Section 3.2.2 (aluminium; page 65).

5.2.8 Preparation of DNA templates for cell-free expression

Preparation of the DNA constructs coding for *E. coli* K12 MinD (*minD*) and MinE (*minE*) was done by amplification with a standard PCR with Phusion High Fidelity DNA polymerase (ThermoFisher Scientific) from chromosomal *E. coli* MG1655 (K12). Primers ChD 511 and ChD 382 (*minD*), and ChD 512 and ChD 384 (*minE*) were utilized (Table 5.4). These primers contain overhangs for the pET11-a backbone plasmid. The PCR products and linearized backbone pET11-a DNA were checked on a 1% agarose gel stained with SYBR safe, imaged with a ChemiDoc™ Imaging System (BioRad Laboratories) and purified with Wizard SV Gel kit (Promega). The purified DNA was incubated with DpnI (New England BioLabs® Inc.) to remove residual plasmid and the linear DNA was purified again with Wizard SV Gel kit. DNA concentration and purity were measured using a ND-1000 UV-Vis Spectrophotometer (Nanodrop Technologies). Gibson assembly (Gibson Assembly® Master Mix of New England BioLabs® Inc) was performed at equimolar concentrations of linearized plasmid (pET11-a) and DNA fragments for 1 h at 50 °C. Transformation of the Gibson assembly products into *E. coli* TOP10 competent cells was done by heat shock, after which cells were resuspended in 200 µL of fresh prechilled liquid LB medium and incubated for 1 h at 37 °C and 250 rpm. Then, the cultures were plated in solid LB medium with ampicillin and grew overnight at 37 °C. Colonies were picked up and cultured in 1 mL of liquid LB medium with 100 µg/mL of ampicillin for 16 h at 37 °C and 250 rpm. Plasmid purification was performed using the PureYield™ Plasmid Miniprep System (Promega). Plasmid concentration and purity were checked on NanoDrop. All sequences were confirmed by sequencing. Additionally, DNA templates *minD* and *minE* sequence optimized for codon usage, CG content and 5' mRNA secondary structures were purchase from GenScript. Both optimized *minD* (*minD_{op}*) and *minE* (*minE_{op}*) constructs came inserted in a pCC1 and pUC57, respectively.

Linear DNA constructs were prepared by polymerase chain reaction (PCR) from a parental plasmid using the primers ChD 194 and ChD 181 (Table 5.4) annealing to the T7 promoter and T7 terminator sequences, respectively. Amplification products were checked on a 1% agarose gel and were further purified using Wizard SV gel (standard column protocol).

Table 5.4 List of primers and sequence

Name	Sequence (5' to 3')
ChD 181	CAAAAAACCCCTCAAGACCCGTTTAGAGG
ChD 194	TAATACGACTCACTATAGGGGAATTGTGAGCGGATAACAATTCCCCT
ChD 382	TCCTTTCGGGCTTTGTTAGCAGCCGGATCCTTATCTCCGAACAAGCGTTTG
ChD 384	TCCTTTCGGGCTTTGTTAGCAGCCGGATCCTTATTTAGCTCTTCTGCTCC
ChD 511	TTAACTTTAAGAAGGAGATATACATATGGCACGCATTATTGTTG
ChD 512	TTAACTTTAAGAAGGAGATATACATATGGCATTACTCGATTCTTTCTC

Concentration and purity were measured by NanoDrop. A detailed account of the DNA sequences and their features can be found in the Appendix (page 154).

5.2.9 SDS-PAGE analysis of synthesized proteins

Analysis on SDS-PAGE of *minD* and *minE_{op}* was done by expressing 5 nM of DNA template (single expression), or 8 and 4 nM of *minD* and *minE_{op}* in a reaction of PURE_{flex} 2.0 (Table 5.5). The reaction solution was supplemented with 1 μ L of DnaK Mix (GeneFrontier Corporation) and 0.5 μ L of GreenLys reagent (FluoroTectTM GreenLys, Promega). SUPERase was not used. After expression, the samples were treated with RNase (RNaseA Solution, Promega) for 30 minutes and boiled at 90 °C for 10 minutes in 2x Laemmli buffer with 10 mM of DTT. Samples were loaded on a 18% SDS-PAGE gel. Visualization of the fluorescently labeled proteins was performed on a fluorescence gel imager (Typhoon, Amersham Biosciences) using a 488-nm laser and a band pass emission filter of 520 nm.

5.2.10 Activity assays on SLBs

Activity assays with purified proteins utilized eGFP-MinD and MinE. Unless otherwise indicated in the relevant sections, a protein mixture was prepared in a 1.5 mL Eppendorf tube as shown in Table 5.6. Assays were carried out in reaction buffer (50 mM Tris-HCl pH 7.6, 150 mM KCl, 5 mM MgCl₂), PURE_{flex}, PURE_{flex} 2.0 or in home-made PURE buffer (20 mM HEPES pH 7.5, 180 mM Potassium glutamate, 14 mM Magnesium acetate). Next, the protein mix was injected in a glass or aluminium chamber where an SLB was already formed. After sealing of the chamber, the sample was imaged at 37 °C.

Activity assays with synthesized proteins was done similarly as described for purified proteins with a few exceptions. For the synthesis of Min proteins, a standard PURE_{flex} 2.0 reaction was carried out by mixing the reactants shown in Table 5.5 in a PCR tube and incubating for 3 hours at 37 °C. Next, the resulting translation products were mixed with the purified proteins and 2.5 mM of ATP, before being injected in a glass or aluminium reaction chamber with a preformed SLB (composition 2; Table 2.4, page 40). The added volumes of synthesized proteins and the concentration of purified proteins depended on the specific experiment and are indicated in the relevant sections.

Table 5.5 Standard reaction of PURE_{frex} 2.0

Reactant	Volume (μ L)	Final concentration
PURE _{frex} 2.0 I	10	1x
PURE _{frex} 2.0 II	1	1x
PURE _{frex} 2.0 III	2	1x
SUPERase	0.5	0.5 U/ μ L
DNA construct	x	5 nM
Milli-Q water	6.5-x	
Total	20	

Table 5.6 Standard composition of activity assays on SLBs with purified Min proteins.

The added buffer could be reaction buffer, PURE_{frex} or PURE_{frex} 2.0 solution I, or home-made PURE buffer.

Component	Volume (μ L)	Final concentration
20 mM ATP	2	2 mM
20 μ M eGFP-MinD	4	4 μ M
20 μ M MinE	3	3 μ M
Buffer	up to a volume of 20 μ L	1x

5.2.11 Microscopy and image analysis

All activity assays on SLBs were visualized using an Olympus IX81 Inverted TIRF microscope. Images were acquired on an EM-CCD camera (iXon X3 DU897, Andor technologies). The eGFP tag from either eGFP-MinC or eGFP-MinD was excited with a 488 nm excitation laser (Olympus CW lasers). Detection splitting filter cubes for dual channel detection were used with a 552 nm dichroic filter, a 524/29 nm emission filter on channel 1 and a 630/92 nm emission filter on channel 2. Olympus cell[^]TIRF illuminator and Andor IQ3 were used as control and acquisition software. The objective used was a 60x magnification oil immersion (ApoNTIRF, NA 1.49). An extra 2x magnification was present in the detection path right before the camera. All experiments were performed at 37 °C, using a temperature controller (T-unit bold line, Okolab).

Microscopy images were processed and analyzed with Fiji²⁶⁰. In general, images were adjusted for brightness and contrast. Optionally, a background subtraction was carried out with a roll balling radius of 50-250 pixels, depending on the image. If specified, average images (AVG) were computed by taking the average pixel intensity of a sequence of pictures of the same region of the sample during a certain period of time.

Analysis of the wave profile of Figure 5.6 E was done by calculating the average pixel intensity of a circular region in the center of the image over the span of 2 minutes (60 images in total). The period of the wave was calculated by averaging the elapsed time between peaks.

5.3 Results

5.3.1 Cloning, expression and purification of Min proteins

In the first place, we proceeded with the cloning, on *E. coli* TOP10 competent cells, of the plasmids containing the Min genes. Then, the proteins MinC, eGFP-MinC, eGFP-MinD and MinE were purified and the pooled fractions visualized on SDS-PAGE (Figure 5.1). The expected molecular weight for each protein was calculated from the amino acid sequence (Table 5.7) and a band corresponding to the expected molecular weight for each protein was found (Figure 5.1). In each case, this band exhibited the most intense signal in the lane. Additional bands aside of the target proteins could be observed as well (Figure 5.1). Next, we estimated the fraction of carry over for each of the purified proteins (Table 5.7). Although the fractions contained numerous additional bands, the target proteins represented a significant proportion of the total protein mass.

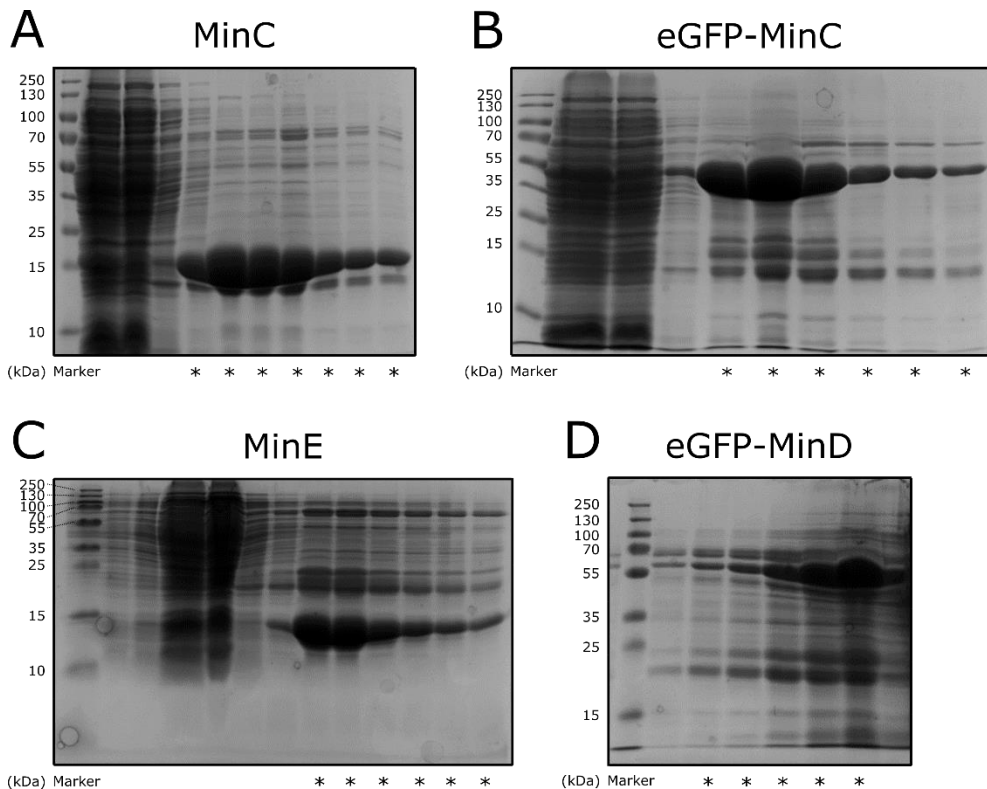


Figure 5.1 SDS-PAGE of the pooled fractions of the purified Min proteins

In all panels, the pooled fractions of each purified protein (*), the cell lysate (CFE), the flow through (FT) and the wash flow through (Wash) is shown. The molecular weight of the protein marker is in kDa. A) Pooled fractions of MinC (~15 kDa). B) Pooled fraction of eGFP-MinC (right below the 55 kDa mark). C) 14 % SDS-PAGE of the pooled fractions of Min E (right below the 15 kDa mark). D) Pooled fractions of eGFP-MinD (right above the 55 kDa mark).

5.3.2 Concentration measurement of purified Min proteins

Next, we assessed the concentration of the purified Min proteins. We reasoned that even a rough approximation would be still useful, since we would have not only an indication about the concentration, but also the ratio at which the purified Min proteins should be employed. We decided to assess the protein concentration by two different but complementary methods.

Table 5.7 Concentration and predicted molecular weight of purified Min proteins

The concentration of the purified Min proteins was calculated based on the Bradford and spectrometry assays. The predicted molecular weight was calculated from amino acid sequence. The carry over for each purified Min protein was calculated. n: number of samples used to calculate the average value. SD: standard deviation.

Stock Protein	Predicted weight (kDa)	Carry Over (%)	Bradford ($\mu\text{M}(n)$, SD)	Spectrometry ($\mu\text{M}(n)$, SD)
MinC	28.5	62	146 (3), 31	--
eGFP-MinC	53.2	55	127 (3), 5	176 (4), 36
eGFP-MinD	60.1	25	64 (6), 3	36 (3), 1
MinE	13.9	36	445 (2), 0.6	--

In one hand, we performed a Bradford assay. Since this assay detects the total protein concentration in a given sample, the results should be considered an overestimation. The standard curve measurements, their calculated linear regressions as well as the measured absorbance values of the different Min proteins can be seen in Figure 5.2. A table summarizing the calculated concentration (μM) for each purified protein can be seen in Table 5.7. In the other hand, we estimated the molar concentration (μM) of the stock proteins by fluorescence spectrometry. This method detects only the presence of a specific fluorophore in the sample, so consequently, only those proteins fused to a fluorophore, i.e. eGFP-MinC and eGFP-MinD, were measured following this approach (Table 5.7).

Because the Bradford assay allowed us to measure the protein concentration of all the purified Min proteins, we resolved to use the results of this method as our working concentrations in future experiments.

5.3.3 Purified MinC, eGFP-MinD and MinE exhibit the expected protein-to-protein and protein-to-membrane interaction in sedimentation assays

Next, we tested the interaction of our purified Min proteins with a phospholipidic membrane and with each other by performing a series of sedimentation assays. We tested the proteins MinC, eGFP-MinD and MinE, both alone and in all possible combinations of two and three proteins in a final concentration of 2, 4 and 6 μM , respectively. We decided not to include eGFP-MinC to avoid possible artifacts caused by the fused eGFP.

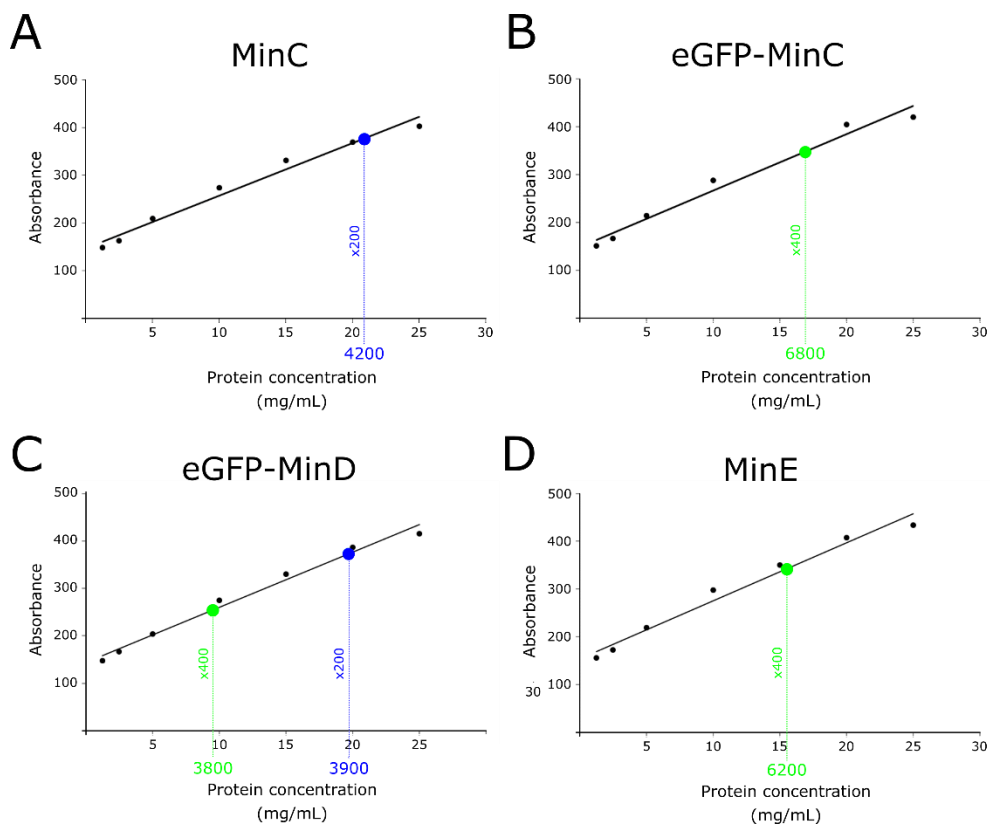


Figure 5.2 Bradford assays performed with the purified Min proteins.

In all panels, small, black dots correspond to the standard made with BSA. Black line corresponds to the linear regression calculated for the standards curve. Each sample was diluted 100, 200 (blue) or 400 (green) times. Each dilution was replicated 3 times. In every panel, the protein concentration (mg/mL) of the original sample has been calculated. Table 5.7 summarizes this information.

Figure 5.3 A-C shows the resulting protein gels of the performed sedimentation assays. For each sample, the percentage of each protein in the pellet was calculated by measuring their integrated band intensities (Equation 5). The calculated percentage should be regarded as a slight overestimation of the real percentage of protein in the pellet, because only an 80% of the supernatant volume was transferred to the wells of the SDS-PAGE gels. However, all samples were treated equally and therefore can be compared to each other.

5.3.3.1 eGFP-MinD binds to the membrane

In the first place, we sought to analyze the capacity of each purified protein to bind to the membrane. To test this, we carried out three different sedimentation assays, only with one protein at a time. Figure 5.3 A shows the resulting SDS-PAGE of these assays and Figure 5.3 D the quantification results. This latter graph, although based only in one repeat, shows the same binding pattern obtained in two other repeats (Figure SI 5.8). The reason we did not included those here is because their conditions were not directly comparable to the following sedimentation assays.

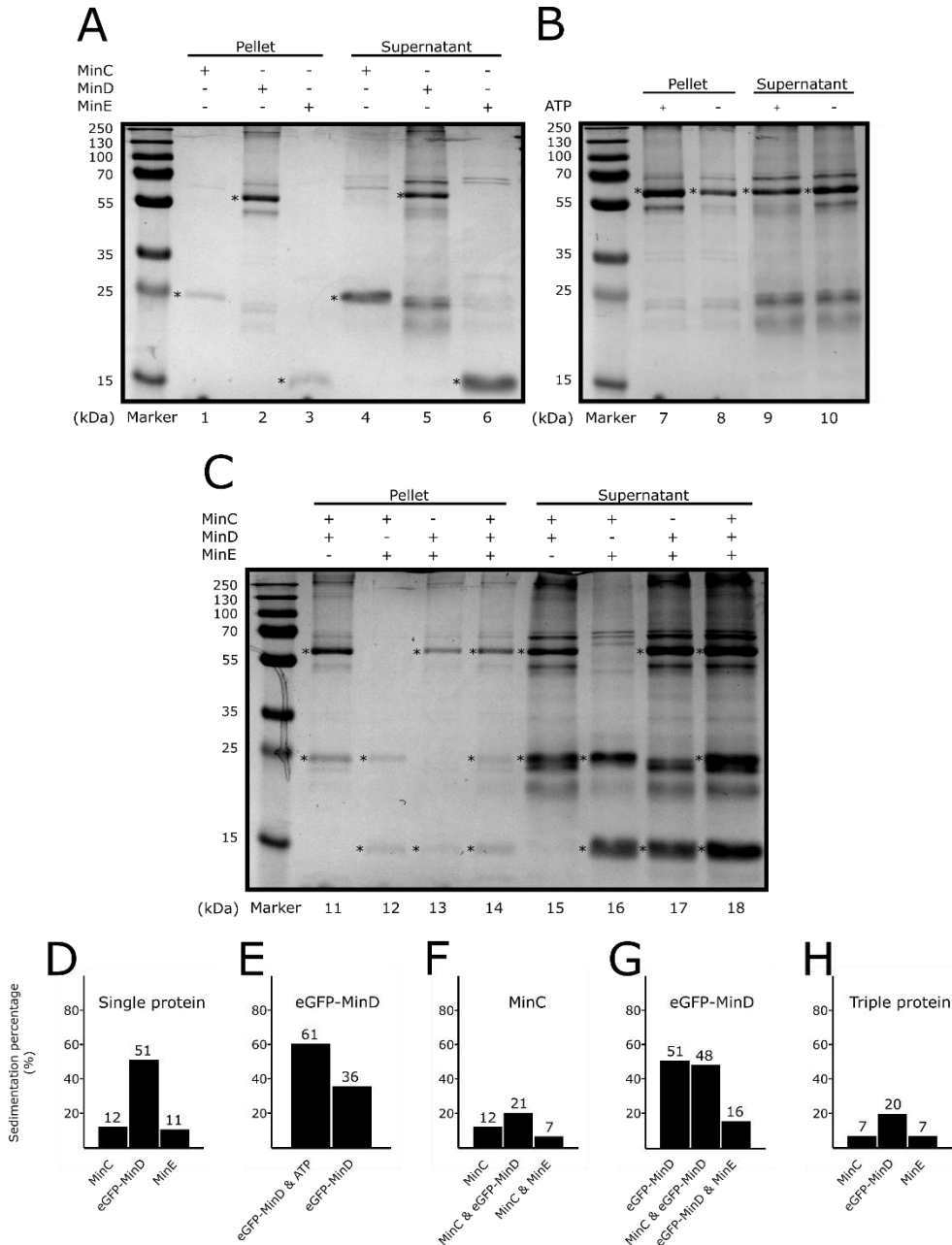


Figure 5.3 Sedimentation assays analyzed by SDS-PAGE and quantification of the fraction of Min proteins associated with the membrane.

In panels from A to C, (*) indicates the band corresponding to MinC (~25 kDa), eGFP-MinD (~55 kDa) and MinE (~15 kDa) and the approximated molecular weight of the protein marker is shown in kDa. The assays were performed with a solution containing 3 mg/mL of *E. coli* polar lipids LMVs and, unless indicated, 1 mM of ATP. The final concentration of each protein was always 2, 4 and 6 μ M of MinC, eGFP-MinD and MinE, respectively. A) SDS-PAGE of sedimentation assays performed with the purified proteins MinC, eGFP-MinD and MinE (assayed alone). B) SDS-PAGE of

sedimentation assays performed with the purified eGFP-MinD with and without 1 mM of ATP. C) SDS-PAGE of sedimentation assays performed with a combination of two or three purified proteins. D) Fraction of each Min protein found in the pellet when assayed alone. E) Fraction of protein found in the pellet when eGFP-MinD was assayed alone, with and without 1 mM of ATP. F) Fraction of MinC found in the pellet when assayed with eGFP-MinD or with MinE. G) Fraction of eGFP-MinD found in the pellet when assayed with MinC or with MinE. H) Fraction of each Min protein found in the pellet when assayed together.

While the fraction found in the pellet for both MinC and MinE was around 10% (12% for MinC and 11% for MinE), MinD exhibited a clear 51%. This result indicates that the purified eGFP-MinD interacts with the membrane in a greater extent than the purified MinC and MinE, in agreement with the current model.

5.3.3.2 eGFP-MinD membrane binding capacity is influenced by the presence of ATP

An important, essential feature of the Min system is the influence of ATP in MinD's membrane recruitment capability. Upon nucleotide binding, MinD dimerizes, heavily increasing its affinity for the membrane¹¹². To assess whether eGFP-MinD membrane affinity is ATP dependent or not, a sedimentation assay was performed with eGFP-MinD alone, in the presence and in the absence of ATP. The results were visualized by SDS-PAGE (Figure 5.3 B).

A graph displaying the percentage of eGFP-MinD sedimentation in both conditions can be seen in Figure 5.3 E, showing that in the presence of ATP, about 61% of eGFP-MinD is found in the pellet, while this percentage lies around 36% in its absence. Such outcome indicates that the affinity of eGFP-MinD for the membrane is increased in the presence of ATP.

5.3.3.3 The fraction of MinC found in the pellet increases in the presence of eGFP-MinD

Next, we sought to verify the interaction between the purified MinC and eGFP-MinD proteins. This feature is capital for the correct functioning of the Min

system *in vivo*, since it couples the FtsZ polymerization inhibitory capacity of MinC with the topological specificity given by the MinDE complex^{111,172,226,227,239,242}. We have already established that the fraction of purified eGFP-MinD able to cosediment with the pellet reaches levels of around 50% (Figure 5.3 D). Therefore, we should also expect the purified MinC to sediment in a larger extent when in the presence of eGFP-MinD than when assayed alone. To test this, we carried out two sedimentation assays where we combined the purified MinC with eGFP-MinD or with MinE as a control (Figure 5.3 C, lanes 11, 12, 15 and 16).

Then, we analyzed the levels of MinC alone, in the presence of eGFP-MinD or together with MinE (Figure 5.3 F). In the absence of eGFP-MinD, the sedimentation levels of MinC remained in a 12% (MinC alone; data taken from Figure 5.3 D) and 6.9% (MinC with MinE). However, when assayed together with eGFP-MinD this percentage almost tripled up to a 21%, indicating an interaction between MinC and eGFP-MinD.

5.3.3.4 MinE releases eGFP-MinD from the membrane

To generate protein oscillations *in vivo*, MinE must be able to release MinD from the membrane. To test whether the purified eGFP-MinD and MinE respond to each other adequately, we performed a sedimentation assay where eGFP-MinD was combined with MinE (Figure 5.3 C, lanes 13 and 17).

Next, we calculated and compared the percentage of eGFP-MinD that cosedimented with the pellet when only eGFP-MinD, eGFP-MinD plus MinC or eGFP-MinD plus MinE were mixed (Figure 5.3 G). While samples containing only eGFP-MinD or eGFP-MinD plus MinC presented a similar percentage of around 50% (51% (from Figure 5.3 D) and 48%, respectively), the sample containing eGFP-MinD plus MinE dropped to a 16%. These results not only suggest that our purified eGFP-MinD responds as expected to the presence of a purified, functional MinE, but also that the purified protein MinE retains the ability to influence the membrane binding capability of the purified MinD.

5.3.3.5 Only eGFP-MinD reaches non-background sedimentation levels when the complete Min system is assayed

So far, we tried assays involving individual or combinations of two proteins. However, the Min system is designed to act as a whole in order to regulate cell division *in vivo*. For example, if only the oscillatory proteins MinD and MinE are present, but not the FtsZ inhibitor MinC, then the system cannot influence the location of the divisome. A similar situation arises when only MinD or MinE are absent. In the presence of the three proteins, MinD is expected to bind first to the membrane, followed by MinC recruitment into a MinCD complex^{112,226,243}. Finally, and after some lagging time, MinE releases MinCD from the membrane^{112,132,133,256}. To assess whether our purified proteins follow similar dynamics, we performed a sedimentation assay with the three Min proteins combined and visualized it as usual with an SDS-PAGE (Figure 5.3 C, lanes 14 and 18).

Then, we calculated the percentage of each individual protein in the pellet. The results can be seen in Figure 5.3 H and revealed that the percentage of eGFP-MinD (20%) was higher than the percentage of both MinC (7%) and MinE (7%). At the same time, eGFP-MinD levels were also lower than the obtained when eGFP-MinD was assayed alone (51%; Figure 5.3 D) and similar to the one obtained when both eGFP-MinD and MinE were combined (16%; Figure 5.3 G). The fraction of MinC in the pellet (7%) was close to the one obtained when only MinC was tested (12%) and clearly lower than the one obtained when both MinC and eGFP-MinD were assayed together (21%). A discussion about this low value can be read in Section 5.4.2.3. Similar binding patterns were obtained for the three Min proteins when a repeat of this experiment was carried out (Figure SI 5.8). Together, this was the expected pattern to observe when the three Min proteins are combined.

5.3.4 Purified Min proteins display spatiotemporal waves on SLBs

In order to capture the local spatiotemporal activity of the Min system, we performed a series of activity assays on supported lipid bilayers (SLBs). Such type of experiments work as follows. First, a phospholipidic membrane is produced on top of a solid support. Due to the success of the previous sedimentation assays and unless otherwise specified, the composition of the membrane will be again *E. coli* polar lipids for the following set of experiments. Second, the proteins of interest are placed on top of the membrane and let to interact. In our case, only the purified proteins eGFP-MinD and MinE will be used. eGFP-MinC will be omitted because it interferes with the read-out signal from eGFP-MinD. Finally, the dynamic protein behavior on the membrane is observed with fluorescence microscopy.

5.3.4.1 MinD and MinE display spatiotemporal waves in simple buffer conditions

First, we wanted to know whether our purified proteins were able to generate Min waves. To test this, we prepared an SLB composed of *E. coli* polar lipids. Then, 4 μM of purified eGFP-

MinD plus 3 μM of purified MinE were added on top of the membrane in reaction buffer. Due to the importance of ATP for the functioning of MinD, 2 mM of this nucleotide was added to the reaction solution.

After addition of the proteins onto the membrane, the membrane showed a non-homogeneous distribution of recruited eGFP-MinD in the form of *bright patches* (Figure SI 5.9 A shows a typical *bright patch*). We were unable to observe any protein dynamics on these areas. To reassure that the signal originated from recruitment of purified eGFP-MinD onto the membrane, and not by unspecific binding of eGFP-MinD to bare glass, we passivated our chamber with BSA right after the formation of the SLB. Still, we observed once more the presence of *bright patches*. This indicates that, while eGFP-MinD was recruited to these areas of the membrane, there were no protein dynamics. Outside the *patches*, not all the surface looked homogenous, but some regions exhibited a slightly higher signal than others. In a subfraction of these regions, the signal did not stay static but shifted along the membrane with a defined direction and forming a wave-like pattern (Figure 5.4 A). The waves presented a front and a rear, although these did not end up organizing into extended fronts of clear and parallel waves. Therefore, we named these patterns *chaotic travelling waves*. Interestingly, it seemed like there were some focal points where new fronts could be formed or obstacles where the fronts collapsed, not allowing the *chaotic waves* to organize in extended parallel fronts. These results show that the purified proteins eGFP-MinD and MinE are able to generate wave-like protein dynamics in reaction buffer.

5.3.4.2 MinD and MinE display spatiotemporal waves in the complex background of the PURE system only if extra ATP is added

Next, we sought to investigate whether the purified proteins eGFP-MinD and MinE were able to generate waves in the complex background of the PURE system. Therefore, we prepared a sample containing again 4 μM of purified eGFP-MinD and 3 μM of purified MinE in a PURE_{flex} background. ATP was not added because it is already present in the PURE system. After addition of the proteins on the membrane, we were not able to detect the formation of Min waves (Figure SI 5.9 B). This was unexpected, given that the same purified proteins, in the same concentrations, were able to generate wave-like patterns in reaction buffer (Figure 5.4 A). Still, *bright patches* as the ones observed in the previous assays (Section 5.3.4.1) were observed.

We proposed several hypotheses to explain this discrepancy. First, the difference in salt concentration and composition between the reaction buffer and PURE_{flex} might cause the inactivation of one or several of the purified Min proteins. Additionally, salt concentration is known to influence wave formation¹³⁴. To test this, we proposed to carry out an activity assay in the context of a home-made PURE_{flex} buffer instead of the whole system. The home-made PURE_{flex} buffer roughly contains the same components than the original, commercial PURE_{flex} buffer. Therefore, we performed an SLB activity assay as done before in Section 5.3.4.1. After 4 μM of eGFP-MinD and 3 μM of MinE were mixed together with the home-made PURE buffer and placed on top of the SLB, wave-like patterns were observed (Figure 5.4 B). In total, three repeats of this activity assay were performed, and the results were positive and consistent (another example is shown in the supplementary Figure SI 5.9 C). Interestingly, the presence of waves on the membrane shifted from the darker areas to the *bright patches* mentioned earlier when reaction buffer, instead of the home-made PURE buffer was used. Due to this new location, the dynamic protein patterns looked more confined and irregular than before, yet similar to the *chaotic waves* described earlier (compare with Figure 5.4 A). Despite this difference, the occurrence of waves was very clear, and we concluded that the PURE_{flex} buffer was not directly responsible for the absence of the Min waves.

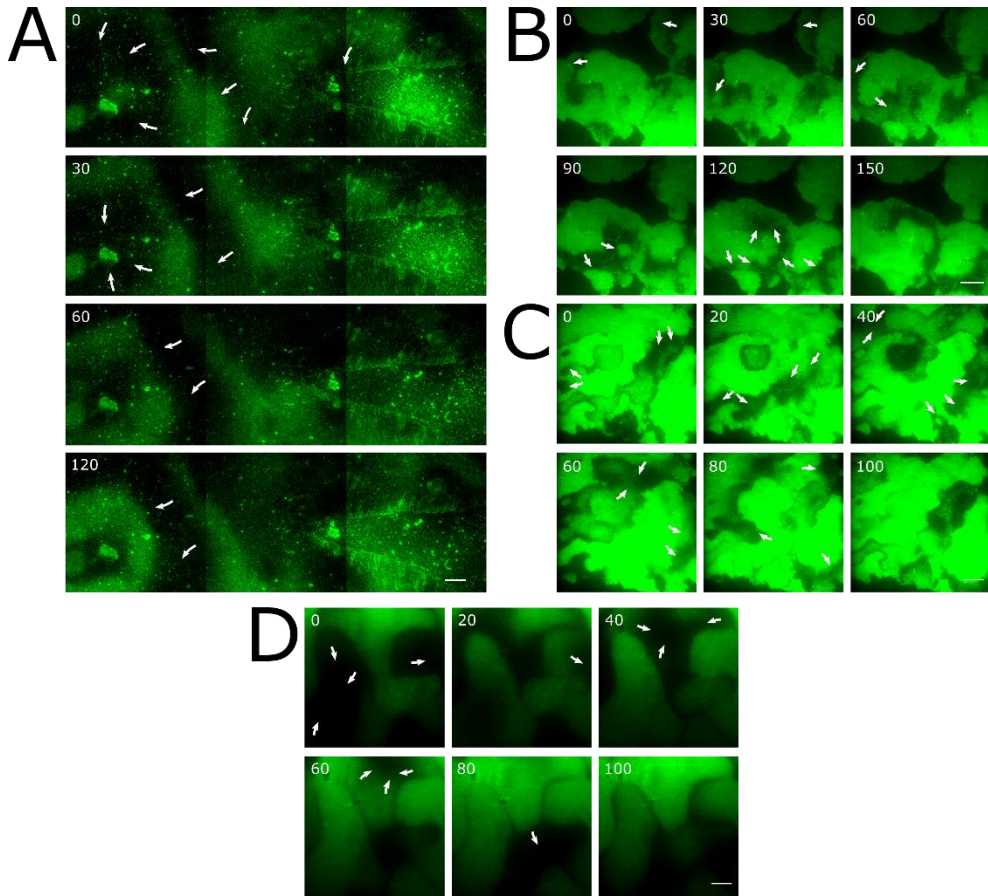


Figure 5.4 Activity assays with the purified Min proteins eGFP-MinD and MinE

TIRFM time-lapse images. Time is shown in seconds. White arrows indicate progression of the wave front. All scale bars: 10 μm . A) Montage of an activity assay performed in reaction buffer. B) Activity assay performed in home-made PUREflex buffer. C) Activity assay in commercial PUREflex, supplemented with 2 mM of ATP. D) Activity assay in commercial PUREflex on top of a DOPC:DOPG minimal membrane.

Second, in view of the latter conclusions, we reasoned that in physiological conditions, the absence of spatiotemporal waves could be due to a high MinE concentration or low levels of effective ATP concentration. The high MinE concentration hypothesis is impossible because the amount of added protein (3 μM) is the same in all the previous assays. However, in the case of the activity assay with the complex, PUREflex background, we relied on the already present ATP to allow the correct functioning of the purified eGFP-MinD. In this case, it is possible that the available levels of this nucleotide are lower due to a network of ATP-consuming reactions occurring in the system and in turn reducing the recruitment of eGFP-MinD to the membrane. To test this hypothesis, we performed a set of SLB activity assays with PUREflex as background plus the addition of an extra amount of 2.5, 5 or 7.5 mM of ATP. Waves were detected for all the three ATP concentrations (Figure 5.4 C; figure only shows waves obtained with 2.5 mM ATP). Once more, the presence of waves was restricted to the *bright patches* referred earlier and showed a very similar wave morphology and dynamics. In conclusion, we

have shown that the limiting factor avoiding Min wave formation in the PURE system was not the PURE_{flex} buffer per se, but the low levels of available ATP.

5.3.4.3 MinD and MinE display spatiotemporal waves on a minimal lipid membrane composition.

So far, we have successfully utilized the purified Min proteins eGFP-MinD and MinE to generate Min waves on SLBs. Additionally, we have optimized the conditions to allow these proteins to operate in the complex background of the PURE system. This is an important step towards the implementation of an oscillatory protein complex in a PURE system based, biomimetic cell. In the case of a minimal cell, it is appealing to use a lipid composition as minimal as possible. In Chapter 2 and Chapter 4 we described and worked with a minimal SLB membrane. We would like the Min system to function also with this membrane composition. Consequently, we decided to assay the activity of the purified proteins eGFP-MinD (4 μ M) and MinE (3 μ M), on top of an SLB (composition 2; Table 2.4, page 40) in PURE_{flex} 2.0. Right after the addition of the protein on the membrane, we observed the formation of waves (Figure 5.4 D).

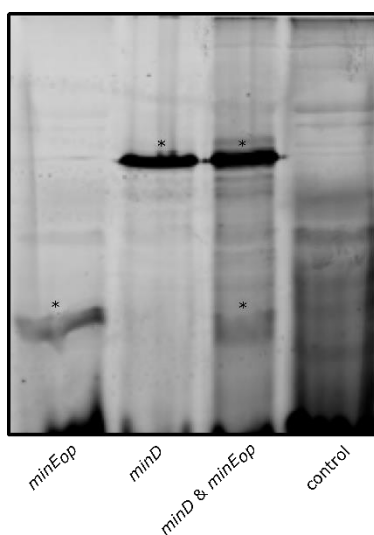


Figure 5.5 Synthesized MinD and MinE_{op} analyzed on SDS-PAGE

DNA templates *minD* and *minE_{op}* were expressed in a PURE_{flex} 2.0 reaction both alone (5 nM) or together (8 nM of *minD* and 4 nM of *minE_{op}*). Translation products were analyzed in a 18% SDS-PAGE. Asterisks (*) mark the corresponding bands of MinE_{op} (~10 kDa) and MinD (~29 kDa). Control sample corresponds with a reaction with no genes.

5.3.5 Cell-free synthesized Min proteins exhibit functional behavior on SLBs

In the previous section we have shown that purified Min proteins eGFP-MinD and MinE are capable of generating Min waves on SLBs, not only in the context of a simple buffer but very importantly also in the background of the PURE system (Section 5.3.4.2; Figure 5.4 B-D). Consequently, the MinDE working system will be used in following experiments to test the activity of cell-free synthesized Min proteins. As discussed in other parts of this thesis, the use of synthesized proteins is crucial to achieve the construction of a minimal cell from a bottom-up approach with self-maintaining and self-reproducing capabilities.

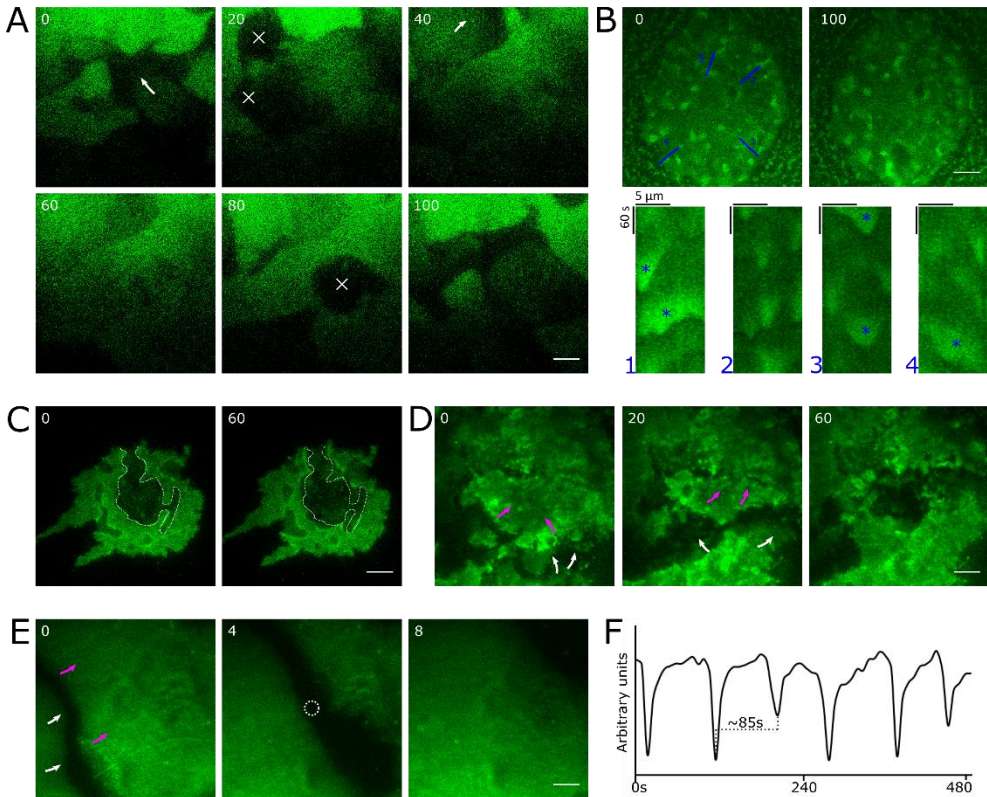


Figure 5.6 Activity assays of synthesized MinD with purified MinE

TIRFM images of activity assays of synthesized MinD and purified MinE plus 100 nM of eGFP-MinD for visualization purposes on top of SLBs. White arrows indicate wave front extension. Magenta arrows indicate wave rear withdrawing. White crosses indicate a homogeneous increase in signal intensity in the area. All scale bars: 10 μm . A) Activity assay with a minimal DOPC:DOPG (80:20 mol%) membrane composition. Although the protein patterns did not seem to occur inside the bright patches with this membrane composition, the dynamics were still similar to the chaotic waves. B) Activity assay on an SLB with an *E. coli* polar lipid composition. In this region we observed the presence of small waves able to appear and disappear quickly. They were able, sometimes, of travelling a short distance before disappearing. *Top*, time-lapse of the region at time 0 and 100 seconds. *Bottom*, kymographs of the profiles shown as blue lines in the top over a span of 6 minutes. Here, it can be seen how the small waves were able to appear and disappear (kymographs number 2 and 3; waves marked with asterisks [*]) and travel short distances on the membrane (kymographs 1 and 4; waves marked with asterisks [*]). C) Activity assay on an SLB with an *E. coli* polar lipid composition. The region corresponds to a bright patch of a chaotic wave with extremely low wave velocity. The dashed line marks the rear of the wave at time 0 seconds. D) Activity assay on an SLB with an *E. coli* polar lipid composition. The region showed a chaotic wave inside a bright patch. E) Activity assay on an SLB with an *E. coli* polar lipid composition. This is the first example of a travelling wave obtained in our experiments. F) Integrated intensity of the circular region in the photograph at 4 seconds over the span of 2 minutes. The average period reached to approximately 84 seconds.

First, we validated the expression of the *min* DNA templates by expressing 5 nM of *minD* or *minE* in a single reaction of PURE_{flex} 2.0 or by co-expressing 8 nM of *minD* and 4 nM of *minE_{op}*. We obtained bands at the expected molecular weights for MinD (~29 kDa) and MinE_{op}

(~10 kDa) in both cases (Figure 5.5). This confirmed that our DNA templates can be used in subsequent experiments.

5.3.5.1 Synthesized MinD and purified MinE resume spatiotemporal waves

Next, we sought to test the activity of synthesized MinD. In the first place, we expressed *minD* in standard conditions. Next, we mixed the translation products with 3 μM of purified MinE and 100 nM of purified eGFP-MinD as a fluorescence reading-out molecule. After injection of the proteins on top of the SLB, *chaotic travelling waves* were detected (Figure 5.6 A). Interestingly, the waves were not occurring inside the areas referred before as *bright patches* (Section 5.3.4.1). To assure that the presence of residual amounts (100 nM) of the purified protein eGFP-MinD was not causing the formation of Min waves, we assayed samples containing only 100 nM of purified eGFP-MinD but not with synthesized MinD. In these conditions, no protein dynamics were generated (Figure SI 5.10 B). The overall morphology and dynamics of the waves when synthesized MinD was present, was very similar to the assays where only purified proteins were tried, despite the lack of confinement of these waves in *bright patches* (Figure 5.6 A). However, other experiments with an *E. coli* membrane lipidic composition showed the presence of regions with protein dynamics inside *bright patches* that largely differed from the already mentioned *chaotic waves*. For example, Figure 5.6 B-E shows several images that, despite their apparent diversity, belong to various regions of the same sample. In Figure 5.6 B we observed the presence of small areas with an increased fluorescent signal, able to appear and move on the membrane before quickly disappearing. The direction of movement of these waves was very irregular. Also, as can be seen in Figure 5.6 C, some *bright patches* exhibited an exceptionally low wave velocity, while keeping the typical morphology of a *chaotic wave*. In this sample, we also obtained the typical *chaotic waves* inside a *bright patch* (Figure 5.6 D; Figure SI 5.10 A), but we also observed the presence of the most canonical travelling Min wave to date in our experiments (Figure 5.6 E). This wave presented a prolonged front with a consistent direction of propagation, even when confined in a *bright patch* (Figure SI 5.10 B). It exhibited an averaged wave velocity and period of 1.86 $\mu\text{m/s}$ and 89 s (Figure SI 5.10 F), respectively, resulting in a wave length of 165 μm . In order to assess the robustness of the synthesized MinD activity assay, we also carried out a set of experiments on SLBs with different membrane compositions, buffer background and volume of synthesized protein. The results are summarized in Table 5.8, and show that the synthesized MinD is able to generate Min waves in the presence of purified MinE in the range of conditions tested.

5.3.5.2 Synthesized MinE and purified eGFP-MinD are unable to resume spatiotemporal waves

Next, we decided to test the activity of cell-free synthesized MinE on SLBs. We expressed in standard conditions 5 nM of *minE* in PURE_{flex}. Then, we combined it with 4 μM of the purified protein eGFP-MinD in order to enable the generation of Min waves and also as a read-out molecule. After the addition of the protein mix on top of an *E. coli* polar lipids SLB, we could not detect the presence of Min waves or any type of protein dynamics. Still, the *bright patches* were present.

We proposed several hypotheses to explain the absence of waves and experimentally investigated them. Table 5.9 shows a summary of various of the different conditions at which we assayed synthesized MinE. First, we hypothesized that the concentration of synthesized MinE might be such that its ratio with eGFP-MinD is unbalanced. To test this, we assayed different eGFP-MinD:MinE ratios. None of them exhibited any Min dynamics. Second, the expression of *minE* might be too low and therefore might not be enough protein to trigger the formation of waves. To test this hypothesis, we designed a new, PURE_{flex} optimized *minE* DNA

Table 5.8 Set of experiments performed on SLBs with synthesized MinD and purified MinE under different conditions.In all cases 100 nM of eGFP-MinD and 6 μ M of MinE was utilized.

Experiments	MinD (μ L)	MinD _{op} (μ L)	ATP (mM)	Background	Membrane composition	Ficoll70 (m/v%)	Results
1	16	--	2.5	PURE <i>frex</i>	<i>E. coli</i> polar lipids	--	waves
2	--	16	--	PURE <i>frex</i> 2.0	<i>E. coli</i> polar lipids	--	no waves
3	--	--	--	PURE <i>frex</i>	<i>E. coli</i> polar lipids	--	no waves
4	16	--	2.5	PURE <i>frex</i>	DOPC-DOPG-DGSNTA	--	waves
5	--	16	2.5	PURE <i>frex</i> 2.0	DOPC-DOPG-DGSNTA	--	waves
6	16	--	2.5	PURE <i>frex</i> 2.0	DOPC-DOPG	--	waves
7	16	--	2.5	PURE <i>frex</i> 2.0	DOPC-DOPG	50	waves
8	10	--	2.5	PURE <i>frex</i> 2.0	DOPC-DOPG	50	waves
9	7	--	2.5	PURE <i>frex</i> 2.0	DOPC-DOPG	50	waves
10	4	--	2.5	PURE <i>frex</i> 2.0	DOPC-DOPG	50	waves

Table 5.9 Set of experiments performed on SLBs with synthesized MinE or MinE_{op} and purified eGFP-MinD or synthesized MinD under different conditions

In all cases, 2.5 mM of ATP was utilized.

Experiment	eGFP-MinD (μ M)	MinD (μ L)	MinE (μ L)	MinE _{op} (μ L)	Background	Membrane composition	Expression	Results
1	4	--	16	--	PURE <i>frex</i>	<i>E. coli</i> polar lipids	3 hours at 37 °C	No waves
2	4	--	13	--	PURE <i>frex</i>	<i>E. coli</i> polar lipids	3 hours at 37 °C	No waves
3	4	--	10	--	PURE <i>frex</i>	<i>E. coli</i> polar lipids	3 hours at 37 °C	No waves
4	4	--	5	--	PURE <i>frex</i>	<i>E. coli</i> polar lipids	3 hours at 37 °C	No waves
5	4	--	16	--	PURE <i>frex</i>	<i>E. coli</i> polar lipids	6 hours at 25 °C	No waves
6	0.1	8	8	--	PURE <i>frex</i>	DOPC-DOPG-DGSNTA	3 hours at 37 °C	No waves
7	0.1	8	8	--	PURE <i>frex</i> 2.0	DOPC-DOPG-DGSNTA	3 hours at 37 °C	No waves
8	2	--	16	--	PURE <i>frex</i> 2.0	DOPC-DOPG-DGSNTA	3 hours at 37 °C	No waves
9	2	--	--	16	PURE <i>frex</i> 2.0	DOPC-DOPG-DGSNTA	3 hours at 37 °C	No waves

template (*minE_{op}*). We expected *minE_{op}* to be able to reach a higher final active protein concentration than the wild-type *minE* construct. Yet, the expression of *minE_{op}* in standard conditions in PURE_{flex} did not trigger the formation of Min waves when combined with 4 μM of eGFP-MinD and placed on top of an *E. coli* polar lipids SLB. Third, the levels of active, functional MinE might be too low. The most probable factor contributing to the activity of synthesized MinE is the protein folding. In one hand, we thought that we could circumvent the problem by combining the synthesized MinE with a synthesized MinD instead of its purified counterpart (eGFP-MinD) and relegate the function of the latter to a mere read-out molecule. We reasoned that a partially misfolded synthesized MinE might function better when exposed to a non-tagged MinD. Consequently, we synthesized 5 nM of both *minE* and *minD* in standard conditions in separated reactions. Then, the resulting translation products were placed together with 100 nM of eGFP-MinD as a read-out molecule on top of an SLB. Still, no protein dynamics were detected. In the other hand, it is possible to influence the folding of a PURE system synthesized protein by reducing the incubation temperature²⁶¹, for example, at 25 °C instead at the standard 37 °C. This way, the nascent peptide enjoys of longer time to fold adequately. However, we must expect the translation rate to slow down and therefore incubation time should be extended, for example from 3 to 6 hours. We attempted this strategy and expressed 5 nM of the *minE* DNA template at 25 °C for 6 hours in PURE_{flex}. Upon addition of the translation products with 4 μM of eGFP-MinD on top of an *E. coli* polar lipids SLB, no waves were observed.

5.3.5.3 A completely cell-free synthesized MinDE system exhibits

spatiotemporal waves only when *minE* is expressed with chaperones

Next, we sought to investigate further the reasons for the absence of synthesized MinE activity. We reasoned that supplementing the PURE_{flex} reaction with molecular chaperones, like for example DnaK and the protein complex GroE, would facilitate the correct folding of the nascent peptide and of misfolded proteins²⁶²⁻²⁶⁵. We started with two standard separated expressions in PURE_{flex} 2.0 of *minD* and *minE_{op}* (5 nM each). The reaction containing *minE_{op}* was supplemented with DnaK. Then, 8 μL of synthesized MinD and 8 μL of synthesized MinE_{op} were added on top of a DOPC-DOPG membrane (composition 2; Table 2.4, page 40) together with 100 nM of eGFP-MinD for visualization purposes and GroE. Strikingly, we observed extensive areas of the SLB showing Min waves (Figure 5.7 A).

Interestingly, this time most of the spatiotemporal patterns could be considered canonical travelling waves as seen in the literature^{133,172,256}. The waves were organized in clear and extended parallel fronts with a defined direction over time and no *chaotic waves* were observed. Furthermore, we detected the presence of a new type of pattern on the membrane. It consisted on an eGFP-MinD patch (core) with smooth and very well-defined edges, surrounded by a ring of low fluorescence signal (Figure SI 5.11 A). This pattern was present always together with many other eGFP-MinD cores and seemed to undergo no travelling over the membrane. Sometimes, canonical travelling waves were found next to these static patterns (Figure SI 5.11 B and C).

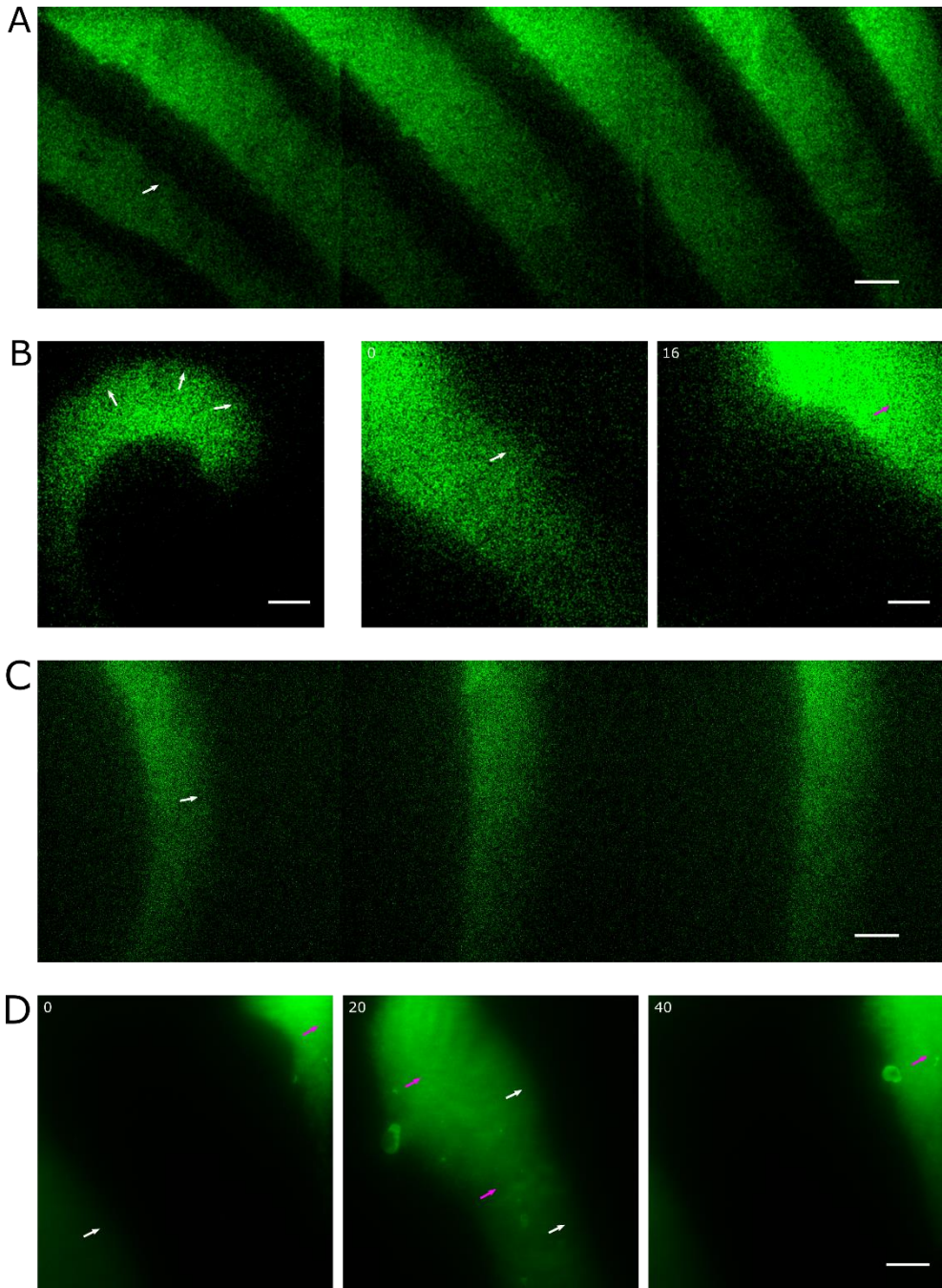


Figure 5.7 Activity assays with synthesized MinD and MinE_{op}

TIRFM images. White arrows indicate wave front extension. Magenta arrows indicate wave rear withdrawing. All scale bars: 10 μm . A) Montage of a region of a sample with synthesized MinD and MinE_{op}. B) Activity assay of co-synthesized MinD and MinE_{op}. *Left*, image of a spiral node on the membrane. *Right*, time-lapse of a travelling wave on the membrane. C) Montage of an activity

assay with a reduced volume (10 μL) of co-synthesized MinD and MinE_{op}. D) Co-synthesized MinD and MinE_{op} together with 1 μM of purified eGFP-MinC. The images show a time-lapse of a travelling Min wave, indicating that the purified protein is able to follow the dynamics generated by MinD and MinE_{op}.

Additionally, we wanted to explore the possibilities of co-expression as a method to implement the synthetic MinDE system in artificial cells. In a biomimetic cell, like for example a liposome in which transcription and translation reactions are taking place, a separated expression of proteins and an eventual mixing is impossible or rather extremely difficult. This means that both *minD* and *minE* must still produce functional proteins even when expressed in the same reaction. Consequently, we carried out a one-pot, single co-expression of 5 nM of *minD* and 5 nM of *minE_{op}* in standard conditions, supplemented with the molecular chaperone DnaK. Then, 16 μL of the resulting translation products were mixed with 100 nM of the purified eGFP-MinD as a read-out molecule and supplemented with GroE. After injection of this mix on the SLB, similar travelling waves as described when separately synthesized proteins were assayed, were observed (Figure 5.7 B; Figure SI 5.12). Furthermore, we performed a second experiment where we reduced the volume added to the protein mix of the synthesized MinD and MinE_{op} by a 40% (from an added volume of 16 μL to 10 μL). Even with a reduced concentration of synthesized proteins, the SLB exhibited the presence of travelling waves (Figure 5.7 C). These results show that we have been able to successfully cell-free synthesized active, functional MinD and MinE_{op} not only in two separately PURE system reactions, but also when both constructs were expressed together.

5.3.5.4 MinC follows along dynamic, co-synthesized MinDE travelling waves

MinC, despite having no part in the generation of waves, plays an important role by regulating the divisome protein complex and therefore cell division *in vivo*. This makes MinC a key component and its implementation in a functional Min system essential. Consequently, we investigated how eGFP-MinC behaved on an SLB with the co-synthesized MinD and MinE_{op}. According to literature²²⁷, if both the purified eGFP-MinC and the co-synthesized MinDE complex work as expected, we should observe recruitment of the purified protein MinC to the MinDE wave-like pattern. First, we co-expressed in standard conditions *minD* and *minE_{op}* in the presence of the molecular chaperone DnaK as already done in Section 5.3.5.3. Then, we placed the resulting reaction on top of an SLB, together with 1 μM of the purified protein eGFP-MinC and GroE. Because eGFP-MinC already contains a fluorescence tag, it also served as a read-out molecule.

After several minutes, we detected the presence of eGFP-MinC travelling waves on the membrane (Figure 5.7 D; Figure SI 5.13 and Figure SI 5.14). Again, there were numerous locations on the membrane exhibiting travelling waves and we could not detect any *chaotic wave* as before. These results indicate that not only the co-synthesized MinD and MinE_{op} generate Min waves in the presence of eGFP-MinC, but also that the purified protein is able to interact with them in the expected manner.

5.4 Discussion and conclusions

In the next section, we will discuss the findings regarding the reconstitution of a cell-free synthesized Min system on supported lipid bilayers (SLBs), while exploring some of the lessons learned during the process. Additionally, we will draw some general conclusions regarding the

use of an *in vitro* transcription and translation (IVTT) machinery like the PURE system to reconstitute a cell-free synthesized *E. coli* Min system on SLBs

First, we will discuss the level of purity of the purified Min proteins, the validity of their concentration measurements and the implications that these two single topics had in the subsequent experiments. Then, we will discuss the results regarding the sedimentation assays. Next, we will discuss the reconstitution of spatiotemporal patterns on SLBs with purified and synthesized Min proteins and will examine these patterns in the light of previous literature. Furthermore, we will stress the importance of optimizing the PURE system, and will finish with an evaluation of the state of our research and how our findings match our original goals.

5.4.1 Purification and concentration measurement of Min proteins

To achieve the reconstitution of a cell-free synthesized Min system on supported lipid bilayers, we first established a working system with purified proteins. The first steps were the purification of each protein and their concentration measurements.

5.4.1.1 Purity

Proteins MinC, eGFP-MinC, eGFP-MinD and MinE were purified and the pooled fractions visualized on SDS-PAGE (Figure 5.1). The presence of additional bands aside of the target proteins is clear and most probably, the majority of these bands correspond to contaminating proteins from the bacterial cell. In Section 5.3.3 we performed a series of sedimentation assays with the purified proteins. The results were analyzed in an SDS-PAGE and it was still possible to observe these extra bands (Figure 5.3), especially in the lanes where the supernatant was analyzed. For example, in lanes 1 and 4 of Figure 5.3 A, additional bands between the 55 and 70 kDa marks can be seen as well as in lanes 2 and 5 between the 20 to 25 kDa and right below the 55 kDa mark, close to the assigned eGFP-MinD band. Also, in lane 6, extra bands can be observed around the region of the 25 kDa mark and right on the 70 kDa mark. In Figure 5.3 B, where only the purified eGFP-MinD was assayed, it is possible to observe a similar pattern to lanes 2 and 5 in Figure 5.3 A, while in Figure 5.3 C the pattern of additional bands is quite ubiquitous and especially clear in the lanes 11 to 14.

Another explanation for the existence of additional bands could be the presence of truncated proteins generated during their expression inside the host cell. Because all the purified Min proteins contain a 6-histidine tag at their N-terminal position, we might see truncated proteins at the C-terminus that purified together with the target protein. These truncations might in the pellet lanes (Figure 5.3 A-C) if they still retain the capacity to interact with another membrane protein. For example, in Figure 5.3 B the extra group of bands around 55 kDa responded to the presence or absence of ATP in the same manner as the target protein eGFP-MinD did (marked with asterisk (*)). This behavior could be explained if this group of bands were truncated versions of the complete eGFP-MinD. We can conclude that there is an obvious contamination with non-target proteins from the host cell.

5.4.1.2 Concentration measurements

In order to measure the concentration of the purified proteins, we utilized two different methods, a Bradford assay²⁶⁶ and a fluorescence spectrometry approach. In the latter case, we only measured the stock solutions containing eGFP-MinC and eGFP-MinD. The results of these assays can be seen in Table 5.7. The calculated concentrations show, in one hand, that both methods disagree regarding the concentration of eGFP-MinD, while in the other the concentration of MinE is high when compared with the rest of the proteins.

A plausible explanation for the high value obtained for the purified MinE might rest on the employed technique. The Bradford assay is based on the binding of the dye Coomassie Brilliant Blue G-250 to the carboxyl group of the aminoacidic chain of the proteins present in the sample²⁶⁶. Thus, a correlation between the absorbance in the wavelength of the color of the sample and the concentration of the target protein can be established through the production of a standard curve with a protein of known concentration. In all our Bradford assays, we made use of the bovine serum albumin (BSA) as standard protein. BSA molecular weight is approximately 69 kDa. This would mean that only target proteins that are closer to this molecular weight would make a good estimation. Since the purified protein MinE has an estimated molecular weight of 14 kDa, we may obtain an inaccurate measure. In the case of the purified protein MinC, the estimated molecular weight lays around 29 kDa so we should expect less bias, while eGFP-MinC and eGFP-MinD have a molecular weight fairly close to the standard protein (Table 5.7).

Additionally, the level of purity that we have seen in Section 5.3.2 influences the results observed with the Bradford assay. The presence of contaminant proteins will add up to the measured mass, and therefore increase the calculated concentration. In order to have an estimation of the proportion of contaminant proteins, we measured the protein carry over for each purified protein (Table 5.7) from the pooled fractions SDS-PAGE (Figure 5.1). For MinE, we found that only 36 % of the total protein mass constituted this protein.

In the other hand, fluorescence spectrometry measurements were also performed only with the purified proteins eGFP-MinC and eGFP-MinD (Section 5.3.2). The results obtained can be seen in Table 5.7 and present some differences with the Bradford assay measurements. For example, the concentration of eGFP-MinD obtained with the fluorescence spectrometry method is two times lower (36 μM) than with the Bradford assay (64 μM), and the concentration of eGFP-MinC obtained with the fluorescence spectrometry method (176 μM) is significantly higher than the one obtained with the Bradford assay (127 μM). One factor influencing the accuracy of the results is the path length, which in our case was of 0.1 cm. A possible measure to take is to use cuvettes with longer path length. However, we did not consider this approach because we would have needed to use a high volume of the stock proteins while diluting the stock protein into the right volume would lead to a protein concentration that is too low to detect.

As we can see, both methods, the Bradford assay and the fluorescence spectrometry, have limitations. Nonetheless and despite the differences, the concentrations obtained with both methods were in the same range. Because the Bradford assay could be applied to the four purified Min proteins, we decided to use these measures as the working concentrations.

5.4.1.3 Implications of purity and concentration of Min proteins in activity assays

The purity of the stock solutions of the purified proteins as well as their calculated concentration might have implications in future assays.

If we assume the presence of C-terminal truncated Min proteins, they might have an impact in activity assays. A truncated protein might be able to interact with a partner, but unable to carry out a particular enzymatic reaction. This would lower the efficiency of the system and virtually abolish it in extreme cases. For example, MinE contains roughly two distinct protein domains. First, the N-terminal domain ($_{1-32}\text{MinE}$) which mediates the interaction with MinD and is able to release the MinCD complex from the cell membrane. And second, the C-terminal domain (MinE_{33-88}), responsible for homodimerization of MinE. Importantly, the

total absence or even mutations in the MinE₃₃₋₈₈ domain lead to Min⁻ phenotypes *in vivo*^{235,236}. As can be seen, the presence of a hypothetical truncated MinE might still conserve the capacity to interact with MinD but a MinCD-E₁₋₃₂ might promote the production of abnormal proteins dynamics.

Additionally, the presence of contaminant proteins has implications regarding the accuracy of the concentration measurements. While this might not be a problem concerning the general activity of the system, it is nonetheless important to count with an accurate description of the conditions. If the real concentration of the purified proteins greatly differs from the calculated one, we would find it difficult to compare our results with previous literature. Another way in which this mismatch might influence future experiments is in the planning of activity assays with synthesized proteins. For example, if we have overestimated the concentration of our purified stock, we might believe, erroneously, that replicating the results with a synthesized protein is impossible due to the low protein yield typically obtained with IVTT's.

5.4.2 Min protein interactions in sedimentation assays

Sedimentation assays with the purified proteins MinC, eGFP-MinD and MinE were performed in order to test whether these purified proteins retained the capacity to interact with each other and with a lipidic membrane.

All sedimentation assays were carried out with 2 μ M of MinC, 4 μ M of eGFP-MinD and 6 μ M of MinE, both when assayed alone and in combination of two or three proteins. It has been calculated that there are approximately 400, 2000 and 1400 molecules of MinC, MinD and MinE respectively per *E. coli* cell^{236,247,248,123}. Taking into account that a standard *E. coli* cell can be considered to occupy a volume equivalent to 1 fL, the concentrations for MinC, MinD and MinE would be 0.65 μ M, 3.3 μ M and 2.3 μ M, respectively. The chosen concentrations for eGFP-MinD and MinE in the *in vitro* sedimentation assays are close to the ones exhibited *in vivo* by *E. coli*. However, their ratio was slightly modified in order to better match previous literature where Min waves were observed on SLBs^{133,256,132}. Additionally, we increased the concentration of the purified MinC four times, compared to the *in vivo* value, to facilitate its detection in the SDS-PAGE. The composition of the large multilamellar vesicles (LMVs) was the *E. coli* polar lipids mix. There are several publications where successful reconstitution of the Min system were established on *E. coli* polar lipid SLBs^{59,112,133,249}. Finally, we decided to use reaction buffer as medium. The use of a more complex background like the PURE system would increase the economic cost.

With the performed sedimentation assays (Section 5.3.3), we showed that the purified proteins MinC, eGFP-MinD and MinE retained the capacity to interact with each other and with the membrane in the expected manner. First, we confirmed that the purified eGFP-MinD is able of membrane binding in the presence of ATP (Figure 5.3 D and E). In fact, the fraction of eGFP-MinD found in the pellet was similar to the 56% reported in literature¹¹². Second, we showed that the presence of the purified protein eGFP-MinD increased the sedimentation levels of MinC up to a 21% (Figure 5.3 F), indicating the formation of a MinCD-membrane complex. Third, we observed how the presence of the purified protein MinE reduced the sedimentation levels of eGFP-MinD down to a 16% (Figure 5.3 G), showing that MinE was able to promote eGFP-MinD's ATPase enzymatic activity and subsequent membrane release. Both the decrease in sedimentation levels as well as the actual levels are in line with literature^{112,249}. Finally, we obtained the expected sedimentation pattern when the three purified proteins MinC, eGFP-MinD and MinE were assayed together (Figure 5.3 H).

Below, we will analyze some details regarding the sedimentation assays and will place them in context with previous literature.

5.4.2.1 Sedimentation levels of MinC and MinE in the absence of eGFP-MinD were higher than expected

According to literature, we should expect only MinD to bind to the membrane but not MinC or MinE^{112,249,267}. Yet, Figure 5.3 D shows that the fraction of purified MinC and MinE found in the pellet was of around 10% when assayed alone.

Although unexpected, this result could be explained by the procedure employed. First of all, only 80% of the supernatant fraction is loaded into the SDS-PAGE wells. This was done to avoid overfilling and sample leaking out of the wells, as well as to assure that all samples contained the same amount of supernatant. Therefore, the real sedimentation levels for all samples should be slightly lower, albeit still close to the reported 10%. Second, it is possible to have a contamination of supernatant during the recovery of the pellet fraction despite the washing steps. This would increase the fraction of protein in the pellet for all samples regardless of the ability of the Min proteins to bind to the membrane.

Alternatively, MinC and MinE might have acquired the ability to bind to the membrane, directly or not. Hsieh et al.²⁴¹ found that physiologically active MinE interacts with phospholipids in *in vitro* assays, reaching bound-to-membrane percentages as high as 16% and that this interaction is essential to generate effective Min oscillations *in vivo*. However, this was done under no salt conditions. In fact, they found that under the same salt concentration as we used in this chapter (150 mM KCl), the percentage of protein in the pellet dropped below 5% and was virtually undetectable under 200 mM KCl. For MinC, a direct, specific binding mechanism is highly unlikely because there are no membrane targeting sequences in this protein. Still, it is possible that a subfraction of the MinC population exhibits unstructured, misfolded or hydrophobic regions on its surface. In turn, these regions might unspecifically integrate in the phospholipid membrane or even aggregate and sediment under centrifugal force. In this case, artifacts might be created when activity assays on SLBs will be carried out. In Section 5.4.1.1 we have also discussed the presence of contaminant proteins both in the SDS-PAGE visualization of the pooled fractions as well as in the pellet fraction of the sedimentation assays. Therefore, there is still the possibility that a certain contaminant protein would interact with the membrane and with MinC or MinE, as a sort of linking molecule. Finally, there is also the possibility of rupture and fusion of vesicles. When this happens, proteins might get encapsulated inside the LMVs and increase the overall signal of the pellet fraction.

Therefore, the levels of around 10% exhibited by the purified proteins MinC and MinE when assayed alone, can be considered background levels.

5.4.2.2 Membrane binding of MinD in the absence of ATP was significant

MinD contains a membrane targeting sequence (MTS) that mediates its recruitment to the phospholipid membrane. This MTS is unstructured when in solution and transposes into a α -helix upon internalization into the membrane²⁰⁸. This poses MinD in a dynamic membrane-cytoplasmic equilibrium. However, the affinity of a single MTS to the membrane is relatively low and therefore the equilibrium is heavily shifted towards the cytoplasmic state²⁰⁸. Interestingly, MinD dimerizes in the presence of ATP, forming a bivalent MTS. As a consequence, the affinity for the membrane increases significantly, pushing the equilibrium towards the membrane-bound state^{112,208}. For this reason, we included 1 mM of ATP in most of our sedimentation assays. In Section 5.3.3.1 and Figure 5.3 C and D, we showed how the

purified eGFP-MinD sedimented in a greater extent (51-61%) than the purified MinC and MinE (about 10%). Similar percentages (50%-60%) have been reported in literature before^{112,208}. When ATP was absent in our assays, the sedimentation levels of eGFP-MinD dropped to 36% (Figure 5.3 D). However, this value is higher than the 15% reported in literature^{112,249}.

As discussed in Section 5.4.2.1, we must consider the experimental procedure to explain part of the eGFP-MinD signal observed in the absence of ATP. There, we resolved that around 10% of the total protein mass will unspecifically contribute to the pellet fraction and can be considered as background signal. Taking this into account, we arrive at a more realistic sedimentation value of 25% for eGFP-MinD in the absence of ATP. Still, this significantly exceeds the 15% previously reported^{249,112}. Another possible cause for the relatively high sedimentation percentage might lie on the presence of the fused eGFP tag at the N-terminus of eGFP-MinD. In fact, it is known that eGFP tends to dimerize²¹⁵. Consequently, the presence of the fused fluorescence protein might shift the monomer-dimer equilibrium towards the dimerized state, even in the absence of ATP. In turn, the recruitment of eGFP-MinD to the membrane is increased.

5.4.2.3 Sedimentation levels of MinC were lower than expected when assayed together with purified eGFP-MinD

As seen in Figure 5.3 E, the fraction of MinC in the pellet when in the presence of eGFP-MinD was higher (21%) than when only MinC or MinC plus MinE were assayed (13% and 7%, respectively). In the latter two cases, this percentage stayed in the range of what we considered as background signal. This result was expected due to the capacity of MinC to interact with MinD. As a consequence, the local concentration of MinC on the membrane must be indirectly increased. However, in the experiments carried out by Lackner et al.¹¹² and under similar conditions, they observed a striking sedimentation percentage for MinC of 86%.

A plausible explanation for the discrepancy of our results and the ones obtained by Lackner et al. could be the MinC:MinD ratio. Lackner et al. noticed that they were already at saturation levels for the 1:4 (MinC:MinD) ratio they assayed. In our case, we performed the experiment at a 1:2 (MinC:eGFP-MinD) ratio. Therefore, in our case, a higher proportion of MinC is expected to be found in the supernatant compared to literature. Alternatively, the fraction of active MinC protein might be significantly lower than the one used by Lackner et al.¹¹² Some of this non-active protein might have lost the ability to interact with eGFP-MinD. And finally, not all the LMVs should be expected to precipitate with the pellet. Indeed, Lackner et al.¹¹² obtained a consistent 2 to 8% of lipids in the supernatant during similar experiments.

5.4.2.4 MinCDE shows the expected interaction pattern

In Figure 5.3 H and Section 5.3.3.5 we reported the results of a sedimentation assay where the three purified proteins MinC, eGFP-MinD and MinE were assayed together. There, we observed a dramatic reduction in the fraction of eGFP-MinD (20%) in the pellet with respect to the value obtained when it was assayed alone (51-61%), and only slightly higher than when it was assayed together with MinE (16%). This reduction in the pellet levels of eGFP-MinD was expected due to the presence of the purified protein MinE. In a similar experiment, Lackner et al.¹¹² reported a 21% of MinD found in the pellet. This percentage is in line with our results.

In the other hand, the values obtained for MinC (7%) and MinE (7%) are slightly lower than background levels. For example, MinC showed a 13% when assayed alone. In principle, we should see a positive correlation in the levels of sedimentation between MinC and eGFP-

MinD. This means that a decrease in the percentage of eGFP-MinD should be also accompanied by a decrease in the levels of MinC, as long as they are assayed together. Such a decrease was observed in our experiment (from 21% to 7% for MinC when MinE was included), but we did not expect the signal to drop below background levels. Lackner et al.¹¹² obtained also very similar results. In their study and under comparable experimental conditions, they observed a 13% of MinC sedimentation when all the three proteins were assayed together. As mentioned in Section 5.4.2.3, in our experiments MinC is in excess with respect to eGFP-MinD which means that a significant fraction of MinC will end up in the supernatant. Yet, the percentage that we obtained for MinC (7%) is only slightly lower than the value obtained by Lackner et al. (13%). For MinE, the percentage in the pellet (7%; Figure 5.3 E) was also slightly below the obtained when MinE was assayed alone (11%; Figure 5.3 A). In this case, we must consider the ability of MinE to perform two opposite functions. In one hand, MinE requires MinD to be membrane recruited, but in the other, it triggers MinD's ATPase activity which in turn dislodges MinD from the membrane. As a consequence, MinE should be expected to be short lived in the membrane, and therefore the levels of protein in the pellet should remain very low. In fact, Lackner et al. found only residual amounts of MinE in the pellet when the three proteins were assayed together.

Regardless the causes, the described decrease in the proportion of MinC found in the pellet into background levels when assayed together with eGFP-MinD and MinE, might have implications in experiments concerning the implementation of a purified Min system. Of course, the generation of waves will not be affected. However, the absence of a transient presence of MinC on the membrane would hinder the production of FtsZ waves on SLBs or liposome membranes¹⁷². Still, our sedimentation assay might not be sensitive enough to detect a low, but important subfraction of membrane bound MinC, capable of creating FtsZ waves in at least some areas of the membrane.

In conclusion, the purified Min proteins interact with each other and the membrane as expected. As explained above, a few differences with literature were found regarding the membrane levels of eGFP-MinD in the absence of ATP, or MinC when assayed together with eGFP-MinD. Nonetheless, we considered that the purified proteins exhibited qualitatively the expected activity, which prompted us to investigate their dynamic self-organization on SLBs.

5.4.3 Wave morphology and dynamics

In Section 5.3.4 and Section 5.3.5, we carried out a series of activity assays on SLBs with the Min proteins. Time-lapse fluorescence microscopy allowed us to observe the self-organization and spatiotemporal pattern formation of both the purified and synthesized Min proteins.

First, we established a working system with the purified proteins eGFP-MinD and MinE. Under the background of the simple reaction buffer we readily observed the formation of a type of spatiotemporal pattern that we named *chaotic travelling waves* (Section 5.3.4.1). Then, we tested our MinDE working system under the background of PURE_{flex} and succeeded to obtain similar waves as long as an extra amount of ATP was supplemented (Section 5.3.4.2). Furthermore, we succeeded to emulate the patterns observed with the purified proteins, with the PURE_{flex} synthesized MinD and purified MinE (Section 5.3.5.1). Next, we tested two PURE_{flex} synthesized proteins at the same time, MinD and MinE_{op}. In this case, we did not detect the presence of any Min protein dynamics until we synthesized *minE_{op}* together with the chaperone DnaK and included GroE in the activity assay solution (Section 5.3.5.3). Interestingly, the morphology of the waves changed from the mentioned *chaotic waves* to the most common travelling waves described in literature. Finally, we combined the co-synthesized proteins MinD and MinE_{op} with the purified eGFP-MinC. Here, we observed the formation

of travelling waves, indicating that the purified eGFP-MinC was able to interact and follow the patterns created by MinD and MinE.

5.4.3.1 MinCDE waves with purified proteins

Under regular conditions, the typical Min waves obtained in literature consist of extended, parallel fronts (Figure 1.7 A, page 24). These waves propagate at a constant velocity, with a consistent wavelength, period and direction^{133,172,256,134}. Sometimes, it is possible to observe areas showing a spiral morphology (Figure 1.7 B, page 24). As a whole, this kind of waves have been named travelling waves.

The experiments with purified proteins that we have conducted in Section 5.3.4 have fully captured the basic features of the Min waves. The waves we generated showed the presence of a clear front and a direction, followed by the rear of the wave (characterized by a decrease in the membrane signal of eGFP-MinD). This indicates that the purified eGFP-MinD and MinE are able to carry out the most important functions. Yet, there are obvious differences with literature. In one hand, the *chaotic travelling waves* seemed to be confined to a number of isolated regions on the membrane, compared to the massive areas that the Min waves span in literature^{133,135}. And in the other, the waves did not present extended parallel fronts with a defined direction^{133,172,256,134}.

Although the most common Min waves observed in literature are travelling waves, these are not the only spatiotemporal patterns obtained with the Min proteins. Under various conditions, it is possible to obtain different morphologies. The most straightforward way to alter the morphology and dynamics of the Min waves is to change the MinD:MinE ratio¹³³. Kretschmer et al.¹³⁵ observed that a reduction in the total concentration of MinE and therefore a change in MinD:MinE ratio, led to a loss in the organization of the wave front population. In other words, the wave fronts became not parallel to each other and did not span as much as before. Additionally, other modifications like depriving MinE of its MTS rendered similar results in this regard, as seen again by Kretschmer et al. This was especially clear when they mutated the hydrophobic leucine in position 3 or 4 to code for a glutamic acid¹³⁵.

Schweizer et al.²⁵⁷ explored other ways of wave perturbation. They performed a set of experiments where obstacles were placed on the planar membrane. They found that the larger in size the obstacles, the more distorted were the waves. For example, when the obstacles presented a size larger than the wavelength, independent spirals were formed in between these obstacles. In contrast, when the obstacles were similar in size to the wavelength, the waves became irregular.

Moreover, Ivanov et al.¹³² found that under some conditions, the MinDE patterns organize in the form of what they called *amoebas*. These patterns were formed by a MinD core surrounded by a ring of MinE. *Amoebas* did not stay static but were able to grow, shrink and move over the membrane. In fact, they were able to disappear if they become too small, or even divide by *E-ring septation* if they became too large. These structures were mostly seen on membranes with a lipid head composition similar to the *E. coli* membrane but with a synthetic mixture of 70% double-unsaturated and 30% of mono-unsaturated aliphatic tail groups at a temperature of 20-22 °C or 100% mono-unsaturated aliphatic tail groups at 25 °C. Ivanov et al. also observed that when the density of *amoebas* grew large, sometimes this pattern transitioned into what they called a *mesh*. This pattern is similar to the *amoebas* in that they exhibited a core of MinD surrounded by a MinE ring. However, they were static and highly packed.

Probably, the results presented in this thesis resemble the most to the ones obtained with an increased MinD:MinE ratio (low concentration of MinE) and to the ones obtained with the

reduced membrane-interacting MinE₁₁₋₈₈, MinE_{L3E} or MinE_{L4E}¹³⁵. This would point out to our purified MinE as responsible for the production of the *chaotic waves*. Perhaps, its actual concentration is much lower than what we measured. In Section 5.4.1.2 we discussed the accuracy of the protein concentration measurements. Compared to the other proteins, the purified MinE showed a rather high concentration of 445 μ M using the Bradford assay (Section 5.3.2). The fraction of carry over (36%) as well as its low molecular weight (14 kDa) with respect to the standard protein used in the Bradford assay (69 kDa) might rise suspicion that the actual concentration is much lower. Additionally, the percentage of active protein could be lower than expected. Perhaps, MinE is much more prone to misfold during or after translation. In fact, synthesized MinE was not able to sustain Min waves until we supplemented the expression reaction and the activity assay solution with DnaK and GroE, respectively. Another possibility, not related directly with MinE, is the presence on the membrane of some type of irregularities such as regions with different lipid composition or fluidity, as well as physical obstacles of some kind. This would explain why the Min waves are confined to some areas of the membrane and present an irregular morphology, similarly to the waves observed by Schweizer et al.²⁵⁷

5.4.3.2 Purified versus synthesized

Following the assays with the purified eGFP-MinD and MinE proteins, we sought to assay the activity of the synthesized MinD together with the purified MinE. As can be seen in Figure 5.6, the overall morphology and dynamics of the waves were very similar to the patterns obtained with purified proteins. Strikingly, this time the Min waves occurred outside the *bright patches*. This observation can be related to the lipid membrane composition employed (DOPC:DOPG), since when a similar experiment with an *E. coli* lipid membrane composition was realized, we observed the presence of patches (Figure 5.4 B, C and D). Here, it is also interesting to notice the presence, for the first time, of a travelling wave (Figure 5.6 E). We also obtained Min waves with the co-synthesized MinD and MinE proteins. Remarkably, most of the patterns obtained in this case were travelling waves that followed classic morphology and dynamics. The waves were able to organize in extended fronts of parallel waves with a clear and consistent direction (Figure 5.7). This is much more similar to the waves obtained in literature^{132,133,135,172,256}.

Such a result seems to indicate that the source of the *chaotic waves* originated from the purified proteins MinE and perhaps also eGFP-MinD, or from the storage solution of the purified proteins. Additionally, the use of an *E. coli* SLB might aggravate the effect. In Section 5.4.1.3 we already discussed the influence that contaminant proteins might have on the formation of the spatiotemporal patterns of the Min system. It is possible that some contaminant proteins interact with the purified eGFP-MinD, MinE or with the membrane, causing the patches or chaotic waves. One way to exclude that the stock solution is contaminated with interfering proteins would be to perform a second purification step. If there were any contaminant proteins causing the formation of patches or *chaotic waves*, the canonical travelling waves should be restored.

Additionally, the fusion protein eGFP-MinD might be a source of anomalous patterns. Although the eGFP-tag is located at the N-terminus to minimize the interference with the MinD membrane binding, it might still affect protein dimerization. Aggregation of eGFP molecules is known to occur²¹⁵, which could lead to persistent dimerization. This might explain, at least in part, the unexpectedly high membrane binding of eGFP-MinD in the absence of ATP in the sedimentation assays (Figure 5.3 D). Additionally, the eGFP-tag could have an effect on MinD protein folding, leading to an aberrant MinD activity in the complex background of the PURE system. The influence of the eGFP-tag could be minimized by combining a non-tagged, wild-type MinD with the purified eGFP-MinD during the assays. For example, a 1:9 eGFP-MinD:MinD mol ratio should be sufficient for protein visualization as

seen in Section 5.3.5.1, where only 100 nM of eGFP-MinD was used for visualization purposes (also, Zieske and Schwille used a 10% of eGFP tagged MinD in their experiments²⁵⁸). Alternative fluorescent protein tags are also available for protein visualization, such as the yellow fluorescent protein (YFP) and the cyan fluorescent protein (CFP). However, these proteins are color mutants of GFP and are thus likely to have similar disadvantages^{216,268}. Organic fluorescent dyes are another possibility, of which many types are commercially available. Dyes used for Min protein visualization include BODIPY, Alexa Fluor dyes¹³³ and Cy5²⁵⁷.

5.4.4 Use of the PURE system and its optimization

With the grand goal of building an artificial cell in mind, it was mandatory for us that we tested and optimize the Min proteins to function in the complex context of the PURE system. We started by assaying the Min proteins in a simple buffer (Section 5.3.3), with the purpose of ruling out protein malfunction. However, we quickly moved on to use PURE $_{flex}$, both as buffer solution, as well as the *in vitro* transcription and translation (IVTT) machinery (Section 5.3.4). From that point on, we observed several differences in protein activity and general Min system functioning that are worth discussing.

5.4.4.1 Formation of eGFP-MinD patches and *chaotic waves* on SLBs as a consequence of the use of the PURE system.

PURE $_{flex}$ is a complex mix of enzymes (T7 RNA polymerase, ribosomes, energy regeneration enzymes, aminoacyl-tRNA synthetases, etc.), translation factors, tRNA, amino acids, energy sources in the form of nucleotides and creatine phosphate, and buffer and salt components like Hepes-KOH, potassium glutamate, magnesium acetate, spermidine and others^{139,140}. Therefore, it is reasonable to expect that Min protein dynamics in the PURE system might not be the same as in reaction buffer. Additionally, the PURE system is limited in the protein yield, it lacks a precise control in the final protein concentration, and it shows a higher risk of protein misfolding of said protein both during and after translation compared to expression in cells.

Nonetheless and unlike with cell extracts, the PURE system is an IVTT platform with a very-well defined and characterized composition. Additionally, it allows for the synthesis of proteins *in situ*, right in the place where they will be tested and avoiding the tedious process of purification. This opens the possibility to synthesize wild-type, non-tagged proteins directly on top of SLBs or inside liposomes. We have exploited this feature in a number of instances during this thesis. The *in situ* expression of proteins is clearly advantageous with some recalcitrant proteins like ZipA (Section 2.3.3, page 46) and/or FtsA (Section 2.3.4, page 50)²⁶⁹. Also, a combination of these PURE system features might explain why the synthesized MinD and MinE $_{op}$ produced canonical travelling waves in the PURE system background (as discussed in Section 5.4.3.2), instead of the *chaotic waves* obtained with purified proteins.

5.4.4.2 Use of chaperones in the PURE system for the synthesis of active MinE

In Section 5.3.5.2 we described our efforts in the synthesis of a fully functional synthesized MinE protein. Despite control experiments with purified proteins in the PURE $_{flex}$ background, which showed the formation of at least *chaotic waves*, the synthesized MinE was unable to generate spatiotemporal protein patterns. The lack of expression of the *minE $_{op}$* DNA constructs was ruled out as shown by SDS-PAGE (Figure 5.6), suggesting that the synthesized MinE might be misfolded. Although lowering the expression temperature failed to generate waves, (Section 5.3.5.2), we successfully promoted correct protein folding with the chaperones DnaK (during expression) and GroE (after expression; Section 5.3.5.3 and Figure 5.7 A).

Chaperones as the one mentioned above are not present in the standard PURE_{flex} solutions. This makes the PURE system prone to generate misfolded proteins. To solve it, a sound alternative is to systematically complement the reaction with chaperones²⁷⁰.

5.4.4.3 Customizing the buffer conditions of the PURE system with the addition of extra ATP allows the protein MinD to be active

In Section 5.3.4 we carried out a set of assays on SLBs with purified proteins. We tested the influence of PURE_{flex} on the generation of spatiotemporal patterns on the membrane. We found that supplementing the solution with fresh ATP was necessary to form waves (Figure 5.4 C). This is an important result, raising the question whether the initial amount of NTPs present in the PURE system could be insufficient for the activity of other nucleotide-dependent proteins, e.g. for the GTP-dependent polymerization of FtsZ in Section 2.3.2 (page 46) or Section 3.3.3 (page 72).

5.4.5 Future steps of a cell-free synthesized Min system and outlook

The reconstitution of the Min system dynamics on SLBs with purified proteins started in 2008 with the publication of Loose et al.¹³³. In this thesis, we have shown, through a combination of PURE system and DNA construct optimization, that the cell-free expression of active, fully functional Min components is possible. This synthetic version of the Min system opens the door for a range of different possibilities.

On SLBs, the next natural step would consist on the synthesis of a functional, fully synthesized Min system. This implies that not only MinD and MinE, but also MinC should be cell-free synthesized. In Section 5.3.3.3 we showed that purified MinC is able to interact with purified eGFP-MinD in sedimentation assays, and in Section 5.3.5.4 to follow the Min waves generated by the co-synthesized MinD and MinE_{op}. A synthetic version of MinC should offer similar functionality. For example, an activity assay on SLB could be envisioned where the synthetic MinC is placed together with a tracing amount of purified eGFP-MinC for visualization purposes, in a background of co-synthesized MinD and MinE_{op}. If the synthetic MinC is able to interact with the MinDE waves, we should still observe the generation of MinC waves on the membrane. There are other possibilities. Since the Min system is designed to work in close relationship with the divisome *in vivo*, of which the proteins FtsZ is the link between them²⁷¹, MinC should be able to depolymerize FtsZ filaments on SLBs. Martos et al.¹⁷² already showed how the purified MinCDE is able to generate FtsZ antiphase waves on SLB. In Chapter 2 we have shown many examples of the filament networks exhibited by both purified and synthesized FtsZ on sZipA-SLBs. Therefore, the next step would be to emulate these results using a cell-free synthesized MinC in the background of the PURE system. Such an achievement would clearly indicate that the synthesized MinC retains the basic functionality of the *in vivo* protein, without the need to use any purified eGFP-MinC.

Finally, the *in-vesicle* synthesis of the Min proteins could be tried. Others have assayed the purified Min proteins both from the outside of liposomes as well as the inside of droplets or liposomes^{113,137,138}. In literature, the range of protein dynamics obtained varied from lumen-to-membrane pulses to travelling waves in round vesicles¹³⁷ and oscillations similar to the *in vivo* dynamics in stretched liposomes¹³⁸. A working strategy to emulate these studies would involve first the encapsulation of our purified eGFP-MinD and MinE with the goal of establishing a working system in liposomes, in the same manner we proceeded with the SLB assays. Next, the combination of a synthesized MinD with a purified MinE (and vice versa) should follow. These last steps should serve as check points to validate the functionality of each synthesized protein, separately, inside liposomes. Once the single synthesized protein assays

have been successful, co- or tri-synthesis (this is, the simultaneous in-vesicle synthesis of the three Min proteins) could follow. In the latter case, a residual amount of purified eGFP-MinC or eGFP-MinD should be added for visualization purposes. Some factors could be traded off to optimize the protocol. In one hand, the lipid composition of the liposomes could be changed to compositions designed to obtain a high yield during the natural swelling phase. The new lipid composition should be compatible with the activity of the Min proteins. Additionally, the liposomes could be externally reshaped through a variety of methods to adopt stretched forms. For example, the presence of 1,2-dimyristoyl (C14:0) phospholipids in the liposome membrane is known to deform and elongate liposomes thanks to the tendency of this phospholipid to change shape under thermal expansion²⁷². Also, some type of biological polymer, like for example microtubules, could be used inside the liposomes. When tubulin assembles, it is capable of pushing away the liposome membrane, successfully stretching the vesicle²⁷³. Nonetheless, the most simple and straight forward method would be the direct use of microfluidics with elongated trapping chambers. Regardless the methodology employed, such liposome deformations would facilitate the generation of *in vivo*-like Min protein oscillations with cell-free synthesized Min proteins.

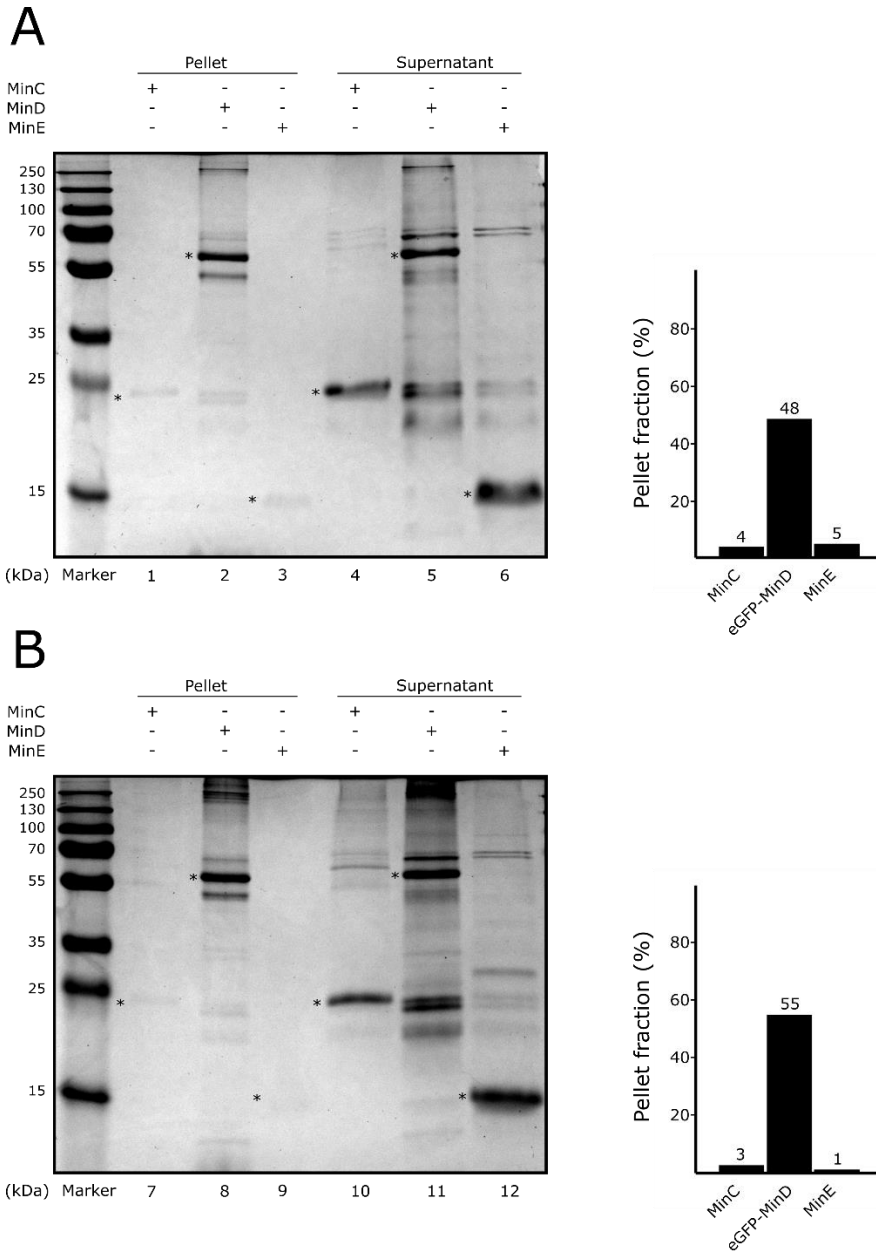
5.4.6 Conclusions

The main goal of the study presented in this chapter, was the cell-free synthesis of a functional Min system and its reconstitution on SLBs. The use of an IVTT like the PURE system was essential in our case, not only due to the novelty of the research (this has not been done yet to the best of our knowledge), but also in the bigger endeavor of building an artificial cell. In this study, we have achieved two of the most important milestones, i.e. the optimization of the PURE system to support the activity of the Min system, and the cell-free synthesis of the Min proteins responsible of the oscillatory activity. These results impart important lessons regarding the use of the PURE system, with general impact for other research lines with a different protein repertoire. Furthermore, these achievements open the door for exciting research paths such as the in-vesicle synthesis of Min proteins and their interaction with FtsZ.

Acknowledgements

We thank Petra Schwille's lab at the Max-Planck-Institut für Biochemie near Munich for providing with plasmids for the Min system proteins. We thank Katja Slangewal and Céline Cleij for outstanding laboratory work and fruitful discussions, as well as Ilja Westerlaken and Esengul Yildirim for technical assistance. We thank Jeremie Capoulade for microscopy training and technical support.

5.5 Supplementary information



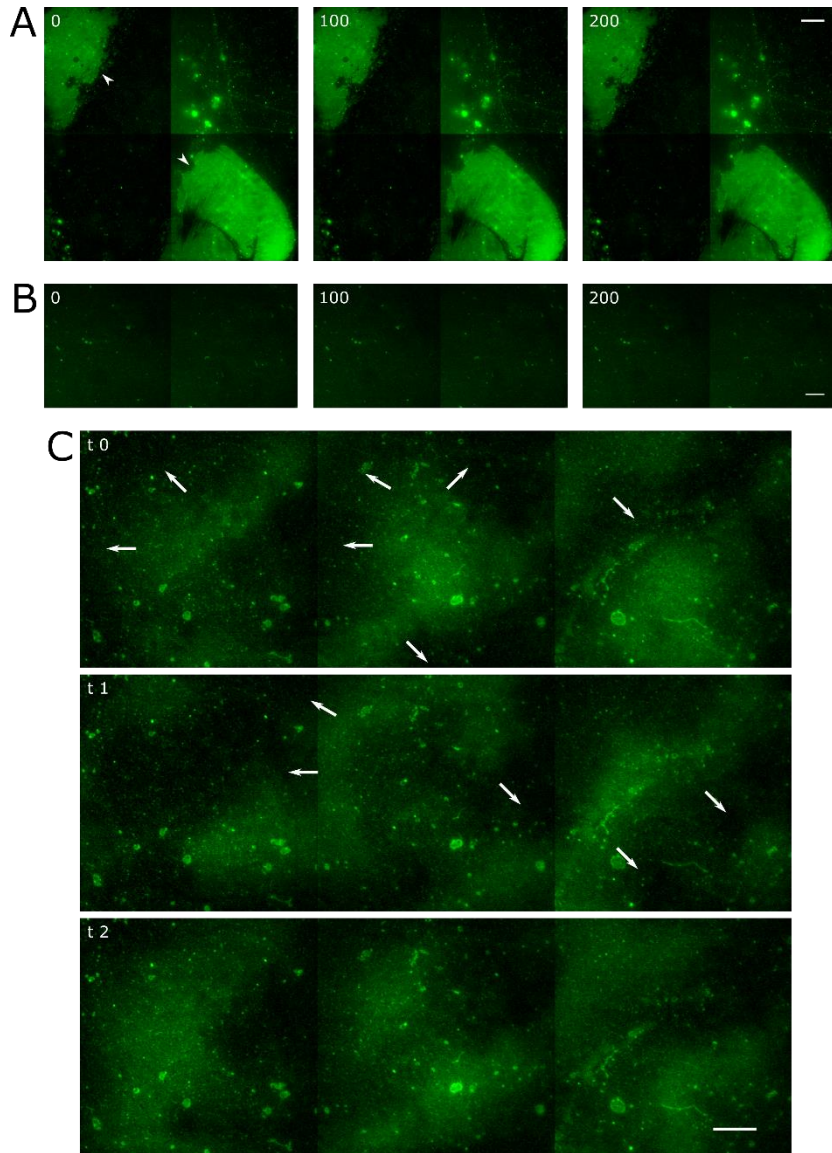


Figure SI 5.9 Dynamics of purified Min proteins

TIRFM time-lapse images of purified Min proteins on SLBs. Time at the upper left corner in seconds, except in C, where the lapsed time is undefined. Scale bars: 10 μm . A) Montage of the activity assay performed on a *E. coli* polar lipids membrane with the purified proteins eGFP-MinD (2 μM) and MinE (3 μM) in reaction buffer plus 1 mM ATP. The presence of *bright patches* is marked with white arrow heads. B) Time-lapse montage of the activity assay performed on a *E. coli* polar lipids SLB with the purified proteins eGFP-MinD (4 μM) and MinE (3 μM) in PUREflex. Typical image of the membrane under these conditions did not exhibit the presence of protein dynamics. C) Montage of the activity assay performed on a *E. coli* polar lipids SLB with the purified proteins eGFP-MinD (4 μM) and MinE (3 μM) in reaction buffer plus 2 mM of ATP. White arrows represent the movement direction of the front of the waves. Time in the upper-left corner is undefined although the time difference between snapshots is around 10 seconds.

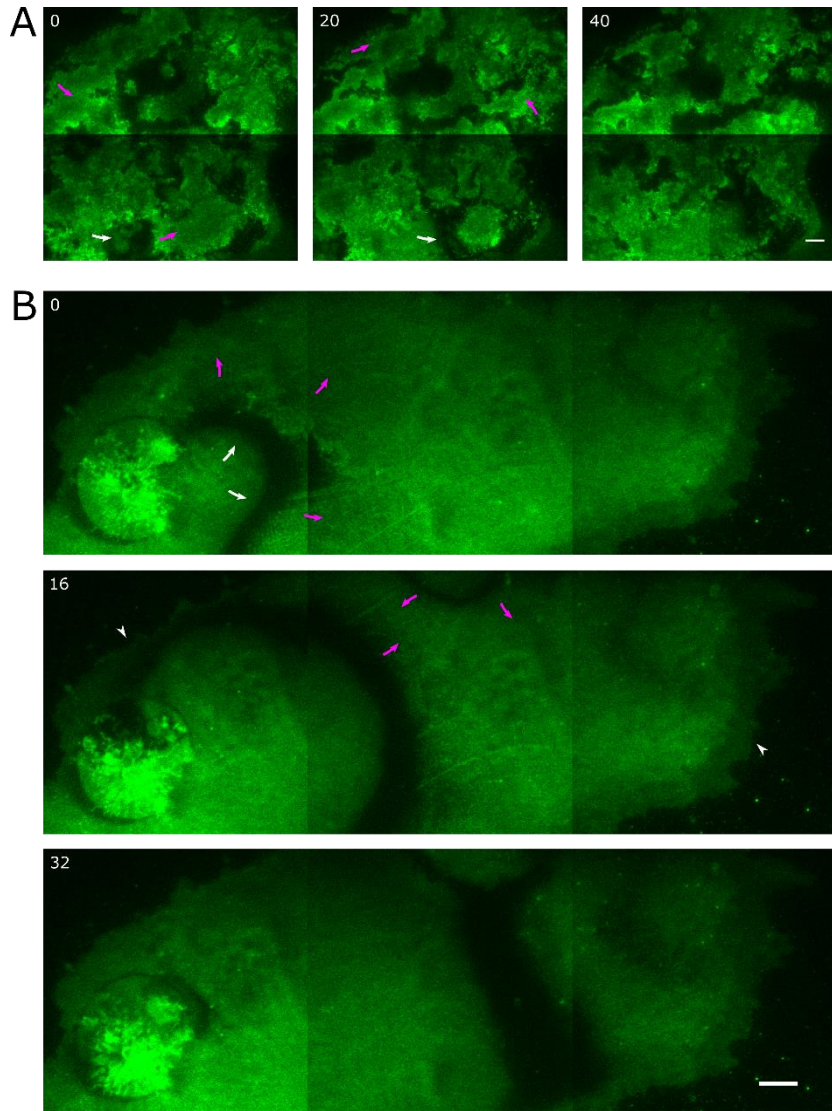


Figure SI 5.10 Activity assays of synthesized MinD

TIRFM images. Both panels correspond to different regions of the same activity assay. Time in the upper-left corner of the images (seconds). White arrows indicate the progression of the wave front. Magenta arrows indicate the withdrawal of the wave rears. This activity assay was performed on an *E. coli* lipids SLB with synthesized MinD, 100 nM of purified eGFP-MinD for visualization purposes and 3 μ M of purified MinE in PURE $_{flex}$. All scale bars: 10 μ m. A) Time-lapse montage of a *bright patch* exhibiting dynamic protein patterns in the form of chaotic waves. B) *Bright patch* exhibiting the most canonical travelling wave so far in our experiments.

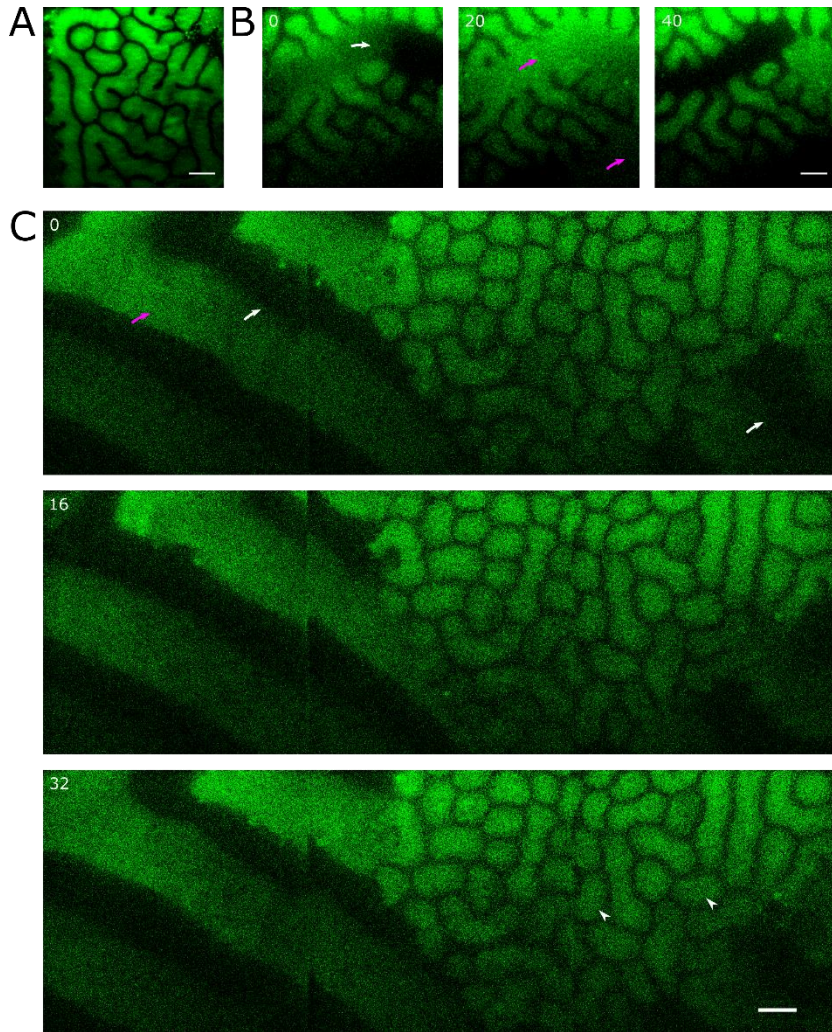


Figure SI 5.11 Activity assay with synthesized MinD and MinE

TIRFM microscopy images. Time in seconds in the upper-left corner when applies. All panels correspond to the same activity assay performed on a DOPC:DOPG (80:20 mol%) membrane with synthesized MinD and synthesized MinE plus 100 nM of eGFP-MinD for visualization purposes in PURE \hat{r} *rex* 2.0. White arrows represent progression of wave front. Magenta arrows indicate the withdrawal of the wave rear. Scale bars: 10 μ M A) Some regions of the membrane showed the presence of static patterns. AVG image. B) Time-lapse of a travelling wave crossing two regions with static patterns. C) Time-lapse montage of a region showing the canonical travelling waves (at the left part of the montage) and static patterns (right region of the montage; white arrows indicate two examples of static patterns).

5 - The cell-free synthesized Min system on SLBs

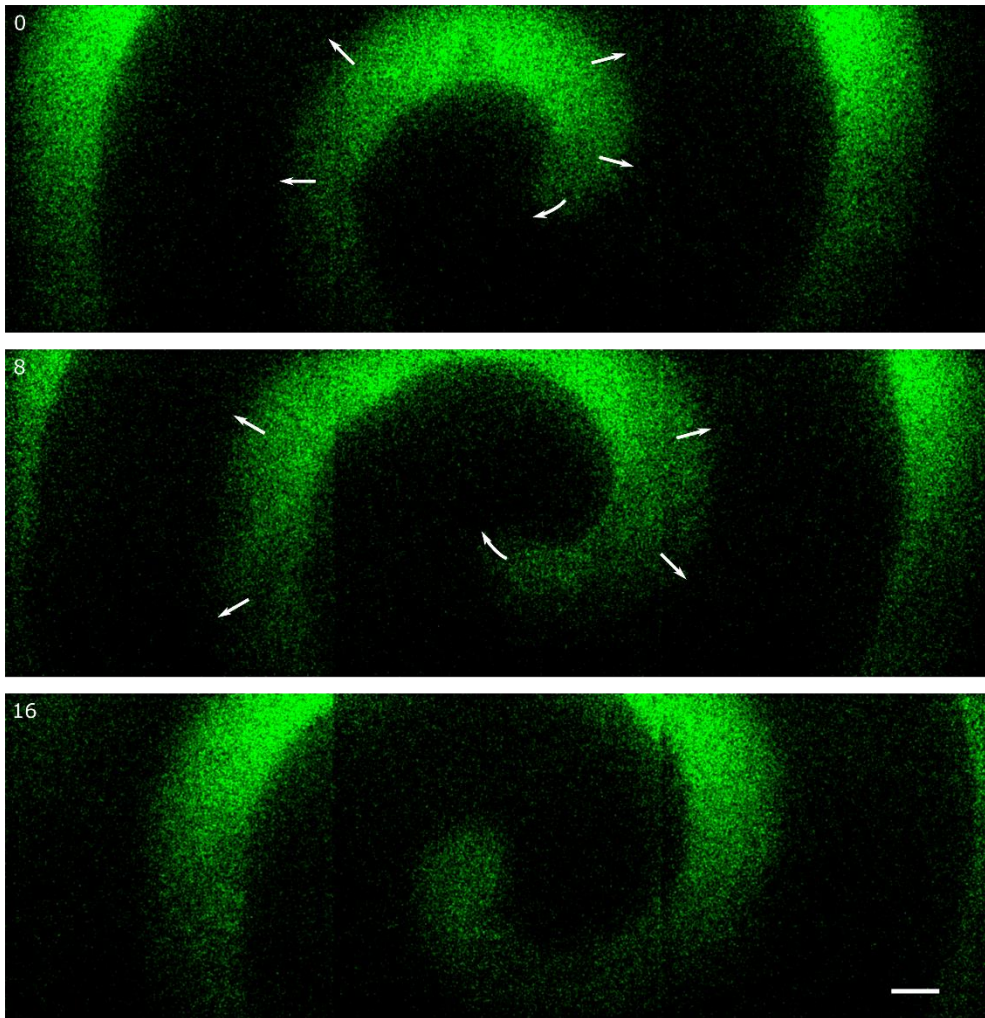


Figure SI 5.12 Spiral motive on SLBs with co-synthesized MinD and MinE_{op}

TIRFM images. Scale bar: 10 μm . Time in the upper-left corner in seconds. White arrows indicate the progression of the wave front. Time-lapse montage activity assay performed on a DOPC-DOPG (80:20 mol%) SLB with co-synthesized MinD and MinE_{op} plus 100 nM of eGFP-MinD for visualization purposes in PURE *flex* 2.0.

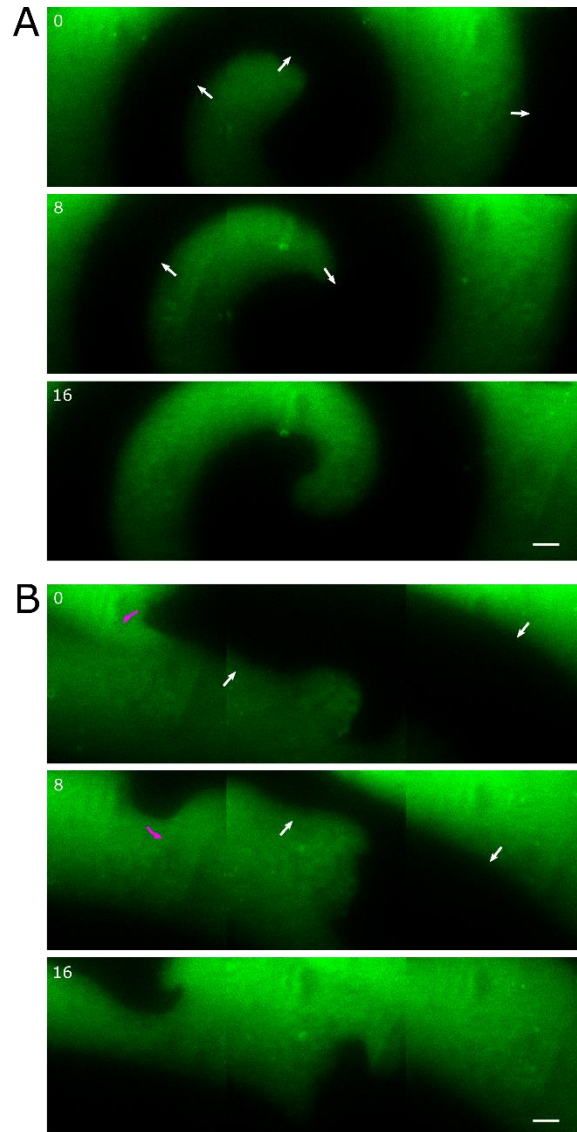


Figure SI 5.13 Activity assay with synthesized MinD and synthesized MinE

TIRFM images. Time in seconds in the upper-left corner of each image. White arrows indicate progression of the wave front. Magenta arrows indicate the withdrawal of the wave rear. Both panels belong to the same activity assay. The assay was carried out on a DOPC:DOPG (80:20 mol%) with synthesized MinD and MinE_{op} plus 100 nM of eGFP-MinD and 2 μM of eGFP-MinC in PURE *frex* 2.0. Scale bars: 10 μm. A) Spiral motive on the SLB. B) Time-lapse montage of two waves progressing in opposite directions and collapsing.

5 - The cell-free synthesized Min system on SLBs

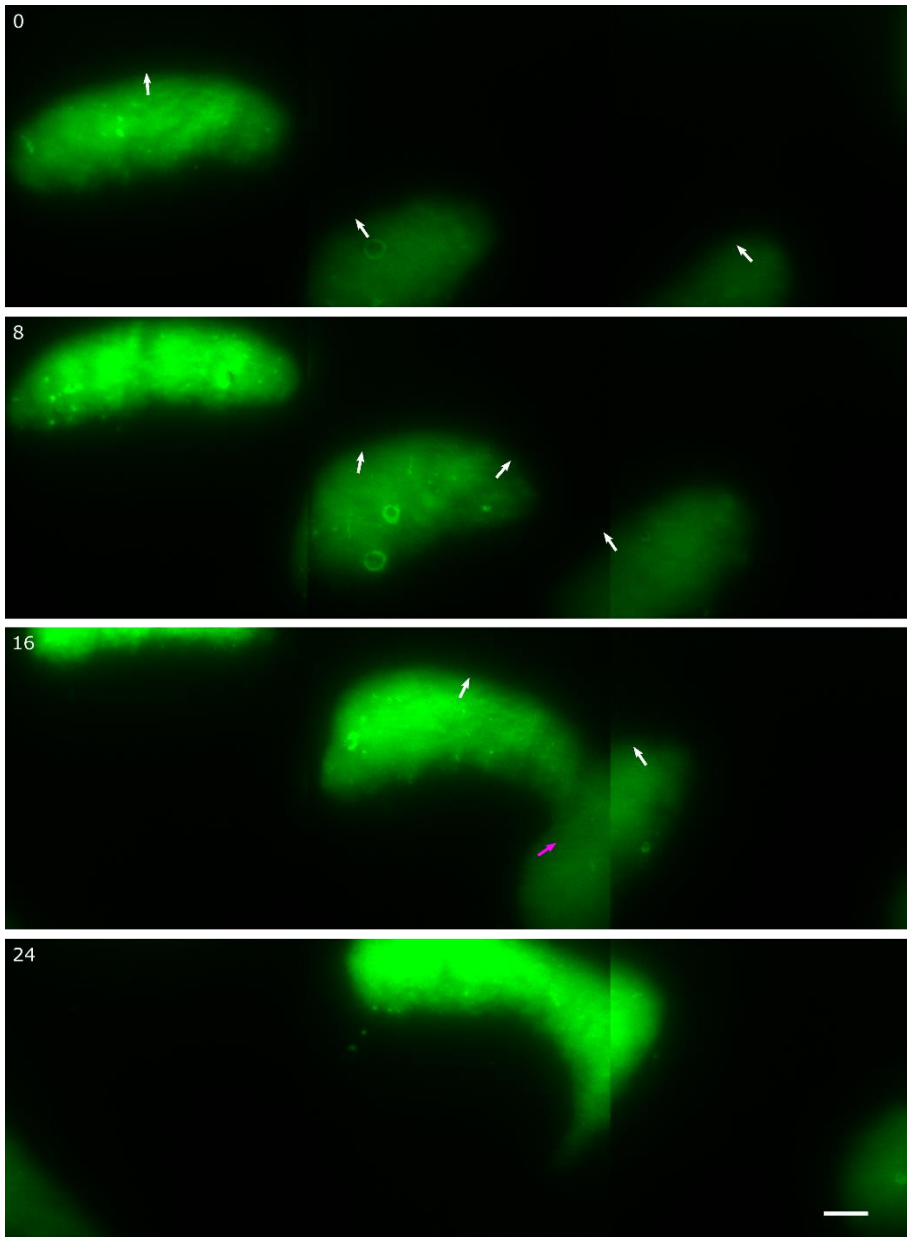


Figure SI 5.14 Activity assay of synthesized MinD and MinE_{op} with purified MinC

TIRFM images. Time in seconds in the upper-left corner of each image. White arrows indicate progression of the wave front. Magenta arrows indicate withdrawal of the wave rear. Time-lapse montage of synthesized MinD and MinE_{op} plus 1 μ M of purified MinC on a DOPC:DOPG (80:20 mol%) SLB in PURE_{flex} 2.0. The presence of travelling waves indicates that the purified MinC interacts with the synthesized MinDE complex. Scale bar: 10 μ m.

Chapter 6

General conclusions

“Omnis cellula e cellula.”

– Aphorism popularized by Rudolf Virchow. Originally by François-Vincent Raspail, in *Annales des Sciences Naturelles*.

Can we engineer an artificial division system for minimal cells, based on the bacterial division machinery? Can this artificial system be spatiotemporally regulated with yet another engineered artificial protein network? These were the two main questions that we asked ourselves at the beginning of this thesis. These questions, or perhaps we should say *challenges*, have been only partially answered. What a humbling truth. It reminds us how little we know about biochemistry, cell division and the fundamental principles of life. What can we conclude?

6.1 The PURE system is a versatile tool and its use should be continued in the development of minimal cells

The PURE system has been without a doubt the lens throughout all experiments of this thesis have been conceived upon. As the vertebral metabolic machinery of our model minimal cell, each one of the chapters explored this technology for the cell-free synthesis of proteins. The PURE system proved itself extraordinarily versatile. For example, in Chapter 2, we showed that lowering down the expression temperature of wild-type ZipA improved the formation of FtsZ/ZipA bundles on SLBs. Although these structures were not as spectacular as the obtained with the soluble version of ZipA (sZipA) or purified sZipA, they might reflect better the physiological state of FtsZ in the cell. The addition of molecular chaperons or enzymes to the expression reaction or to the activity assay buffer, was as well a significant optimization of the PURE system. In Chapter 2, we observed that addition of peptidyl-tRNA hydrolase, an enzyme involved in the recycling of aborted translation products²⁷⁴ that potentially could improve the efficiency of translation, seemed to increase the repeatability of our results with synthesized ZapA. Even more significant was the addition in Chapter 5 of DnaK and GroE to the expression reaction and the assay buffer of synthesized MinE experiments, respectively, since they were required to observe activity.

Other optimizations, perhaps not related with the correct folding of the proteins but with providing a permissive environment for protein activity, were demonstrated. For example, in Chapter 5 we showed that synthesized MinD required extra ATP to operate in a PURE system environment, despite the fact that PURE_{flex} contains 3 mM of this nucleotide. Presumably, the available levels of ATP were too low for an efficient MinD activity in a working PURE system. In Chapter 3, in the other hand, we found that an increase of around 15% in the basal concentration of K⁺ and Mg²⁺, lowered the threshold for the formation of FtsZ bundles inside vesicles. This was key to generate protein filaments that deformed the liposomes. Other type of optimization involved the expression of proteins at low temperature. In Chapter 2, we showed that synthesis of full-length ZipA at 25 °C allowed the formation of FtsZ/ZipA structures on the membrane, while standard expression at 37 °C failed to generate them. Finally, the PURE system proved versatile as well regarding the site of protein synthesis. In Chapter 2, we exploited the *in situ* expression of FtsA and ZipA directly on top of planar membranes. FtsA and ZipA contain a membrane targeting sequence for phospholipid interaction, which can make difficult both purification and cell-free synthesis in batch mode. This is especially true in the case of ZipA because this targeting sequence is a hydrophobic transmembrane domain located at the N-terminus of the protein. Such a feature implies that nascent proteins expose first a highly hydrophobic domain, which might promote aggregation with other nascent, or partially folded ZipAs.

Despite its versatility, the PURE system is limited by the low protein yield obtain in comparison to other cell-free extracts²⁷⁵ and of course expression *in vivo*. A newly developed PURE_{flex}, named PURE_{flex} 2.0, aimed to improve expression efficiency. Indeed, PURE_{flex} 2.0 has been

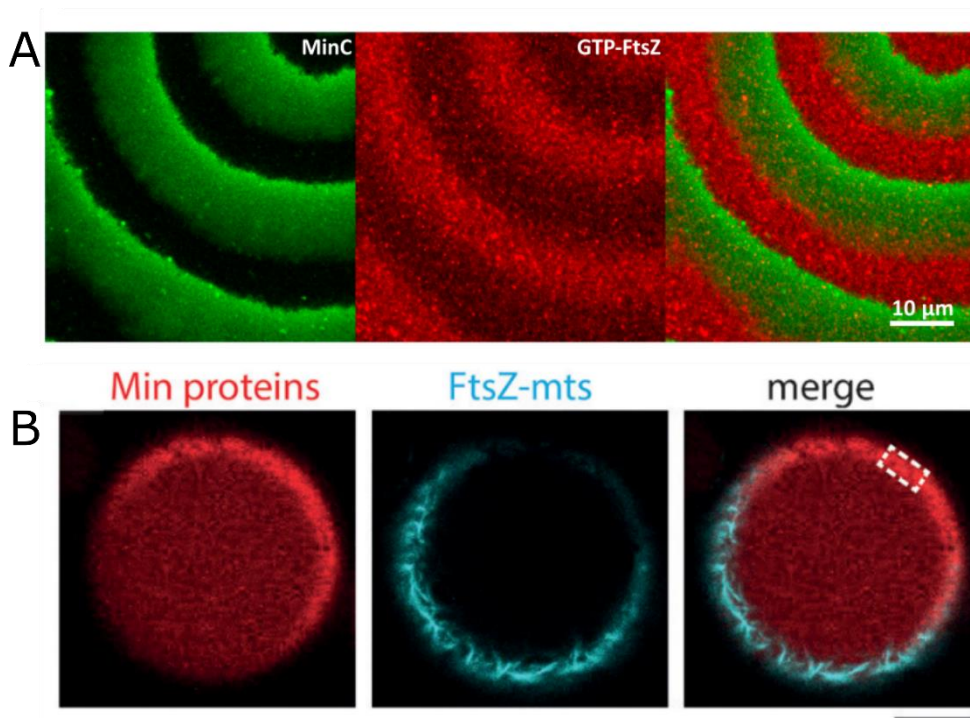


Figure 6.1 Co-restitutions of FtsZ filament networks and Min system with biomimetic membrane models

A) Co-restitution of FtsZ/ZipA with the Min system on SLBs. The Min waves generated an FtsZ/ZipA wave in antiphase. Panel adapted from reference¹⁷². B) Co-restitution of FtsZ-YFP-MTS with the Min system in lipid interfaced droplets. Pole-to-pole Min oscillatory patterns promoted an antiphase, symmetric FtsZ-YFP-MTS pattern. Scale bar: 10 μm . Adapted from reference¹³⁷.

shown to increase the yield of its predecessor by a factor of ~ 5 and the operational life-span by a factor of two¹⁴³. However, this is still far from being sufficient to provide an autonomous metabolic system in artificial cells. Research on this topic cannot but keep improving. Taking all together, we can conclude that the PURE system has been an invaluable tool for the *de novo* synthesis of proteins. Its versatility allows for optimization, its purity for a high level of interpretability of the results, and its defined composition for the rational design of model artificial cells.

6.2 Synthesized *E. coli* division-related proteins can be implemented in artificial cells

Throughout this thesis, we have shown that synthesized FtsZ, FtsZ-His, FtsZ-A, FtsA, sZipA and ZapA supported the formation of cytoskeletal structures on

planar membranes, even in co-synthesis conditions (FtsZ/ZapA and FtsZ-His/ZapA). In liposomes, we have demonstrated FtsZ expression and liposome deformation. And finally, we have shown spatiotemporal patterns generated by synthesized MinD and MinE on planar

membranes. With these data we can conclude that the synthesis of functional *E. coli* related division proteins is possible. However, we have not attempted the co-reconstitution of both systems yet.

In 2015, Martos et al¹⁷² reconstituted on planar membranes MinCDE waves together with FtsZ-sZipA networks. They confirmed that FtsZ waves were formed in antiphase with the Min waves (Figure 6.1 A). Moreover, they reported that the modulation value of the FtsZ waves, i.e. the difference between the fluorescence on the waves and the fluorescence outside the waves, was dependent on the membrane density of ZipA. They also found that the modulation value was positively correlated with the crowded environment. This could be of relevance in our minimal division machinery (MDM) model, since the generation of high values would help a strong positioning of the Z-ring at midcell. In vesicles, an interesting example was reported by Zieske and colleagues¹³⁷. They addressed the generation of patterns with reconstituted MinCDE and FtsZ-YFP-MTS inside lipid-interfaced droplets. Indeed, they observed a sustained antiphase oscillation of FtsZ-YFP-MTS and MinCDE (Figure 6.2 B).

As done in the above-mentioned studies, we could address the same questions with synthesized proteins, both in SLBs and in vesicles. Something to take into account is the relatively low yield of the PURE system. This implies that the synthesis of a 5-protein system is probably not in the reach of the current technology. Yet, the use of small protein-synthesizing compartments might be key in this regard, since it has been shown that some of these vesicles favor the production of *de novo* synthesized proteins²⁷⁶. Nonetheless, a mixed approach with both purified and synthetic proteins could be tried. Reconstitution of the Min waves could be done with purified MinC and synthesized MinD and MinE, as long as extra ATP and a suitable chaperon was added to the mix. As for FtsZ, since it is a soluble protein, it would be probably best to use it purified. This way, FtsA could be synthesized in vesicle to avoid difficulties in the encapsulation of this protein by natural swelling. By using two purified proteins (FtsZ and MinC), the PURE system could be still in reach of synthesizing the other three. Of course, other synthesized-purified combinations should be explored. An important consideration is the stoichiometry of the DNA templates. It could be expected that with increasing number of genes, the interaction of the protein synthesis machinery and the DNA templates becomes highly complex. Optimization will require to adjust the copy number of each gene, or to group the different genes under the same operon to ensure a correct stoichiometry.

6.3 A new minimal machinery model arises

In Chapter 1 (page 11), we proposed an idealized minimal cell model, whose function was to guide our research in the consecution of an evolving, self-maintaining, self-reproducing artificial cell. We described as well an idealized model of an MDM. After the data gathered and discussed in this thesis, a new, extended minimal division machinery (EMDM) model emerges (Figure 6.2).

Here, as in the MDM model, FtsZ occupies a central position. FtsZ's role is to assemble at midcell, forming a constricting protein ring. In this task, FtsZ is aided by ZapA or ZapC, small FtsZ crosslinkers that help the condensation of FtsZ protofilaments in coherent bundles. Since the FtsZ to Zap ratio is important for the generation of bundles, in the EMDM model, artificial

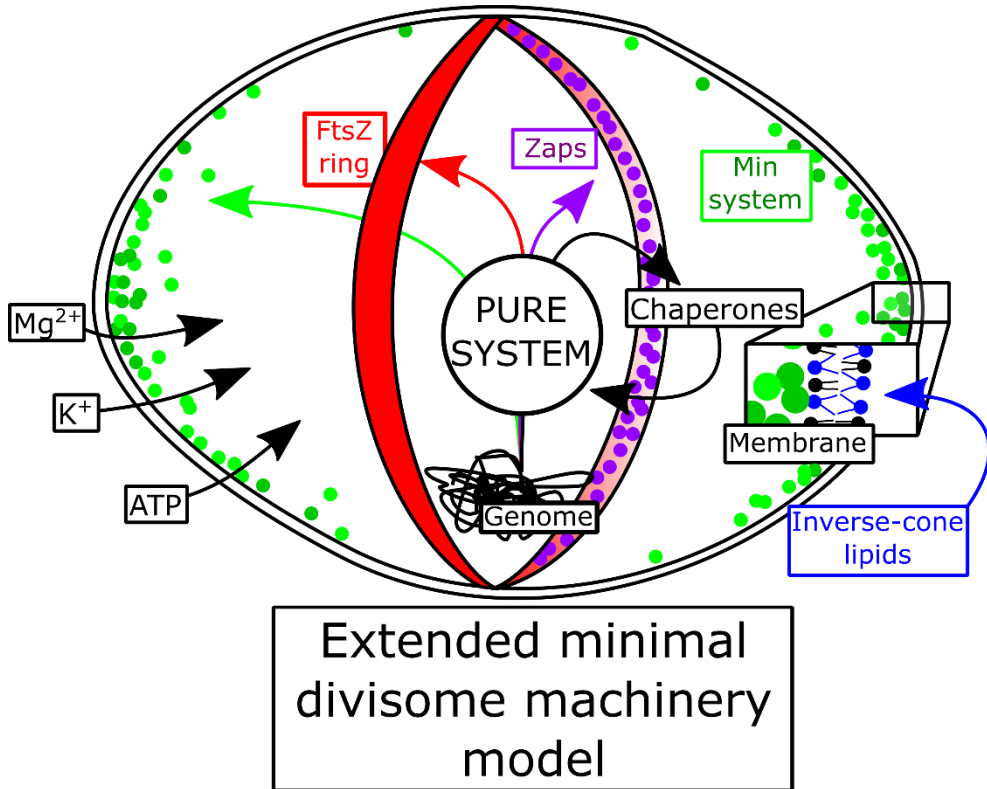


Figure 6.2 Extended minimal divisome machinery model

In Figure 1.1 , (page 12), we presented our minimal division machinery (MDM) model. This consisted in an idealized vision of a division machinery to be implemented in artificial cells. Throughout this thesis, this model has been expanded. In our extended minimal divisome machinery (EMDM) model, FtsZ occupies a central role. After expression by the PURE system, FtsZ assembles at midcell into a constricting ring-like structure (red). FtsZ is aided in this by Zap's proteins, which promote the cohesion of the ring (violet). The FtsZ/Zap assembly is anchored to the membrane by FtsA or ZipA, thus a constriction force can be transmitted to the membrane. The location of the FtsZ-ring at midcell is guided by the Min system (green). In the EMDM model, the media is rich in K^+ , Mg^{2+} and ATP. Chaperones are synthesized as well to ensure that MinE is functional. Finally, to facilitate Min system oscillations, the cell is elongated through the insertion on the membrane of inverse-cone lipids.

chromosomes containing a different copy number per gene are used. The FtsZ-Zap structure is anchored to the membrane through FtsA and ZipA, and guided to the midcell by the MinCDE system. To allow correct expression of ZipA, the optimal temperature is 25 °C. In the other hand, the media is rich in K^+ , Mg^{2+} and ATP to reduce the FtsZ bundling threshold (K^+ , Mg^{2+}) and to permit the activity of MinD (ATP). DnaK or other suitable molecular chaperone are synthesized in the cell as well, to ensure the correct folding and activity of MinE. Finally, the liposome membrane contains a proportion of inverse-cone lipids to promote the elongation of the cell to recreate Min pole-to-pole oscillatory patterns.

Appendix

DNA constructs and sequences

7.1 DNA sequences for expression of Min proteins in *E. coli*.

All sequences were kindly provided by the laboratory of Petra Schwille in the Max-Plank-Institute of Biochemistry, Germany. All genes are inserted in pET28-a. Here, only the region between the promoter and terminator of each gene is shown. A schematic of the following DNA constructs can be seen in Figure 7.1. The color and symbol code for the DNA sequences can be seen in Table 7.1.

Table 7.1 Code of colors and symbols for the DNA sequences for expression of Min proteins in *E. coli*.

Genetic part	Color and symbol code
Promoter (t7)	red
Operator (lacO)	orange
Ribosome binding site sequence	purple
Start codon	CAPITALS
Thrombin cleavage site	<u>underlined</u>
T7 leader sequence	brown
Wild-type DNA sequence of target protein	blue
egfp	green
6 histidine tag DNA sequence	dark blue
Stop codon	CAPITALS
Terminator (t7)	red

7.1.1 *minC*

taatacgaactcactataggggaattgtgagcggataacaattccctctagaataattttgtttaactttaagaaggagatataaccATGggc agcagccatcatcatcatcatcacagcagcggcctggctgccgcggcagccatattggctagcatgactggtggacagcaaatgggtcgcgga tccgaattcagcaacacgccaatcgagcttaaggcagtagcttcaactttatctgtggttcatctgcatgaggcagaaacctaagggtatccatca ggcgctggaagacaaaatcgctcaggcccccgatttttaaaacatgccccgttgtaactcaacgtcagtcactggaagaccggtaactgg tcagcgatgcataaggcgttttcgcaaccggtttcgggttattggcgtaagtggtcgtgcaagatgctgcaacttaagccgaaattgaaaaga tggggctgcctatcctgacggaaggaaaggaaaaagcgccaagtcagctcccaacccgaggtccagcgcgaaatacaacgcccgtcac aaaaacgcgttaatagataccccggctcgttcggtcagcgtatttatgtccacaatgtgatctgattgttacaagccagcttagcgtggggc cgaattgattccgatgggaacattcatgtctatggcatgatgcggtcgtgctgctggcaggggcaagtggtgaccgggaaacgcaaatatgtt gtacgaacctgatggcgaactggtgtccatcgaggtgaatactggctgagtgatcaaatcccagcagaattttatggcaaacggcgcgact gcagttatgctgaaaacgctttgaccgttcaaccgttaaatTGAgtcagcaccaccaccaccactgagatccggctgctaaacaaagcc cgaaggaagctgagttggctgctgccaccgctgagcaataactagcataacccttggggcctctaaacgggtcttgaggggtttttg

7.1.2 *egfp-minC*

taatacgaactcactataggggaattgtgagcggataacaattccctctagaataattttgtttaactttaagaaggagatataaccATGagg catcatcatcatcatcatcacagtaaaaggagaagaacttttactggagttgtccaattctgttgtaattagatggtgatgtaatggcacaaa ttttctgcagtgagaggggtgaaggtgatgcaacatacggaaaactacccttaaatattttgactactggaaaaactacctgttccatgcca acactgtcactactttcgcgtatggtctcaatgctttgagagataccagatcatatgaacagcagatgacttttcaagatgccaatgcccga ggttatgtacaggaaagaactatttttcaagatgacgggaactacaagacacgtgctgaagtcaagttgaaggtgataccctgttaattag

Appendix – DNA constructs and sequences

aatcagtgtaaaaggattgatttttaagaagatggaaacattcttggacacaaattggaatacaactataactcacacaatgtatacatcatgg
cagacaaaacaaagaatggaatcaaaagttaacttcaaaatfagacacaacattggaatggaagcgttcaactagcagaccattatcaacaaa
atactcaattggcgatggccctgtcctttaccagacaaccattactgtccacacaatctgccctttcgaagatcccaacgaaaagagaga
ccacatggtcctctttagttgtaacagctgctgggattacacatggcatggatgaactatacaagggtgcagcgggtgaattcagcaacacgc
caatcgagcttaaaggcagtagcttcaacttattctgtggttcatctgcatgaggcagaacctaaaggttatccatcaggcgtggaagacaaaatc
gctcaggccccgcatttttaaacatgccccctgttactcaacgtcagctgactggaagaccccgtaaaactggtcagcgtgcaataaggcgg
tttcggcaaccggtttgctgggttattggcgtaaagtgctgcaaaagatgcaacttaaacgcaaatgtaaaagatggggctgctatctgacg
gaaggaaaggaaaaagcgccacgtccacgtccacacccgaggtccacagcgaatacaacgcccgttcaaaaaacgcgttataatagata
ccccggtgcttccggtcagcgtatttatgtccacaatgtgatctgattgtaacaagccacgttagcgtggggccgaattgattgctgagggga
acattcatgtctatggcatgatgcgcggtctgctgctggcaggggcaagtggtgaccgggaaacgcaaatatttgtacgaacctgatggcgga
actggttccatcgaggtgaactggctgagtgatcaatccagcagaattttatggcaaaagcggcgcgactgcagtttagtcaaaacgct
ttgaccttaaccgtTAAattgagtcgagcaccaccaccaccactgagatccgctgctaacaagccccgaaaggaagctgagttgg
ctgctgccaccgctgagcaataa**ctagcataacccttggggcctctaaacgggtcttgagggtttttt**

7.1.3 *egfp-minD*

taatacgactcactataggggaattgtgagcggataacaattccctctagaataat**ttgtttaa**ctttaagaaggagatataccATGggc
agcagccatcatcatcatcatcagcagcggcctggtgcccgcggcagccatattgctagcatgactggtggaagcagcaaatgggtcgcgga
tccgtgagcaaggcagggagctgttaccggggtggtgcccactctggtcagctggaagcagcgttaaacggccacaagtgcagctgttcc
ggcagggcgagggcagtcacactacggcaagctgaccctgaagttcatctgcaccacggcgaagctgcccgtgcccaccctcgtg
accaccctgacctacggcgtgagctttagcggctaccggaccacatgaagcagcagacttcttcaagtccgcatgcccgaaggctac
gtccaggagcgcaccattcttcaaggacgacggcaactacaagaccgcccaggtgaagttcagggcgcacaccctggaaccgcat
cgagctgaaggcatcagcttcaaggaggcgaacatctggggcacaagctggagtaactacaactacaacagccacaacgtctatatcatgg
ccgacaagcagaagaacggcatcaagggtgaactcaagatccccaacaatcgaggacggcagcgtgagctgcccgaccactaccagca
gaacacccccatcgcgacggccccgtgctgctcccgaacaaccactactgagcaccagtcgcccctgagcaaaagacccccaacgagaag
cgcgatcacatggtcgtggtgagttcgtgaccgcccgggatacctcggcatggacgagctgtacaagaa**ttcgcacgcattattgtt**
tacttccggcaaaagggtgtgtgtaagacaacctccagcgcggccatgccactggtttggccagaaggaagaaactgtcgtgataga
ttttgatatcggcctgtaatactcagctgattatgggtgtgaaacgggctgtttacgatttctgtaaacgctcattcagggcagcacaacgta
aatcagggcgttaataaagataagcgtactgaaatctctatattctgcccgcacgcaaaacacgcgataaagatgcccctcaccgtgaagggg
tcgcaaaagtcttgatgatcgaagcagatgattttgaaatctggttctgactcccggcagggattgaaacccggtgctgtaattgcaactcta
ttttgagacgaagcattattaccaccaaccgggaagtctcctcagtagcgcgactctgaccgatttttaggcattctggctgcaaatcacgcc
gcgcagaaaaatggcgaagagcctataaagagcacctgctgttaacgcgctataaccaggccgctgaagcagaggtgacatgctgagcatg
gaagatgtgctggagatctcgcgcatcaaacctgctggcgtgatcccagaggatcaatcagattgctgccccttaaccaggggtgaaccggtca
ttctcgacattaacgccgatcgggtaagcctacgcagataaccgtagaacgtctgttgggagaagaacgtcctttccgcttcattgagaaga
gaagaaaggcttctcaaacgcttcttgggaggaTAAaagcttggggccgactcagcaccaccaccaccactgagatccggtgct
aacaagccccgaaaggaagctgagttggctgctgccaccgctgagcaataa**ctagcataacccttggggcctctaaacgggtcttgagggt**
ttttt

7.1.4 *minE*

taatacgactcactataggggaattgtgagcggataacaattccctctagaataat**ttgtttaa**ctttaagaaggagatataccATGggc
agcagccatcatcatcatcatcacagcagcggcctggtgcccgcggcagccatattgctagcatgactggtggaagcagcaaatgggtcgcgga
tccgaattcgacttactcgtattcttctcgcggaagaaaaacacagccaacattgcaaaagAACGGCTGcagattattgtgctgaacgccc
tcgacgcatgcagaaaccgattatctgccagttgctgtaaaatattcttgaggtcattgtaaatagctacaatgatcctgagatgtaac
cgtacagcttgagcaaaaagatggcgtatattctattctgagctgaacgtgacctaccggaagcagaagagctgaaaTAAaagcttgcgg
ccgactcagcaccaccaccaccactgagatccggtgctcaacaagccccgaaaggaagctgagttggctgctgccaccgctgagca
taactagcataacccttggggcctctaaacgggtcttgagggtttttt

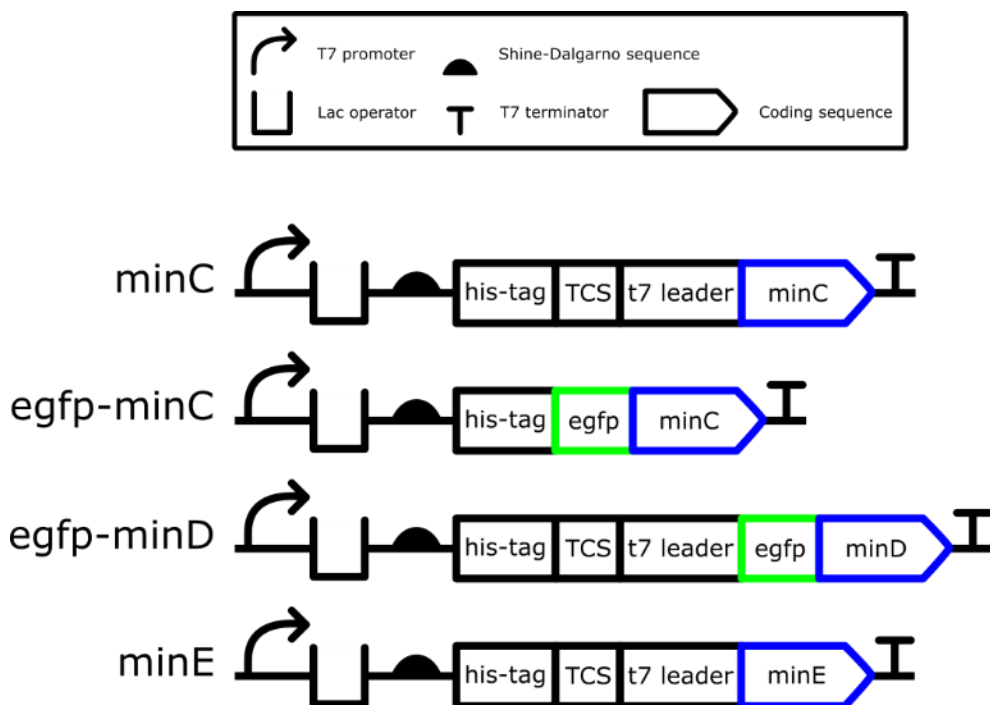


Figure 7.1 Schematic of DNA constructs used in this thesis for expression in *E. coli*.

7.2 DNA sequences for expression in the PURE system

All sequences are inserted in pET11-a except the optimized sequences *minD_{op}* and *minE_{op}* which are inserted in pCC1 and pUC57, respectively. Here, only the region between the promoter and terminator of each gene is shown. A schematic of the following DNA constructs can be seen in Figure 7.2 (divisome proteins), Figure 7.3 (min proteins) and Figure 7.4 (other sequences). The color and symbol code can be seen in Table 7.2.

Appendix – DNA constructs and sequences

Table 7.2 Code of colors and symbols for DNA templates for the cell-free expression in the PURE system.

Genetic part	Color and symbol code
Promoter (t7)	red
Operator (lacO)	orange
Ribosome binding site sequence	purple
Start codon	CAPITALS
DNA sequence of target protein	blue
6 histidine tag DNA sequence	dark blue
FtsA membrane targeting sequence	dark green
Stop codon	CAPITALS
Terminator (t7)	red

7.2.1 *ftsZ*

taatacgactcactataggggaattgtgagcggataacaattcc
cctctagaataat
ttgtttaactttaagaaggagata
tatacat
ATG
tttgaaccaatggaacttacc
aatgatgacgcggtgattaaagtcacggcgtcggcggcggcggtaatctgttgaacacatggtcgcgagcgcattgaagggttgaattcttcgcggtaaataccgatgcacaagcgtcgcgtaaacagcggttggacagacgattcaaatcggtagcgggtacacaaaggactggcgtggcgtactccagaagtggccgcaatgcggctgatgaggatcgcgatgcattgcgtcggcgtggaaggtgcagacatggctcttattgctgcgggtatgggtggtgtaccggtacaggtgcagcaccagtcgtcgtgaagtggcaaaaatttgggtatcctgaccgttctgtctcactaagcctttcaactttgaaggcaagaagcgtatggcattcgcggagcaggggatcactgaactgtccaagcatgtggactctgatcactatcccgaacgacaaaactgctgaaagtctgggcccgggtatctcctgctggatgcgtttggcgcagcgaacgatgactgaaaggcgtgtgcaaggtatcgcgtgaactgattactgctccgggtttgatgaactggactttgcagacgtacgcaccgtaattctctgagatggctacgcgaatgatgggtctggcgtggcgcgagcgggtgaagaccgtgcggaagaagctgctgaaatggctatcttctccgctgctggaagatctacgcgaatgatgggtctggcgtggcgcgagcgggtgaagaccgtgcggaagaagctgctgaaatggctatcttctccgctgctggaagatcgcacctgtctggcgcgcgcggtgctgggttaacatcacggcggccttcgactcgtctggatgagttcgaacggtaggtaacaccatccgtgcatttctccgacaacgcgactgtgggtatcggtacttcttggaccggatataatgacgagctgcgtaaccgttgttgcacaggtatcgcgatggacaaacgtcgaatacactctggtgaccaataagcaggttcagcagccagtgatggatcgtaccagcagcatgggatggctccgtgaccaggagcagaagccggttgcataaagctgtaataatgcagcgcgcaaaactgcgaaagagccggattatctggatcccagcattccgcgtaagcaagctgat
TAA
ggatccggctgctaacaagcccgaaggaagctgagttggctgctgccaccgctgagcaataa
ctagcat
aacccttggggcctcaaacgggtcttgaggggtttttg

7.2.2 *ftsZ-his*

taatacgactcactataggggaattgtgagcggataacaattcc
cctctagaataat
ttgtttaactttaagaaggagata
tatacat
ATG
tttgaaccaatggaacttacc
aatgatgacgcggtgattaaagtcacggcgtcggcggcggcggtaatctgttgaacacatggtcgcgagcgcattgaagggttgaattcttcgcggtaaataccgatgcacaagcgtcgcgtaaaacagcggttggacagacgattcaaatcggtagcgggtatccaaaggactggcgtggcgtactccagaagtggccgcaatgcggctgatgaggatcgcgatgcattgcgtcggcgtggaaggtgcagacatggctcttattgctgcgggtatgggtggtgtaccggtacaggtgcagcaccagtcgtcgtgaagtggcaaaagatttgggtatcctgaccgttctgtctcactaagcctttcaactttgaaggcaagaagcgtatggcattcgcggagcaggggatcactgaactgtccaagcatgtggactctgatcactatcccgaacgacaaaactgctgaaagtctgggcccgggtatctcctgctggatgcgtttggcgcagcgaacgatgactgaaaggcgtgtgcaaggtatcgtgaactgattactcgtccgggtttgatgaactggactttgcagacgtacgcaccgtaattctctgagatgggctacgcaatgatgggtctggcgtggcgcgagcgggtgaagaccgtgcggaagaagctgctgaaatggctatcttctccgctgctggaagatcgcaccgtctggcgcgcgcgctgctggttaacatcacggcggccttcgacctgctgctgatgagttcgaacggtaggtaacacatccgtgcatttgcctccgacaacgcgactgtgggtatcggtacttcttggaccggatataatgacgagctgcgtaaccgttgttgcacaggtatccgcatggacaaacgtcctgaaatcactctggtgaccaataagcaggttcagcagccagtgatggatcgtaccagcagcatgggattggctccgctgaccagagcagaagccggttgcataaagctgtaataatgcgcccgaactgcgaaagaccggattatctggatcccagcattcctgctg

taagcaagctgatcatcacatcatcacatTAAggatccggctgctaacaagcccgaaggaagctgagttggctgctgccaccgctga
gcaataactagcataacccttggggcctctaaacgggtcttgagggtttttt

7.2.3 *ftsZ-a*

taatacgaactactataggggaattgtgagcggataacaattccctctagaataattttgtttaactttaagaaggagatacatATGttt
gaaccaatggaacttaccatgacgcgggtattaaagtcacggctcggcggcggcgggtaattgctgtgaaacacatggtgcgcgagcgc
attgaaggtgtgtaattcttcgcggtaaataccgatgcacaagcgtcgtgaaacagcggttggacagacgattcaaatcggtagcggatca
ccaaaggactggcgcgtgcgtaaatccagaagttggcgcgaatgcggctgatgaggatcgcgatgattgctgcgcgctggaaggtgag
acatggtctttattgctgcgggtatgggtgtgtgtaccggtacaggtgcagcaccagtcgctcgtgaagttggcaaaagattttgggtatcctgacc
gtgctgtcgtcactaagcctttcaactttgaaggcaagaagcgtatggcattcgcggagcaggggatcactgaaactgctcaagcatgtggactc
tctgatcactatccgaacgacaaactgctgaaattctgggcccgggtatctccctgctggatgctgtttggcgcagcgaacgatgactgaaag
gcgctgtgcaaggtatcgtgaaactgattactcgtcgggtttgatgaaactggacttttcagacgtacgcaccgtaagtctgagatgggctac
gcaatgatgggtctggcgtgagcgggtgaagaccgtcgggaagaagctgctgaaatggctatctcttccgctgctggaagatatcgacc
tgtctggcgcgcggcgtgctggttaacatcacggcgggtctgacctgcgtctggatgagttcgaacggtaggtaacacacccgtgacattt
gcttccgacaacgcgactgtggtatcggtaacttcttgaaccggatgatgaatgacgagctgcgtaaccgttgttgcagaggtatcggcat
ggacaaactgctgaaactcctgtgtgaccaataagcaggttcagcagccagtgatggatcgtaccagcagcatgggatggctccgctgac
ccaggagcagaagccggttctaaagctgtaatagcaatgcgcccgaactcgaagagcgggattatcgtgatatccagcattcctgcg
taagcaagctgatggctcgtgatcaagcgaactcaatagttggctgcgaaagagtttTAAggatccggctgctaacaagcccgaaggaag
a

7.2.4 *zipA*

taatacgaactactataggggaattgtgagcggataacaattccctctagaataattttgtttaactttaagaaggagatacatATGatg
caggatttgcgtctgataatfaactattgttggcgcgatcgcataatcgtttactgtgacatggtttctggaccagcgtaaagaacgatcttcta
tgttccgcatcggcattaaacgaatgaagtcaaaacgtgacgacattcttatgacgaggatgctgaagatgatgagggcgttggtaggt
tctgtttaccgcgtgaatcatgccccggtaacgctcaggagcatgaggctgctcgtcgcgcgcaacaccagtaaccaaccgcttatgcg
tctgcgagccgctcaaccggtccagcagccgctgaagcgcaggtaccgccaacatgctccgcatccagcgcagccggtgagcagcc
tgcctatcagccgagcctgaacagcgttgcagcagccagtttcccaacaggtcgcgccagcggcagcctgtcattcagcaccgcaacc
ggcacaacaggttttcagcctgcagaaaccgtagcggcaccacagcctgagcctgtagcggaaactgctccagttatggataaaaccgaagcg
caaagaagcgggtattatcatgaagctcgcggcgcacacggtagcagtaaacgggtgaactgcttcttaacagcattcaacaagcgggctt
atttttggcgaatgaatattaccatcgtcatcttagcccggatggcagcggcccggcgttattcagcctggcgaatattgtgaaaccgggaac
ctttgatcctgaaatgaagatttactactcgggtgtcactactctttagcaggtaccgtcttacggtgacgagctgcagaactcaagctgat
gctgcaatctgcgcagcatattgcatgaagttggcgggtgctgctgctgacgatcagcggctatgatgactccgcagaatttgcgcgagtac
caggacatcatccgcgaagtcaaaagcgaacgcTGAggatccggctgctaacaagcccgaaggaagctgagttggctgctgccac
cgtgagcaataactagcataacccttggggcctctaaacgggtcttgagggtttttt

7.2.5 *szpA*

taatacgaactactataggggaattgtgagcggataacaattccctctagaataattttgtttaactttaagaaggagatacatATGcat
caccatcatcacatcatggtttctggaccagccgtaaaagaacgatcttctatgttccgcatcggccattaaaacgaatgaagtcaaaacgtg
acgacgattcttatgacgaggatgctgaagatgatgagggcgttggtaggttctgtttaccgcgtgaatcatccccggtaaacgctcagga
gcatgaggtgctcgtcgtcgcgaacaccagtaaccaaccgcttatgctcgtcgcagccgctcaaccggtccagcagccgctgaagc
geaggtaccgccaacatgctccgatccagcgcagccggtgacgacgctgctatcagccgcagcctgaacagcgttgcagcagccag
tttccacaggtcgcgcagcgcgcagcctgtgattcagcaccgcaaccggcaacaaggtttccagcctgcagaaccgtagcggcac
cacagcctgagcctgtagcgaacctgctccagttatggataaacggaagcgaagagcgggtattatcatgaacgtcgcggcgcacag
gtagcagctaaacgggtgaactgcttctaacagcattcaacaagcgggtctcattttggcgaatgaatattaccatcgtcatcttagcccgg
atgacgcccggcgttattcagcctggcgaatattggtgaaaccgggaaccttggatcctgaaatgaaggatttcaactctccgggtgctact
atctttatgaggtaccgcttaccggtgacgagctgcagaaactcaagctgatgctgcaatctgcgcagcataattgcatgaaagttggcgtg
cgtgcttgcagatcagcggctgatgactcgcgaaattgcgcgagtagcagcagcagcagcagcagcagcagcagcagcagcagcagcagc
ggatccggctgctaacaagcccgaaggaagctgagttggctgctgccaccgctgagcaataactagcataacccttggggcctctaaacg
ggtcttgagggtttttt

Appendix - DNA constructs and sequences

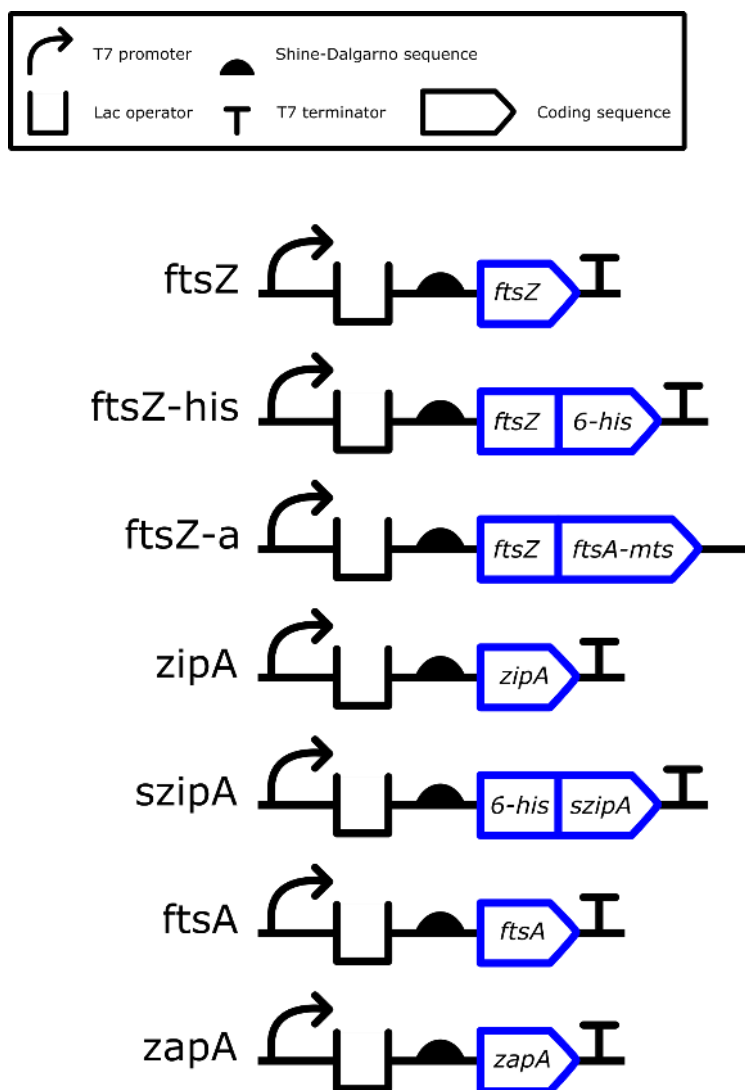


Figure 7.2 Schematic of *E. coli* divisome DNA constructs for cell-free expression in the PURE system.

7.2.6 *ftsA*

taatacgaactcactataggggaattgtgagcggataacaattccctctagaataattttgtttaactttaagaaggagatatatcatATGatc
aaggcgacggacagaaaaactgtagtaggactggagattggtaccgcgaaggttgcgctttagtaggggaagtctgcccacggtatggc
aataatcattggcgtgggcagctgccgctgcgtggtatggataaaggcggggtgaacgacctcgaatccgtggtcaagtgcgtacaacgcgc
attgaccaggcagaattgatggcagattgtcagatctctcggatatactggcctttctggaagcacatcagctccagaatgaaattggtatg
gtgcctattctgaagaagaagtgacgcaagaagatgtggaaaacgtcgtccataccgcgaaatcgggtgctgctgcgatgagcatcgtgtgc
tgcattgtatcccgaagagatgcatgattgactatcaggaaggatcaagaatcggtaggactttcgggcgtgctggatgcaggcaaaagtgc
acctgatcacatgtcacaacgatatggcgaaaaacatcgtcaaacggttgaacgttggggctgaaagttgaccaactgatatttgcggact
ggcatcaagttattcggattatgacggaagatgaactggaactgggtgtctgctgctgcgatatcgggtggtgataatggatgcgctttatc
cgggtgggcattgctgcccactaaggaattccttatgctggaatgtcgtgaccagtgatctgcttacgctttggcagccgccaagcgcag

ccgaagcgattaaagttgccacgggtgtgctgggtccatcgttggaaaagatgagagcgtggaagtgcgagcgtaggtggtcgtccgcc
acggagctgcaactcagacactggcagaggtgatcagcgcgctaaccgagctgctcaacctgtcaacgaagatattgcagttgca
ggaaaagcttcccaacaagggttaaacatcacctggcggcaggcattgtattaacgggtggcgcagcgcagatcgaagcttgcagcgtg
tgctcagcgcgtttcatagcgaagtcgfatcggcgcgcgctgaacattaccgggttaacggattatgctcaggagccgtattattcagcgg
cgggtggattgcttactatgggaaagatcacatctaacggtgaagctgaagtagaaaaactgttacagatcagttgctcgtggtatcaa
gcgactcaatagttggctgcaaaaagagtttTAAggatccggctgctaacaagcccgaaggaagctgagttggctgctgccaccgctga
gcaataa**ctagcataacccttggggcctctaacgggtcttgagggttttttg**

7.2.7 *zapA*

taatacgaactcactataggggaattgtgagcggataacaattcccctctagaataat**ttgtttaactttaagaaggagata**tatacat**ATG**tct
gcacaaccgctgatattcaaatTTTTGGCCGTTCACTGCTGTGAAGTCCCGCTGACCAAGGGATGCGTTGAATCAGGCAGCGGACGATC
TGAACCAACGGTTGCAAGATCTGAAAGAAGCACTAGAGTCAAAATCTGAACAGTTGGTCTTATTGCCGATGAATATCAGCTATGAGTTA
GCGCAAGAAAAAGCAAGACTCGTACTACGCGGAAGTATGGAACAGCGTATTCCGATGCTGCAGCAGACCATAGAACAAGCGTTACTTGA
ACAAGTGCATACCAGAAAACTAACAAAACTTTGAA**TGA**ggatccggctgctaacaagcccgaaggaagctgagttggctgctg
ccaccgctgagcaataa**ctagcataacccttggggcctctaacgggtcttgagggttttttg**

7.2.8 *minD*

taatacgaactcactataggggaattgtgagcggataacaattcccctctagaataat**ttgtttaactttaagaaggagata**tatacat**ATG**gc
acgcatattgtgttacttccgggcaaggggggtgtgtaagacaacctccagcgcggccatcgccactggtttggcccagaagggaaagaaa
actgtcgtgatagattttgatctggcctgtaattctcgacctgattatgggttgaacgccgggtcgtttacgatttcgtaacgctattcagg
gcatgcaacgctaaatcaggcgtfaaattaaagataagcgtactgaaaatctctataattcgcggcatcgaaaacacgcgataaagatccct
caccctggaagggctgcgcaaaagtcttgatgatctgaaagcgtggattttgaaattatcgttttgactccccggcagggatgaaaccggtg
cgttaatggcactctattttgcagacgaagccattattaccaccaaccggaaagtctctcagtacgcgactcagctgaccgtattttaggcattctgg
cgtcgaaatcacgccgcgagaaaatggcgaagagcctattaaagagcacctgctgtaacgcgctataaccaggccgctgtaagcagaggt
gacatgctgagatggaagatgtgctggagatctcgcgcatcaaacctcgtcggcgtgatccagaggatcaatcagattgctgcgccttaacc
agggtgaaccggtcattctcgacattaacgccgatgcccggtaagcctacgcagataccgtagaacgtctgtttgggagaagaacgtcctttccg
cttcattgaaagaagaagaaagggttcctcaaacgctgttcggagga**TAA**ggatccggctgctaacaagcccgaaggaagctgagtt
ggctgctgccaccgctgagcaataa**ctagcataacccttggggcctctaacgggtcttgagggttttttg**

7.2.9 *minD_{op}*

taatacgaactcactataggggaattgtgagcggataacaattcccctctagaataat**ttgtttaactttaagaaggagata**tatacat**ATG**gcg
cgtattattgttttaccagcggcaagggcggcgtttggcaagaccagcagcgcggcgattgacaccggcctggcgcagaagggcaagaa
aaccgtggtatcgactcgcgatattggtctcgttaacctggactgatcatggcctgcgagcgtcgtgtggtttacgactttgtgaacgtgattcag
ggtgatcgaccctgaaccaggcgtgatcaaggataaacgtaccgagaacctgtatattcgcggcgagccagaccgctgacaagatgctg
ctgaccctggaagcgtggcgaaggttctggacgatctgaagcgtatggacttgcgagttatctgtgtgcatagccggcgggtattgaaaccg
gcgcgctgatggcgtgtacttgcggcagaggcgtattaccaccaaccggaaagtgagcagcgtgctgacagcgtatctctgggtat
tctggcagcaagagcctcgtcgggagaaacggcaggaaccgatcaagaacacctgctgctgacccgttataatccgggtcgtgtgagccg
tggcgacatgctgacatggaggaagtctggaatctcgcgtataaacgttgggtgtgatcccggaggaccagagcgtgctgctgctgagc
aaccaaggtgaaccggtattctggacattaacgcggatgcccggcaagcgtacgcggataccgttgaacgtcgtggtggcaggaacgtccg
ttctgtttattgaaagaagaagaaggggttctgaagcgtctgtttggcggc**TAA**ggatccggctgctaacaagcccgaaggaagctg
agttggctgctgccaccgctgagcaataa**ctagcataacccttggggcctctaacgggtcttgagggttttttg**

7.2.10 *minE*

taatacgaactcactataggggaattgtgagcggataacaattcccctctagaataat**ttgtttaactttaagaaggagata**tatacat**ATG**gc
attactgatttcttctcgcggaaagaaaaacacagccaacttgcaaaaagacggctgcagattattgtgctgaacccgtcgcagcgtg
cagaaccgattatctgcgcgcaagatattcttgaggtcatttgtaataactgatacaaatgctgagatggtaaccgtaacgctgagctg
agcaaaaagatggcgatatttcttctgagctgaacgtgacctaccggaagcagaagagctgaaa**TAA**ggatccggctgctaacaag
cccgaaggaagctgagttggctgctgccaccgctgagcaataa**ctagcataacccttggggcctctaacgggtcttgagggttttttg**

Appendix – DNA constructs and sequences

7.2.11 *minE_{op}*

taatacgaactcactataggggaattgtgagcggataacaattccctctagaataatttgtttaactttaagaaggagatatacatATGgcgctgctggattcttctgagccgtaagaaaaacaccgcgaacatcgcgaaagagcgtctgcaaatcattgttgcggagcgtcgtcgtgacgatgcggaaccgcactactcggcagctgcgtaaaagatactctggaagtgttgcgaagtgttcaaattgacccggagatggtgaccgttcagctggaacaaaaggacggtgatcagcattctggagctgaacgttacctgccggaagcggaggaaactgaagTAAggatccggctgctaacaagcccgaaggagactgagttggctgctgccaccgctgagcaataac**tagcataacccttggggcctctaaacgggtcttgaggggttttttg**

7.2.12 *p3-phi29*

taatacgaactcactatagggagaccacaacggttcctctagaataatttgtttaactttaagaaggagatatacatATGgcacgcagcccgcgatccgcatcaaagataacgacaaagccgaatacggcctggtgaaaaatacgaagctaaaatcgacgtaccaagaaaaaatggcgtggatctgacggctgaaattgacatccggatctggactcattgaaacccgcgcagttcaataatggaagaacaagctagctctttacgaaccgtgcgaatgatcgctatcagttcgagaaaaacgctacggctggtgcatcgaaagctaaaattgcggaatgcaacgtaaaccaaagaagttcaacgcctggtgatgaaaaaatcaagccatgaaagacaagaatattacgcaggcgtaaaccgcagggcagcattgaaacacgctatcgccatgacctaccggcagatgtgacgggtatcaaccgtccgcagcattttgacttcagtaaagttcgcagttactccgctcgcaccctggaagaatccatggaatgcccagcggatccgcagattacgaaaagaaatgattcagctgcaactgaaatttatcaaaagcgtcgaaaggctcatttaactgctgacggccgacgaactgattgaagaactgaagaaaaatccgccgatgactttatgaactgttcctgctattagcgaatctctttgaaagaattcattctgaaggcaaccgctgaaaaatgtggaggtaacgtttacaaaattctgtctatctggaacaatatcgtcgtggtgattttgatctgctgctgaaaggcttcTAA**tagcataacccttggggcctctaaacgggtcttgaggggttttttg**

7.2.13 *eyfp*

aagatttaggtgacactatagaatacaagcttgggctgcagcgcgaaat**taatacgaactcacta**tagggagaccacaacggttcctctagaaataatttgtttaactttaaga**aggag**atatacatATG**cggggttctcatcatcatcatcat**ggtatggtagcatgactggtggacagcaaatgggtcgggatctgtacgacgatgacgataaggatccgatggtgagcaagggcagggagctgttcaccgggtggtcccatcctggtcgaactgagcggcgacgtaaacggccacaagttcagcgtgtccggcgagggcgatgccacctacggcaagctgacctgaagttcatctgcaccaccgcaagctgcccgtgcccctggcccaccctcgtgaccacctcggctacggcctgcagtgcttcgcccgtaccggacacatgagcagcagcacttctcaagtcgcccattgcccgaaggctacgtccaggagcgcaccatcttctcaaggacgacggcaactacaagaccgcgcccaggtgaaagttcagggcgacaccctggtgaaccgcatcgagctgaaggcatcgacttcaaggaggacggcaacatcctggggcacaagctggagtacaactacaacgccacaacgcttatatcattgcccgaagcagaagaacggcatcaagggtgaacttcaagatccgccacaacatcgaggacggcagcgtgacgtcgcgaccactaccagcagaacacccccaacggcagcggccccgtcgtcgtcggcacaaccactactgagctaccagtcgaagctgagcaaacgcccacgagaagcgcgatcacatggtcctgctggagttcgtgaccgccggggaatcctcggcattggcagcgtgtaaacTAA**aagcttcccgggaaagtataatgatgaaagatatgcagcaactgaaatggtgaaaggacgggtccagggtgctgctgctcggcagtcagctgttgaagtagagtgtagctccgtaactagtcgctcgat**atccccggctagcataacccttggggcctctaaacgggtcttgaggggttttttaaaaaaaaaaaaaaaaaaaaaaaaaaaaaa

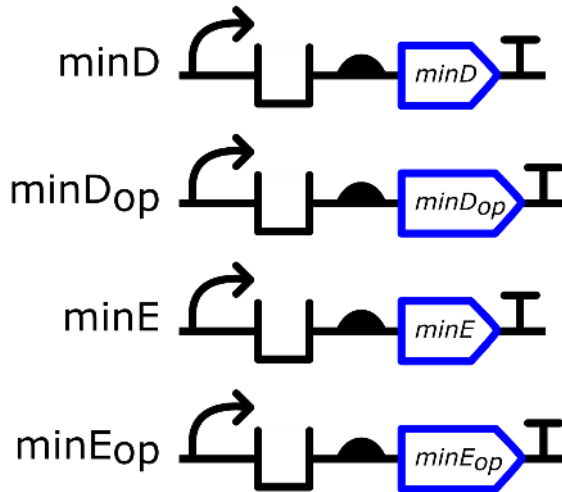
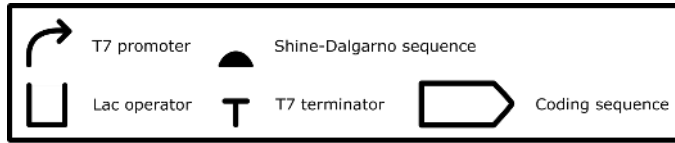


Figure 7.3 Schematic of *E. coli* min system DNA constructs for cell-free expression in the PURE system

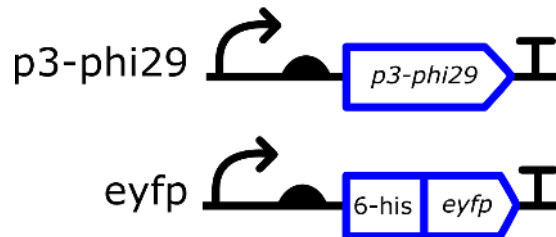
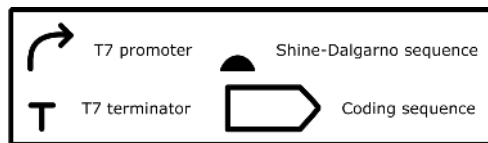


Figure 7.4 Schematic of DNA constructs for cell-free expression in the PURE system for control experiments

References

1. Dawkins, R. *The selfish gene*. (Oxford University Press, 1989).
2. Maturana, H. & Varela, F. *De maquinas y seres vivos*. (1973).
3. Fernández, N., Maldonado, C. & Gershenson, C. Information Measures of Complexity, Emergence, Self-organization, Homeostasis, and Autopoiesis. in 19–51 (Springer, Berlin, Heidelberg, 2014). doi:10.1007/978-3-642-53734-9_2.
4. Gershenson, C. Requisite variety, autopoiesis, and self-organization. doi:10.1108/K-01-2015-0001.
5. Giovannoni, S. J. *et al.* Genome Streamlining in a Cosmopolitan Oceanic Bacterium. *Science* (80.). **309**, 1242–1245 (2005).
6. Keseler, I. M. *et al.* The EcoCyc database: reflecting new knowledge about *Escherichia coli* K-12. *Nucleic Acids Res.* **45**, 543–550 (2016).
7. Ye, Y.-N. *et al.* A novel proposal of a simplified bacterial gene set and the neo-construction of a general minimized metabolic network OPEN. *Sci. Rep.* **6**, 1–10 (2016).
8. Mushegian, A. R. & Koonin, E. V. A minimal gene set for cellular life derived by comparison of complete bacterial genomes. *Proc. Natl. Acad. Sci.* **93**, 10268–10273 (1996).
9. Gil, R., Silva, F. J., Peretó, J. & Moya, A. Determination of the Core of a Minimal Bacterial Gene Set. *Microbiol. Mol. Biol. Rev.* **68**, 518–537 (2004).
10. Luisi, P. L. Conceptual framework of research on the origin of life on Earth. in *The Emergence of Life* 1–16 (Cambridge University Press, 2006). doi:10.1017/CBO9780511817540.002.
11. Luisi, P. L. About Various Definitions of Life. *Orig. Life Evol. Biosph.* **28**, 613–622 (1998).
12. Xavier, J. C., Raosaheb, K. & Rocha, I. Systems Biology Perspectives on Minimal and Simpler Cells. *Microbiol. Mol. Biol. Rev.* **78**, 487–509 (2014).
13. Gibson, D. G. *et al.* Creation of a Bacterial Cell Controlled by a Chemically Synthesized Genome. *Science* (80.). **329**, 52–56 (2010).
14. Xu, C., Hu, S. & Chen, X. Artificial cells: from basic science to applications. *Mater. Today* **19**, 516–532 (2016).
15. Moya, A. *et al.* Toward minimal bacterial cells: evolution vs. design. *FEMS Microbiol. Rev.* **33**, 225–235 (2009).
16. Cho, M. K. *et al.* Global Transposon Mutagenesis and a Minimal *Mycoplasma* Genome. *Science* (80.). **286**, 2087–2090 (1999).
17. Zohreh Nourian. Towards the assembly of a minimal oscillator. (2015).
18. Rasmussen, S., Chen, L., Nilsson, M. & Abe, S. Bridging Nonliving and Living Matter. *Artif. Life* **9**, 269–316 (2003).

19. Mann, S. Systems of Creation: The Emergence of Life from Nonliving Matter. *Acc. Chem. Res.* **45**, 2131–2141 (2012).
20. Hammer, D. A. & Kamat, N. P. Towards an artificial cell. *FEBS Lett.* **586**, 2882–2890 (2012).
21. van Nies, P. *et al.* Self-replication of DNA by its encoded proteins in liposome-based synthetic cells. *Nat. Commun.* **9**, 1–12 (2018).
22. Scott, A. *et al.* Cell-Free Phospholipid Biosynthesis by Gene-Encoded Enzymes Reconstituted in Liposomes. *PLoS One* **11**, 1–23 (2016).
23. Bi, E. & Lutkenhaus, J. FtsZ ring structure associated with division in *Escherichia coli*. *Nature* **354**, 161–164 (1991).
24. Errington, J., Daniel, R. A. & Scheffers, D.-J. Cytokinesis in bacteria. *Microbiol. Mol. Biol. Rev.* **67**, 52–65, table of contents (2003).
25. Trip, E. N. & Scheffers, D.-J. A 1 MDa protein complex containing critical components of the *Escherichia coli* divisome. *Sci. Rep.* **5**, 1–10 (2015).
26. Bernhardt, T. G. & De Boer, P. A. J. The *Escherichia coli* amidase AmiC is a periplasmic septal ring component exported via the twin-arginine transport pathway. *Mol. Microbiol.* **48**, 1171–1182 (2003).
27. Bernhardt, T. G. & De Boer, P. A. J. Screening for synthetic lethal mutants in *Escherichia coli* and identification of EnvC (YibP) as a periplasmic septal ring factor with murein hydrolase activity. *Mol. Microbiol.* **52**, 1255–1269 (2004).
28. Ogino, H. *et al.* FtsZ-dependent localization of GroEL protein at possible division sites. *Genes to Cells* **9**, 765–771 (2004).
29. Bertsche, U. *et al.* Interaction between two murein (peptidoglycan) synthases, PBP3 and PBP1B, in *Escherichia coli*. *Mol. Microbiol.* **61**, 675–690 (2006).
30. Ebersbach, G., Galli, E., Møller-Jensen, J., Löwe, J. & Gerdes, K. Novel coiled-coil cell division factor ZapB stimulates Z ring assembly and cell division. *Mol. Microbiol.* **68**, 720–735 (2008).
31. Gerding, M. A., Ogata, Y., Pecora, N. D., Niki, H. & De Boer, P. A. J. The trans-envelope Tol-Pal complex is part of the cell division machinery and required for proper outer-membrane invagination during cell constriction in *E. coli*. *Mol. Microbiol.* **63**, 1008–1025 (2007).
32. Gueiros-Filho, F. J. & Losick, R. A widely conserved bacterial cell division protein that promotes assembly of the tubulin-like protein FtsZ. *Genes Dev.* **16**, 2544–2556 (2002).
33. Samaluru, H., Saisree, L. & Reddy, M. Role of SufI (FtsP) in cell division of *Escherichia coli*: Evidence for its involvement in stabilizing the assembly of the divisome. *J. Bacteriol.* **189**, 8044–8052 (2007).
34. Schmidt, K. L. *et al.* A Predicted ABC Transporter, FtsEX, Is Needed for Cell Division in *Escherichia coli*. *J. Bacteriol.* **186**, 785–793 (2004).
35. Huang, K. H., Durand-Heredia, J. & Janakiraman, A. FtsZ ring stability: Of bundles, tubules, crosslinks, and curves. *J. Bacteriol.* **195**, 1859–1868 (2013).
36. Hale, C. A. *et al.* Identification of *Escherichia coli* ZapC (YcbW) as a component of

- the division apparatus that binds and bundles FtsZ polymers. *J. Bacteriol.* **193**, 1393–1404 (2011).
37. Vaughan, S., Wickstead, B., Gull, K. & Addinall, S. G. Molecular Evolution of FtsZ Protein Sequences Encoded Within the Genomes of Archaea, Bacteria, and Eukaryota. *J. Mol. Evol.* **58**, 19–39 (2004).
 38. RayChaudhuri, D. & Park, J. T. Escherichia coli cell-division gene ftsZ encodes a novel GTP-binding protein. *Nature* **359**, 251–254 (1992).
 39. Mukherjee, A. & Lutkenhaus, J. Guanine nucleotide-dependent assembly of FtsZ into filaments. *J. Bacteriol.* **176**, 2754–8 (1994).
 40. Erickson, H. P., Taylor, D. W., Taylor, K. A. & Bramhill, D. Bacterial cell division protein FtsZ assembles into protofilament sheets and minirings, structural homologs of tubulin polymers. *Proc. Natl. Acad. Sci. U. S. A.* **93**, 519–23 (1996).
 41. Löwe, J. & Amos, L. A. Tubulin-like protofilaments in Ca²⁺-induced FtsZ sheets. *The EMBO Journal* vol. 18 <https://www.ncbi.nlm.nih.gov/pmc/articles/PMC1171319/pdf/002364.pdf> (1999).
 42. Oliva, M. A., Cordell, S. C. & Löwe, J. Structural insights into FtsZ protofilament formation. *Nat. Struct. Mol. Biol.* **11**, 1243–1250 (2004).
 43. Bramhill, D. & Thompson, C. M. GTP-dependent polymerization of Escherichia coli FtsZ protein to form tubules. *Proc. Natl. Acad. Sci. U. S. A.* **91**, 5813–7 (1994).
 44. Scheffers, D.-J., De Wit, J. G., Den Blaauwen, T. & Driessen, A. J. M. GTP Hydrolysis of Cell Division Protein FtsZ: Evidence that the Active Site Is Formed by the Association of Monomers. *Biochemistry* **41**, 521–529 (2002).
 45. de Boer, P., Crossley, R. & Rothfield, L. The essential bacterial cell-division protein FtsZ is a GTPase. *Nature* **359**, 254–256 (1992).
 46. Stricker, J., Maddox, P., Salmon, E. D., Erickson, H. P. & Mcintosh, J. R. Rapid assembly dynamics of the Escherichia coli FtsZ-ring demonstrated by fluorescence recovery after photobleaching. *Proc. Natl. Acad. Sci.* **99**, 3171–3175 (2002).
 47. Anderson, D. E., Gueiros-Filho, F. J. & Erickson, H. P. Assembly dynamics of FtsZ rings in Bacillus subtilis and Escherichia coli and effects of FtsZ-regulating proteins. *J. Bacteriol.* **186**, 5775–81 (2004).
 48. Erickson, H. P., Taylor, D. W., Taylor, K. A. & Bramhill, D. Bacterial cell division protein FtsZ assembles into protofilament sheets and minirings, structural homologs of tubulin polymers. *Proc. Natd. Acad. Sci. USA* **93**, 519–523 (1996).
 49. Oliva, M. A. *et al.* Assembly of archaeal cell division protein FtsZ and a GTPase-inactive mutant into double-stranded filaments. *J. Biol. Chem.* **278**, 33562–70 (2003).
 50. Peters, P. C., Migocki, M. D., Thoni, C. & Harry, E. J. A new assembly pathway for the cytokinetic Z ring from a dynamic helical structure in vegetatively growing cells of Bacillus subtilis. *Mol. Microbiol.* **64**, 487–499 (2007).
 51. Erickson, H. P., Anderson, D. E. & Osawa, M. FtsZ in bacterial cytokinesis: cytoskeleton and force generator all in one. *Microbiol. Mol. Biol. Rev.* **74**, 504–28 (2010).
 52. Di Lallo, G., Anderluzzi, D., Ghelardini, P. & Paolozzi, L. FtsZ dimerization in vivo. *Mol. Microbiol.* **32**, 265–274 (1999).

53. Löwe, J. Crystal Structure Determination of FtsZ from *Methanococcus jannaschii*. *J. Struct. Biol.* **124**, 235–243 (1998).
54. Dyer, N. Tubulin and its prokaryotic homologue FtsZ: a structural and functional comparison. *Sci. Prog.* **92**, 113–37 (2009).
55. Arkus Gardner, K. A. J., Moore, D. A. & Erickson, H. P. The C-terminal Linker of *Escherichia coli* FtsZ functions as an intrinsically disordered peptide. *Mol. Microbiol.* **89**, 264–275 (2013).
56. Ma, X. & Margolin, W. Genetic and functional analyses of the conserved C-terminal core domain of *Escherichia coli* FtsZ. *Journal of bacteriology* vol. 181 <https://www.ncbi.nlm.nih.gov/pmc/articles/PMC94211/pdf/jb007531.pdf> (1999).
57. Mosyak, L. *et al.* The bacterial cell-division protein ZipA and its interaction with an FtsZ fragment revealed by X-ray crystallography. *EMBO J.* **19**, 3179–91 (2000).
58. Ma, X., Ehrhardt, D. W. & Margolin, W. Colocalization of cell division proteins FtsZ and FtsA to cytoskeletal structures in living *Escherichia coli* cells by using green fluorescent protein. *Cell Biol.* **93**, 12998–13003 (1996).
59. Loose, M. & Mitchison, T. J. The bacterial cell division proteins FtsA and FtsZ self-organize into dynamic cytoskeletal patterns. *Nat. Cell Biol.* **16**, 38–46 (2013).
60. Wang, X., Huang, J., Mukherjee, A., Cao, C. & Lutkenhaus, J. Analysis of the interaction of FtsZ with itself, GTP, and FtsA. *J. Bacteriol.* **179**, 5551–5559 (1997).
61. Pichoff, S. & Lutkenhaus, J. Unique and overlapping roles for ZipA and FtsA in septal ring assembly in *Escherichia coli*. *EMBO J.* **21**, 685–93 (2002).
62. Rueda, S., Vicente, M. & Mingorance, J. Concentration and Assembly of the Division Ring Proteins FtsZ, FtsA, and ZipA during the *Escherichia coli* Cell Cycle. *J. Bacteriol.* **185**, 3344–3351 (2003).
63. Dai, K. & Lutkenhaus, J. The Proper Ratio of FtsZ to FtsA Is Required for Cell Division To Occur in *Escherichia coli*. *J. Bacteriol.* **174**, 6145–6151 (1992).
64. Kabsch, W. & Holmes, K. C. The actin fold. *FASEB J.* **9**, 167–74 (1995).
65. Ent, F. van den & Lowe, J. Crystal structure of the cell division protein FtsA from *Thermotoga maritima*. *EMBO J.* **19**, 5300–5307 (2000).
66. Herricks, J. R., Nguyen, D. & Margolin, W. A thermosensitive defect in the ATP binding pocket of FtsA can be suppressed by allosteric changes in the dimer interface. *Mol. Microbiol.* **94**, 713–727 (2014).
67. Yim, L. *et al.* Role of the carboxy terminus of *Escherichia coli* FtsA in self-interaction and cell division. *J. Bacteriol.* **182**, 6366–6373 (2000).
68. Krupka, M. *et al.* Role of the FtsA C Terminus as a Switch for Polymerization and Membrane Association. *MBio* **5**, 1–9 (2014).
69. Pichoff, S. & Lutkenhaus, J. Identification of a region of FtsA required for interaction with FtsZ. *Mol. Microbiol.* **64**, 1129–1138 (2007).
70. Pichoff, S. & Lutkenhaus, J. Tethering the Z ring to the membrane through a conserved membrane targeting sequence in FtsA. *Mol. Microbiol.* **55**, 1722–1734 (2005).

71. Shiomi, D. & Margolin, W. Compensation for the loss of the conserved membrane targeting sequence of FtsA provides new insights into its function. *Mol. Microbiol.* **67**, 558–569 (2015).
72. Geissler, B., Elraheb, D. & Margolin, W. A gain-of-function mutation in ftsA bypasses the requirement for the essential cell division gene zipA in Escherichia coli. *Proc. Natl. Acad. Sci.* **100**, 4197–4202 (2003).
73. Hale, C. A. & De Boer, P. A. J. Direct Binding of FtsZ to ZipA, an Essential Component of the Septal Ring Structure That Mediates Cell Division in E. coli. *Cell* **88**, 175–185 (1997).
74. Skoog, K. Cell division in Escherichia coli. (Stockholm University, 2011).
75. Ohashi, T., Hale, C. A., de Boer, P. A. J. & Erickson, H. P. Structural evidence that the P/Q domain of ZipA is an unstructured, flexible tether between the membrane and the C-terminal FtsZ-binding domain. *J. Bacteriol.* **184**, 4313–5 (2002).
76. Hale, C. A. & de Boer, P. A. Recruitment of ZipA to the septal ring of Escherichia coli is dependent on FtsZ and independent of FtsA. *J. Bacteriol.* **181**, 167–76 (1999).
77. Raychaudhuri, D. ZipA is a MAP-Tau homolog and is essential for structural integrity of the cytokinetic FtsZ ring during bacterial cell division. *EMBO J.* **18**, 2372–2383 (1999).
78. Skoog, K. & Daley, D. O. The Escherichia coli Cell Division Protein ZipA Forms Homodimers Prior to Association with FtsZ. *Biochemistry* **51**, 1407–1415 (2012).
79. Martos, A. *et al.* Characterization of Self-Association and Heteroassociation of Bacterial Cell Division Proteins FtsZ and ZipA in Solution by Composition Gradient–Static Light Scattering. *Biochemistry* **49**, 10780–10787 (2010).
80. Hale, C. A. & De Boer, P. A. J. ZipA is required for recruitment of FtsK, FtsQ, FtsL, and FtsN to the septal ring in Escherichia coli. *J. Bacteriol.* **184**, 2552–2556 (2002).
81. Jimenez, M., Martos, A., Vicente, M. & Rivas, G. Reconstitution and organization of Escherichia coli proto-ring elements (FtsZ and FtsA) inside giant unilamellar vesicles obtained from bacterial inner membranes. *J. Biol. Chem.* **286**, 11236–11241 (2011).
82. Dajkovic, A., Pichoff, S., Lutkenhaus, J. & Wirtz, D. Cross-linking FtsZ polymers into coherent Z rings. *Mol. Microbiol.* **78**, 651–668 (2010).
83. Buss, J. *et al.* In vivo organization of the FtsZ-ring by ZapA and ZapB revealed by quantitative super-resolution microscopy. *Mol. Microbiol.* **89**, 1099–1120 (2013).
84. Bailey, M. W., Bisicchia, P., Warren, B. T., Sherratt, D. J. & Männik, J. Evidence for divisome localization mechanisms independent of the Min system and SlmA in Escherichia coli. *PLoS Genet.* **10**, e1004504 (2014).
85. Buss, J. *et al.* A Multi-layered Protein Network Stabilizes the Escherichia coli FtsZ-ring and Modulates Constriction Dynamics. *PLOS Genet.* **11**, e1005128 (2015).
86. Buss, J. A., Peters, N. T., Xiao, J. & Bernhardt, T. G. ZapA and ZapB form an FtsZ-independent structure at midcell HHS Public Access. *Mol Microbiol* **104**, 652–663 (2017).
87. Small, E. *et al.* FtsZ Polymer-bundling by the Escherichia coli ZapA orthologue, YgfE, involves a conformational change in bound GTP. *J. Mol. Biol.* **369**, 210–221 (2007).

88. Pacheco-Gómez, R. *et al.* Tetramerization of ZapA is required for FtsZ bundling. *Biochem. J.* **449**, 795–802 (2013).
89. Galli, E. & Gerdes, K. FtsZ-ZapA-ZapB interactome of *Escherichia coli*. *J. Bacteriol.* **194**, 292–302 (2012).
90. Aarsman, M. E. G. *et al.* Maturation of the *Escherichia coli* divisome occurs in two steps. *Mol. Microbiol.* **55**, 1631–1645 (2005).
91. Yu, X.-C., Weihe, E. K. & Margolin, W. Role of the C Terminus of FtsK in *Escherichia coli* Chromosome Segregation. *J. Bacteriol.* **180**, 6424–6428 (1998).
92. Liu, G., Draper, G. C. & Donachie, W. D. FtsK is a bifunctional protein involved in cell division and chromosome localization in *Escherichia coli*. *Mol. Microbiol.* **29**, 893–903 (1998).
93. Begg, K. J., Dewar, S. J. & Donachie, W. D. A New *Escherichia coli* Cell Division Gene, *ftsK*. *J. Bacteriol.* **177**, 6211–6222 (1995).
94. Wang, L. & Lutkenhaus, J. FtsK is an essential cell division protein that is localized to the septum and induced as part of the SOS response. *Mol. Microbiol.* **29**, 731–740 (1998).
95. Buddelmeijer, N. & Beckwith, J. A complex of the *Escherichia coli* cell division proteins FtsL, FtsB and FtsQ forms independently of its localization to the septal region. *Mol. Microbiol.* **52**, 1315–1327 (2004).
96. Liu, B., Persons, L., Lee, L. & Boer, P. A. J. de. Roles for both FtsA and the FtsBLQ subcomplex in FtsN- stimulated cell constriction in *Escherichia coli*. **6**, 356–372 (2015).
97. Lara, B. & Ayala, J. A. Topological characterization of the essential *Escherichia coli* cell division protein FtsW. *FEMS Microbiol. Lett.* **216**, 23–32 (2002).
98. Mercer, K. L. N. & Weiss, D. S. The *Escherichia coli* cell division protein FtsW is required to recruit its cognate transpeptidase, FtsI (PBP3), to the division site. *J. Bacteriol.* **184**, 904–912 (2002).
99. Dai, K., Xu, Y. & Lutkenhaus, J. Topological Characterization of the Essential *Escherichia coli* Cell Division Protein FtsN. *J. Bacteriol.* **178**, 1328–1334 (1996).
100. Busiek, K. K., Eraso, J. M., Wang, Y. & Margolin, W. The Early Divisome Protein FtsA Interacts Directly through Its 1c: Subdomain with the Cytoplasmic Domain of the Late Divisome: Protein FtsN. *J. Bacteriol.* **194**, 1989–2000 (2012).
101. Tsang, M.-J. & Bernhardt, T. G. Guiding divisome assembly and controlling its activity. *Curr. Opin. Microbiol.* **24**, 60–65 (2015).
102. Du, S. & Lutkenhaus, J. Assembly and Activation of the *Escherichia coli* Divisome. *Mol. Microbiol.* **105**, 177–187 (2017).
103. Tsang, M.-J. & Bernhardt, T. G. A role for the FtsQLB complex in cytokinetic ring activation revealed by an *ftsL* allele that accelerates division. *Mol. Microbiol.* **95**, 1–54 (2014).
104. Bisson-Filho, A. W. *et al.* Treadmilling by FtsZ filaments drives peptidoglycan synthesis and bacterial cell division. *Science* **355**, 739–743 (2017).

105. Loose, M. & Mitchison, T. J. The bacterial cell division proteins FtsA and FtsZ self-organize into dynamic cytoskeletal patterns. *Nat. Cell Biol.* **16**, 38–46 (2013).
106. Ramirez-Diaz, D. A. *et al.* Treadmilling analysis reveals new insights into dynamic FtsZ ring architecture. *PLOS Biol.* **16**, e2004845 (2018).
107. Cabre, E. J. *et al.* Bacterial division proteins FtsZ and ZipA induce vesicle shrinkage and cell membrane invagination. *J. Biol. Chem.* **288**, 26625–26634 (2013).
108. Furusato, T. *et al.* De Novo Synthesis of Basal Bacterial Cell Division Proteins FtsZ, FtsA, and ZipA Inside Giant Vesicles. *ACS Synth. Biol.* **7**, 953–961 (2018).
109. Osawa, M. & Erickson, H. P. Liposome division by a simple bacterial division machinery. *Proc. Natl. Acad. Sci. U. S. A.* **110**, 11000–4 (2013).
110. Raskin, D. M. & De Boer, P. A. J. Rapid pole-to-pole oscillation of a protein required for directing division to the middle of *Escherichia coli*. *Cell Biol.* **96**, 4971–4976 (1999).
111. Hu, Z. & Lutkenhaus, J. Topological regulation of cell division in *Escherichia coli* involves rapid pole to pole oscillation of the division inhibitor MinC under the control of MinD and MinE. *Mol. Microbiol.* **34**, 82–90 (1999).
112. Lackner, L. L., Raskin, D. M. & de Boer, P. A. J. ATP-dependent interactions between *Escherichia coli* Min proteins and the phospholipid membrane in vitro. *J. Bacteriol.* **185**, 735–49 (2003).
113. Martos, A., Petrasek, Z. & Schwille, P. Propagation of MinCDE waves on free-standing membranes. *Environ. Microbiol.* **15**, 3319–3326 (2013).
114. Meacci, G. *et al.* Mobility of Min-proteins in *Escherichia coli* measured by fluorescence correlation spectroscopy. *Phys. Biol. Biol. Phys. Biol.* **3**, 255–263 (2006).
115. Hu, Z., Mukherjee, A., Pichoff, S. & Lutkenhaus, J. The MinC component of the division site selection system in *Escherichia coli* interacts with FtsZ to prevent polymerization. *Proc. Natl. Acad. Sci.* **96**, 14819–14824 (1999).
116. Arumugam, S., Petrašek, Z. & Schwille, P. MinCDE exploits the dynamic nature of FtsZ filaments for its spatial regulation. *Proc. Natl. Acad. Sci. U. S. A.* **111**, 1192–1200 (2014).
117. Yang, S. *et al.* Characterization of C-terminal structure of MinC and its implication in evolution of bacterial cell division. *Sci. Rep.* **7**, 7627 (2017).
118. Shen, B. & Lutkenhaus, J. Examination of the interaction between FtsZ and MinC^N in *E. coli* suggests how MinC disrupts Z rings. *Mol. Microbiol.* **75**, 1285–1298 (2010).
119. Shen, B. & Lutkenhaus, J. The conserved C-terminal tail of FtsZ is required for the septal localization and division inhibitory activity of MinC(C)/MinD. *Mol. Microbiol.* **72**, 410–24 (2009).
120. Hu, Z. & Lutkenhaus, J. Analysis of MinC Reveals Two Independent Domains Involved in Interaction with MinD and FtsZ. *J. Bacteriol.* **182**, 3965–3971 (2000).
121. Shiomi, D. & Margolin, W. The C-terminal domain of MinC inhibits assembly of the Z ring in *Escherichia coli*. *J. Bacteriol.* **189**, 236–43 (2007).
122. Taviti, A. C. & Beuria, T. K. MinD directly interacting with FtsZ at the H10 helix

- suggests a model for robust activation of MinC to destabilize FtsZ polymers. *Biochem. J.* **474**, 3189–3205 (2017).
123. De Boer, P. A. J., Crossley, R. E., Hand1, A. R. & Rothfield, L. I. The MinD protein is a membrane ATPase required for the correct placement of the Escherichia coli division site. *EMBO J.* **10**, 4371–4380 (1991).
 124. Wu, W., Park, K.-T., Holyoak, T. & Lutkenhaus, J. Determination of the structure of the MinD-ATP complex reveals the orientation of MinD on the membrane and the relative location of the binding sites for MinE and MinC. *Mol. Microbiol.* **79**, 1515–28 (2011).
 125. Mileykovskaya, E. *et al.* Effects of phospholipid composition on MinD-membrane interactions in vitro and in vivo. *J. Biol. Chem.* **278**, 22193–8 (2003).
 126. Zhang, Y., Rowland, S., King, G., Braswell, E. & Rothfield, L. The relationship between hetero-oligomer formation and function of the topological specificity domain of the Escherichia coli MinE protein. *Mol. Microbiol.* **30**, 265–273 (1998).
 127. Kang, G. B. *et al.* Crystal structure of Helicobacter pylori MinE, a cell division topological specificity factor. *Mol. Microbiol.* **76**, 1222–1231 (2010).
 128. Park, K.-T. *et al.* The Min Oscillator Uses MinD-Dependent Conformational Changes in MinE to Spatially Regulate Cytokinesis. *Cell* **146**, 396–407 (2011).
 129. Park, K.-T., Wu, W., Lovell, S. & Lutkenhaus, J. Mechanism of the asymmetric activation of the MinD ATPase by MinE. doi:10.1111/j.1365-2958.2012.08110.x.
 130. Loose, M., Fischer-Friedrich, E., Herold, C., Kruse, K. & Schwille, P. Min protein patterns emerge from rapid rebinding and membrane interaction of MinE. *Nat. Struct. Mol. Biol.* **18**, 577–583 (2011).
 131. Kleckner, N. Mesoscale spatial patterning in the Escherichia coli Min system: Reaction-diffusion versus mechanical communication. *PNAS* **107**, 8053–8054 (2010).
 132. Ivanov, V. & Mizuuchi, K. Multiple modes of interconverting dynamic pattern formation by bacterial cell division proteins. *Proc. Natl. Acad. Sci. U. S. A.* **107**, 8071–8 (2010).
 133. Loose, M., Fischer-Friedrich, E., Ries, J., Kruse, K. & Schwille, P. Spatial regulators for bacterial cell division self-organize into surface waves in vitro. *Science* **320**, 789–92 (2008).
 134. Vecchiarelli, A. G., Li, M., Mizuuchi, M. & Mizuuchi, K. Differential affinities of MinD and MinE to anionic phospholipid influence Min patterning dynamics in vitro. *Mol. Microbiol.* **93**, 453–63 (2014).
 135. Kretschmer, S., Zieske, K. & Schwille, P. Large-scale modulation of reconstituted Min protein patterns and gradients by defined mutations in MinE's membrane targeting sequence. *PLoS One* **12**, (2017).
 136. Zieske, K. & Schwille, P. Reconstitution of self-organizing protein gradients as spatial cues in cell-free systems. (2014).
 137. Zieske, K., Chwastek, G. & Schwille, P. Model Membranes Protein Patterns and Oscillations on Lipid Monolayers and in Microdroplets. *Angew. Chem. Int. Ed. Engl.* **55**,

- 13455–13459 (2016).
138. Litschel, T., Ramm, B., Maas, R., Heymann, M. & Schwille, P. Beating vesicles: Encapsulated protein oscillations cause dynamic membrane deformations. *Angew. Chemie Int. Ed.* **57**, 16286–16290 (2018).
 139. Shimizu, Y. *et al.* Cell-free translation reconstituted with purified components. *Nat. Biotechnol.* **19**, 751–755 (2001).
 140. Shimizu, Y., Kanamori, T. & Ueda, T. Protein synthesis by pure translation systems. *Methods* **36**, 299–304 (2005).
 141. Rolf, J. *et al.* Application of Cell-Free Protein Synthesis for Faster Biocatalyst Development. *Catalysts* **9**, 190 (2019).
 142. Nourian, Z., Scott, A. & Danelon, C. Toward the assembly of a minimal divisome. *Syst. Synth. Biol.* **8**, 237–47 (2014).
 143. Blanken, D., van Nies, P. & Danelon, C. Quantitative imaging of gene-expressing liposomes reveals rare favorable phenotypes. *Phys. Biol.* **16**, (2019).
 144. Castellana, E. T. & Cremer, P. S. Solid supported lipid bilayers: From biophysical studies to sensor design. *Surf. Sci. Rep.* **61**, 429–444 (2006).
 145. Richter, R. P., Bérat, R. & Brisson, A. R. Formation of solid-supported lipid bilayers: an integrated view. *Langmuir* **22**, 3497–505 (2006).
 146. Elender, G., Kühner, M. & Sackmann, E. Functionalisation of Si/SiO₂ and glass surfaces with ultrathin dextran films and deposition of lipid bilayers. *Biosens. Bioelectron.* **11**, 565–577 (1996).
 147. Hillebrandt, H., Wiegand, G., Tanaka, M. & Sackmann, E. High Electric Resistance Polymer/Lipid Composite Films on Indium-Tin-Oxide Electrodes. *Langmuir* **15**, 8451–8459 (1999).
 148. Nuzzo, R. G. & Allara, D. L. Adsorption of Bifunctional Organic Disulfides on Gold Surfaces. *J. Am. Chem. Soc.* **105**, 4481–4483 (1983).
 149. Tamm, L. K. & McConnell, H. M. Supported phospholipid bilayers. *Biophys. J.* **47**, 105–13 (1985).
 150. Brian, A. A. & McConnell, H. M. Allogeneic stimulation of cytotoxic T cells by supported planar membranes (class I major histocompatibility antigen/membrane reconstitution/antigen processing/LFA-1 cell surface protein/lateral diffusion). *Immunology* **81**, 6159–6163 (1984).
 151. Richter, R., Mukhopadhyay, A. & Brisson, A. Pathways of Lipid Vesicle Deposition on Solid Surfaces: A Combined QCM-D and AFM Study. *Biophys. J.* **85**, 3035–3047 (2003).
 152. Albertorio, F. *et al.* Fluid and Air-Stable Lipopolymer Membranes for Biosensor Applications. *Langmuir* **21**, 7476–7482 (2005).
 153. Zhang, L., Spurlin, T. A., Gewirth, A. A. & Granick, S. Electrostatic stitching in gel-phase supported phospholipid bilayers. *J. Phys. Chem. Lett.* **110**, 33–35 (2006).
 154. Nourian, Z., Roelofsen, W. & Danelon, C. Triggered gene expression in fed-vesicle microreactors with a multifunctional membrane. *Angew. Chemie - Int. Ed.* **51**, 3114–

3118 (2012).

155. Zylberberg, C. & Matosevic, S. Pharmaceutical liposomal drug delivery: a review of new delivery systems and a look at the regulatory landscape. *Drug Deliv.* **23**, 3319–3329 (2016).
156. Yu, W. *et al.* Synthesis of Functional Protein in Liposome. *Journal of Bioscience and Bioengineering* vol. 92 (2001).
157. Bangham, A. D., Standish, M. M. & Watkins, J. C. Diffusion of univalent ions across the lamellae of swollen phospholipids. *J. Mol. Biol.* **13**, 238–252 (1965).
158. Nomura, S. M. *et al.* Gene Expression within Cell-Sized Lipid Vesicles. *ChemBioChem* **4**, 1172–1175 (2003).
159. Pereira de Souza, T., Stano, P. & Luisi, P. L. The Minimal Size of Liposome-Based Model Cells Brings about a Remarkably Enhanced Entrapment and Protein Synthesis. *ChemBioChem* **10**, 1056–1063 (2009).
160. Tsuji, G., Sunami, T. & Ichihashi, N. Production of giant unilamellar vesicles by the water-in-oil emulsion-transfer method without high internal concentrations of sugars. *J. Biosci. Bioeng.* **126**, 540–545 (2018).
161. Saito, H. *et al.* Time-resolved tracking of a minimum gene expression system reconstituted in giant liposomes. *Chembiochem* **10**, 1640–1643 (2009).
162. Karzbrun, E., Tayar, A. M., Noireaux, V. & Bar-Ziv, R. H. Synthetic biology. Programmable on-chip DNA compartments as artificial cells. *Science* (80.). **345**, 829–832 (2014).
163. Mattheyses, A. L., Simon, S. M. & Rappoport, J. Z. Imaging with total internal reflection fluorescence microscopy for the cell biologist. *J. Cell Sci.* **123**, 3621 (2010).
164. Söderström, B. *et al.* Disassembly of the divisome in *Escherichia coli*: evidence that FtsZ dissociates before compartmentalization. *Mol. Microbiol.* **92**, 1–9 (2014).
165. Carettoni, D. *et al.* Phage-display and correlated mutations identify an essential region of subdomain 1C involved in homodimerization of *Escherichia coli* FtsA. *Proteins Struct. Funct. Bioinforma.* **50**, 192–206 (2003).
166. Shiomi, D. & Margolin, W. Dimerization or oligomerization of the actin-like FtsA protein enhances the integrity of the cytokinetic Z ring. *Mol. Microbiol.* **66**, 1396–1415 (2007).
167. Szwedziak, P., Wang, Q., Freund, S. M. V & Löwe, J. FtsA forms actin-like protofilaments. *EMBO J.* **31**, 2249–60 (2012).
168. Pichoff, S., Shen, B., Sullivan, B. & Lutkenhaus, J. FtsA mutants impaired for self-interaction bypass ZipA suggesting a model in which FtsA's self-interaction competes with its ability to recruit downstream division proteins. *Mol. Microbiol.* **83**, 151–67 (2012).
169. Hale, C. A., Rhee, A. C. & de Boer, P. A. ZipA-induced bundling of FtsZ polymers mediated by an interaction between C-terminal domains. *J. Bacteriol.* **182**, 5153–66 (2000).
170. Zorrilla, S., Minton, A. P., Vicente, M. & Andreu, M. Magnesium-induced Linear Self-association of the FtsZ Bacterial Cell Division Protein Monomer. **275**, 11740–11749

- (2000).
171. Rueden, C. T. *et al.* ImageJ2: ImageJ for the next generation of scientific image data. *BMC Bioinformatics* **18**, 529 (2017).
 172. Martos, A. *et al.* FtsZ polymers tethered to the membrane by ZipA are susceptible to spatial regulation by min waves. *Biophys. J.* **108**, 2371–2383 (2015).
 173. Haney, S. A. *et al.* Genetic analysis of the Escherichia coli FtsZ-ZipA interaction in the yeast two-hybrid system. *J. Biol. Chem.* **276**, 11980–11987 (2001).
 174. Matsui, T., Han, X., Yu, J., Yao, M. & Tanaka, I. Structural change in FtsZ induced by intermolecular interactions between bound GTP and the T7 loop. *J. Biol. Chem.* **289**, 3501–3509 (2013).
 175. Huang, K., Mychack, A. & Tchorzewski, L. Characterization of the FtsZ C-terminal variable (CTV) region in Z-ring assembly and interaction with the Z-ring stabilizer ZapD in *E. coli* cytokinesis. *PLoS One* **11**, e0153337 (2016) doi:10.1371/journal.pone.0153337.
 176. Buske, P. J. & Levin, P. A. Extreme C terminus of bacterial cytoskeletal protein FtsZ plays fundamental role in assembly independent of modulatory proteins. *J. Biol. Chem.* **287**, 10945–10957 (2012).
 177. Caldas, P. *et al.* ZapA stabilizes FtsZ filament bundles without slowing down treadmilling dynamics. *bioRxiv* 580944 (2019) doi:10.1101/580944.
 178. Pichoff, S. & Lutkenhaus, J. Identification of a region of FtsA required for interaction with FtsZ. *Mol. Microbiol.* **64**, 1129–1138 (2007).
 179. Krupka, M., Sobrinos-Sanguino, M., Jiménez, M., Rivas, G. & Margolin, W. Escherichia coli ZipA Organizes FtsZ Polymers into Dynamic Ring-Like Protofilament Structures. *MBio* **9**, 1–15 (2018).
 180. Concha-Marambio, L., Maldonado, P., Lagos, R., Monasterio, O. & Montecinos-Franjola, F. Thermal adaptation of mesophilic and thermophilic FtsZ assembly by modulation of the critical concentration. *PLoS One* **12**, 1–20 (2017).
 181. Kuznetsova, I. M., Turoverov, K. K. & Uversky, V. N. What macromolecular crowding can do to a protein. *Int. J. Mol. Sci.* **15**, 23090–23140 (2014).
 182. Low, H. H., Moncrieffe, M. C. & Löwe, J. The Crystal Structure of ZapA and its Modulation of FtsZ Polymerisation. *J. Mol. Biol.* **341**, 839–852 (2004).
 183. Roach, E. J., Kimber, M. S. & Khursigara, C. M. Crystal structure and site-directed mutational analysis reveals key residues involved in Escherichia coli ZapA function. *J. Biol. Chem.* **289**, 23276–86 (2014).
 184. Thalmeier, D., Halatek, J. & Frey, E. Geometry-induced protein pattern formation. *Proc. Natl. Acad. Sci. U. S. A.* **113**, 548–53 (2016).
 185. Turing, A. M. *The Chemical Basis of Morphogenesis. Philosophical Transactions of the Royal Society of London. Series B, Biological Sciences* vol. 237 <http://www.jstor.org/about/terms.html>. (1952).
 186. Gierer, A. & Meinhardt, H. A theory of biological pattern formation. *Kybernetik* **12**, 30–39 (1972).

187. Osawa, M. & Erickson, H. P. Liposome division by a simple bacterial division machinery. *Proc. Natl. Acad. Sci. U. S. A.* **110**, 11000–11004 (2013).
188. Szwedziak, P., Wang, Q., Bharat, T. A. M., Tsim, M. & Löwe, J. Architecture of the ring formed by the tubulin homologue FtsZ in bacterial cell division. *Elife* 1–22 (2014) doi:10.7554/eLife.04601.
189. van Nies, P. *et al.* Unbiased tracking of the progression of mRNA and protein synthesis in bulk and in liposome-confined reactions. *ChemBioChem* **14**, 1963–1966 (2013).
190. Viola, P. ; & Jones, M. *Rapid Object Detection Using a Boosted Cascade of Simple Features.* <http://www.merl.com> (2004).
191. Ahijado-Guzmán, R. *et al.* Control by potassium of the size distribution of Escherichia coli FtsZ polymers is independent of GTPase activity. *J. Biol. Chem.* **288**, 27358–65 (2013).
192. Chen, Y. & Erickson, H. P. FtsZ filament dynamics at steady state: subunit exchange with and without nucleotide hydrolysis. *Biochemistry* **48**, 6664–73 (2009).
193. Liechti, G. *et al.* Pathogenic Chlamydia Lack a Classical Sacculus but Synthesize a Narrow, Mid-cell Peptidoglycan Ring, Regulated by MreB, for Cell Division. *PLOS Pathog.* **12**, e1005590 (2016).
194. Daley, D. O., Skoglund, U. & Söderström, B. FtsZ does not initiate membrane constriction at the onset of division. *Sci. Rep.* **6**, 33138 (2016).
195. Coltharp, C. & Xiao, J. Beyond force generation: Why is a dynamic ring of FtsZ polymers essential for bacterial cytokinesis? *BioEssays* **39**, 1–11 (2017).
196. Osawa, M., Anderson, D. E. & Erickson, H. P. Curved FtsZ protofilaments generate bending forces on liposome membranes. *EMBO J.* **28**, 3476–84 (2009).
197. Osawa, M., Anderson, D. E. & Erickson, H. P. Reconstitution of Contractile FtsZ Rings in Liposomes. *Science* **320**, 792–794 (2008).
198. Osawa, M. & Erickson, H. P. Inside-out Z rings - constriction with and without GTP hydrolysis. *Mol. Microbiol.* **81**, 571–579 (2011).
199. Kato, N. *et al.* Effects of lipid composition and solution conditions on the mechanical properties of membrane vesicles. *Membranes (Basel)*. **5**, 22–47 (2015).
200. Erickson, H. P. & Osawa, M. Cell division without FtsZ - a variety of redundant mechanisms. **78**, 267–270 (2011).
201. Jiménez, M., Martos, A., Vicente, M. & Rivas, G. Reconstitution and organization of Escherichia coli proto-ring elements (FtsZ and FtsA) inside giant unilamellar vesicles obtained from bacterial inner membranes. *J. Biol. Chem.* **286**, 11236–41 (2011).
202. Mellouli, S. *et al.* Self-organization of the bacterial cell-division protein FtsZ in confined environments. *Soft Matter* **9**, 10493 (2013).
203. Schramke, H. *et al.* Revisiting regulation of potassium homeostasis in Escherichia coli: the connection to phosphate limitation. *Microbiologyopen* **6**, 1–16 (2017).
204. Cayley, S., Lewis, B. A., Guttman, H. J. & Record, M. T. Characterization of the cytoplasm of Escherichia coli K-12 as a function of external osmolarity: Implications for protein-DNA interactions in vivo. *J. Mol. Biol.* **222**, 281–300 (1991).

205. Blaauwen, T. Den, Hamoen, L. W. & Levin, P. A. The divisome at 25 : the road ahead. *Curr. Opin. Microbiol.* **36**, 85–94 (2017).
206. Dai, K. & Lutkenhaus, J. FtsZ is an essential cell division gene in Escherichia coli. *J. Bacteriol.* **173**, 3500–3506 (1991).
207. Ortiz, C., Natale, P., Cueto, L. & Vicente, M. The keepers of the ring : regulators of FtsZ assembly. *FEMS Microbiol. Rev.* 1–11 (2015) doi:10.1093/femsre/fuv040.
208. Szeto, T. H., Rowland, S. L., Habrukowich, C. L. & King, G. F. The MinD membrane targeting sequence is a transplantable lipid-binding helix. *J. Biol. Chem.* **278**, 40050–6 (2003).
209. Redfearn, J. C. *A Comprehensive Model of the Structure and Function of the FtsZ Ring of Escherichia Coli.* https://etd.ohiolink.edu/!etd.send_file?accession=kent1460475643&disposition=inline (2016).
210. Schneider, C. A., Rasband, W. S. & Eliceiri, K. W. NIH Image to ImageJ: 25 years of image analysis. *Nat. Methods* **9**, 671–675 (2012).
211. Mohammadi, T. *et al.* The GTPase activity of Escherichia coli FtsZ determines the magnitude of the FtsZ polymer bundling by ZapA in vitro. *Biochemistry* **48**, 11056–11066 (2009).
212. Arumugam, S. Reconstitution of bacterial cytokinesis: the Z-ring. (2012).
213. Mingorance, J. *et al.* Visualization of single Escherichia coli FtsZ filament dynamics with atomic force microscopy. *J. Biol. Chem.* **280**, 20909–14 (2005).
214. Osawa, M., Anderson, D. E. & Erickson, H. P. Curved FtsZ protofilaments generate bending forces on liposome membranes. *EMBO J.* **28**, 3476–84 (2009).
215. Krasowska, J., Olasek, M., Bzowska, A., Clark, P. L. & Wielgus-Kutrowska, B. The comparison of aggregation and folding of enhanced green fluorescent protein (EGFP) by spectroscopic studies. *J. Spectrosc.* **24**, 343–348.
216. Nagai, T. *et al.* A variant of yellow fluorescent protein with fast and efficient maturation for cell-biological applications. *Nat. Biotechnol.* **20**, 87–90 (2002).
217. FPbase :: The Fluorescent Protein Database. <https://www.fpbases.org/>.
218. Deshpande, S., Caspi, Y., Meijering, A. & Dekker, C. Octanol-assisted liposome assembly on chip. *Nat. Commun.* **accepted**, 1–9 (2015).
219. Bernhardt, T. G. & De Boer, P. A. J. SlnA, a nucleoid-associated, FtsZ binding protein required for blocking septal ring assembly over chromosomes in E. coli. *Mol. Cell* **18**, 555–564 (2005).
220. Jia, S. *et al.* Effect of the Min system on timing of cell division in Escherichia coli. *PLoS One* **9**, e103863 (2014).
221. Männik, J. *et al.* Absence of the Min system does not cause major cell division defects in Agrobacterium tumefaciens. *Front. Microbiol.* **1**, 1–14 (2018).
222. Gerdes, S. Y. *et al.* Experimental determination and system level analysis of essential genes in Escherichia coli MG1655. *J. Bacteriol.* **185**, 5673–5684 (2003).

223. Joyce, A. R. *et al.* Experimental and computational assessment of conditionally essential genes in *Escherichia coli*. *J. Bacteriol.* **188**, 8259–8271 (2006).
224. Baba, T. *et al.* Construction of *Escherichia coli* K-12 in-frame, single-gene knockout mutants: the Keio collection. *Mol. Syst. Biol.* (2006) doi:10.1038/msb4100050.
225. de Boer, P. A., Crossley, R. E. & Rothfield, L. I. A division inhibitor and a topological specificity factor coded for by the minicell locus determine proper placement of the division septum in *E. coli*. *Cell* **56**, 641–9 (1989).
226. Hu, Z., Saez, C. & Lutkenhaus, J. Recruitment of MinC, an inhibitor of Z-ring formation, to the membrane in *Escherichia coli*: role of MinD and MinE. *J. Bacteriol.* **185**, 196–203 (2003).
227. Raskin, D. M. & de Boer, P. A. MinDE-dependent pole-to-pole oscillation of division inhibitor MinC in *Escherichia coli*. *J. Bacteriol.* **181**, 6419–24 (1999).
228. Halatek, J., Brauns, F. & Frey, E. Self-organization principles of intracellular pattern formation. *Philos. Trans. R. Soc. B Biol. Sci.* **373**, 20170107 (2018).
229. Raskin, D. M. & de Boer, P. A. Rapid pole-to-pole oscillation of a protein required for directing division to the middle of *Escherichia coli*. *Proc. Natl. Acad. Sci. U. S. A.* **96**, 4971–6 (1999).
230. A Hale, C., Meinhardt, H. & Boer, P. A. J. de. Dynamic localization cycle of the cell division regulator MinE in *Escherichia coli*. *EMBO J.* **20**, 1563–1572 (2001).
231. Kruse, K. A Dynamic Model for Determining the Middle of *Escherichia coli*. *Biophys. J.* **82**, 618–627 (2002).
232. Adler, H. I., Fisher, W. D., Cohen, A. & Hardigree, A. A. Miniature (i)*Escherichia coli*(i) cells deficient in DNA. *Proc. Natl. Acad. Sci. U. S. A.* **57**, 321–6 (1967).
233. de Boer, P. A., Crossley, R. E. & Rothfield, L. I. Roles of MinC and MinD in the site-specific septation block mediated by the MinCDE system of *Escherichia coli*. *J. Bacteriol.* **174**, 63–70 (1992).
234. Akerlund, T., Bernander, R. & Nordström, K. Cell division in *Escherichia coli* minB mutants. *Mol. Microbiol.* **6**, 2073–2083 (1992).
235. Pichoff, S., Vollrath, B., Touriol, C. & Bouché, J.-P. Deletion analysis of gene minE which encodes the topological specificity factor of cell division in *Escherichia coli*. *Mol. Microbiol.* **18**, 321–329 (1995).
236. Zhao, C.-R., De Boer, P. A. J. & Rothfield, L. I. Proper placement of the *Escherichia coli* division site requires two functions that are associated with different domains of the MinE protein. *Proc. Natl. Acad. Sci. U. S. A.* **92**, 4313–4317 (1995).
237. Raskin, D. M. & de Boer, P. A. The MinE ring: an FtsZ-independent cell structure required for selection of the correct division site in *E. coli*. *Cell* **91**, 685–94 (1997).
238. Park, K.-T., Du, S. & Lutkenhaus, J. MinC/MinD copolymers are not required for Min function. *Mol. Microbiol.* **98**, 895–909 (2015).
239. De Boer, P. A. J., Crossley, R. E. & Rothfield, L. I. Roles of MinC and MinD in the Site-Specific Septation Block Mediated by the MinCDE System of *Escherichia coli*. *J. Bacteriol.* **174**, 63–70 (1992).

240. Fu, X., Shih, Y.-L., Zhang, Y. & Rothfield, L. I. The MinE ring required for proper placement of the division site is a mobile structure that changes its cellular location during the *Escherichia coli* division cycle. *Proc. Natl. Acad. Sci.* **98**, 980–985 (2000).
241. Hsieh, C.-W. *et al.* Direct MinE-membrane interaction contributes to the proper localization of MinDE in *E. coli*. *Mol. Microbiol.* **75**, 499–512 (2010).
242. Johnson, J. E., Lackner, L. L. & de Boer, P. A. J. Targeting of (D)MinC/MinD and (D)MinC/DicB complexes to septal rings in *Escherichia coli* suggests a multistep mechanism for MinC-mediated destruction of nascent FtsZ rings. *J. Bacteriol.* **184**, 2951–62 (2002).
243. Hu, Z. & Lutkenhaus, J. A conserved sequence at the C-terminus of MinD is required for binding to the membrane and targeting MinC to the septum. *Mol. Microbiol.* **47**, 345–355 (2003).
244. Juarez, J. R. & Margolin, W. Changes in the Min oscillation pattern before and after cell birth. *J. Bacteriol.* **192**, 4134–42 (2010).
245. Männik, J. *et al.* Robustness and accuracy of cell division in *Escherichia coli* in diverse cell shapes. *Proc. Natl. Acad. Sci. U. S. A.* **109**, 6957–62 (2012).
246. Bisicchia, P., Arumugam, S., Schwille, P. & Sherratt, D. MinC, MinD, and MinE drive counter-oscillation of early-cell-division proteins prior to *Escherichia coli* septum formation. *MBio* **4**, e00856-13 (2013).
247. Szeto, T. H., Rowland, S. L. & King, G. F. The dimerization function of MinC resides in a structurally autonomous C-terminal domain. *J. Bacteriol.* **183**, 6684–7 (2001).
248. Shih, Y.-L., Fu, X., King, G. F., Le, T. & Rothfield, L. Division site placement in *E. coli*: mutations that prevent formation of the MinE ring lead to loss of the normal midcell arrest of growth of polar MinD membrane domains. *EMBO J.* **21**, 3347–57 (2002).
249. Hu, Z., Gogol, E. P. & Lutkenhaus, J. Dynamic assembly of MinD on phospholipid vesicles regulated by ATP and MinE. *Proc. Natl. Acad. Sci. U. S. A.* **99**, 6761–6 (2002).
250. Suefuji, K., Valluzzi, R. & RayChaudhuri, D. Dynamic assembly of MinD into filament bundles modulated by ATP, phospholipids, and MinE. *Proc. Natl. Acad. Sci. U. S. A.* **99**, 16776–81 (2002).
251. Zhou, H. & Lutkenhaus, J. Membrane binding by MinD involves insertion of hydrophobic residues within the C-terminal amphipathic helix into the bilayer. *J. Bacteriol.* **185**, 4326–35 (2003).
252. Zhou, H. & Lutkenhaus, J. The switch I and II regions of MinD are required for binding and activating MinC. *J. Bacteriol.* **186**, 1546–55 (2004).
253. Park, K.-T., Wu, W., Lovell, S. & Lutkenhaus, J. Mechanism of the asymmetric activation of the MinD ATPase by MinE. *Mol. Microbiol.* **85**, 271–81 (2012).
254. An, J. Y. *et al.* Crystal structure of the N-terminal domain of MinC dimerized via domain swapping. *J. Synchrotron Radiat.* **20**, 984–8 (2013).
255. Conti, J., Viola, M. G. & Camberg, J. L. The bacterial cell division regulators MinD and MinC form polymers in the presence of nucleotide. *FEBS Lett.* **589**, 201–206 (2015).
256. Loose, M., Fischer-Friedrich, E., Herold, C., Kruse, K. & Schwille, P. Min protein

- patterns emerge from rapid rebinding and membrane interaction of MinE. *Nat. Struct. Mol. Biol.* **18**, 577–83 (2011).
257. Schweizer, J. *et al.* Geometry sensing by self-organized protein patterns. *Proc. Natl. Acad. Sci. U. S. A.* **109**, 15283–8 (2012).
258. Zieske, K. & Schwille, P. Reconstitution of pole-to-pole oscillations of min proteins in microengineered polydimethylsiloxane compartments. *Angew. Chem. Int. Ed. Engl.* **52**, 459–62 (2013).
259. Caspi, Y. & Dekker, C. Mapping out Min protein patterns in fully confined fluidic chambers. *Elife* **5**, (2016).
260. Schindelin, J. *et al.* Fiji: an open-source platform for biological-image analysis. *Nat. Methods* **9**, 676–682 (2012).
261. van Nies, P. Y. B. Virus-inspired dna replication coupled with gene expression in a minimal cell framework. (2017) doi:10.4233/UUID:F572409D-366D-4042-BA02-3BED8209B4A0.
262. Ziemienowicz, A. *et al.* Both the Escherichia coli chaperone systems, GroEL/GroES and DnaK/DnaJ/GrpE, can reactivate heat-treated RNA polymerase. *J. Biol. Chem.* **268**, 25425–25431 (1993).
263. Teter, S. A. *et al.* Polypeptide flux through bacterial Hsp70: DnaK cooperates with trigger factor in chaperoning nascent chains. *Cell* **97**, 755–765 (1999).
264. Deuerling, E., Schulze-Specking, A., Tomoyasu, T., Mogk, A. & Bukau, B. Trigger factor and DnaK cooperate in folding of newly synthesized proteins. *Nature* (1999) doi:10.1038/23301.
265. Schroder, H., Langer, T., Hartl, F.-U. & Bukau, B. DnaK, DnaJ and GrpE form a cellular chaperone machinery capable of repairing heat-induced protein damage. *EMBO J.* **12**, 4137–4144 (1993).
266. Bradford, M. M. A rapid and sensitive method for the quantitation of microgram quantities of protein utilizing the principle of protein-dye binding. *Anal. Biochem.* **72**, 248–254 (1976).
267. Di Ventura, B. & Sourjik, V. Self-organized partitioning of dynamically localized proteins in bacterial cell division. *Mol. Syst. Biol.* **7**, 457 (2011).
268. Demachy, I. *et al.* Cyan fluorescent protein: Molecular dynamics, simulations, and electronic absorption spectrum. *J. Phys. Chem.* **109**, 24121–33 (2005).
269. Martos, A. *et al.* Isolation, characterization and lipid-binding properties of the recalcitrant FtsA division protein from Escherichia coli. *PLoS One* **7**, 1–6 (2012).
270. Niwa, T., Kanamori, T., Ueda, T. & Taguchi, H. Global analysis of chaperone effects using a reconstituted cell-free translation system. *Proc. Natl. Acad. Sci. U. S. A.* **109**, 8937–42 (2012).
271. Bi, E. & Lutkenhaus, J. Cell division inhibitors SulA and MinCD prevent formation of the FtsZ ring. *J. Bacteriol.* **175**, 1118–25 (1993).
272. Sakuma, Y. & Imai, M. Model system of self-reproducing vesicles. *Phys. Rev. Lett.* **107**, (2011).

273. Tanaka, S., Takiguchi, K. & Hayashi, M. Repetitive stretching of giant liposomes utilizing the nematic alignment of confined actin. *Commun. Phys.* **1**, 18 (2018).
274. Das, G. & Varshney, U. Peptidyl-tRNA hydrolase and its critical role in protein biosynthesis. *Microbiology* **152**, 2191–2195 (2006).
275. Caschera, F. & Noireaux, V. Synthesis of 2.3 mg/ml of protein with an all Escherichia coli cell-free transcription-translation system. *Biochimie* **99**, 162–8 (2014).
276. Kato, A. *et al.* Cell-Sized confinement in microspheres accelerates the reaction of gene expression. (2012) doi:10.1038/srep00283.

Summary

The creation of artificial cells with the minimal set of components to exhibit self-maintenance, self-reproducibility and evolvability (in other words, to be considered alive) is one of the most exciting areas within the field of synthetic biology. Such entities, here called minimal cells, are constructed by either the top-down or bottom-up approach. The top-down approach attempts to realize a minimal cell starting from an already existing unicellular organism and stripping down non-essential genes. In the bottom-up approach, separate biochemicals, such as phospholipids, DNA and proteins are assembled from scratch to reconstitute cell-like functions. On the way to tackle this curiosity-driven building challenge, we also expect to learn more about the most fundamental processes that define a living cell.

In the Christophe Danelon lab, we propose to build a minimal cell using a bottom-up synthetic biology approach. The scaffold consists of three core modules. First, a liposome is used as a compartment model that defines the minimal cell as a physical entity. Its phospholipid membrane controls the exchange of matter and energy. Second, the information about the composition of the cell (lipid, RNA, protein) is encoded in DNA in the form of genes. Third, the protein synthesis using recombinant elements system, or PURE system, is implemented as a metabolic machinery to synthesize proteins from DNA templates. We believe that such a minimal cell model has the potential to ultimately meet the requirements for being recognized as living.

One of the essential processes required for achieving self-reproduction is division. In this thesis, we asked two questions: can we engineer a division system for liposome-based minimal cells by mimicking the bacterial division machinery? Can this reconstituted division apparatus be spatiotemporally regulated with yet another engineered protein network inspired from bacteria? To answer these questions, our strategy involved the in-vesicle synthesis of a carefully selected, *Escherichia coli* division protein set. In *E. coli*, division starts with the polymerization of the cytosolic protein FtsZ into a ring-like structure positioned at midcell. This FtsZ ring is anchored to the inner membrane by the partner proteins FtsA and ZipA. On time, the FtsZ ring constricts until division is completed as a binary fission event. Proper localization of the division ring is ensured by a three-protein system, the Min system, that dynamically self-organizes and specifically enables formation of the FtsZ ring at midcell. We hypothesize that, in analogy to cellular division, synthesis of FtsZ, FtsA, ZipA and the Min system will stimulate formation of an active FtsZ ring that will eventually split our minimal cell in two. This gene set and associated protein functionality is what we call the minimal division machinery model.

In order to implement this minimal division machinery model, we began by exploring the potential of the cell-free synthesized *E. coli* division proteins FtsZ, FtsA and ZipA to recapitulate basic cytoskeletal properties. Protein activity was assayed on planar supported membranes. We found that Ficoll70, a general macromolecular crowder, was necessary to trigger formation of filament networks with the purified proteins FtsZ and ZipA under the tested conditions. More importantly, the cell-free synthesized FtsZ, FtsA and ZipA were able to self-organize into filaments of distinct morphologies, curved with FtsA and straight with ZipA. To bypass the need of Ficoll70, we demonstrated that cell-free expressed ZapA, a natural FtsZ crosslinker, was able to trigger bundling of FtsZ filaments when mixed with purified or cell-free synthesized FtsZ.

Next, we sought to reconstitute an FtsZ-based membrane deforming machinery inside liposomes. We first tested the dynamics of encapsulated purified FtsZ. While in standard conditions we were unable to detect in-vesicle FtsZ polymerization, we found that increasing

K^+ and Mg^{2+} concentrations mediated assembly of FtsZ into straight bundles. This new condition was also compatible with filament assembly of synthesized FtsZ. Next, we quantified the shape of FtsZ filament-containing liposomes, and revealed that internal FtsZ filaments are capable of deforming liposomes into elongated and lemon-shapes.

To reduce the load of the PURE system's metabolic machinery, we designed and studied the activity of two chimeric versions of FtsZ, engineered to target phospholipid bilayers in the absence of its native membrane-anchoring proteins FtsA and ZipA. We found that our chimeric proteins could be recruited to planar membranes and self-organize into dynamic cytoskeletal structures. Dynamical behaviours included condensation of filaments and constriction of protein rings. These artificial structures could also form on the outer leaflet of free-standing liposome membranes. However, no activity was detected when the chimeric FtsZ proteins were synthesized in vesicles.

Finally, we attempted to reconstitute a functional Min system on planar membranes with the ultimate goal of spatially and temporally regulating FtsZ polymerization in synthetic cells. We found that cell-free synthesized Min proteins resumed reaction-diffusion-like patterns on planar membranes, granted an optimization of the ATP concentration, gene sequence and presence of suitable chaperones.

In conclusion, this work provides experimental evidence for DNA-directed production and functional assembly of key *E. coli* division proteins. Many of the typical properties of FtsZ, FtsA, ZapA and Min proteins have been validated when expressed and assayed on supported lipid bilayers. In liposomes, we have demonstrated the link between FtsZ expression and membrane deformation. Yet, the anchoring of cell-free synthesized FtsZ to the inner leaflet of the liposomes, the organization into a contractile division ring and its dynamic positioning by in situ expressed Min proteins are specific goals that remain to be achieved. In light of the presented results, we propose a new picture of our minimal division machinery model. Specifically, we suggest to extend the chosen set of genes to include chaperons that will assist the correct folding of synthesized proteins, as well as one of the proteins of the Zap family, like ZapA, for FtsZ-ring condensation. Additionally, increasing the concentration of K^+ and Mg^{2+} may facilitate FtsZ filament formation by lowering the FtsZ polymerization critical concentration, while an increase of ATP concentration will ensure sustained functioning of the Min system. We believe that implementation of the above conditions in future experiments will bring us closer to an FtsZ-based dividing liposome.

Samenvatting

Het creëren van artificiële cellen die met een minimale set componenten zichzelf in stand kunnen houden, kunnen reproducieren en evolueren, (met andere woorden als levend beschouwd kunnen worden), is een van de meest veelbelovende onderwerpen op het terrein van de synthetische biologie. Dergelijke entiteiten, hier 'minimale cellen' genoemd, worden volgens een top-down of bottom-up benadering geconstrueerd. Bij de top-down benadering wordt getracht een minimale cel te verwezenlijken door niet-essentiële genen te verwijderen uit een al bestaand eencellig organisme. Bij de bottom-up benadering worden afzonderlijke biomoleculen zoals fosfolipiden, DNA en eiwitten vanaf de basis opgebouwd en geassembleerd tot een eenheid met celachtige eigenschappen. In de loop van dit door nieuwsgierigheid gedreven, uitdagende onderzoek, verwachten we ook meer inzicht te verwerven in de meest fundamentele processen eigen aan een levende cel.

In het laboratorium van Christophe Danelon stellen we voor om een minimale cel te bouwen met een bottom-up benadering. Het frame bestaat uit drie kernmodules. Ten eerste wordt een liposoom gebruikt als compartimentmodel om de minimale cel te definiëren als een fysieke onafhankelijke eenheid. Het fosfolipidemembraan van het liposoom reguleert de uitwisseling van materiaal en energie. De tweede module betreft de informatie over de samenstelling van de cel (lipide, RNA, eiwit): deze informatie is als genen geëncodeerd in DNA. De derde module omvat het metabole netwerk om eiwitten te synthetiseren op basis van de code in het DNA. Hiervoor wordt het PURE (protein synthesis using recombinant elements) systeem gebruikt. Dit minimale cel model heeft volgens ons het potentieel om uiteindelijk aan de voorwaarden van leven te voldoen.

Een van de essentiële processen voor reproductie is deling. In deze thesis komen twee vragen aan de orde: kunnen we een delingssysteem voor liposomen ontwerpen door het bacteriële systeem voor celdeling na te bootsen? Kan dit geassembleerde delingsapparaat vervolgens in ruimte en tijd gereguleerd worden door een ontworpen eiwitnetwerk dat ook gebaseerd is op bacteriën? Om deze vragen te kunnen beantwoorden, hanteerden we als strategie de in-vesikel synthese van een zorgvuldig geselecteerde set van delingseiwitten van *Escherichia coli*. In *E. coli* begint de celdeling met de polymerisatie van het cytosolische eiwit FtsZ tot een ringvormige structuur in het midden van de cel. Deze FtsZ-ring wordt dankzij de eiwitten FtsA en ZipA verankerd in de binnenmembraan. Constrictie van de FtsZ-ring deelt de cel uiteindelijk in twee. Een driedelig eiwitsysteem, het Min-systeem, garandeert de correcte localisatie van de delingsring. De dynamische zelf-organisatie van het Min-systeem zorgt specifiek voor de assemblage van de FtsZ-ring in het midden van de cel. Onze hypothese is dat, in analogie met celdeling, synthese van FtsZ, FtsA, ZipA en het Min-systeem de vorming van een actieve FtsZ-ring zal stimuleren, wat uiteindelijk de minimale cel in twee deelt. De verzameling van deze genen en hun eiwitfuncties noemen we het minimale delingsapparaatmodel (minimal division machinery model).

Voor de implementatie van dit minimale delingsapparaatmodel onderzochten we eerst de mogelijkheden van de cel-vrij gesynthetiseerde delingseiwitten FtsZ, FtsA en ZipA van *E. coli* om een basaal cytoskelet te vormen. De eiwitactiviteit werd gevolgd op vlakke membranen onder de microscoop. We ontdekten dat onder de door ons geteste condities Ficoll70, een algemeen macromoleculair vulmiddel (crowding agent), nodig was om de vorming van filamentnetwerken van opgezuiverd FtsZ en ZipA te initiëren. Belangrijker nog, de cel-vrij gesynthetiseerde FtsZ, FtsA en ZipA waren in staat om zelf te assembleren tot filamenten met een specifieke morfologie, gebogen met FtsA en recht met ZipA. We toonden aan dat door het

toevoegen van cel-vrij gesynthetiseerd ZapA, een natuurlijke crosslinker van FtsZ, Ficoll70 niet nodig was om bundels van opgezuiverde of cel-vrij gesynthetiseerde FtsZ-filamenten te vormen.

Vervolgens wilden we een op FtsZ gebaseerd membraan vervormend molecuair apparaat in liposomen reconstrueren. We hebben eerst de dynamiek van ingekapseld opgezuiverd FtsZ getest. Hoewel we in standaardomstandigheden geen FtsZ-polymerisatie in het blaasje konden detecteren, vonden we dat toenemende concentraties K^+ en Mg^{2+} de assemblage van FtsZ tot rechte bundels veroorzaakten. Deze nieuwe conditie was ook compatibel met de assemblage van gesynthetiseerde FtsZ tot filamenten. Vervolgens kwantificeerden we de vorm van FtsZ-filamenten bevattende liposomen en onthulden we dat interne FtsZ-filamenten liposomen kunnen vervormen tot langwerpige en citroen-vormen.

Om de belasting van de metabole machines van het PURE-systeem te verminderen, hebben we de activiteit van twee chimerische versies van FtsZ ontworpen en bestudeerd, ontworpen om dubbellellagse fosfolipide te binden in afwezigheid van de native membraan verankerende eiwitten FtsA en ZipA. We ontdekten dat onze chimere eiwitten konden binden aan vlakke membranen en zichzelf in dynamische cytoskeletstructuren organiseren. Dynamisch gedrag zoals condensatie van filamenten en vernauwing van eiwitringen werd door de eiwitten vertoont. Deze kunstmatige structuren kunnen zich ook vormen op de buiten kant van vrije liposoommembranen. Er werd echter geen activiteit gedetecteerd wanneer de chimere FtsZ-eiwitten in blaasjes werden gesynthetiseerd.

Ten slotte probeerden we een functioneel Min-systeem op vlakke membranen te reconstrueren met het uiteindelijke doel om FtsZ-polymerisatie in synthetische cellen ruimtelijk en tijdelijk te reguleren. We vonden dat celvrij-gesynthetiseerde Min-eiwitten reactie-diffusie-achtige patronen op vlakke membranen toonden, als de ATP-concentratie, gensequentie en aanwezigheid van geschikte chaperones geoptimaliseerd waren.

Concluderend biedt dit werk experimenteel bewijs voor DNA-gerichte productie en functionele assemblage van belangrijke *E. coli*-divisie-eiwitten. Veel van de typische eigenschappen van FtsZ, FtsA-, ZapA- en Min-eiwitten zijn gevalideerd wanneer ze tot expressie worden gebracht en getest op ondersteunde lipidemembranen. In liposomen hebben we het verband aangetoond tussen FtsZ-expressie en membraanvervorming. Toch zijn de verankering van celvrij gesynthetiseerde FtsZ eiwitten aan de binnenkant van de liposomen, de organisatie in een contractiele scheidingsring en de dynamische positionering door in situ tot expressie gebrachte Min-eiwitten specifieke doelen die nog moeten worden bereikt. In het licht van de gepresenteerde resultaten stellen we een nieuw beeld voor van ons model met een minimale divisie apparaat. Specifiek stellen we voor om de gekozen set genen uit te breiden met chaperons die helpen bij het correct vouwen van gesynthetiseerde eiwitten, evenals een van de eiwitten van de Zap-familie, zoals ZapA, voor FtsZ-ringcondensatie. Bovendien kan het verhogen van de concentratie van K^+ en Mg^{2+} de vorming van FtsZ-filamenten vergemakkelijken door de kritieke concentratie van de FtsZ-polymerisatie te verlagen, terwijl een toename van de ATP-concentratie zal zorgen voor een duurzame werking van het Min-systeem. Wij geloven dat de implementatie van de bovenstaande voorwaarden in toekomstige experimenten ons dichterbij een op FtsZ gebaseerd scheidend liposoom zal brengen.

Acknowledgements

Tens of thousands of years ago -let's pretend that this is actually true-, cavemen already knew that *it takes a town to raise a child*. After millennia of enlightenment, science and a lot of television, academic people realized of a similar, key principle: *it takes a town to raise a PhD*. In other words: many are needed to bring a PhD student to success. Here, I would like to briefly thank those people, *my town*, to whom I owe so much.

Christophe, what an honor. Right from the beginning, during the interview, I was impacted by how you care for your students. I can say now, in the best sense of the sentence, that I did not decide to join the lab necessarily because of the science you do -which is by the way of the highest levels- but by your personality. More than four years in your lab did nothing but to confirm such a great first impression. You are kind, understanding, prone to have a personal relationship, always available for questions, discussions and doubts. Christophe, thanks for the time invested in me. **Marileen**, thanks as well for everything. I remember the annual meetings, when I had to present the progress of my PhD. You had always been a great support of my research, asking always the right questions and offering advice. It has been as well an honor to have you as my promotor.

Alicia, back in the beginning of 2014, you were the one who told me about the open position in the department. Thanks to you I got in! But you did not stop there and continued to give me more than four fantastic years in the office, in the lab, in town. Parties, dinners, walks, conversations, all in all you have been a terrific friend, always so generous and so funny. You made the whole experience more than worth it. Thanks for accepting being my paranymph: with you, the whole defense process has been a piece of cake. **Johannes**, my double in the department. I will miss your dirty jokes, the games at the foosball table, the scientific conversations, the whisky club to which I only attended once... and you were the only one there. I believe I now tolerate whisky thanks to you. Sorry I did not have a white shirt or the like to wear at that moment. Thanks for being such a fantastic friend who had supported me in the difficult moments and, of course, for being my paranymph.

During my first days in the lab, I met incredible people who helped me get one foot in front of the other in the right way. **Ilja**, it is marked in my memory one of the first conversations that we had. It was right after the interview. You came to talk to me. You made me feel welcomed even when I did not know if I was getting the position or not. And you kept helping me in the lab from day one. **Zohreh**, thanks for starting me in the lab and teaching me the basic protocols. I will always remember your smile. **Fabrizio**, thanks for the scientific conversations and help in the lab. **Huong**, I will always miss you. You are very especial and sweet. **Andrew**, you also helped in my first steps in the lab. I will always remember as well the times we had dinner, or simply hanged out. Thank you. **Pauline**, it was an honor to be one of your colleagues. I learned many things from you even if you did not realize of it, and we shared quite personal stories. I will always remember those. **Duco**, it has been a pleasure to be your laboratory colleague. Thanks a lot for the tips about the confocal microscope and the funny moments through all this time. **Anna**, you have always been a model of working efficiency. I admire you for it. Thanks for all the help of scientific nature. **Essengul**, I will always remember with a smile how you were able to get anything you wanted. Lab supplies, rooms to do a meeting, you name it. **David**, thanks for everything. The help in the lab, the good moments having a beer, or simply your uncountable number of jokes. You will be definitely missed. **Elisa**, thanks a lot for taking charge of the projects. I cannot think of a better person to continue the

good work. **Zhanar**, although we have not spent much time together, I can already say from the few conversations we initiated, that you have already taught me quite a lot. Thanks for it.

Of course, I could not forget many of the students that in some way or another have passed by the lab. **Katja**, my first student. What a pity you could only join one day per week. We really had fun. Thanks a lot for taking with me the first steps with the Min system project. **Ilias**, do you remember how you asked me to be my student? You put a lot of time and effort in the FtsZ project and as a consequence many of the results in this thesis are linked to your work. Thanks for been a kind, good person and for been a friend. **Céline**, I have a lot to thank you as well. You did a fantastic job with the Min system project. I think we made a wonderful team. You are smart and fun. I am sure you will have a bright future wherever your steps will lead you. So many students and so few lines: **Mischa, Jurjen, Miranda, Roy, Emma, Adriana, Gemma, Sophie, Gabriele, Gabriella...** Thanks for making working side by side with you a more-than-awesome experience.

Other people in, or out the department have contributed to my success in many different ways: with conversations, with activities, with friendships. **Nicole and Meheran**. Thanks a lot for letting me ask you my doubts about any scientific topic. Thanks for the dinners, the beers, the cocktails at café Luna or simply thanks for your company throughout this time. **Roland**, I am so glad that Alicia found you. You are a true friend, and to be honest, you brought the lab movies to a whole new level. **Elena, Sumit, Viktorija**, it has been an honor to enter the department at the same time than you. Thanks for the good moments. **Maurits**, thanks for your patience every time I asked you for help with the TIRF microscope. **Benjamin**, your self-defense classes were awesome. Thanks for everything. **Eve**, you are a technician superstar. Ok, forget about the technician part, you are simply a superstar. **Carsten**, I will never forget that you always beat me at sleigh racing in Courchevel back then in my first year in the department. May I have one day my revenge! **Mathia**, you were one of the first people I had the pleasure to meet during my first Kavli day in Brussels. Since then, I always felt that I could count on you for anything. Talking about Kavli days in Brussels, I will be always impressed by you, **Pawel**, and your infinite ability to party hard. **Laura**, thanks for showing me what means to give it all on the dancefloor. **Daniël and Jeremy**, thanks for your training. You open up the fluorescence microscopy universe to me. **Michela**, I will always remember our conversations about life, those sunny evenings in the old building while you were writing your thesis. **Victor**, my Mexican friend, I think I have never drunk so much tequila as when hanging out with you... and I mean that as a compliment. **Mohammed, Anthony, Roy, Luuk, Jakub, Thijs, Federico** and many others. I will always associate you with foosball and a generous, healthy dose of competitiveness. Thank you. So many people, so few lines: **Vanessa, Hiram, Natalia, Richard, Stephanie, Fabai, Nuria, Kim, Patrick, Daniel, Mahipal, Jorine, Yoonis, Dijana, Jolijn, Sophie Roth, Becca...** You all contributed to make my PhD an unforgettable, superb experience.

Way before I came to Delft, a number of people, in a way or another, contributed to help me to get where I now stand. **Cynthia Slagter**, thanks for believing in me and giving me the opportunity to meet the wonderful family that you guys are at Calvin University. **Anding Shen** and **Mary Dekker**, thank you for accepting me in your lab and tolerating a dummy Spaniard who barely could speak English at the time. **Teun Boekhout** and **Bart Theelen**, a small bird told me that you were the ones responsible for selecting me to do the internship at the Westerdijk Fungal Biodiversity Institute among many other possible candidates. Such experience opened many doors for me. Many, many thanks. **Anna Kolecka, Aleja, Sandra, Liana, Rhiana...** thanks for being of such support in Utrecht. How was it? Ah, yes... CBS is fun!

Y por fin, mi familia. **Raquel**, es increíble pensar que esa llamada que hice años antes de conocerte, de alguna manera, me trajo a ti, paso a paso. Ya conoces la historia. ¡Tantas historias! ¡Recuerdas ese día en el CBS, cuando había tenido un mal día en el laboratorio, hacía frío afuera, estaba oscuro y llovía? De camino a tu casa mi bici rompió. Llegue a tu casa molesto, cansado, enfadado y sintiéndome miserable. Entonces, tú me hiciste sentar en tu sofá, pusiste una manta sobre mis hombros, me diste una toalla para secar mi pelo, y pusiste un plato de comida en mis manos. En un instante, me sentí feliz de nuevo. ¿Cómo lo hiciste? El milagro es que tú has seguido confortándome y apoyándome, en lo bueno y en lo malo, hasta este mismo día. Nunca podría haber ido tan lejos sin ti. Muchas gracias. Mis **abuelitos**, nunca me olvidaré de los paseos que dábamos con mis hermanos a Roces en aquellos días cálidos de verano de mi dulce infancia. Para mí era como una aventura, viajar, caminando entre prados a un lejano lugar. Nunca me olvidaré de los veranos en Madrid, ¡ni de los veranos en Fuengirola! De las navidades en familia, de las visitas a nuestra casa. Nunca me olvidaré de que vosotros también me criasteis con amor. Gracias por ser tan maravillosos. Mis hermanos, Natán, Daniel y Juan. ¡Qué increíble es saber que nunca podría haber tenido mejor compañía para afrontar mi vida que a vosotros! De todos y cada uno he aprendido mucho. **Natán**, tú me enseñaste a ser sociable, abierto, a conversar... recuerdo cómo ya desde pequeño te miraba y quería ser más como tú. Desde que te marchaste a Madrid no he dejado de echarte de menos, pero siempre me alegra cada vez que nos vemos, aunque sea mucho menos a menudo de lo que desearía. Muchas gracias por todo. **Daniel**, tú me has enseñado a saber aceptar la situación en la que uno se encuentra, aunque no sea en la que uno desearía estar. Me has enseñado resiliencia, a esperar, a ser paciente. Sé que en el futuro encontrarás lo que buscas. Te lo mereces. Gracias por los buenos momentos, las risas, las experiencias... **Juan**, tú me has enseñado a tener una voz propia, un criterio propio. Me has enseñado lealtad y a no callarme para denunciar las injusticias. Tu forma de ser es arriesgada. Pero el que no arriesga no gana. Gracias por todo. Y por fin, mis **padres**. Qué podría decir, sino que vosotros sois el origen de todo. Siempre habéis creído en mí. Siempre me habéis soportado. Empujado. Amado. Me habéis regalado todo. Habéis sido una guía en mi vida, tanto moral como espiritualmente. Me habéis hecho una persona. En fin, no estaría aquí donde ahora me hallo, si no fuera por vosotros. Este éxito, que yo alcance el título de doctor, es un éxito vuestro también. Enorgulleceos, como yo me enorgullezco de vosotros.

Gracias, gracias y más gracias.

Curriculum vitae

Jonás Noguera López

18-5-1987

Born in Gijón, Spain

- | | |
|-------------|--|
| 1999 - 2005 | Secondary Education
Instituto Doña Jimena, Spain |
| 2005 - 2011 | Licenciatura en Biología
Universidad de Oviedo, Spain |
| 2012 | Research Internship in HIV
Calvin University, United States of America |
| 2013 | Research Internship in Ascomycetes
Westerdijk Fungal Biodiversity Institute, The Netherlands |
| 2014 - 2019 | PhD in Synthetic Biology
Technische Universiteit Delft, The Netherlands
Title 'An FtsZ-centric approach to divide gene-expressing liposomes'
Promotors: Dr. C. Danelon & Prof.Dr. M. Dogterom |

List of publications

Godino, E. *, López, J.N. *, Zarguit, I., Doerr, A., Jiménez, M., Rivas, G., Danelon, C. **Cell-free biogenesis of bacterial division proto-rings that can constrict liposomes.** *In preparation.*
(* denotes equal contribution)

Godino, E., López, J.N., Foschepoth, D., Cleij, C., Doerr, A., Ferrer Castellà, C., Danelon, C. **De novo synthesized Min proteins drive oscillatory liposome deformation and regulate FtsA-FtsZ cytoskeletal patterns.** *Nat Commun* 10, 4969 (2019) doi:10.1038/s41467-019-12932-w